BUCKLING BEHAVIOUR OF STEEL BOX-GIRDER BRIDGES

François-Xavier Tupula Yamba

A Thesis

in

The Faculty

of

Engineering

Presented in Partial Fulfillment of the Requirements
for the degree of Doctor of Philosophy at
Concordia University
Montréal, Québec, Canada

April 1981

To my parents

PROLOGUE

PROLOGUE

...The story of bridges is an epic of human vision and courage, high hopes and disappointments, heroic efforts and inspiring achievements.

A bridge is more than a sum of stresses and strains... it is the symbol of humanity's heroic struggle toward mastery of the forces of nature.

Bridges symbolize the ideals and aspirations of humanity. They span the barriers that divide, and they bring peoples, communities, and nations into closer unity...

- D.B. Steinman and S.R. Watson

(1941)

ABSTRACT

ABSTRACT

BUCKLING BEHAVIOUR OF STEEL BOX-GIRDER BRIDGES

François-Xavier Tupula Yamba, Ph.D.
Concordia University, 1981

The steel box-girder is now a favoured shape for bridge engineers. It offers many structural advantages, if compared to the conventional plate girder and truss bridges, and it constitutes a good solution in the intermediate and long-span range. The progress accomplished in fabrication, and in particular, of welding techniques, contribute to the wide use of steel box-girder bridges.

This type of bridge is often designed by using theory and design standards established for plate-girder bridges. However, due to numerous accidents which have occurred with this type of bridge, it is now proven that these design standards are not appropriate for use on steel box-girder bridges. New investigations accounting for all parameters which influence the behaviour of steel box-girder bridges are needed before design recommendations can be established.

It has been found that the major steel box-girder bridge failures are due to buckling. In fact, steel box-girder bridges are an assembly of thin plates and stiffened panels,

and for the sake of economy, the range of plate width-to-thickness ratio used requires a careful buckling consideration. It has been proven that the classical elastic buckling theory does not accurately predict the buckling behaviour of plates and stiffened panels used in steel box-girder bridges, and only the large deflection (non-linear) theory accounting for the effect of initial imperfections need therefore, to be considered. In fact, the initial geometrical imperfections and residual welding stresses have great weakening effect on the buckling strength of plates in the range of width-to-thickness ratios often used in steel box-girder bridges.

There is a need for extensive experimental tests before establishing appropriate design recommendations intended to be used on steel box-girder bridges.

In the present study, the ultimate buckling strength of steel box-girder bridges, as governed by their buckling performance is investigated, considering different structural parameters which may influence them.

An evaluation of the actual bridge design standards, with regard to the buckling is made. The effect of initial geometrical imperfections and residual welding stresses is demonstrated. The ultimate buckling strength, as given by the large deflection (non-linear) theory is reviewed and

compared with some approximate methods.

An extensive experimental investigation of the buckling behaviour of steel box-girder bridges was conducted on three models. It was possible to study the buckling performance of all components such as flanges and webs, the interaction between their components, the overall buckling behaviour and influence of stiffener spacings and rigidities; to determine the required optimum rigidity for the stiffener to remain straight and rigid up to and after buckling of the plate, to study the influence of any initial geometrical imperfections and of any residual welding stresses. Finally, the influence of the failure mode upon the ultimate strength was determined.

The theoretical and experimental results were compared and it was found that only the non-linear theory accounting for the effect of any initial imperfections could accurately predict the ultimate buckling behaviour of steel box-girder bridges.

ACKNOWLEDGEMENTS

ACKNOWLEDGEMENTS

The author is sincerely grateful to Professor M.S. Troitsky, for having accepted the task of supervising this study, and would like to thank him for his guidance, criticism, correction and encouragement throughout the course of this research.

Thanks also to all Civil Engineering Departmental Professors for their advice.

Special thanks to Louis Stankevicius, Harold Leroux and Daniel Roy for their friendship and cooperation during the experimental stage of this research. Thanks also to Gerard Viger, Daniel Plamandon and all the plumbers for their help; and to Miss M. Stredder for the typing of the manuscript.

I would like to express my deep gratitude to my wife, Mariette and to my son, Gabriel-Bandeja, for their understanding and patience; and finally, to all my brothers and sisters for their encouragement.

TABLE OF CONTENTS

TABLE OF CONTENTS

PAGE

LIST OF FIGURES

LIST OF FIGURES

LIST OF FIGURES

LIST OF FIGURES

LIST OF FIGURES

LIST OF FIGURES

LIST OF FIGURES

LIST OF FIGURES

LIST OF FIGURES

LIST OF FIGURES

APPENDIX "A"

LIST OF FIGURES

APPENDIX "B"

LIST OF TABLES

LIST OF TABLES

LIST OF TABLES

APPENDIX "A"

NOTATIONS

NOTATIONS

Due to the size of this thesis, the notations are separated into two parts:

N-1 for the main part

N-2 for Appendix B

NOTATIONS

N-1 MAIN PART

a_x, a_y	Stiffeners spacing in x and y-directions
A, A'	Cross-sectional area of the original and effective plate/stiffener column
A_s	Cross-sectional area of the stiffener
A_w	Coefficient used in calculation of residual welding stresses
b	Width of plate
$(b/t)_y$	Plate width-to-thickness ratio at which the critical buckling stress σ_{cr} is equal to yield stress σ_y
b_e	Effective width of plate
B	Width of flange between webs
B_B	Width of the bottom flange
B_p	Length of the cantilever part
B_T	Width of the top flange
C	Coefficient used for calculating the sectant stiffness
d	Depth of the cross-section
D_x, D_y	Flexural rigidity of the stiffened plate
e	Deflection of plate due to load
e_o	Initial deflection of plate
e_{ult}	Ultimate deflection of plate at collapse

E, E_x, E_y	Modulus of elasticity
E_t	Tangent modulus
f_b	Allowable compression stress
f_o	Maximum magnitude of plate initial imperfections
F	Stress functions
g	Gauge length to be used for measuring of initial geometrical imperfections
G	Shear modulus $G = \frac{E}{2(1+\nu)}$
$2H$	Effective torsional rigidity of stiffened plate
I_x, I_y	Moment of inertia of the stiffener in x and y-direction
I'	Moment of inertia of the effective plate/stiffener column
K	Buckling coefficient
K_{bs}	Secant stiffness coefficient
ℓ	Buckling length of column
ℓ_e	Effective buckling length
ℓ_c	Length of flange transverse stiffener
ℓ/r	Column slenderness ratio
$(\ell/r)_y$	Slenderness ratio at which the critical buckling stress σ_{cr} is equal to yield stress σ_y
ℓ_o	Coefficient used for the reduction of initial imperfections
L	Length of stiffened panel
m	Magnification factor of initial imperfections
M_x, M_y, M_{xy}	Bending and torsion moment per unit width in x and y-directions

$\overline{M}, \overline{MN}$	Quadratic stress interstices
n_x, n_y, n_{xy}	Membrane forces per unit width
n_a	Average membrane force per unit width
$\overline{n}$	Mean membrane force per unit width
N	Number of flange longitudinal stiffeners
N_x, N_y, N_{xy}	Membrane forces
$\overline{N}$	Quadratic stress intensity
P	Pressure per unit surface
P_s	Compression load carried by stiffener
P_y	Compression load in y-direction
P_{ult}	Ultimate compression load
r	Radius of gyration
r'	Radius of gyration of the effective plate/stiffener column
S	Stiffener spacing
S_t, S_b	Section modulus for compression and Tensile stress
t	Plate thickness
t_i	Thickness of flange transverse stiffener
t_s	Thickness of flange longitudinal stiffener
u,v	Strain function in x and y-directions
w	Deflection surface function
w_o	Initial deflection surface function
Z_{sk}	Distance from centroid of plate/stiffener column to mid-plane of plate

α	Aspect ratio of plate (α=a/b)
γ	Relative stiffener rigidity = $\frac{10.92\ I_s}{bt^3}$
δ	Relative cross-sectional area of stiffener = $\frac{A_s}{bt}$
δ_o	Overall initial imperfections
δ_{ox}, δ_{oy}	Overall initial imperfections in x and y-directions
Δ	Shift of position of neutral axis (original, and effective plate/stiffener column)
Δ_{sx}, Δ_{sy}	Measured initial imperfection of flange longitudinal stiffener in x and y-directions
Δ_x, Δ_y	Measured plate initial imperfections in x and y-directions
Δ_{x1}, Δ_{x2}	Plate initial imperfection measured on gauge g equal to b and 2b, respectively
$\Delta_{sy1}, \Delta_{sy2}$	Longitudinal stiffener initial imperfection measured on gauge g length equal to be and 2b,respectively
ε	Strain
$\varepsilon_x, \varepsilon_y$	Unit strain in x and y-directions
$(\varepsilon_y)_{FP}$	Longitudinal strain of flange plate at flange/web edge
$(\varepsilon_y)_w$	Longitudinal strain of web
ν	Poisson's ratio
λ	Buckling factor, $\lambda = \sqrt{\sigma_y/\sigma_{cr}}$
σ	Direct stress
σ_o	Uniaxial yield stress
$\bar{\sigma}$	Maximum mean membrane stress
$\sigma_a, (\sigma_a')$	Collapse stress of the cross(effective) plate/stiffener column

σ_{am}	Maximum average stress
σ_{cr}	Critical buckling stress
$\sigma_e, (\sigma'_e)$	Critical Euler's buckling stress of the cross (effective) plate/stiffener column $\sigma_e = \pi^2 E/(\ell/r)^2$
σ_m	Maximum stress
σ_r	Compressive residual welding stress
σ_Y	Yield stress
σ_{YP}	Yield stress of plate
σ_{YD}	Yield stress of stiffener
σ_{YT}	Torsional buckling limiting stress
σ_{ult}	Ultimate stress
τ	Shear stress

APPENDIX "B"

N-2 SECOND PART

a	Length of plate
a_x, a_y	Stiffeners spacing in x and y-direction respectively
A_x, A_y	Cross-sectional area of stiffeners in x and y-direction respectively
b	Width of plate
B	Unit flexural and torsional rigidity of plate $= \frac{Et^3}{12(1-\nu^2)}$
B_x, B_y	Flexural unit rigidity of stiffened plate $B_x = \frac{1}{a_x}\int_{a_x} E(z)(z-e_x)^2\, dA_x$ $B_y = \frac{1}{a_y}\int_{a_y} E(z)(z-e_y)^2\, dA_y$
B_{xy}, B_{yx}	Torsional unit rigidity of stiffener in x and y-direction respectively $= \frac{1}{3} G \leq h_s t_s^3$
D	Extensional unit rigidity of the stiffened plate $= \frac{Et}{(1-\nu^2)}$
D_x, D_y	Extensional unit rigidity of the stiffened plate

$$D_x = \frac{1}{a_x} \int_{a_x} E(z)\, dA_x$$

$$D_y = \frac{1}{a_y} \int_{a_y} E(z)\, dA_y$$

e_x, e_y — Eccentricities of the center of gravity of the stiffener about the middle plane of the plate in the x and y-direction, respectively

$$e_x = \frac{1}{a_x D_x} \int_{a_x} E(z) z\, dA_x$$

$$e_y = \frac{1}{a_y D_y} \int_{a_y} E(z) z\, dA_y$$

E — Modulus of elasticity

f — Function of deflection

f_o — Function of initial deflection

F — Airy's stress function

F_x, F_y — Component of F in the x and y-direction respectively

G — Shear modulus

$$= \frac{E}{2(1+\nu)}$$

h_s — Depth of stiffener or the largest dimension of rectangular elements that compose cross-section of the stiffener

I_x, I_y — Moment of inertia of stiffener in x and y-direction respectively about the middle plane of the plate

Lo — Location or point where the reading is taken

M_x, M_y	Bending moment per unit length in x and y-direction, respectively
n_x, n_y	In-plane forces per unit width in x and y-direction respectively
n_{xy}, n_{yx}	Shear forces per unit width in x and y-direction respectively
N_x, N_y	In-plane forces in x and y-direction
N_{xy}, N_{yx}	Shear forces in x and y-direction
P	Lateral load per unit area of plate
P_x	Compressive force per unit width in x-direction
PR	Pressure in the jack
t	Plate thickness
t_s	Width of stiffener or the smallest dimension of rectangular elements that compose cross-section of the stiffener
u,v	Displacements function in x and y-direction
u_x, v_y	Unit displacements in x and y-direction
w	Deflected surface function
w_o	Initial deflection surface function
α	= a/b
γ_{xy}, γ_{xy}	Shear strains in x and y-direction
ε_{pl}	Normal strain in plate
ε_{st}	Normal strain in stiffener
$\varepsilon_x, \varepsilon_y$	Normal strains in x and y-direction

ν	Poisson's ratio
σ_{pl}	Normal stress in plate
σ_{st}	Normal stress in stiffener
σ_x, σ_y	Normal stresses in x and y-direction
τ_{xy}, τ_{yx}	Shear stresses in x and y-direction
U_b	Strain energy of bending
U_m	Strain energy of membrane stresses
U_t	Total strain energy
$\int_{a_x} dA_x$	Surface integral in x direction on width a_x
$\int_{a_y} dA_y$	Surface integral in y-direction on width a_y

CHAPTER I

INTRODUCTION

CHAPTER I

INTRODUCTION

1.1 DESCRIPTION OF A STEEL BOX-GIRDER BRIDGE

A box-girder may be used as simply supported, continuous, in cable-stayed or suspension bridges.

The cross-section generally consists of a single or multi-cell box carrying a steel or concrete deck (Figure 1.1).

The web is composed of two vertical or inclined walls. The number of web walls can be increased if shear stresses are predominant, or if the width-to-span ratio may be increased to take into account the number of traffic lanes to be carried. The web panels may be stiffened with vertical and/or horizontal stiffeners.

The upper flange serves as a deck to carry the traffic so that it is stiffened with longitudinal ribs and transverse beams, as in the case of an orthotropic steel deck. The upper flange may also be of concrete, acting as a composite construction.

The bottom flange plate may be unstiffened for a narrow girder, but it is generally reinforced with longitudinal stiffeners in the region of the negative bending moment (over intermediate supports) in continuous construction.

Longitudinally, the girder is stiffened with transverse diaphrams over the supports, together with some intermediate diaphrams, if necessary.

Figure 1.2 shows the different components of a steel box-girder bridge.

1.2 HISTORICAL NOTE: THE DEVELOPMENT OF STEEL BOX-GIRDER BRIDGES

The available literature takes us as far back as 1839, with Roebling and Homere [1] - [4], who proposed three tubular spans of 500 feet to bridge the Mississippi, but the proposal was not executed.

The first tubular bridge realized is the Britannia Bridge, (Figure 1.3), built during 1845-1850, by Robert Stephenson, in England.

Robert Stephenson also designed other tubular bridges in England and abroad. These are the Conway Bridge (England), the Victoria Bridge over the St. Lawrence River, in Montreal, a bridge over the Damietta branch of the Nile (Africa), and the Brotherton Bridge over the Aire River.

A pony tubular girder, with a span of 60 feet over the Leeds and Liverpool Canal, was erected in 1846 by William Fairbairn. The same year, James Mill-Holland built a tubular plate-girder bridge with a span of 50 feet, over the Baltimore and Ohio Railroad.

In 1849, for bridging the Rhine at Cologne, Fairbairn submitted two alternate plans, one of them had two tubular spans of 570 feet, with double tubes for the lines of railroad and an open 24-foot highway between them.

In 1858, Boyd proposed a tubular bridge over the English Channel between France and England, with 500-foot spans, but the project was abandoned because of its cost.

Some of the earliest tubular bridges are the Pennith Bridge over the Nepean River, New South Wales (1864) and the Gainsborough Bridge over the Trent River, England (1865).

For almost a century, no steel box-girders were built and no explanation has been given for this situation.

In 1947-48, the Cologne-Deutz Bridge (Figure 1.4) was built over the Rhine in Germany.

Because a steel box-girder bridge comprises an assembly of thin plates interconnected with each other, it may be stated that its actual development is associated with the progress accomplished in welding techniques, as well as the introduction of orthotropic steel decks, especially since the Second World War. Since that time, many steel box-girder bridges have been built across the world, some of the biggest being the Severn Bridge, England (Figure 1.5), the Bosporus Bridge, Turkey (Figure 1.6), the Erskine Bridge, England (Figure 1.7), and the West Gate Bridge, Australia (Figure 1.8).

1.3 ADVANTAGES OF BOX-GIRDER BRIDGES

The steel box-girder is now preferred-shaped for bridge engineers. This is due to positive structural characteristics, among which are:

(a) The theoretically good distribution of the metal, resulting in its great strength in bending and torsion, and consequently, economical by saving in its weight and in construction costs.

(b) A box shape has a high torsional rigidity, thus providing efficient support upon the eccentric loads and effective distribution of such loads in the transverse direction.

(c) It is convenient to provide high aerodynamic stability; therefore providing a more suitable shape for suspension bridges, (Severn Bridge, Figure 1.5) as well as long spans exposed to wind forces (The Europa Bridge, Figure 1.9).

(d) For a given number of webs, a box-girder bridge has a larger upper flange width than that of an I-section girder bridge. This increased flange results in a reduced depth. Therefore, a great span-to-depth ratio can be used. This is an advantage in a case where the depth is limited, for example, in clear-

ance for navigation.

(e) A box-girder may be completely fabricated in the shop and the components shipped to the erection site, (Concordia Bridge, Figure 1.10).

This saves both in its fabrication and erection costs. Shop fabrication also permits a better control of work, and therefore, a better quality can be achieved.

(f) The graceful appearance of a box-girder, especially in urban areas, is generally regarded as attractive, the increased slenderness and the effect of inclined web walls being considered as esthetical advantages.

(g) The interior space of the girder may be used for the passage of services and its maintenance is also reduced.

1.4 DEFICIENCIES OF PRESENT ANALYTICAL METHODS

Box-girder bridges are often designed by using theories and specifications established for plate-girder bridges.

Following the failure of a few box-girder bridges [5]-[8] (1969-1971), (Figures 1.11-1.14), a number of commissions [9]-[16], committees [17],[18], and research teams [19],[20], took place. The general conclusion was that both analytical and experimental research is needed to improve the actual design

criteria and to carry out the theories and design recommendations accounting for all parameters typical to that of box-girder bridges. Since that time, several investigations on the behaviour of steel box-girder bridges have been undertaken in a number of countries [17],[18],[19].

Because buckling failure has been associated with all major bridge collapse, it was concluded [14],[17],[18] that:

> "The linear plate buckling theory appears to be sufficiently on the unsafe side for sections that are wide, in comparison with their length, so that consideration of the ultimate strength theory of initially deformed stiffened panels need to be used in design."

In awaiting the development of design rules, based upon this ultimate strength theory, some countries [17],[21] recommended an increase of the actual buckling safety factor, considering the importance of buckling upon the strength of steel box-girder bridges, and the need of rigorous buckling investigation, both analytical and experimental.

Because a box-girder is an assembly of plate and stiffened panels, its buckling behaviour may be well understood by (a) first considering the buckling behaviour of each component separately, and (b) secondly, considering the buckling of the bridge, as a whole structure, considering the interaction between its components.

1.4.1 Compression Flange

The actual bridge standards by AASHO [22], (American Association of Highway Officials) and CSA [23], (Canadian Standards Association), for the design of steel box-girder bridges, are derived from that research as outlined by Fountain [24], and are based upon the elastic linear buckling theory of plates and stiffened plates, as presented by Timoshenko [25].

It is recognized [18] that these standards do not treat the buckling behaviour of such steel box-girder bridges deeply, as may be encountered in practice. One of these deficiencies is the design of the compression flanges.

Figure 1.15 summarizes the present design rules. A design curve may be explained as follows:

(a) It is considered that the yield stress F_y of the steel will be developed if λ is less than 0.6. For this portion of the curve, the allowable stress is equal to $0.55\ F_y$.

(b) When λ is greater than 1.3, an elastic buckling stress F_{cr} of the plate will occur and the allowable stress will then be equal to $0.55\ F_{cr}$.

(c) When λ is between 0.6 and 1.3, failure will occur by buckling at a stress less than that of both the

yield stress F_y and the critical elastic buckling stress F_{cr}. The allowable stress in this intermediate region corresponds to a smooth transition curve tangential to $f_b = 0.55\ F_y$ at $\lambda = 0.6$ and to $f_b = 0.55\ F_{cr}$ at $\lambda = 1.3$.

These rules fail to take advantage of the extra available strength produced as the result of either strain hardening at low b/t ratios ($\lambda < 0.6$), or the development of post-buckling strength at higher b/t ratios ($\lambda < 1.3$).

The transition curve ($0.6 < \lambda < 1.3$) which covers the practical range of width-to-thickness ratios, and which is intended to account for the effect of residual stresses, is similar to that used for the elastic buckling of columns. This transition curve is derived solely upon a similarity between the column and the plate buckling. Such application is questionable [18].

The rules do not account for the effect of initial imperfections and it has been proven [19],[20],[26] - [28]), that they may reduce the buckling capacity to an unexpected low value, and similar to this influence, that of the residual stresses is more predominant in the intermediate region ($0.6 < \lambda < 1.3$), as will be shown in Chapter II.

The design stress, such as that given by References [22] and [23], is based solely on the elastic buckling behaviour of

the plate between the stiffeners and not upon the overall buckling behaviour of the stiffened panel. It is assumed that the stiffeners are rigid enough and remain so, before and after elastic buckling of the plate. By doing so, the stiffeners constitute only the nodal lines of the buckling modes of the plate, and consequently, there is little interaction between the plate and stiffeners. An economical design may be obtained by making the design in such a way that the local and overall critical buckling stress occurs at approximately the same level.

The required rigidity for the stiffener to remain rigid is also derived by an approximate elastic method.

Dubas [29], Massonnet [30],[32], and other researchers [33],[34], have proven the inadequacy of the actual elastic buckling theory when applied to steel box-girder bridges. In fact, Dubas [29] has demonstrated that to remain rigid and straight up to the elastic buckling of a plate, the stiffeners require a rigidity five times greater than that given by elastic buckling theory.

In investigation of the buckling, it is important to consider its overall behaviour in respect to that of the stiffened panel. It is thus possible, in this way, to differentiate the mode of buckling. Two modes of failure are observed [35] - [40]:

(a) Plate failure, and

(b) stiffener failure

depending on which plates and stiffeners initiate failure, (Figure 1.16).

The buckling capacity of the stiffened panel may change considerably, depending upon which failure mode occurs first [37] - [40].

It has also been shown [14],[17],[20],following the aforementioned bridge failure, that the compression flange is the most weakest component; if buckling takes place, there is no post-buckling strength reserve that may retain the collapse, as is the case in web panels, where some post-buckling strength reserve exists due to tension field action.

The above-outlined deficiencies of analysis methods deal with the compression flange. Steel box-girder bridges are also composed of webs and transverse diaphrams. The buckling behaviour of those components needs to be considered. Finally, box-girders need to be analyzed as whole structures, thus enabling the influence of interaction between the components on the ultimate buckling strength of steel box-girder bridges to be more clearly defined.

1.4.2 Web Plates

Normally, webs are simultaneously subjected to shear and bending. The state of stress in the pre-buckling state is shown to be linear, as given by the general elastic theory of bending and stress-state changes after the appearance of buckling. When shear stress reaches a critical value, there is a diagonal stress field between the flanges and the stiffening. After reaching a critical value, the structure can then collapse by the failure of the diagonal tensile strips, if the material is not ductile, or by kinematic mechanism, in a longitudinal and transverse stiffening frame.

The problem of critical stress in a web has already been treated by many researchers, however, a more complete theory is given by Kloppel [41],[42]. For an ultimate load theory of a web, it appears that a reliable method is given by Rockey [43] and Ostapenko -[44],[45].

One of the main difficulties encountered for accurately predicting the ultimate strength of webs of steel box-girder bridges, is the accurate consideration of the interaction between the web and the flange. Although current approximate treatment has provided acceptable results for rolled and welded plate girders, its application to web panels of steel box-girder bridges is far to be recommended.

In a box-girder, the behaviour of the web panels depends upon the degree of restraint against the membrane forces at the web/flange junction, as well as upon the capacity of the box-girder to accommodate redistribution of its longitudinal bending or direct stress. It also depends upon whether the webs are stiffened transversely and/or longitudinally [46]. The web inclination has also had an influence on its behaviour. This latter factor can be investigated by comparing the rectangular and trapezoidal shapes, such as those shown in Reference [47].

Due to the difficulty in analytically considering web/flange interaction, as well as the interaction between flexural and shear stresses, current practice is to treat the web and flange separately. Another difficulty is the interaction between the elastic buckling strength(that is, the tension field strength) of the web. Although there is no question about the application of the tension field action to plate-girders because the flanges provide sufficient anchorage to the web panel, in a box-girder, the tension field action can be applied if the flange/web edges connecting the member resists the vertical forces due to tension field action.This is why most proposed approximate methods consider the lower capacity of the tension field action. This means an assumption of negligible flange rigidity. This treatment is known,in technical literature,

as the "true Basler solution".

The ultimate strength of the webs is now determined by simply adding the beam shear strength (elastic buckling) and the tension field strength (post-buckling). But, this is a very conservative solution. A survey of several different proposed methods for predicting the ultimate buckling strength of those webs that are typical of steel box-girder bridges, has been conducted in Reference [48]. However, the conclusion is that further investigations, especially those of an experimental nature, are needed before establishment of appropriate web design recommendations.

1.4.3 Diaphragms

The stiffness, number and location of the diaphragms influence the behaviour of a steel box-girder as a whole structure, longitudinally and transversely. By designing the box-girder by the line analysis method, it is assumed that the cross-section does not distort. This means that the box-girder has closely-spaced diaphragms, having great rigidity in the plane of the cross-section, but are more flexible in the longitudinal direction [49],[50],[51],[52].

So, an intermediate diaphragm provides cross-sectional rigidity for torsion, which constitutes one of the main advantages of a box-girder. The support diaphragms also have to be capable of transferring the shear forces through

to the bearings. The post-buckling behaviour in a web is also influenced by the behaviour of the diaphragm [47].

The effects upon the elastic and ultimate load diaphragm behaviour of the initial imperfections, as well as the vertical and rotational misalignment of the bearings need to be studied.

Many attempts are made to develop a basis for predicting the strength and theoretical critical buckling load of a diaphragm, especially the load-bearing diaphragms. Some theoretical works [53] - [56] and tentative recommendations, based upon experimental tests [20], have been reported. However, it seems that the problem remains complex and the post-buckling reserve is not well-known.

1.4.4 Overall Box Behaviour

In the previous sections, each component of a steel box-girder has been considered separately, and is described by considering any different parameters that may influence in some way, the strength and stability of that component under investigation.

However, each component has been described by considering the other parts adjacent to it, to ensure the realistic boundary conditions.

The problem of investigating the behaviour of a steel box-girder as a whole, remains very complex and is the objective of many research programs. In Reference [20], the collapse behaviour of a rectangular steel box-girder is investigated by considering the box as a whole structure, and by taking into account the interaction between the different components. The state of each component is so analyzed. Tests have also been reported on the behaviour of a continuous two-span box-girder as a whole structure. The results found give an important conclusion to the collapse behaviour in continuous construction when flange buckling occurs, and the moment distributions and deflections, relating these to initial imperfections. The influence of shear-lag throughout the effect of vertical misalignment of the center bearings on the behaviour of a box-girder have also been considered, and the results obtained may be considered useful for design purposes.

Mathematical formulation of the behaviour of a steel box-girder as a whole structure, is very complex and therefore, experimental tests are recommended for better understanding of the problem.

1.5 SCOPE AND OBJECTIVE

The objective of this thesis is the investigation of the ultimate strength of steel box-girder bridges, as limited by their buckling performances, mainly their compression

flanges.

A steel box-girder offers advantageous structural characteristics and it is a suitable solution for bridges in the intermediate and long-span ranges. However, its buckling behaviour needs more investigation, as outlined in Section 1.4. A survey of available information on the subject was conducted [57], from which it was concluded that the present work would contribute by providing additional information to the buckling behaviour, in consideration of the following factors:

a) The influence of stiffener spacing and rigidity.

b) The required optimum rigidity for the stiffener to remain rigid and/or straight, up to and after the buckling of the plate elements.

c) The influence of initial geometrical imperfections of the plate, stiffeners and overall imperfections of the cross-section, as a whole. The influence of residual welding stresses.

d) The influence of the interaction between the web and flange on their respective buckling strength, and on the overall buckling behaviour of the cross-section.

e) The influence of the failure mode on the overall buckling strength.

1.6 ORGANIZATION OF THE THESIS

In Chapter I, an introduction on steel box-girder bridges, together with an analysis of some design problems associated with it, is presented.

Different components that compose the cross-section are described. A brief note is given on the historical development of this particular bridge-type, as well as on the advantageous structural characteristics that are offered.

A summary of deficiencies of the existing bridge design standards in accurately predicting the ultimate strength of steel box-girder bridges is made, from which the factors requiring further investigation can be deduced.

Chapter II, is the evaluation of the influence of initial geometrical imperfections, of residual welding stresses and of fabrication and erection imperfections. The main objective of this Chapter is the definition of those factors, the determination of appropriate mathematical expressions for their consideration in analytical methods, and the influence of their shape or direction.

Chapter III deals with the analytical evaluation of ultimate buckling strengths of stiffened panels, with a consideration of the effect of both the initial imperfections and residual welding stresses. A steel box-girder bridge is

an assembly of stiffened panels, therefore its buckling behaviour can be studied by considering first, the buckling behaviour of different components separately, and secondly, by considering the behaviour of the cross-section, as a whole structure.

The analysis made in Chapter III, is based upon the first alternative, and treats the compression flange. A review of different proposed approximate methods intended as ultimate ones is made. A non-linear method taking into account the initial imperfections is developed. The main objective of this Chapter is to compare those proposed methods with the purpose of making some recommendations.

Chapter IV is an experimental investigation of the overall buckling behaviour. There is an extensive source of available literature dealing with the buckling strength of stiffened panels, however, most of them are purely theoretical and their application to the wide stiffened panels, typical of steel box-girder bridges, is questionable. All these proposed methods consider separately, the behaviour of each component of the cross-section. Such consideration fails to accurately account for the interaction between their components. The reason for this trend is the complexity of mathematical formulations of the buckling behaviour of the cross-section, as a whole.

Due to the above reasons, a study of the ultimate buckling strength accounting for the real interaction between the components, is possible, only by experimental investigation. This alternative is most frequently recommended [14],[18],[20] and the results obtained will supplement the analytical methods.

For this thesis, a full experimental investigation has been conducted on three models. The design is made in such a way as to cover all factors considered in the objective. Special tools have been designed, example for reading of the initial geometrical imperfections and automatic reading of the deformation mechanism of the model during loading stage.

The models have been fabricated by a licensed steel shop and care has been taken to follow the sequence of operations normally used for bridge components in the shop fabrication. All models have been loaded up to complete failure.

Experimental investigation can be divided into five steps: the design, fabrication, preparation, testing and interpretation of the results.

Finally, Chapter V contains the conclusions of the present work and tentative design recommendations , together with further studies in this area.

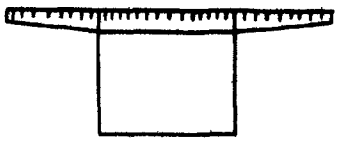

– a single cell box
orthotropic deck

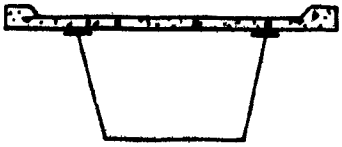

– a single cell box
concrete deck

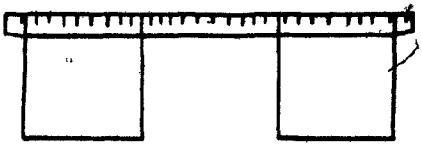

– two separate boxes
orthotropic deck

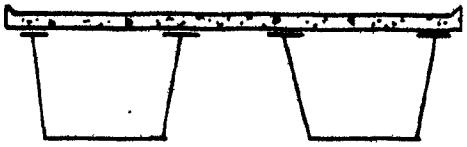

– two separate boxes
concrete deck

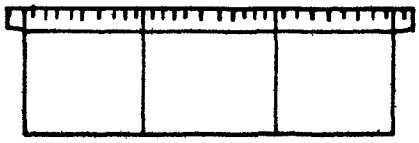

– multicell box
orthotropic deck

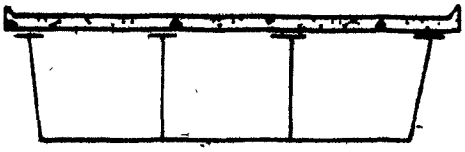

– multicell box
concrete deck

FIG. 1.1 CROSS-SECTION GEOMETRY OF A STEEL BOX GIRDER BRIDGE

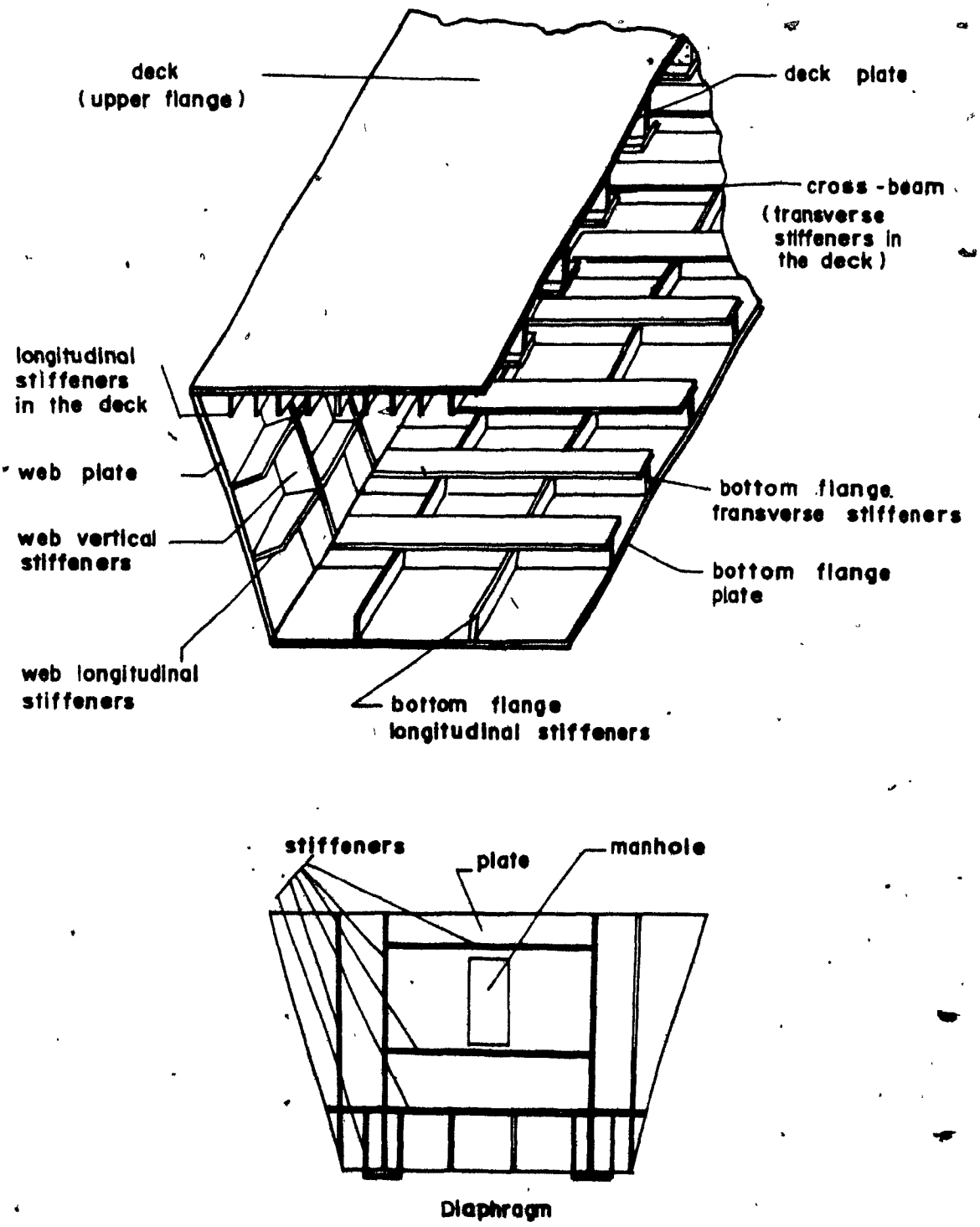

FIG. 1.2 COMPONENTS OF A STEEL BOX GIRDER BRIDGE

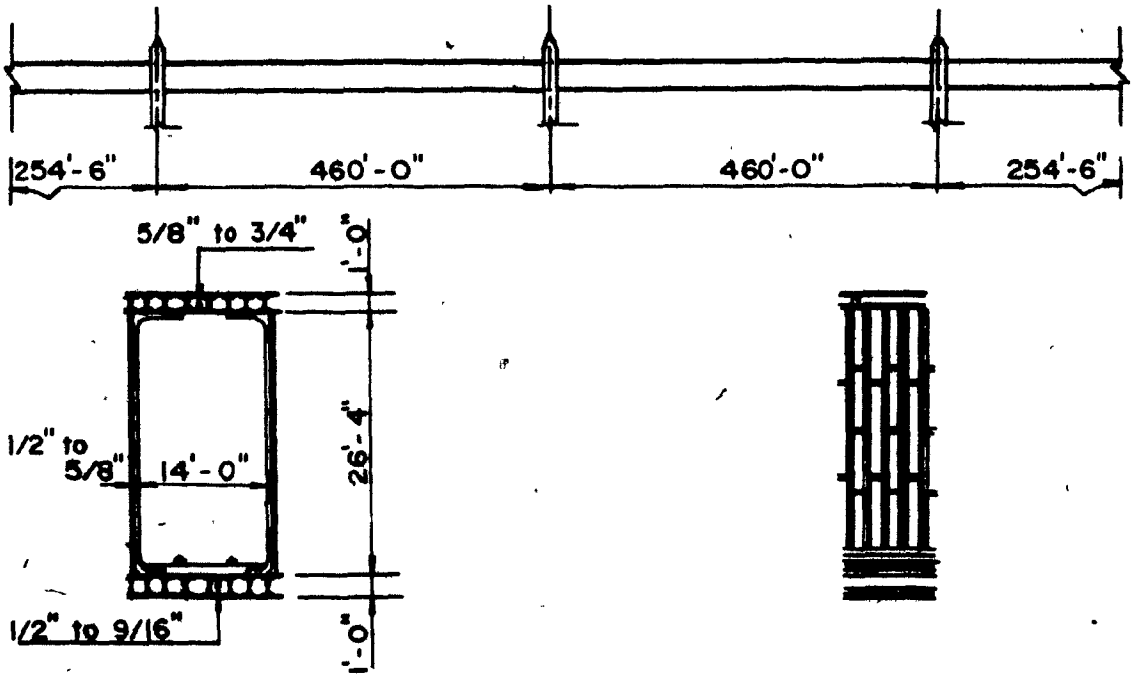

FIG. 1.3 BRITANNIA BRIDGE, ENGLAND, 1850

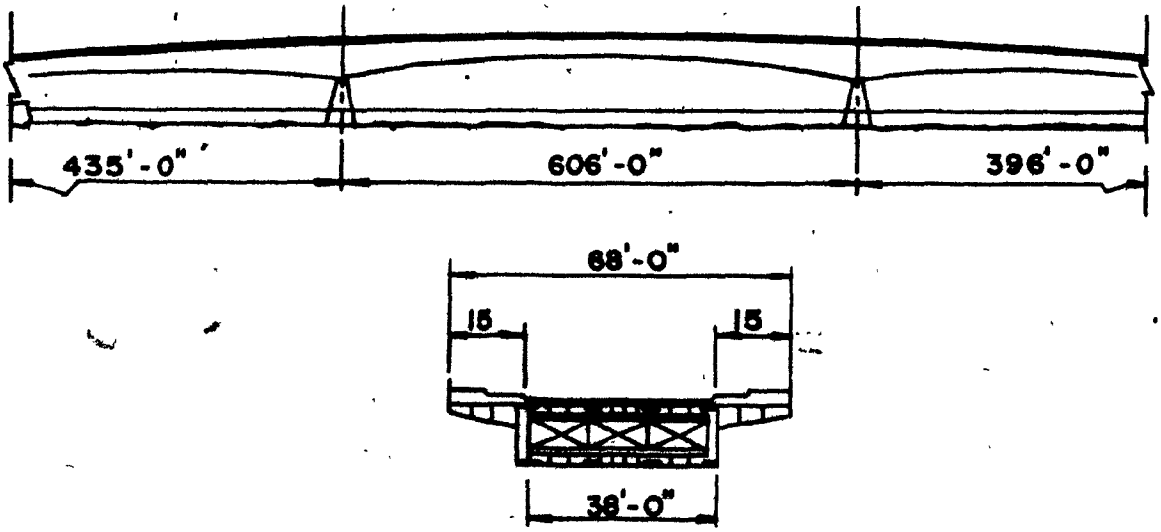

FIG. 1.4 COLOGNE-DEUTZ BRIDGE, GERMANY, 1948

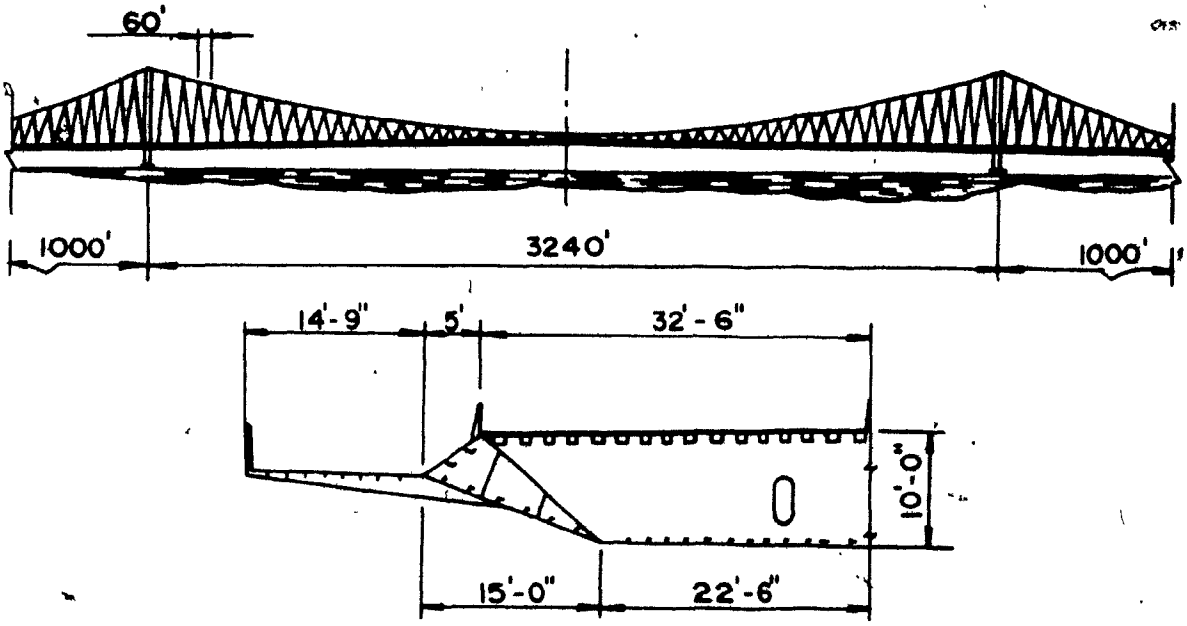

FIG. 1.5 SEVERN BRIDGE, ENGLAND, 1966

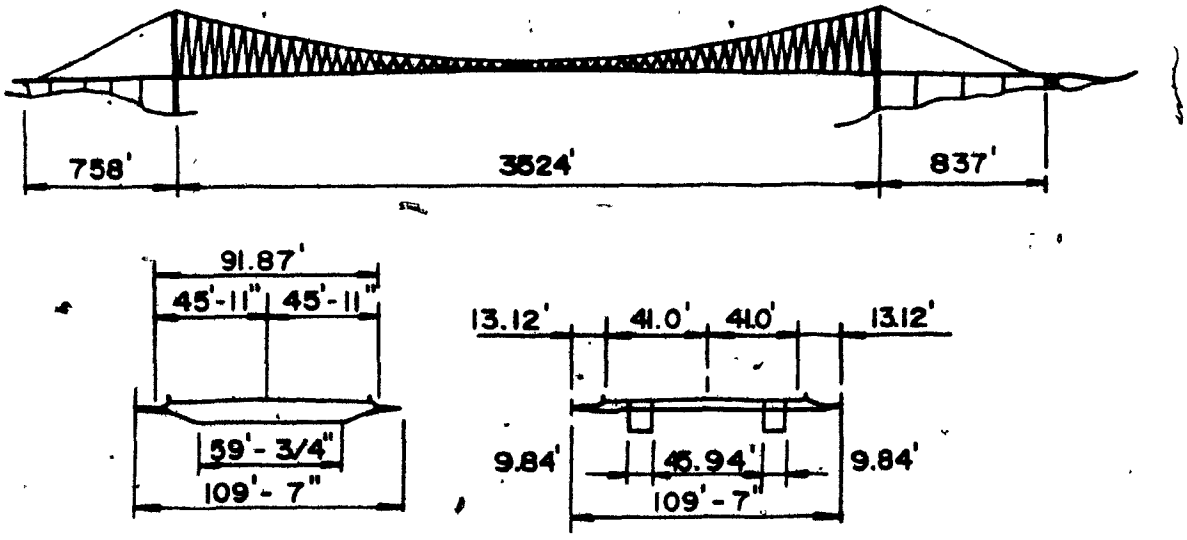

FIG. 1.6 BOSPORUS BRIDGE, TURKISH REPUBLIC,1975

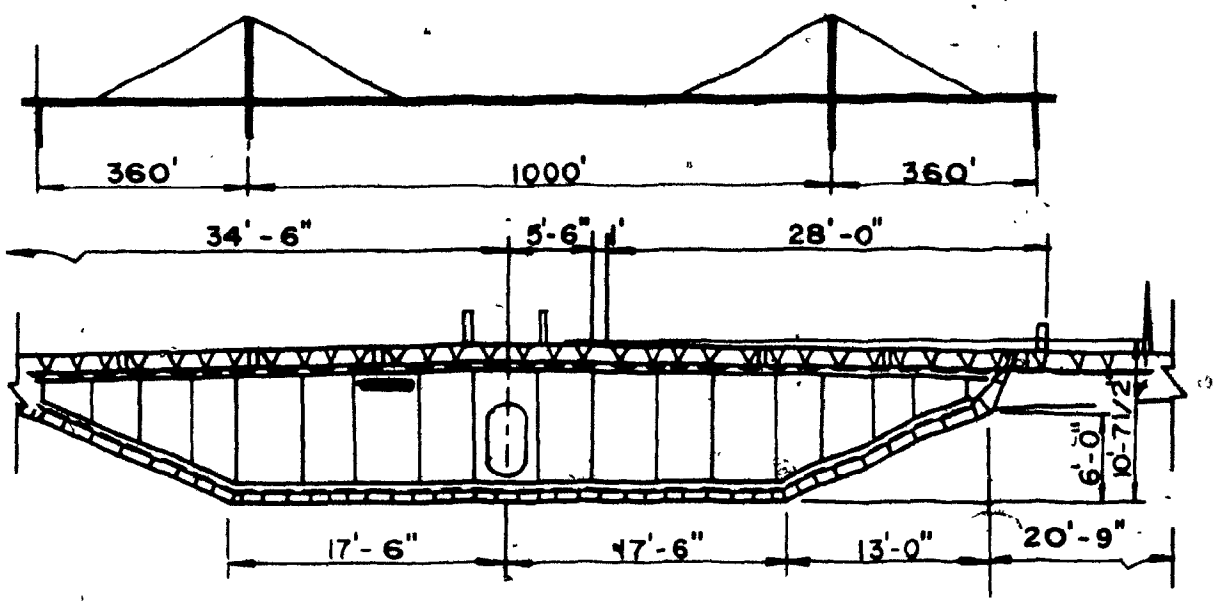

FIG. 1.7 ERSKINE BRIDGE, ENGLAND, 1971

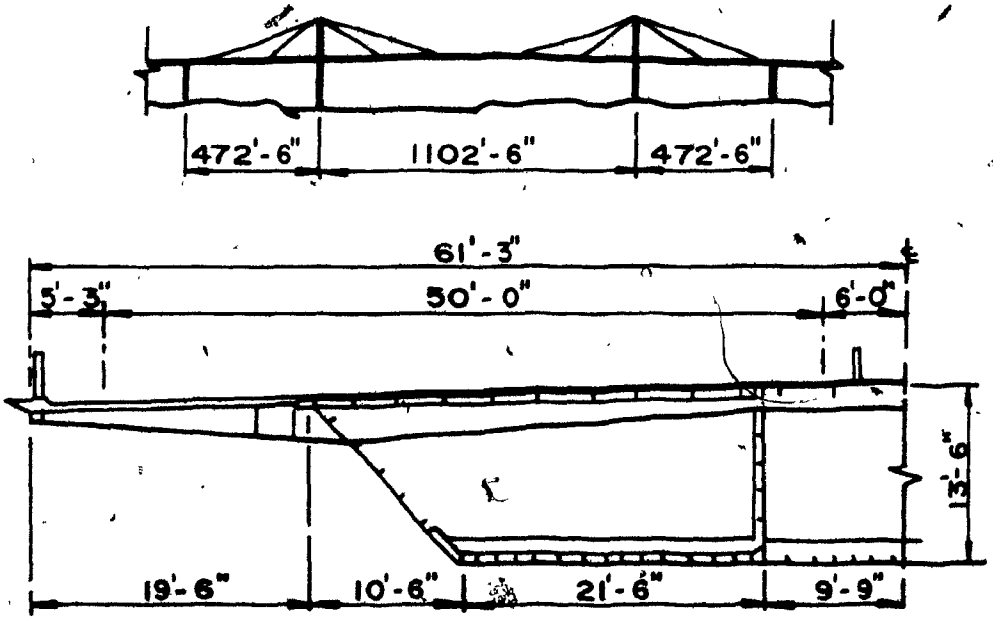

FIG. 1.8 WEST GATE BRIDGE, AUSTRALIA, 1974

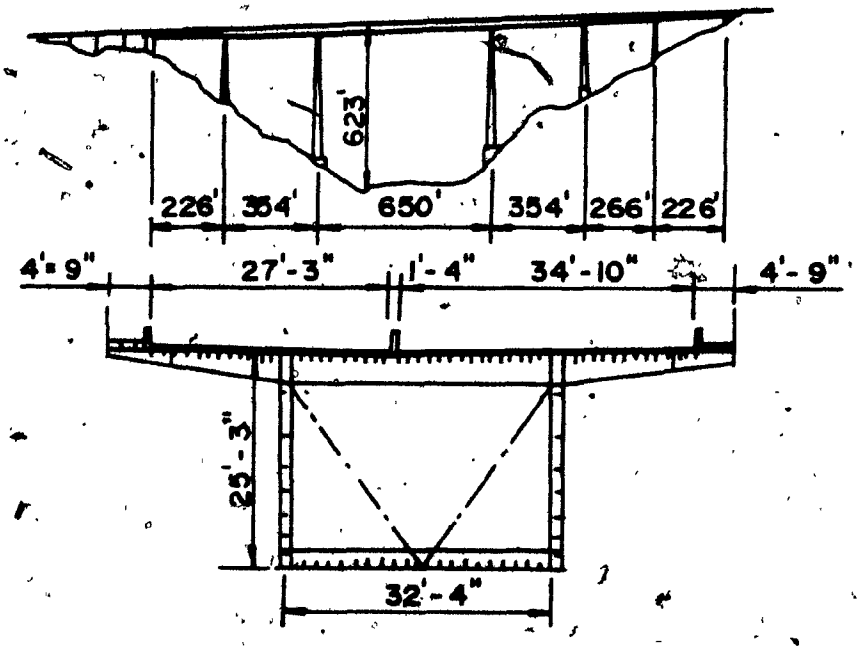

FIG. I.9 EUROPA BRIDGE, AUSTRIA, 1964

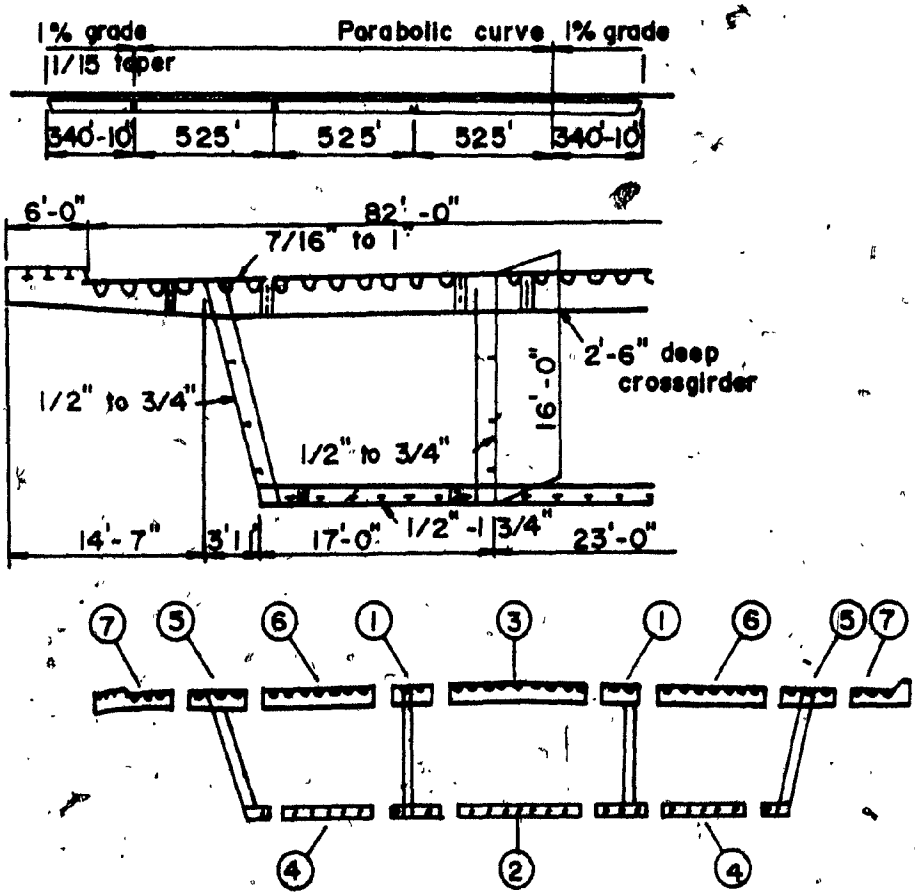

End view of shipping components

FIG. 1.10 PONT DE LA CONCORDE, MONTREAL, 1967

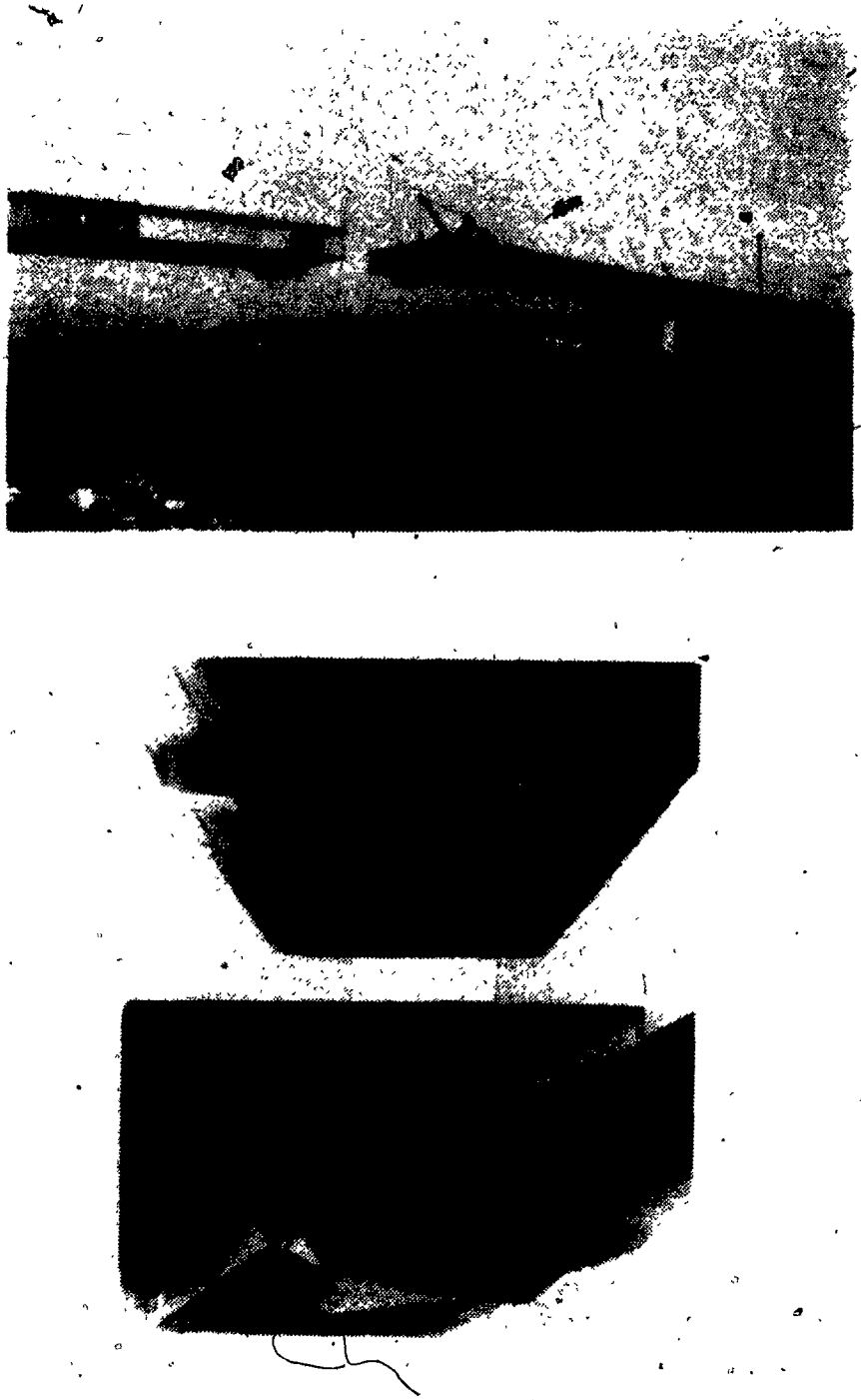

FIG. 1.11 COLLAPSE OF THE FOURTH DANUBE BRIDGE, VIENNA, 1969

The bottom flange that was under compression during the construction stage buckled causing failure.

FIG. 1.12 COLLAPSE OF THE MILFORD HAVEN ROAD BRIDGE, ENGLAND, 1970

Insufficient buckling strength.

FIG. 1.13 COLLAPSE OF THE WEST GATE BRIDGE, AUSTRALIA, 1970

Insufficient buckling strength.

FIG. 1.14 COLLAPSE OF BRIDGE OVER THE RHINE AT KOBLENZ, WEST GERMANY, 1971

Inadequate plate stiffening over the gap.

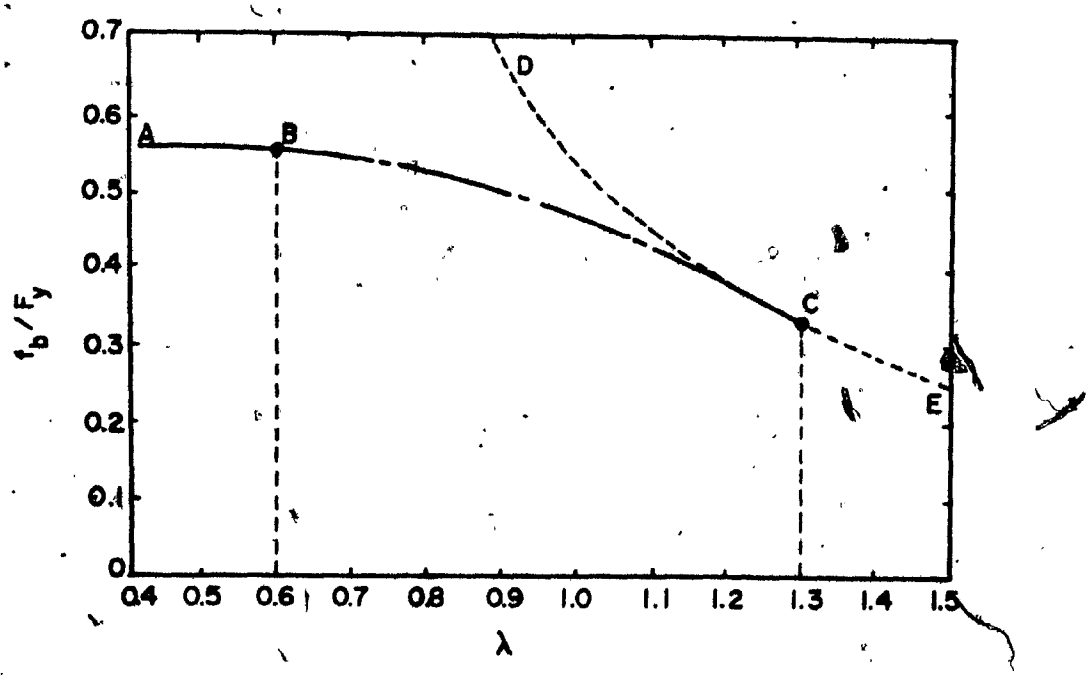

FIG. 1.15 NON-DIMENSIONAL PLATE BUCKLING CURVE FOR DESIGN OF COMPRESSION FLANGES BY AASHO [22] AND CSA-S6 [23]

$$\lambda = \sqrt{\frac{F_y}{F_{cr}}} = b/t = \sqrt{\frac{F_y}{E} \cdot \frac{12(1-\nu)^2}{\pi^2 K}}$$

B is at $b/t = \frac{3070\sqrt{K}}{\sqrt{F_y}} = \frac{6140}{\sqrt{F_y}}$ if $K = 4$

C is at $b/t = \frac{6650\sqrt{K}}{\sqrt{F_y}} = \frac{13300}{\sqrt{F_y}}$ if $K = 4$

Curve AB: $f_b = 0.55\, F_y$

Curve BC: $$f_b = 0.55 - 0.224\ F_y \left[1 - \sin\frac{\pi}{2}\left(\frac{6650\sqrt{K} - b/t\sqrt{F_y}}{3580\ K}\right)\right]$$

$$\text{for } \frac{3070\sqrt{K}}{\sqrt{F_y}} < b/t < \frac{6650\sqrt{K}}{\sqrt{F_y}}, \text{ if } K = 4$$

$$f_b = 0.55F_y - 0.224\ F_y \left[1 - \sin\frac{\pi}{2}\left(\frac{13300\sqrt{K} - b/t\sqrt{F_y}}{7160}\right)\right]$$

$$\text{for } \frac{6140}{\sqrt{F_y}} < b/t < \frac{13300}{\sqrt{F_y}}$$

DCE: $$f_b = 0.55F_{cr} = 14.4\ K(t/b)^2 \times 10^6$$

F_y = yield stress

F_{cr} = critical elastic buckling stress

f_b = allowable stress

K = buckling coefficient

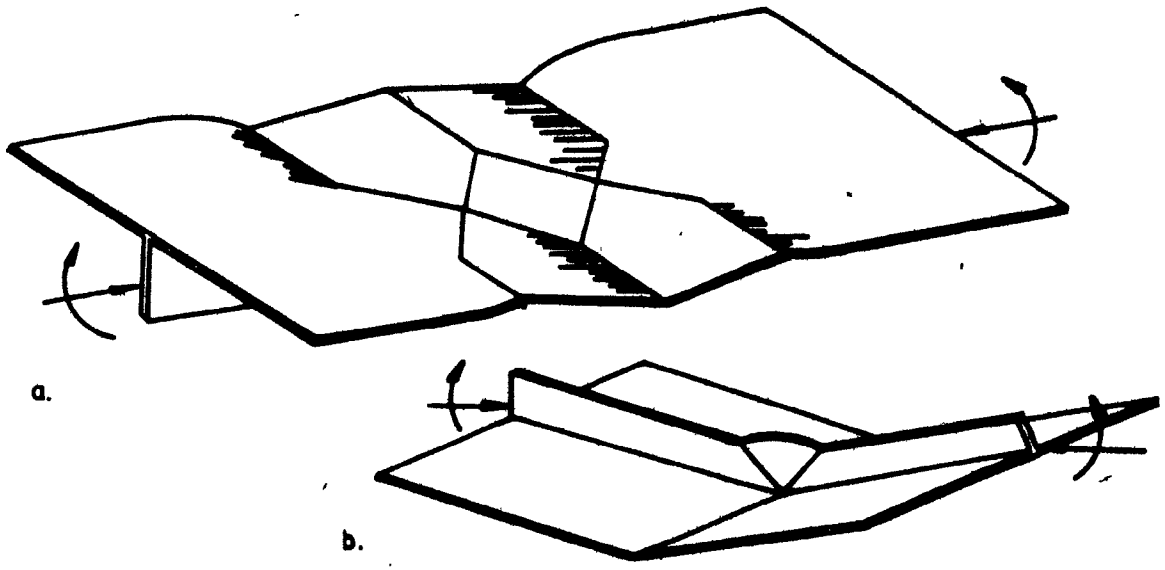

FIG. 1.16 MODES OF STIFFENED PLATES FAILURE IN THE PLASTIC STAGE:

a) PLATE FAILURE MODE

b) STIFFENER FAILURE MODE

CHAPTER II

INFLUENCE OF INITIAL IMPERFECTIONS ON THE BUCKLING STRENGTH OF STEEL BOX-GIRDER BRIDGES

CHAPTER II

INFLUENCE OF INITIAL IMPERFECTIONS ON THE BUCKLING STRENGTH OF STEEL BOX-GIRDER BRIDGES

2.1 INTRODUCTION

It is well-known that, in providing safety, the classical elastic buckling theory should account for the effects of initial imperfections, both geometrically as well as for locked-in residual stresses. In fact, the imperfections of the various members can reduce the buckling safety of such thin-walled box structures under compression as those of axially loaded columns, to an unexpectedly low value.

From past research, it has been proven that the imperfections have their maximum weakening effect over a range of intermediate slendernesses, or a b/t ratio range which is the most practical (Figure 2.1).

In the past, in cases of plates and plated structures in compression, it was believed that the imperfections effect could be compensated by the post-buckling reserve (Curve 4, Figure 2.1(b)) possessed by such structures. Unfortunately, in many practical cases, the slendernesses used in the design are in the range (b/t = 30 to b/t = 70) where post-buckling reserve is negligible and the weakening effect of imperfections is not.

The greatest weakening effect of the imperfections occurs at the slenderness $(\ell/r)_y \simeq 90$ or at $b/t \simeq 55$. This corresponds closely to the Von Karman's critical point $(b/t)_y = (b/t)$ or $\sigma_{cr} \simeq \sigma_y$. However, at lower and at higher slendernesses or b/t ratios, some factors may reduce and may even compensate for the effect of imperfections and residual stresses.

In fact, at low values of b/t or ℓ/r strain-hardening may cause the failure load to rise above the squash load (Curve 5, Figure 2.1(b)), while at higher b/t values, the membrane action in plates can cause the failure load to rise above the elastic instability curve (Curve 6, Figure 2.1(b)).

One example of membrane stress action is by tension field action, which can occur if the members bounding a plate in shear are sufficiently stiff and strong enough to prevent inward movement at the boundaries. In such circumstances, it is found that imperfections and residual stresses have negligible significance in relation to the failure load [58]. It is for this reason that the web plate tends to be less imperfection-sensitive.

It is also shown [27] that the residual stress influences the behaviour of the stiffened panel after the latter has begun to buckle. At this stage, the stiffened panel then begins to deform, causing the residual stresses to affect the stiffness, and therefore the rate of buckling growth; and consequently, the strength.

2.2 TYPES OF IMPERFECTIONS

In a steel box girder bridge, the imperfections can be classified into three types, as follows:

(a) Geometrical imperfections

(b) Residual stresses due to welding

(c) Construction imperfections

In the design, the effect of geometrical imperfections and residual stresses may either be accounted for by the same imperfection factor, or may be treated separately. The first approach has been used more frequently in the past, and is still being used currently.

With an advancement of knowledge in the determination of both geometrical imperfections and residual stresses, some design approaches treat them separately, this being the case proposed in Merrison's Rules [14,59].

Construction imperfections are usually considered during the design stage, by using the tolerances specified,

these tolerances being both fabrication and erection imperfections.

In the following sections, a review of some suggested methods of accounting for such imperfections is made, and the weakening effect of these imperfections on the buckling strength of compression and stiffened panels is shown.

2.3 GEOMETRICAL IMPERFECTIONS

By evaluating the critical load of stiffened plates by the classical stability theory, we assume the plate to be plane, and the stiffener to be straight. Unfortunately, this assumption is found to be far from exact. There are geometrical deviations from the planeness of the plates and from the straightness of the ribs and stringers, either by curvature, or by not being in line, especially near the joints or splices.

These imperfections introduce internal eccentricities which add to the load eccentricities. As a result, the bending deformation/load ratio is non-linear, and consequently, the stress-deformation diagram has an increasing curvature. Thus, to take into account the influence of these imperfections, the ultimate strength must be computed by second-order theory, and the load-carrying capacity can be exact only if the initial deformations due to the geometrical and structural imperfections are known.

It is shown that two flanges of similar cross-section and material may have a significant difference in their load-carrying capacity, depending upon which mode of failure occurs, since the factor which controls the critical mode of failure is the net eccentricity at the centre of the stiffened panel. This eccentricity depends upon the direction and magnitude of the initial bow in the panel and the eccentricity of an in-plane loading, with respect to the centroid of the stiffened cross-section.

The resulting net eccentricity which influences the direction of the moment of the critical panel is the algebraic sum of those eccentricities. Therefore, since the mode of buckling depends upon the difference of the two small eccentricities and the strength depends upon the buckling mode, the importance of the geometrical imperfections then becomes apparent.

2.3.1 Influence of the Shape of Geometrical Imperfections

By considering the geometrical imperfections of the plates, it appears that their shape, as well as their consequently effective values, are of importance in determining the failure load.

In considering a one-sided stiffened plate (Figure 2.2), a survey of its geometrical imperfections reveals that the

plate imperfections have a tendency to be markedly barrel-shaped, the average Δy imperfection being considerably greater than the average Δx_1 or Δx_2 imperfection. The worst effects of these imperfections on the collapse of a plate are obtained when there are ripples in the plate in the direction of the stiffeners, of a wave-length similar to that of the elastic critical buckling mode. It is observed that Δy has a tendency to be positive, due to the plate/stiffener welds, and this influences markedly the effect of any plate imperfections upon the collapse load. For a longitudinally stiffened panel, the mean effective imperfection is found to be similar to that of the mean imperfection of a sub-panel (between two cross-frames) taken singly.

It is sometimes argued that the tendency for stiffener imperfections to be located on one side (towards the stiffener outstand) implies an effective length for its buckling, that is, less than the distance between the cross-frames.

Figure 2.3 is an idealization of the geometrical imperfections for a stiffened plate, and Figure 2.4 shows the gauge length to be used for measurement.

Figure 2.5 shows two observed modes of failure and the types of imperfections causing them, while Figure 1.16 shows two failure modes in their plastic stages.

It is observed that the stiffener failure mode is the most critical, because it is abrupt and less failure load is associated with it. Therefore, it can be concluded that the shape of any initial geometrical imperfections does have a greater influence on the failure mode, and consequently, on the ultimate buckling strength of the stiffened plates.

2.3.2 Suggested Methods For Considering Geometrical Imperfections

An exact evaluation of the effective values for geometrical imperfections is very complex, due to the number and nature of factors to be considered. However, some tentative recommendations have been made, based upon both theoretical and experimental works. The following are some of these recommendations.

Beer and Shulz [60] have investigated the influence of geometrical and/or structural imperfections upon the buckling of columns.

Leonhardt and Hommel [61] have studied the influence of geometrical imperfections on the buckling of the bottom flange of a steel box-girder bridge. It seems that the most sensitive part of a box-girder is the bottom flange, which acts as a chord member for bending and obtains either the axial tension or axial compression. The bottom flange has proven to be the weak point in the collapse of several bridges [27]. Therefore, it must be well stiffened against buckling under axial compression. Because, if such buckling takes place, there is no post-

buckling strength which could hold up the collapse of the box-girder, as could be expected in the case of webs where a post-buckling strength may be expected, due to the effect of tension field action [14,58], and where post-buckling safety is more or less independent of any geometrical or structural imperfections of the web plate, itself [27].

Lebnhardt and Hommel [61] have shown the influence of imperfections of longitudinal stiffeners on the required flexural stiffness of the cross-beam and also upon the buckling strength of the bottom flange. This is given in Equation (2.1) as the function of a ratio of the transverse-to-longitudinal flexural stiffness, and is plotted in Figure 2.6.

$$\frac{I_y}{I_x}\alpha^4 = \frac{2\varepsilon}{\pi^4}\frac{1}{q}\frac{\varepsilon\cos\varepsilon}{\sin\varepsilon - \varepsilon\cos\varepsilon} \qquad (2.1)$$

where

$$\varepsilon^2 = \frac{\ell^2 p}{EI_x}$$

q = quotient of two succeeding load increments (second-order theory)

For practical purposes, $0.6 \leq \varepsilon < 1.4$, and q should be kept below 0.3. Horne and Flint [62] define the factor q as the ratio of the longitudinal thrust in the flange to a thrust that would be sufficient to cause critical buckling conditions in the cross-frame, and they suggest a maximum

value of q to be 0.6.

From the classical buckling theory (no imperfections), the ratios of the transverse-to-longitudinal flexural stiffness (I_y/I_x) is equal to 0.25 and 0.318 for the cross-beam's spacing of ℓ and 2ℓ, respectively. It is also found that the load on the cross-beam can lie between 4% and 6% of the longitudinal compressive force P. This ratio is much higher than the usual ratio of 1% used in the design of stiffening elements in structures under compression.

It may therefore be concluded that the influence of any imperfections upon the effectiveness of the bottom flanges in a box girder for service conditions cannot be neglected for the limit state strength, but whether or not they influence the working load stresses and deformations must be established.

It can be assumed that no reduction of the effective cross-sectional area is necessary owing to the imperfections for analyzing the working load stresses and deformations. Such imperfections have to be taken into account only for limit state calculations, chiefly for safety against yielding, due to the deformations of second-order.

The influence of these imperfections on the buckling loads of orthotropic plates can be accounted for by introducing some factors, as in the case of a slender column in which case, any geometrical imperfections and error in load eccentricity are

expressed as a fraction of the buckling length, ranging between 1/1,000 and 1/500. However, in the case of a plate, it seems reasonable to vary, i.e., to decrease with the actual size of the panel or of the span of the cross-girder, and should also depend upon the type of stiffener used, and especially on its sensitivity against torsional buckling.

From Reference [61], the initial imperfections or displacement might lie between $\ell/300$ and $\ell/600$ for an I-shaped stiffener, and for a stiffener span length of 6.56 feet and 32.81 feet, respectively. For closed stiffeners such as those of triangular or trapezoidal shape, the above limits could be 30% smaller. The initial distortion of steel plates should be limited to about 1/300 of the stiffener's spacing.

Although there has been some disagreement with Reference [61] on the effective magnitude of the vertical flexural loading upon transverse stiffeners or cross-beams due to initial imperfections of the longitudinal stiffeners, Horne, Flint [62] and Charterjee [63] agree on the limitations of any initial imperfections which should lie between 1/1,200 to 1/900 for the transverse stiffeners. For longitudinal stiffeners, the maximum allowable initial imperfections should be 1/600, however, if the effective value of the imperfections of a stiffened panel does not exceed 70% of the specified limit, the maximum allowable initial imperfections of the longitudinal stiffeners should be limited to 1/900 or 1/1,200.

Dowling, Loe and Dean [47] have studied the effect of initial geometrical imperfections on the behaviour of load-bearing diaphragms in rectangular and trapezoidal stiffened steel box-girder bridges. The imperfections of the stiffeners have been limited to $\ell/400$ towards the outstands and $\ell/600$ away from the outstands, as specified in the appraisal rules [14, 59]. Local panel deformations were about 15% of the plate thickness, and the average misalignment of the plates at the transverse butt weld was about 0.05 in. The tests showed that in general, the plate elements which buckled first, did so in the direction of their initial deformations. The direction of the first plate buckling had more influence on the direction in which the adjacent plates subsequently buckled, than were the latter's own initial deformations. Buckling of the stiffeners in a rectangular diaphragm appeared to be influenced more by the eccentricity of the loading at the change in section and the restraining moments from the bearing, than by their own initial bowings.

Massonnet and Maquoi [64] have developed a non-linear (elastoplastic) theory for the ultimate strength (collapse strength) of a stiffened box-girder subjected to pure bending. The initial deformations are taken into account and expressed by an eigenfunction (Equation (2.2)), similar to that representing the first buckling mode of a compressed orthotropic plate, according to the classical linear theory of buckling.

$$w_o(x,y) = f_o \cos\frac{\pi x}{a} \cos\frac{\pi y}{b} \qquad (2.2)$$

where

f_o is the average initial deflection of the plate determined by the measurements made upon the plate.

Maquoi [65] recommended that f_o could be $f_o/t \simeq 0.92 \simeq 1$, for a plate having $t \geq 10$ mm, and should be increased for the lower value of $t \simeq 3$ to 5 mm.

In the Merrison Rules [14,59], regarding the checking of the stiffened panels under compression, the magnification factor of an initial imperfection is assumed to be the ratio of elastic critical stress/(elastic critical stress-applied stress).

$$f = \frac{\sigma_{cr}}{\sigma_{cr} - \sigma_m} \qquad (2.3)$$

In the interim design rules [14], the plate imperfections δ_o for the plate panels of a stiffened panel with N stiffeners, are expressed as

$$\frac{\delta_o}{t} = \frac{1}{600}\left(\frac{b}{t}\right)\left[0.4\sqrt{\left(\frac{As}{bt}\, b/t\right)} + \left(\frac{1}{200}\, b/t\sqrt{\frac{1}{(N+1)}}\right.\right. \qquad (2.4)$$

The above formula gives an error of ±7% [66]. The value of δ/t can be decreased for the ratios $b/t \geq 50$.

The maximum values for δ_o/t are as follows:

$$\frac{\delta_o}{t} = 0.4 - \frac{1}{14000}(b/t)^2 \quad \text{for restrained panels}$$

$$\frac{\delta_o}{t} = 0.5 - \frac{1}{12800}(b/t)^2 \quad \text{for unrestrained panels} \qquad (2.5)$$

In the revisions to the German Standard (DIN 414) [21], the critical initial deflection of the longitudinal stiffeners is

$$f_o = \frac{\ell}{700(0.9+1/\ell)} \qquad (2.6)$$

where

ℓ is the effective length,

and the initial geometrical deformation of the steel plates between the longitudinal stiffeners is limited to $\leq b/150$, where

b is the width of the plate between the webs.

Dwight [26] has studied the effect of imperfection on the strength of unwelded panels. He classified the imperfections in three ways: longitudinal, transversal and spherical. For the ranges of plate panels considered (b/t = 45 to 60), it was found that the transversal imperfections had the greatest sensitivity, compared to the longitudinal ones. This greatest sensitivity was in a region where $\sigma_{cr} = \sigma_y$, the

reduction in strength was of the order of 17%, as compared to a perfect panel; this, for an amplitude of transverse imperfections of b/2000 or t/36. It was also shown that the effect of spherical imperfections is of the order of that of a transverse one of the same amplitude. For an edge-welded plate, a spherical imperfection of amplitude b/1000 is suggested, although the imperfections observed are mostly longitudinal.

Dawson and Walker [67,68] have investigated the post-buckling of geometrically imperfect plates. They assumed the shape of initial imperfections to be the same as that of the buckling mode of a perfect plate with stress-free edges. They referred to the work of Coan [69], who suggested that the initial imperfections could be based upon the first three terms of the deflection series given by

$$w_o = t \sum_{m=1,\,3\ldots}^{\infty} \sum_{n=1,\,3\ldots}^{\infty} a_{o(m,n)} \cos m\frac{\pi x}{a} \cos n\frac{\pi y}{b} \qquad (2.7)$$

where

$a_{o(m,n)}$ are prescribed deflection coefficients,

such that

$$t \sum_{m=1,\,3\ldots}^{\infty} \sum_{n=1,\,3\ldots}^{\infty} a_{o(m,n)} = e_o t \qquad (2.8)$$

where

$e_o t$ is the amplitude of initial imperfections.

But, Equation (2.8) requires a long computation and is therefore not suitable for design purposes. For this reason, it is preferable to carry out some generalized parameter for e_o, which on an average, can be taken to describe the initial geometrical imperfections of all plates. This is possibly only in comparison with the test data.

Equations (2.9) to (2.12), have been investigated and

$$e_o = \alpha t \tag{2.9}$$

$$e_o = \beta(\sigma_y/\sigma_{cr})^{1/2} \tag{2.10}$$

$$e_o = \sigma_y b^2/t^2 = \gamma(\sigma_y/\sigma_{cr}) \tag{2.11}$$

$$e_o = 0.2(\sigma_y/\sigma_{cr}) \tag{2.12}$$

compared [70]-[72]. The factors α, β, and γ can have a conservative value of 0.2. However, Equation (2.12) is recommended as the most rational in that it is geometrically sounder and is found to be in agreement with current rolling practice.

Equation (2.12) applies specifically to uniformly loaded stiffened elements of cold-rolled sections. It may also be suggested that it be applicable to rolled sections, in which the unstiffened element can be regarded as critical. Also, Equation (2.12) has been developed for a square plate which can

buckle into square wave forms [73].

In his work for the analysis and design of stiffened plates for a collapse load, Murray [38] combined the effect of initial imperfections with that of load misalignment in one factor δ_o. The initial imperfections are of two forms, the transverse barrelling of the plate (called "hungry horse", Figure 2.3(b)), and the longitudinal bowing (Figure 2.3(c)). He assumed that the initial deflection δ at the centre of the column (here, the column is defined as "formed by a stiffener and effective width of the plate on its sides, (Figure 2.7)), to be given by

(a) For $\sigma < \sigma_c$ $$\delta = \frac{\delta_o}{1 - \frac{\sigma}{\sigma_c}} \qquad (2.13)$$

and for

(b) $$\sigma_c < \sigma < \sigma_f$$

In this case, the panel behaves as an eccentrically loaded column with a different cross-section to that of the original plate. In this case δ is given by

$$\delta = \frac{\delta_o + \Delta^1}{1 + (\sigma^1/\sigma^1_e)} \qquad (2.14)$$

In Equations (2.13) and (2.14), the terms are defined as follows:

σ = axial stress

σ_c = axial buckling stress of the plate (classical theory) of the plate

$$\sigma_c = \frac{k\pi^2 E}{12(1-\nu^2)}(t/b)^2$$

σ_e = axial stress at which panel buckles as a column, Euler theory

$$\sigma_e = \pi^2 E/(r/\ell)^2$$

σ^1 and σ_e^1 refer to the effective column

σ_f = value of σ at collapse

$$\Delta^1 = \Delta\left(1 - \frac{\sigma_c A/A^1}{\sigma_e^1}\right)$$

Δ = shift in position of neutral axis (original column and effective column)

A = area of cross-section

The failure of the whole panel is assumed to occur when the effective column reaches yield either at the outer surface of the plate (plate failure mechanism, Figure 1.16(a)), or at the free edge of the stiffener (stiffener failure mechanism, Figure 1.16(b)).

The choice of which failure mechanism occurs depends only upon the sign of $(\delta_o + \Delta^1)$ in Equation (2.14). If it is positive, the plate fails and if it is negative, the stiffener fails. Hence, the importance of considering the initial imperfections is shown.

In a previous work, Murray [37] has shown that the mode of a stiffener failure mechanism is more critical because the lower failure loads are associated with it and collapse in this mode is very sudden. This was also confirmed by Horne and Narayanan [39] and by experimental tests performed for this thesis.

Murray [38] derived a new form for expressing the imperfections in such a way that the Perry-Robertson formula can accurately predict the collapse load and the direction of collapse. This expression is given by

$$\eta = \frac{A^1 y^1 (\delta_o + \Delta^1)}{I^1} \tag{2.15}$$

and the Perry-Robertson formula becomes:

$$\frac{\sigma_f^1}{\sigma_y} = \frac{1}{2}\left[1 + (1+\eta)\frac{\sigma_e^1}{\sigma_y}\right] - \sqrt{\frac{1}{4}\left[1 + (1+\eta)\frac{\sigma_e^1}{\sigma_y}\right]^2 - \frac{\sigma_e^1}{\sigma_y}} \tag{2.16}$$

where

σ_f = the value of σ at collapse

σ_y = yield stress

η = is taken as positive

y^1 = the distance to the extreme fibre depending on whether $\delta_o + \Delta^1$ is positive or negative

Horne and Narayanan [74] have suggested an approximate method for the design of stiffened steel compression panels. They allow for the reduction of plate stiffness with large ratios b/t, the effect of residual stresses and plate imperfections. They have assumed that the stiffener be of sufficiently strong cross-section to be able to develop yield at their extreme fibers before collapsing by local torsional buckling.

Referring to their previous work [75], they have established that under a mean longitudinal stress σ_m, a plate having a uniform initial imperfection Δ_x, will have a maximum displacement Δ_{max} of

$$\Delta_{max} = m\ \Delta_x \qquad (2.17)$$

where m is given by

$$\frac{\sigma_m}{\sigma_{cr}} = \left(\frac{m-1}{m}\right)\ [1 + 2m(m+1)C] \qquad (2.18)$$

with

$$C = \frac{3}{16}(1-\nu^2)\,(\Delta_x/t)^2 \qquad (2.19)$$

If the collapse criterion is the attainment of a longitudinal membrane stress at the plate/stiffener boundary equal to the yield stress σ_y, then the mean stress σ_m is given by

$$\sigma_m = K_{bs}\sigma_y \tag{2.20}$$

where

K_{bs} is defined as the secant effective width given by

$$K_{bs} = \frac{1 + 2m(m+1)C}{1 + 4m(m+1)C} \tag{2.21}$$

Equations (2.18) and (2.21) can be solved simultaneously if $\nu, \sigma_y/E$, b/t and Δ_x/t are known.

But Δ_x shall take account of the following factors.

(a) The interaction of the membrane and bending stresses which may produce some plastic zones partially through the plate.

(b) To account for transverse membrane stresses due to the fact that longitudinal edges will be kept straight in plane by adjacent plate panels.

(c) The possible premature collapse of a stiffened panel before the attainment of yield stresses at their boundary in the case of higher b/t ratios.

(d) The effect of residual stresses due to welding.

Then to be complete, Δ_x should be given by

$$\Delta_x = (\delta_x + \frac{1}{2}\delta_{xM})\frac{b}{30t}\sqrt{\frac{\sigma_y}{245}} \qquad (2.22)$$

where

δ_x = the measured plate imperfections

δ_{xM} = the plate tolerance given in the Merrison Rules, as follows:

$$\delta_{xM} = \frac{b}{t}(1+\frac{b}{5000}) \quad \text{for } t < 25$$

$$\delta_{xM} = \frac{b}{375}(1+\frac{b}{5000}) \quad \text{for } t \geq 25 \qquad (2.23)$$

In Equations (2.22) and (2.23), all terms are in metric units.

The failure stress σ_A on the effective column can be computed using the Perry-Robertson formula (Equation (2.16)), where the terms are defined as follows:

$\eta = \alpha(\ell - \ell_o)/r$

$\alpha = a_o\Delta/r$

$\Delta = \Delta_{sx} + 1.2\ e$ (Figure 2.7)

e = eccentricity of applied load with respect to the effective column

a_o = distance of the centroid of effective section from the centre of the plate

Δ_{sx} = overall imperfection of the stiffened plate

ℓ = length of the panel

ℓ_0 = limiting length of strut column $= 0.2\pi \sqrt{E/\sigma_y}$

r = radius of gyration of the effective column.

The axial load P on the stiffened plate is given by

$$P = \sigma_A (K_{bs} bt + A_s) \qquad (2.24)$$

where

A_s = a cross-sectional area of the stiffener

Equation (2.25) has been considered [76],[77] as giving a reasonable value for the amplitude of random initial longitudinal ripples.

$$\delta_0 = b/1000 \qquad (2.25)$$

To-date, the most referred to by actual researchers facing the problems associated with steel box-girder bridges, are the interim design and workmanship rules known as the Merrison Rules [14],[59]. Hereunder are its recommended allowances for initial geometrical imperfections. It should be remembered that these rules are still the object of continuing modification due to the availability of the test results.

1) Plate Panels

For plate panels and the behavior of plate elements acting in association with stiffeners and cross-frames,

the initial distortion of sinusoidal wave-forms corresponds to that of the critical mode of buckling with a maximum displacement from the plane equal to δ_o plus any allowance for residual stresses and interaction with diaphragms or cross-frames.

a) The initial imperfection δ_o is given by

$$\delta_o = \frac{1.2\ b\ \Delta_x}{G}\sqrt[3]{\frac{1}{N+1}} \qquad (2.26)$$

where

δ_o = is in metric measurements

b = smaller dimension of the plate panel

G = gauge length to be adopted for tolerance checking

N = number of longitudinal stiffeners across the cross-section of stiffened panel, for plate panels in a compression flange

N = 0 for plate panels in a web and diaphragm

Δ_x = specified tolerances for flat and curved plate panels in stiffened panels. For curved plate panels in unstiffened flange: the specified tolerances plus $\frac{L_1^2}{8R}$

L_1 = half-wavelength of buckling

R = radius of curvature in elevation of any panel curved out-of-plane along its length with R greater than 40 times the panel width.

b) If the calculations are based upon effective imperfections obtained from measured deformations, δ_o is given by

$$\delta_o = \frac{1.2\ b}{G} |\Delta_x|_{eff.} \qquad (2.27)$$

where

$|\Delta_x|_{eff.}$ = effective imperfections (Ref. [14], Clause 23.2, 23.3b)

c) The equivalent initial imperfection due to the interaction of the diaphragms. When in the stress analysis of a diaphragm, and no portion of the compression flange of the box is assumed to act compositely with the diaphragm plating, allowance shall be made for the transverse strain at the edge of the diaphragm by taking an increased value of the initial out-of-plane deformation of the adjacent flange panels given by

$$\delta_o = \sqrt{(\Sigma\delta)^2 + \frac{8\ b^2\ \varepsilon}{\pi^2}} \qquad (2.28)$$

where

ε = mean transverse compressive strain on the edge of the diaphragm over the panel width plus $(\nu\ \sigma_m)/E$

σ_m = coincident mean longitudinal stresses in the flange panel (ve compression)

b^* = panel width parallel to the diaphragm

$\Sigma\delta$ = the total out-of-plane deformation, initial imperfection plus the equivalent initial imperfection due to residual stress, (Section 4.2)

This increased initial deformation shall be assumed to exist within the proportion of that compression flange contained by the effective widths of the diaphragm flanges (Ref. [14], Clause 11.2, 11.4).

d) In order to allow for the variation of the plate panel initial out-of-plane deformation, δ_o along the lengths of the longitudinal stiffeners and transverse cross-frames may be based upon the effective widths of the plate panels associated with each, appropriate to the reduced values of initial deformations δ_{oR}, of the plate panels given by

$$\delta_{oR} = \delta_o \sqrt[3]{b/L} \qquad (2.29)$$

where

L = half-wavelength of buckling of the stiffened panel in the direction of the longitudinal stiffener or cross-frame under consideration when subjected to applied stress in the same direction.

2) Stiffened Panels

An estimation of the initial imperfections in stiffened panels has been widely considered in the design rules [14], Clause 18.1.3 and Clause 23 "workmanship". To avoid duplication, this will not be reproduced here, as the original may directly be used.

The procedure for carrying out a survey to determine the effective initial imperfections, is given in Appendix A23, of Reference [14], and also in Reference [65].

3) Design Recommendations

In the interim design rules [14], recommendation design formulas are given regarding the stability and strength of plate panels (Art. 19) and of the stiffened panels (Art. 20). In these design formulas, it is possible to account for the effect of initial imperfections as follows:

a) Plate Panels

For in-plane stresses and for plate panels in flanges and diaphragms, and without any distribution of stresses:

$$\sigma_{eult} = \sigma_y \left(1 - \frac{\sigma_y}{8\alpha\ \sigma_{cr}}\right) \text{ but } \not< \alpha\ \delta_y \qquad (2.30)$$

where

σ_{eult} = ultimate equivalent effective stress

$$\alpha = \frac{\text{applied stress to cause first surface yield}}{\sigma_y}$$

$$= \sigma_{ey}/\sigma_y$$

σ_{ey} = value of σ_e which gives σ_e peak = σ_y

$$\sigma_e = \sqrt{\sigma_{n1}^2 + \sigma_{n2}^2 - \sigma_{n1}\sigma_{n2} + 4\tau_{eff}^2}$$

The factor α is obtained from large deflection elastic analysis and varies with b/t, assumed initial imperfections, and the degree of edge restraint present.

But Reference [14] is still subjected to continuing improvement. Then Equation (2.30) is deemed to significantly overestimate the plate strength (Figure 2.8(a)) when compared with the elasto-plastic solution by Frieze, [78]. Frieze also studied the effect of various unloaded edge in-plane boundary conditions on the average stress (σ_{av}/σ_y) - average strain ($\varepsilon_{av}/\varepsilon_y$) curves for plates in compression (Figure 2.8(b)). The effect of an edge in-plane restraint can be seen to vary with the level of initial deformation, δ_o and has also been shown to vary with b/t.

b) Stiffened Panels

In the case of stiffened panels, the approach is to treat the longitudinally stiffened plate as a series of T-section columns. The stress is given by:

$$\sigma = \frac{P}{A}\left[1 + \frac{y_o}{z}\left\{\frac{1}{1 - P^1/P_{cr}}\right\}\right] \qquad (2.31)$$

where

P = axial load at their ends

P^1 = P for flange stiffeners

= P_{eff} for web stiffeners

P_{eff} = additional effective compressive force which magnifies the initial bows present in the stiffener but does not contribute to the applied axial stresses

A = cross-sectional area

z = sectional modulus

P_{cr} = elastic critical load

y_o = initial geometric imperfection

Further information is given in References [27] and [14] regarding the application of Equations (2.30) and (2.31).

2.4 RESIDUAL WELDING STRESSES

Residual stresses are induced by heating during the welding operation. When two plates are welded together, the welding will induce a system of internal stresses usually termed "residual stresses" (Figure 2.9). The thermal expansion of steel per 100°C is about equal to the strain of mild steel at a yield (0.001). The temperature reached in welding is over 1,200°C. This explains the high unavoidable residual stress due to welding.

It is now shown [14,18] that these residual stresses have their weakening effect on the buckling strength of the columns and plates of intermediate practical slenderness (ℓ/r) and b/t ratios. Therefore, they lie in the same zone as the geometrical imperfections.

It is current practice in using the classical elastic buckling theory, that the weakening effect of both imperfections are compensated by a magnification factor applied to the critical stress. At present, some suggestions have been given for treating geometrical imperfections and residual stress separately [14,59].

Several suggested techniques in accounting for the effect of residual stresses are available. It is the responsibility of the designer to adopt one of them. Sometimes, there may exist some disagreement between any two proposed

techniques, i.e., Chapman [79] makes the suggestion that a reduction in the elastic modulus would be one way of considering the residual stresses, but Horne [80] considers that the above approach will cause more difficulties to arise, in that the reduction of an elastic modulus may affect the buckling strength of slender panels, and it is shown that residual stresses do not have much effect in this range.

By considering the research works to-date, it can be argued that residual stresses do not have an effect on the buckling strength of plates having width-to-thickness ratios less than 20.

The residual stresses may be accounted for in two ways: first, their magnitude can be directly deduced from the critical stress, secondly, they may be expressed in an equivalent geometric imperfection, and the total resulting imperfections used for calculation. The following are suggested techniques, using these two methods.

2.4.1 Consideration of the Magnitude of Residual Stresses

The method of directly considering the magnitude of residual stresses and consequently, of the reduction of critical stresses have successfully been used. The magnitude of such residual stress can be computed, using different available techniques, [81], i.e., the following analytical one.

By considering two plates jointed together by welding, (Figure 2.9), it is found that there exists two forms of residual stresses, the welds themselves, together with the metal in their immediate vicinity under tensile stresses, and the remainder of each plate under compression. This system of stresses should meet equilibrium conditions. Crisfield [82] has shown that this stress distribution is only self-equilibrating for an initially flat plate. Consequently, for an imperfect plate, before the application of external loads, the stresses and displacements must be released until an equilibrium configuration is reached.

The width of the tension zone is estimated to be two-to-four times the thickness of the weld, on either side [83]. Then, the width of the tension zone can be defined as the function of a plate thickness, nt (Figure 2.9).

The tests conducted on a box shape column (Figure 2.10), by Dwight, Moxham [83], and Nishiro [84] showed that the pattern of residual stresses persists over most of the lengths of the members, and is only modified by shear-lag close to the ends. For the purpose of analysis, an idealized pattern of residual stresses is used, (Figure 2.9(c)). The stress in the tension zone is assumed to be the yield stress of the parent plate. This means that the higher yield of the actual weld metal is ignored. This treatment can be found to be acceptable, in that the weld metal is a small part of

the tension zone.

Considering the longitudinal equilibrium gives the relation between the residual stress σ_r and the width of the tension zone ηt:

$$\sigma_r = \sigma_y \frac{2\eta}{(b/t - 2\eta)} \qquad (2.32)$$

Equation (2.32) can easily be evaluated if the residual stress is related to the size of the weld, since for a given plate thickness, a large weld can be expected to produce more residual stresses. But, this requires a number of varying conditions.

Tests made by Moxham [83] showed that for a plate of given thickness and providing the thermal history at its edges is known, the width ηt is largely independent of the overall width b, provided that b/t is over about 25, a value below which the local buckling ceases to govern, in any case. Thus, the problem reduces to the relation of ηt to the weld size. For two or more plates meeting at a weld, it is shown that

$$C = \eta_1 t_1 = \eta_2 t_2 \ldots = \frac{CA}{\sigma_y \Sigma t} \qquad (2.33)$$

where

Σt = summary of plate thickness

A = cross-sectional area of added metal

C = coefficient having dimensions of stress

From References [83] and [84], C should be taken as 6,000 N/mm^2 (400 ton/in^2), and from Reference [85], $A = 0.6\ w^2$, with w equal to that of the fillet weld leg. For butt welds, it is shown that $W = \sqrt{A/0.6}$ should be acceptable. Thus, the residual stresses should be related to the weld sizes as follows:

$$\sigma_r = \frac{\sigma_y}{\frac{\sigma_y\ b/t}{[0.6C(W/t)^2 - 1]}} \qquad (2.34)$$

Equations (2.32), (2.33) and (2.34) apply only to a continuous single pass fusion weld, using common processes.

Dwight et al, [35] have studied the theoretical strength of simply-supported square plates, having their unloaded edges able to pull in, but constrained to stay straight. Although his elasto-plastic approach tends to overestimate the strength of a plate of high b/t ratio, because of the assumed constraint at the unloaded edges, his approach gives interesting results in the range of b/t corresponding to $\sigma_{cr} \simeq \sigma_y$, which region is most sensitive to the effect of imperfections. He recommended the following Equation (2.35) be used for the determination of a reduced critical stress in a simply-supported plate.

$$\sigma^{1}_{cr} = \sigma_{cr} - \{(\sigma_r+\sigma_y)\cos\frac{\pi\sigma_r}{2(\sigma_r+\sigma_y)} - \sigma_y\} \qquad (2.35)$$

where

σ^{1}_{cr} = reduced critical stress

σ_{cr} = critical stress for unwelded plates of the same b/t

Equation (2.35) is found to agree fairly closely with the notion that $\sigma^{1}_{cr} = \sigma_{cr} - \sigma_r$ for values of σ_r up to about $0.2\ \sigma_y$ and to overestimate the drop in the critical stress. Figure 2.11 shows how a reduction in the critical stress $(\sigma_{cr}-\sigma^{1}_{cr})$ varies with σ_r, while Figure 2.12 shows the comparison of Ractliffe's findings with that of Von Karman's Equation. It should be outlined here, that Equation (2.35) is carried out by assuming an initial deflection at the centre of the plate, this initial deflection being expressed as a function of the plate width $(b\delta_o)$.

Crisfield [82] extended the approximate method given in the Merrison Rules [14,59], in that he considered the fact that the edge strips remain elastic well beyond the strain, at which point, the stress-free plate would collapse. By doing so, he believed that with the exception of plates with very peaky stress-free load-shortening characteristics, the maximum load would therefore be appreciably higher than that given by subtracting the average residual compression stress from the stress-free collapse load.

By assuming that the load-shortening curve for the stress-free plate is known, i.e.,

$$\sigma^1_{SF} = f(\varepsilon^1_{SF}) \tag{2.36}$$

It is also assumed that Equation (2.36) applies to the central region $(b - \eta t)$ for which the applied stress is σ_1, the strain is ε, and the area $A_1 = bt - \eta t^2$ (Figure 2.13). Thus, the equivalent stress that would be applied to a stress-free plate is therefore

$$\sigma_{SF} = \sigma_1 + \sigma_r \tag{2.37}$$

where

σ_r = residual compressive stress acting upon A_1

$$\sigma_r = \frac{1}{(b/\eta t) - 1} \tag{2.38}$$

From Figure 2.12(b), the following relation should be established:

$$(\sigma^1_r - \sigma^1_1) = f(\varepsilon^1_1 . \varepsilon^1_r) \tag{2.39}$$

The remaining area $A_2 = \eta t^2$ is assumed to remain linearly elastic, up to $\varepsilon^1_2 = 2$, as a consequence of its initial residual stress. Also, the strains applied to areas A_1 and A_2, are equal, so that $\varepsilon^1_2 = \varepsilon^1_1$, i.e.,

$$\sigma_2^1 = \epsilon_1^2 \ , \ \epsilon_1^1 \leq 2$$

$$\sigma_2^1 = 2 \ , \ \epsilon_1^1 > 2$$

Therefore, if σ is the stress applied to the welded plate, the equilibrium conditions will require

$$\sigma(A_1+A_2) = \sigma_1 A_1 + \sigma_2 A_2 \tag{2.40}$$

It follows that

$$\sigma^1 = (1-\frac{\eta t}{b})\phi(\epsilon_1^1) + \frac{\eta t}{b}\sigma_2^1 \tag{2.41}$$

Equation (2.41) may be used for a given load-shortening curve for a stress-free plate to quickly generate a family of curves for a number of different magnitudes of residual stress.

Dwight and Little [86] have proposed the simpler approach of calculating the strength of stiffened steel compression flanges. They accounted for the effect of residual stress by subtracting the residual stress. They used an "effective yield" approach for dealing with the interaction between the local and overall buckling, instead of the "effective width" method.

The exact evaluation of the welding residual stress σ_R still needs more investigation, but after an analysis of the numerous proposed approachs, Equation (2.42) is currently being used in England [87] and applies to the flange plate.

$$\sigma_R = \frac{C_1 A_w}{bt + A_s} \tag{2.42}$$

where

C is the coefficient of shrinkage and is experimentally found to be 10×10^3 N/mm^2 for a single fillet run.

But, the maximum value of Equation (2.42) rarely exceeds $0.10\ \sigma_y$.

2.4.2 Equivalent Out-Of-Plane Deformations Due To Welding Residual Stresses

As outlined at the beginning of this Section, the residual stresses can sometimes be accounted for by evaluating their equivalent initial out-of-plane deformation, that is, added to the initial geometrical imperfection. This approach is used in some design formulas, i.e., the Perry-Robertson formula (Equation (2.16)), and the Merrison Rules [14].

The following are the proposed equations contained in the Merrison Rules for unstiffened plate panels.

$$\Sigma\delta = \sqrt{\delta_o^2 + \frac{8\, L_1^2 \sigma_{R_1} + 8\, L_2^2\, \sigma_{R_2}}{\pi^2 E + \pi^2 E}} \tag{2.43}$$

where

$\Sigma\delta$ = total equivalent initial deformation of the plate panel

δ_o = initial imperfection given by the equations

σ_{R_1},(σ_{R_2}) = effective residual compression stress in direction 1(2) due to welds in this direction 1(2)

L_1,(L_2) = half-wavelength of buckling in the critical mode in direction 1(2)

In equation (2.43), the effective residual compressive stresses σ_{R_1} and σ_{R_2} are calculated in accordance with Clause 7.4 [14] as follows, for plates in stiffened compression flanges and diaphragms:

$$\sigma_{Reff} = 0 \quad \text{for } 0 < b/t < 20 \text{ and for plates attached to concrete slabs.}$$

$$\sigma_{Reff} = \sigma_{RS} \frac{b/t - 20}{20} \quad \text{for } 20 < b/t < 40$$

$$\sigma_{Reff} = \sigma_{RS} \quad \text{for } 40 < b/t$$

where

b = mean spacing of stiffeners

The residual stress σ_{RS} is calculated in accordance with Clause 7.2.1a and 7.3.1 to 7.3.7 [14] for stiffener attachment welds only.

The calculation of residual stress σ_{RS} requires the

determination of the shrinkage force due to welding, this latter force being dependent upon the cross-section of the weld metal at the joint, on the total number of weld runs in the joint, and upon the mean distance between the welds. The shrinkage forces transverse to the weld may be ignored.

2.5 FABRICATION AND ERECTION IMPERFECTIONS

The fabrication and erection of wide stiffened plate panels, which constitute steel box-girder bridges, are often a complex operation due to the varying factors associated with the manufacturing capabilities, their dimensions, and the site of the bridge. High imperfections usually take place during the above operations, therefore, a greater attention should be given during this stage, and all possible imperfections should be accounted for in the design.

One example of these imperfections is the misalignment of the bearings, [14], that is, failure of horizontal planarity (Figure 2.14(a)), and transverse error in the alignment of twin bearings (Figure 2.14(b)).

A typical example showing the importance in accounting for the fabrication and erection imperfections, is the failure of the Milford Haven Road Bridge [17]-[19] which caused much damage. The approximate cause of failure was the buckling of the load-bearing diaphragm over the pier. From a provisional technical report from the coroner investigating the deaths,

three unforeseen hazards may have contributed to the failure:

1) The diaphragm could have been as much as 3/4 inch out of flat, making it susceptible to local buckling;

2) The bearing on the pier was out of line with the neutral axis of the diaphragm and would impose a bending moment on the diaphragm, or

3) Some bolts that were supposed to be loose were tight and under the movement of a load, may have torn the longitudinal stiffeners loose from the bottom flange, making it compressionably unstable.

Another example of the effect of the fabrication imperfections is the failure of the bridge at Koblenz, West Germany [12]. The collapse of this bridge was attributed to an insufficient stiffening above a transverse weld in the compression flange. Figure 2.15 shows the part which caused the failure. The T-stiffener has been cut to permit the use of automatic welding in the bottom flange plate. A stiffener splice was provided after automatic welding of the plate, but there was a gap of one inch between the splice and the bottom flange plate. As the bridge was built by cantilever method, at this stage, the bottom flange was under high compressive stresses. Due to a one-inch gap, the plate was not stiffened at this location and could not resist such high stress. Therefore, the plate buckled and very quickly, all the compres-

sion flange buckled at this section, causing the collapse of the completed bridge.

The above two examples demonstrate the importance of accounting for the effect of fabrication imperfections on the buckling strength of thin plates used for box-girder bridges. In practice, such initial imperfections are accounted for in the factor of safety, but this latter may be insufficient. As an example, for the bridge at Koblenz, Fig. 1.14, the safety factor was 1.7 for buckling, but as it has been proven, this was not sufficient.

2.6 CONCLUSION ON THE INFLUENCE OF INITIAL IMPERFECTIONS

It may be concluded from this Chapter, that initial geometrical imperfections, residual welding stress, fabrication and erection imperfections, have a weakening effect upon the buckling strength of steel box-girder bridges. For economical reasons, the plates used are thin and wide, and deviate from the planeness for plates and from straightness for stiffeners. Those deviations cause internal eccentricities which add to the applied load eccentricity; therefore, the structural elements are subjected to more stresses than those applied. Also, the heating during the welding process introduces residual stresses at their welded edges. Those induced stresses reduce the buckling capacity of the elements.

Unfortunately, the effect of both the initial geometrical imperfections and residual welding stresses is as high and is in the same range of-plate-to thickness ratio (b/t) as it is shown in Figure 2.1. Some initial imperfections are produced during the handling, fabrication and erection. All these factors need to be accounted for in a safe calculation of the buckling strength of steel box-girder bridges.

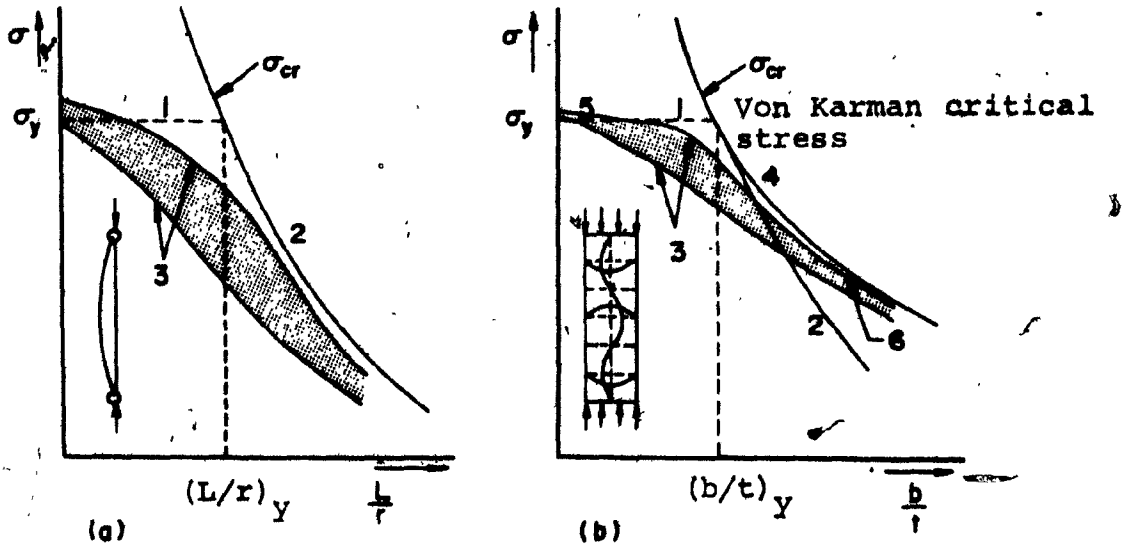

FIG. 2.1 EFFECT OF INITIAL IMPERFECTIONS AND RESIDUAL WELDING STRESSES ON THE CRITICAL BUCKLING STRESS:

a) OVERALL BUCKLING OF A PANEL CONSIDERED AS A COLUMN
b) PLATE BUCKLING

1 = yield

2 = elastic critical stress (perfect)

3 = experimental zone of critical stress with imperfections

4 = post-buckling reserve for perfect plates

5 = increase due to strain hardening

6 = post-buckling reserve for imperfect plates

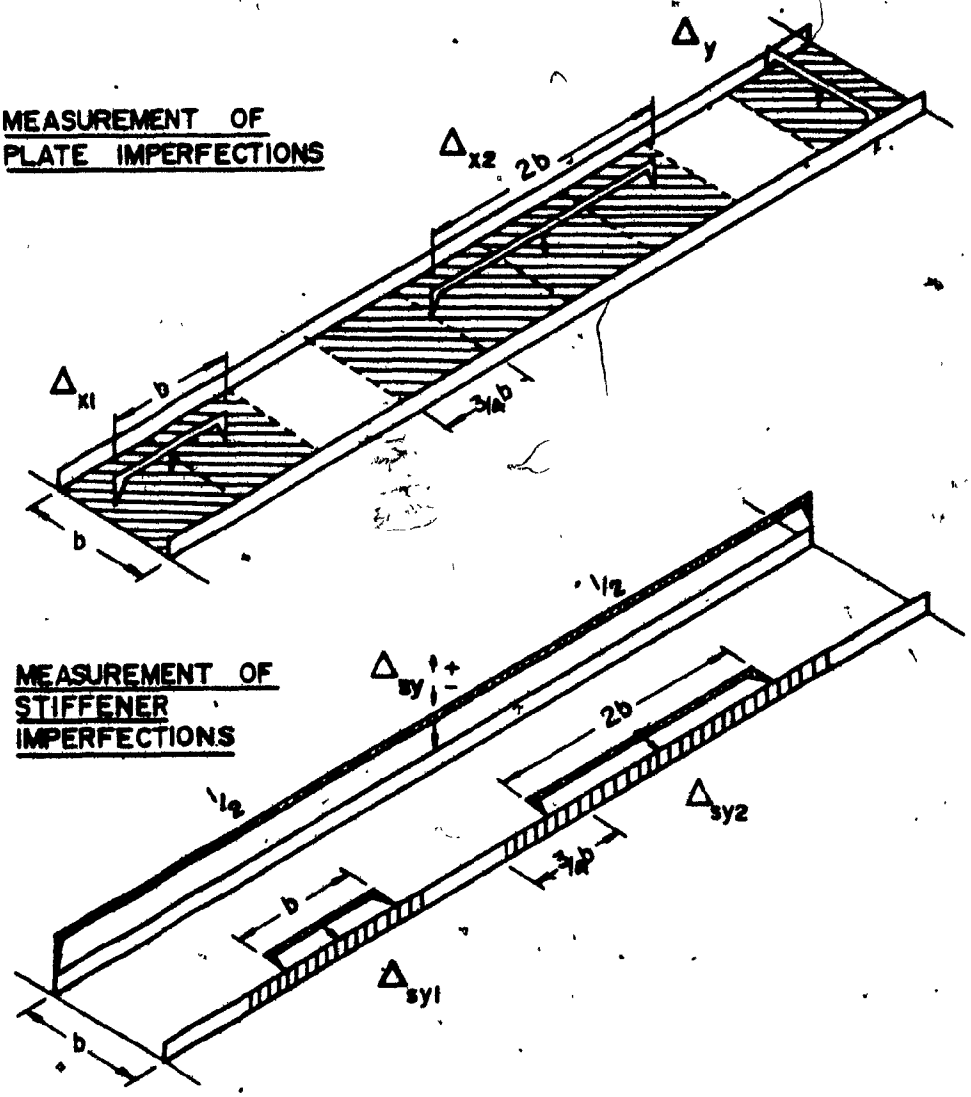

FIG. 2.2 AN EXAMPLE OF INITIAL IMPERFECTIONS SURVEY

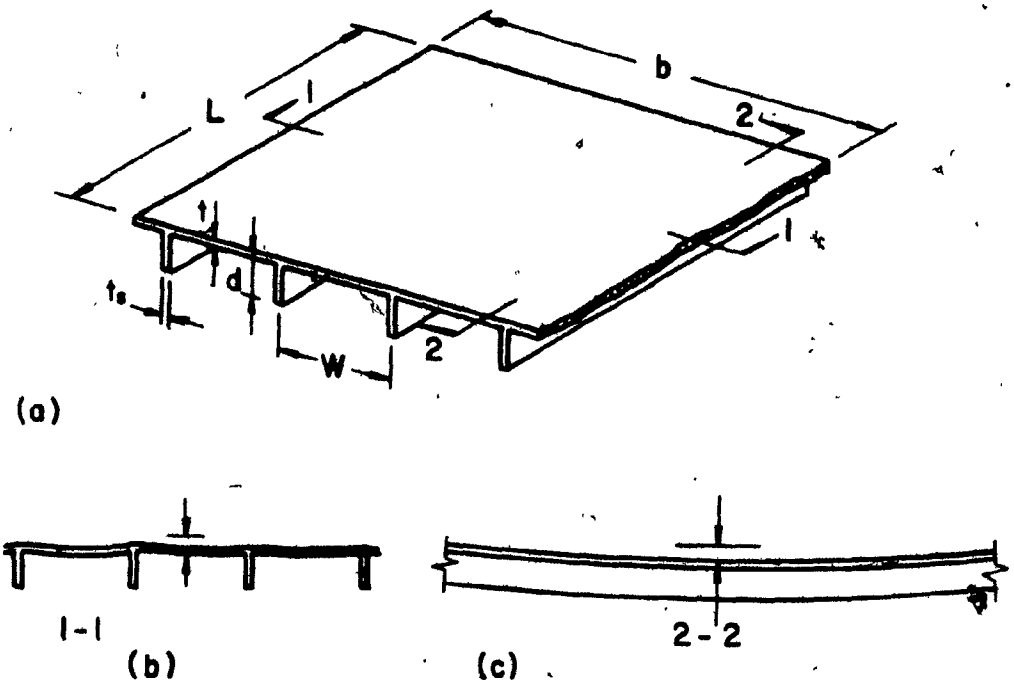

FIG. 2.3 AN EXAMPLE OF INITIAL IMPERFECTIONS IDEALISATION:

a) TYPICAL STIFFENED PLATE b) PLATE IMPERFECTION IN TRANSVERSE DIRECTION c) OVERALL INITIAL IMPERFECTION IN LONGITUDINAL DIRECTION

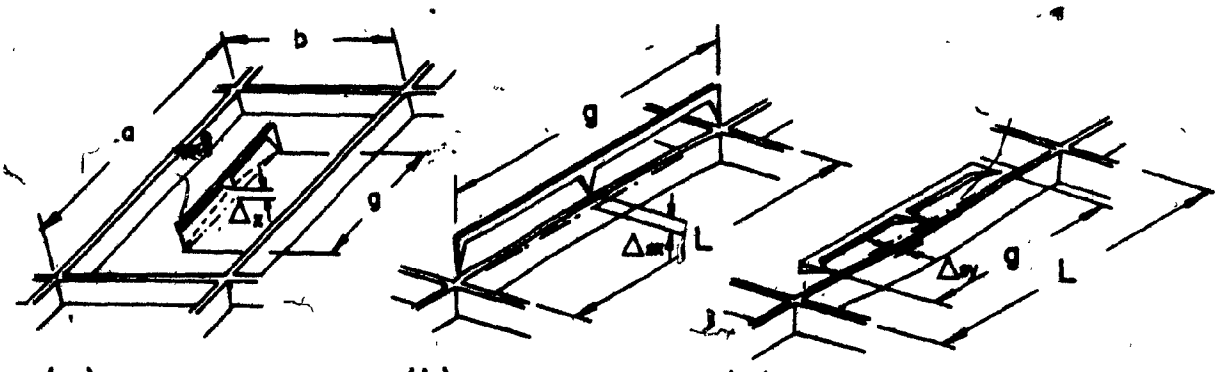

FIG. 2.4 BASIC INITIAL IMPERFECTIONS MEASUREMENTS

a) PLATE PANELS b) AND c) LONGITUDINAL STIFFENERS

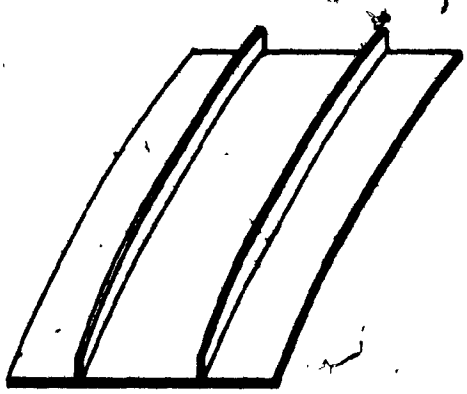

(a)

Plate induced failure
Panel bowing towards the free edges of stiffener

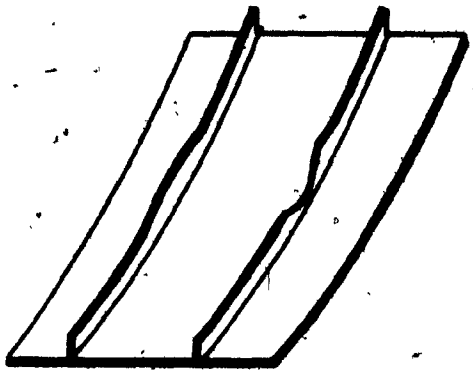

(b)

Stiffener induced failure
Panel bowing towards plate

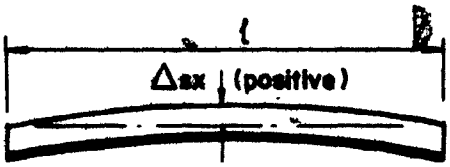

Overall imperfection favouring plate failure (positive)

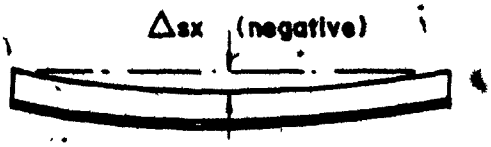

Overall imperfection favouring stiffener failure (negative)

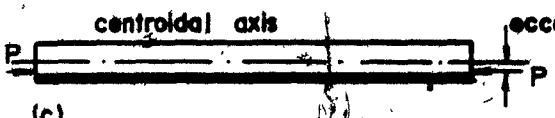

(c)

Eccentricity of load favouring plate failure (positive)

FIG. 2.5 MODES OF FAILURE AND INITIAL IMPERFECTIONS CAUSING THEM

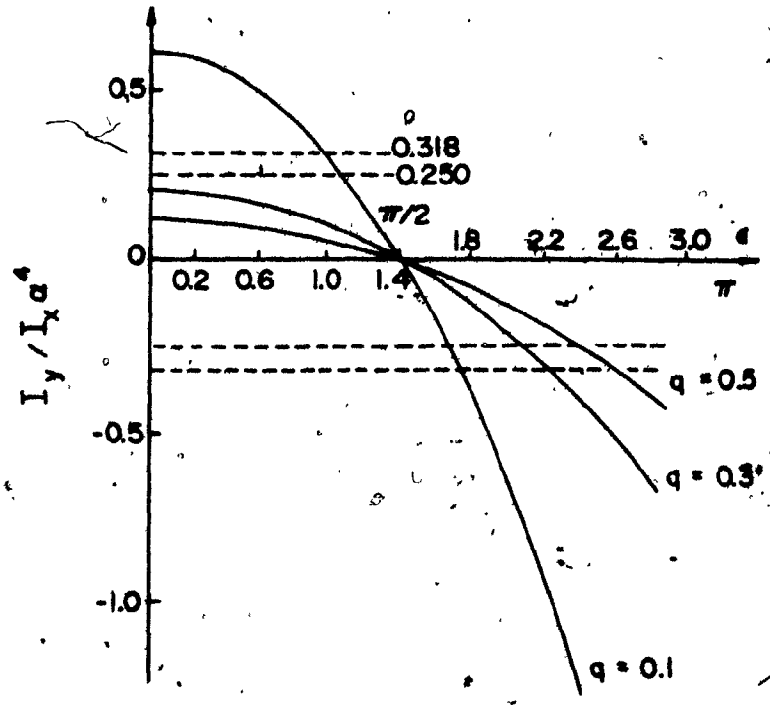

FIG. 2.6 EFFECT OF THE LONGITUDINAL STIFFENER GEOMETRICAL IMPERFECTION ON THE REQUIRED FLEXURAL STIFFNESS OF THE TRANSVERSE STIFFENER (CROSS-BEAM) GIVEN BY EQUATION (2.1)

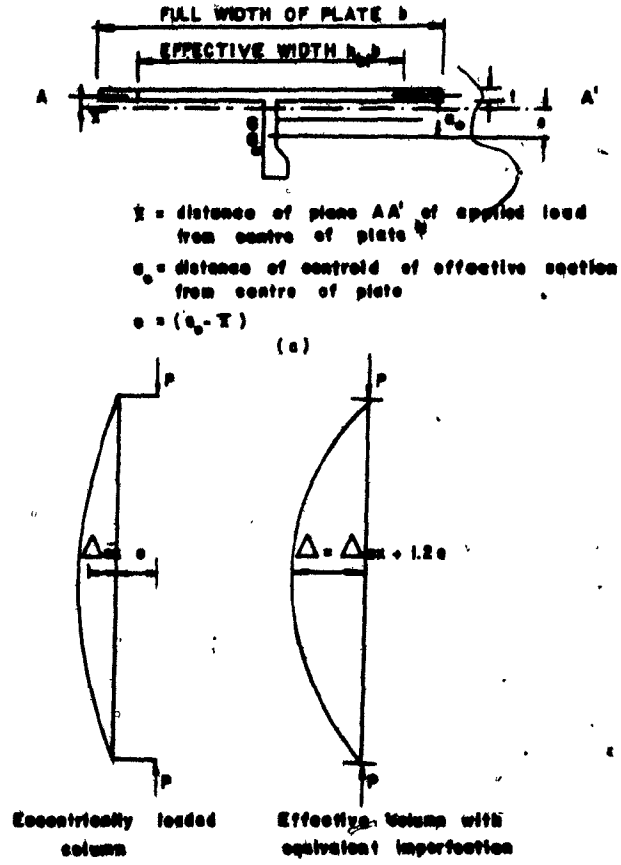

FIG. 2.7 STIFFENED PLATE AS A PLATE-STIFFENER COLUMN ACCOUNTING FOR INITIAL IMPERFECTIONS

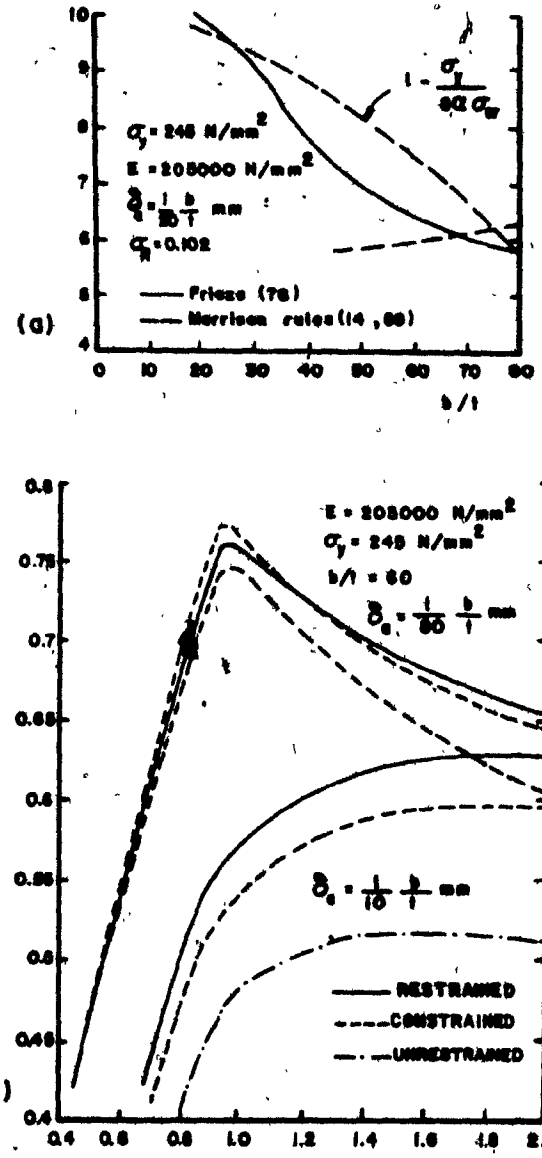

FIG. 2.8 COMPARISON OF INITIAL IMPERFECTIONS TREATMENT OF THE MERRISON RULES [14,59] WITH RESULTS FROM OTHER SOURCES [78]

a) ULTIMATE STRENGTH IN COMPRESSION OF SIMPLY-SUPPORTED CONSTRAINED PLATES
b) EFFECT OF IN-PLANE RESTRAIN ON PLATES IN COMPRESSION

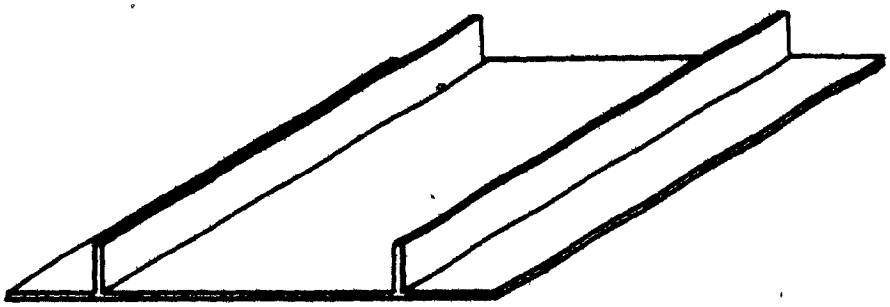

(a)

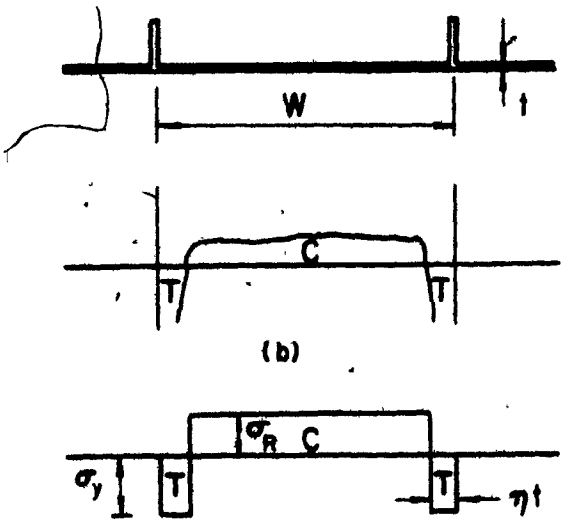

σ_y = yield stress
σ_R = welding residual stress
C = compression
T = tension
ηt = width of tension bloc
η = coefficient to be specified

FIG. 2.9 DISTRIBUTION OF RESIDUAL WELDING STRESSES IN A STIFFENED PLATE

a) TYPICAL STIFFENED PLATE
b) MEASURED DISTRIBUTION
c) IDEALISED DISTRIBUTION FOR ANALYSIS PURPOSE

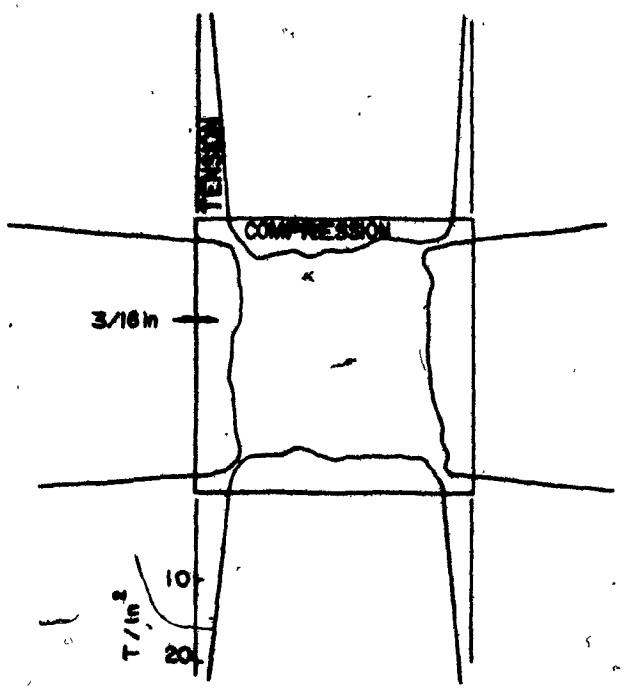

FIG. 2.10 TYPICAL OBSERVED RESIDUAL WELDING STRESSES PATTERN IN A BOX MEMBER

$b/t = 80$, $\sigma_y = 52$ ksi

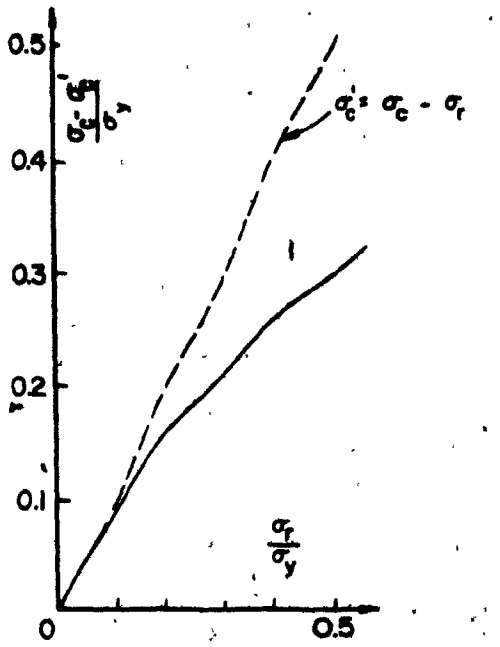

FIG. 2.11 EFFECT OF RESIDUAL COMPRESSIVE STRESS (σ_r) ON THEORETICAL CRITICAL BUCKLING STRESS:

σ_c = UNWELDED CRITICAL STRESS

σ_{c1} = WELDED CRITICAL STRESS

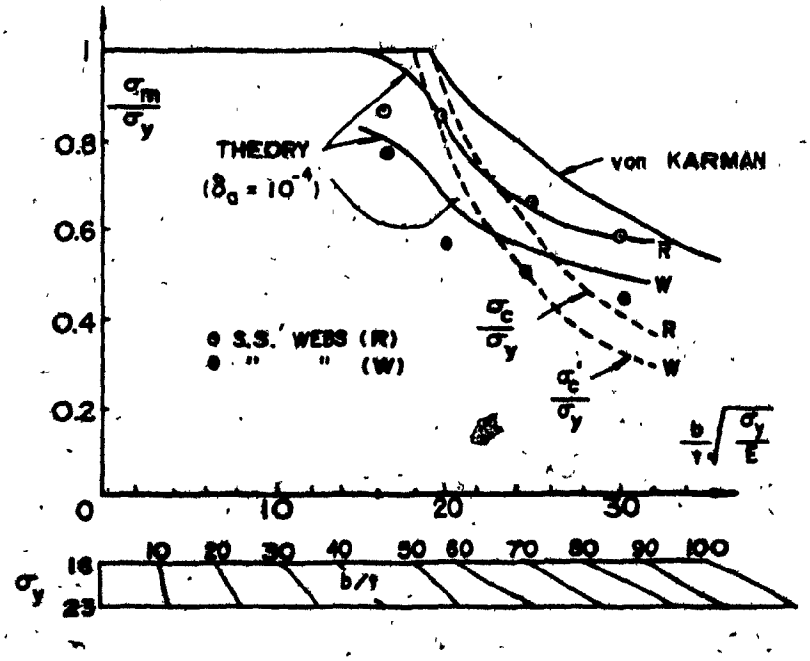

FIG. 2.12 EFFECT OF RESIDUAL STRESSES ON SIMPLY SUPPORTED PLATES. COMPARISON OF VON KARMAN PROPOSAL WITH OTHER SOURCES

R = AS ROLLED, W = AS WELDED

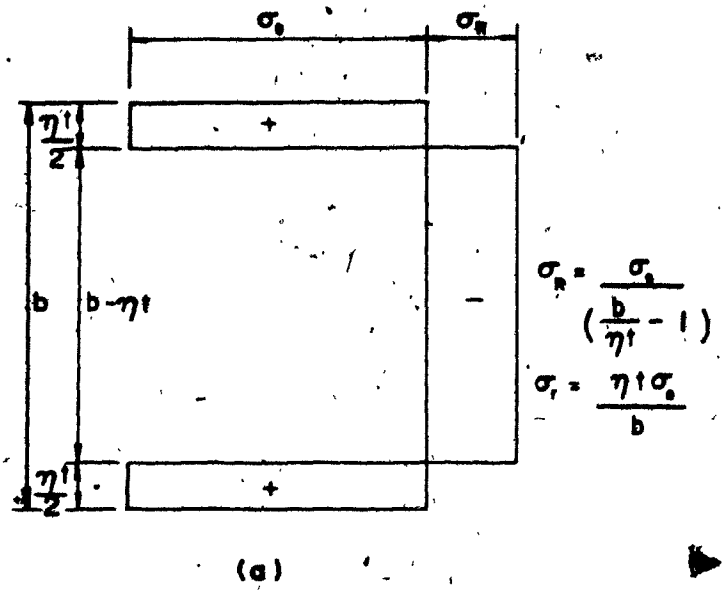

(a)

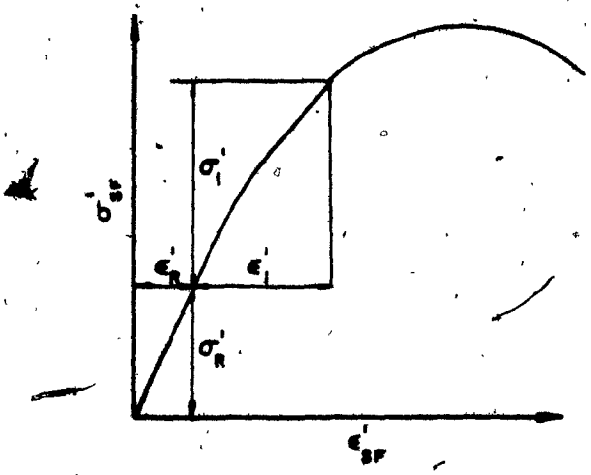

(b)

FIG. 2.13 GENERAL TREATMENT OF RESIDUAL STRESSES

a) ASSUMED PATTERN OF RESIDUAL STRESSES
b) NON-DIMENSIONAL LOAD-SHORTENING CURVE FOR STRESS-FREE PLATES

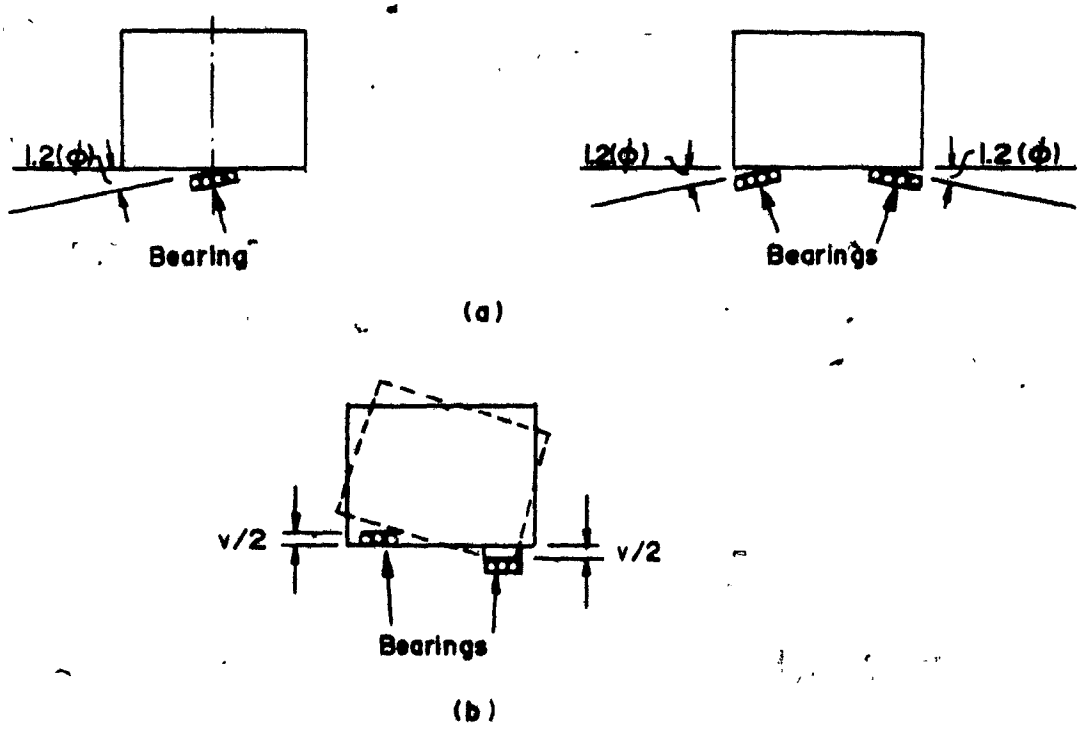

FIGURE 2.14 ERECTION IMPERFECTIONS: MISALIGNMENT OF BEARINGS

a) TRANSVERSE SECTION THROUGH BOX SHOWING DEPARTURE FROM HORIZONTAL PLANARITY OF BEARINGS
b) TRANSVERSE SECTION THROUGH BOX SHOWING TRANSVERSE ERROR OF TWIN BEARINGS

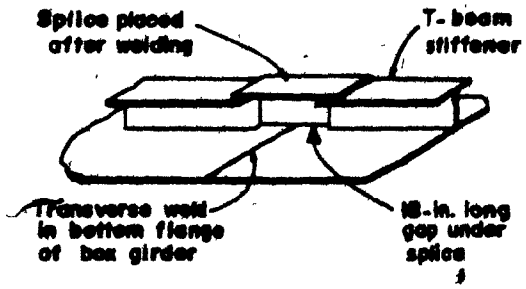

FIGURE 2.15 COLLAPSE OF THE BRIDGE AT KOBLENZ (WEST GERMANY)
INSUFFICIENT PLATE STIFFENING DUE TO PRESENCE OF THE GAP CAUSED BUCKLING

CHAPTER III

EVALUATION OF THE ULTIMATE BUCKLING STRENGTH OF STIFFENED PANELS

CHAPTER III

EVALUATION OF THE ULTIMATE BUCKLING STRENGTH OF STIFFENED PANELS

3.1 INTRODUCTION

In this Chapter, the buckling behaviour of the deck plate is considered. Different formulas are reviewed for the calculation of the critical buckling stress σ_{cr} and the maximum applied stress σ_m at collapse.

Some suggested methods of analysis consider the deck plate, itself, while others take into account the influence of both the longitudinal and transverse stiffeners, as well as the influence of imperfections. Finally, the entire cross-section is treated as a whole, by considering both the deck and bottom flange, including the web plate.

Since the pioneer work by Bryan [88] in 1891, different papers, sometimes in contradiction, have been published on the critical buckling stress of compression plates. This disagreement goes from the basic definition of an ideal, elastic, perfect plate (no imperfections) to the determination of the buckling coefficient to be used in the expression for the buckling stress σ_{cr}. This latter is defined as the theoretically applied stress at which a plate, as defined above, would cease to stay flat.

$$\sigma_{cr} = \frac{k \pi^2 E}{12(1-\nu^2)}(t/b)^2 \qquad (3.1)$$

Codes of practice are continually reviewed to conform with up-to-date research work. Such is the case in the work by Dwight and Moxham [83], who, after an investigation of the interaction between local buckling and overall column buckling, together with the effects of residual stresses by welding, concluded the inadequacy of Equation (3.1) for simply supported webs, as shown in Figure 3.1(a). Figure 3.1(a) indicates that σ_{cr} is overestimated for a small plate aspect ratio b/t and underestimated for higher aspect ratios. Figure 3.1(b) shows that no obvious changes in behaviour can be detected at σ_{cr}.

Due to a disagreement in the determination of the buckling factor k and therefore, the critical stress σ_{cr}, some researchers who faced the buckling problem have claimed [83] σ_{cr} to be purely of academic interest only, and, therefore has no meaning, in practice.

But, in determining the maximum capacity of the plates and stiffened panels under compression, the critical buckling stress criteria, σ_{cr} is generally used more often than others; for example, the yielding stress σ_y.

In this Chapter, the main objective will be the evaluation of the ultimate strength of plates and stiffened panels

under compression, how the critical buckling stress σ_{cr} is used, and how the effects of initial imperfections are considered.

The term "ultimate strength" as used here, means the full capacity as determined on the basis of post-buckling behaviour (post-elastic) of the considered component. The collapse load is that used just to cause collapse (mechanism).

The ultimate strength of a steel box-girder bridge could be determined only by considering the ultimate strength of the stiffened panels composing its cross-section.

In the following sections, some of these analysis methods are reviewed and compared with the purpose of making some tentative design recommendations.

3.2 EMPIRICAL EXPRESSIONS

An exact evaluation of the maximum average applied stress σ_{am} of plates and stiffened panels under compression is complex, due to the number and nature of the factors involved. For this reason, empirical expressions based mostly on test results, have been proposed. However, for the sake of safety, very conservative safety factors are generally applied, since empirical expressions may overestimate the capacity of the element. These conservatisms may lead to an uneconomical design.

Hereunder are some proposed empirical expressions. From the available literature, T. Box [89], in 1883, proposed Equation (3.2) for mild steel panels.

$$\sigma_m = \frac{80}{\sqrt{b/t}} \text{ ton/in}^2 \qquad (3.2)$$

Since this time, many other empirical expressions are proposed for σ_m, for example, Equations (3.3) and (3.4), and different concepts are carried out. These expressions are the effective width approach, the tangent modulus method, and some analytical techniques.

Equation (3.3) was first developed for aluminum, but it is sometimes used for steel by changing the parameters.

$$\sigma_m = C\, \sigma_{cr}\, \eta\, \sigma_y^{1-\eta} \qquad (3.3)$$

where

C and η are based on the appropriate test data for the material being considered [90],[91]

This treatment is also found suitable for light gauge construction [92]. In steel, the coefficient C and η would vary with the level of residual stress, but for a rough design they might be $C = 0.75$, $\eta = 0.3$.

In ship designs, another empirical formula (Equation (3.4)), is used

$$\frac{\sigma_m}{\sigma_y} = 1.18\frac{(b/t)_y}{(b/t)} - 0.35\left[\frac{(b/t)_y}{(b/t)}\right]^2 \qquad (3.4)$$

where

$(b/t)_y = (b/t)$, at which $\sigma_{cr} = \sigma_y$.

One of the early uses of stiffened plates was in ship-building. An example of such design is the Britannia Bridge, for which Fairbairn [1] has applied the techniques developed for ship design.

Empirical Equations (3.3) and (3.4) can be used in region B of Figure 3.1(a), in which the tangent modulus approach when applied, fails to take advantage of the post-buckled strength reserve [26].

The approach for considering failure due to local buckling in isolation from any other instability is reasonable for a short member. But, for most practical cases, an account must be made of any possible interaction between the local buckling and the overall flexural buckling of a column, as a whole. The growth of local waveness with loads reduce the flexural stiffness of the section, thus increasing the susceptibility to overall collapse.

Some design standards such as the British Standards BS 153 and BS 449 for hot-rolled construction, allow this effect by taking a constant effective width and disregarding

the rest of the section, however long the member.

Another empirical method for the calculation of the maximum stress σ_m is the use of a fictitious yield stress. The procedure is to determine σ_m for a short strut of the same section and construct a column curve that would apply to a fictitious material with yield σ_m.

The predicted stress at failure σ_m^1 is read from this curve at the appropriate value L/r, where r is taken as the radius of gyration for the whole section. This approach is used by Bulson [93] by replacing σ_y by σ_m in the Perry-Robertson formula

$$\sigma_m^1 = \frac{x}{2}\left(1 + \sqrt{1 - \frac{4\,\sigma_m \sigma_e}{x^2}}\right) \qquad (3.5)$$

where

$$x = \sigma_m + (1+0.033\ L/r)\sigma_e$$

and

σ_e = Euler critical buckling stress for column

$$= \pi^2 E/(L/r)^2$$

In the United States, [94] a Johnson type parabola is used, Equation (3.6)

$$\sigma_m^1 = \sigma_m - \frac{\sigma_m^2 (L/r)^2}{4\pi^2 E} \qquad (3.6)$$

Equation (3.6) meets the stress axis at $\sigma_m^1 = \sigma_m$ and coincides with the Euler curve at $(L/r) = \pi\sqrt{2E/\sigma_m}$. Figure 3.2 makes a comparison of Equations (3.5) and (3.6). The difference is entirely due to the variation of strut curves between the United States and England, rather than any basic difference in plate-buckling philosophy.

For stiffened panels under compression, Equation (3.7) is proposed by Allen [95] for calculating the failure stress. An attempt is made in considering the effects of the imperfections.

$$\frac{1}{\sigma_f^n} = \frac{1}{\sigma_e^n} + \frac{1}{\sigma_c^n} + \frac{1}{\sigma_y^n} \qquad (3.7)$$

where

σ_c = elastic local buckling stress

σ_e = elastic overall buckling stress (Euler)

σ_f = failure stress

σ_y = yield stress

n = number which can account for imperfections

Equation (3.7) is proposed for dealing with the buckling interaction of a compression panel, and it is an intuitive extension of the buckling design formula (Equation (3.8)).

$$\frac{1}{\sigma_f^n} = \frac{1}{\sigma_e^n} + \frac{1}{\sigma_y^n} \qquad (3.8)$$

If σ_c is ignored and n = 1, Equation (3.7) reduces to the Rankine strut formula.

The ultimate strength of the panel is calculated by applying Equation (3.7) to each element and then adding the strengths.

If σ_c or $\sigma_e \geq 3\sigma_y$, the buckling effect may be neglected. This is equivalent to a cut-off or plateau in the buckling curve (Equation (3.7)).

In the case of a stiffened plate, when $\sigma_e < 3\sigma_y$, the elastic local buckling stress σ_c should be used. This is to account for the fact that the plate buckling can interact with the overall buckling.

When $\sigma_e > 3\sigma_y$, the local buckling cannot interact with the overall buckling, and a pseudo-elastic stress σ_{cs} (Equation (3.9)) is to be used, if greater than σ_c. Allen [95] considers that this is equivalent to the strengths predicted by the effective width concept which allows for additional post-buckling strength.

$$\sigma_{cs} = \frac{1.5\sqrt{E\,\sigma_y}}{(b/t)} \qquad (3.9)$$

In Equation (3.7), the imperfection factor n covers not only the geometrical imperfections, but also the residual welding stresses, non-linearity and a degree of load eccentri-

city. The value of n varies between 1 and 2. The greater the imperfections, the lower the number n, but in general, 2 is an acceptable value.

This value has been compared with the test results in Reference [38] and are found to be in good agreement. But the Rankine formula is well justified for a simple strut, and it is doubtful whether there is enough evidence to support it, or a modified version for thin-walled sections, of which stiffened plates are a sub-group. Thin-walled sections fail by local buckling which is quite a different problem from that of simple strut buckling, as it involves distortions of the cross-section.

3.3 EFFECTIVE WIDTH METHOD

For calculating the maximum average applied stress σ_{am}, the effective width method is the most widely used, and is considered a shorter method.

The effective width method is a concept which originates in the distribution of stress in a plate under compression at failure, as shown in Figure 3.3. The concept can be defined as follows: for a given thin plate of thickness t, there is a portion b_e of b which is fully effective in resisting compressive stress, all portions of b being greater than b_e do not have any contributing effect, therefore, the failure load of the plate will be equal to $\sigma_y b_e t$.

Here, the question arises of what fraction of b is b_e. For that, different approaches are proposed, depending upon the assumptions made, but the first finding was made by Von Karman [96], the father of effective width concept. He suggested, in 1932, that b_e should be a value for which the ratio b_e/t gives $\sigma_{cr} = \sigma_y$ for a simply-supported plate. By the substitution of k by 4 in Equation (3.1), the effective width b_e is given by Equation (3.10).

$$b_e = 1.9\, t\sqrt{E/\sigma_y} \qquad (3.10)$$

In applying the effective width method to the analysis of steel box-girder bridges, two distinct concepts exist; the first one considers only the behaviour of the plate element between the stiffeners. The second concept also accounts for the participation of stiffeners, and also includes the participation of web plates and bottom flanges.

Here, these two concepts are considered and compared, with a purpose of making some tentative recommendations.

3.3.1 Consideration of the Behaviour of Plate Elements Only

The effective width b_e, as given by Equation (3.10), is based only upon the behaviour of those plate elements between the stiffeners, and neglects any contribution by the

stiffeners. Then, the capacity of a stiffened panel is obtained by adding those b_e calculated for each plate element. This concept is widely used and may be considered only as a simplification of the problem. Also, there is some disagreement on the accuracy of Equation (2.[illegible]0) in that the values used in practice are often lower than those given by it. Some researchers simply consider it unsafe [97],[98].

However, most of the proposed formulas for b_e computations are continually modified, based upon the research work. This is the case in Winter's [70],[71] Equation (3.11) used by A.I.S.I. [99] for light gauge construction.

$$\frac{b_e}{b} = \frac{1.9}{(b/t)}\sqrt{\frac{E}{\sigma_{max}}}\left[1 - \frac{0.475}{(b/t)}\sqrt{\frac{E}{\sigma_{max}}}\right] =$$

$$= \sqrt{\frac{\sigma_{cr}}{\sigma_{max}}}\left(1 - 0.24\sqrt{\frac{\sigma_{cr}}{\sigma_{max}}}\right) \qquad (3.11)$$

Winter's effective width expression is a generalized concept of Von Karman, applying to the post-critical longitudinal rigidity.

In Equation (3.11), the value of b_e is computed by a trial and error procedure, due to the value of σ_{max}. This latter is dependent upon three interdependent functions [70].

$$\sigma_{max} = f_1(I_e) = f_2(b_e) = f_3(\sigma_{max}) \qquad (3.12)$$

where

f_1, f_2, f_3 are defined functions.

The plate fails when $\sigma_{max} = \sigma_y$, then the failure load is $b_e \, t \, \sigma_y$.

The same expression has been found to fit well the average test results for annealed stainless steel [100], and has been found to be in good and conservative agreement for carbon steel [101].

In Equation (3.11), the coefficients 0.475 and 0.25 are replaced respectively, by 0.418 and 0.22, to make the equation less conservative [102]. Also, in Equation (3.11), the same value of σ_{max} is used in computation of both the deflections and the maximum stress levels. This is in disagreement with Walker's[73], and Merrison's Rules [14], who suggest the use of two separate values of σ_{max}.

The British Standard [103] (PD 4064), used an empirical expression (Equation (3.13)) derived by Chilver [72], who worked on the ultimate strength of short-length, concentrically loaded, steel struts of various sections and yield stresses.

$$\left(\frac{b_e}{b}\right)_{ult} = \frac{\sigma_{ult}}{\sigma_y} = 0.66 \left(\frac{\sigma_{cr}}{\sigma_y}\right)^{1/3} \qquad (3.13)$$

Equation (3.13) uses an effective width as a constant, and then overcomes the trial and error procedure. By doing so, it can give conservative results for loads below the maximum. Also, (σ_{cr}/σ_y) is a function of b/t, so that σ_{ult} is readily calculable, giving an effective width corresponding to that of the beam collapse.

By using the experimental results on longitudinally-stiffened panels, [104],[105] Faulkner [106],[107] has provided Equation (3.14) for the effective width

$$\frac{b_e}{b} = \frac{2}{B}\sqrt{\frac{\sigma_y}{\sigma_{max}}} - \frac{1}{b^2}\frac{\sigma_y}{\sigma_{max}} \qquad (3.14)$$

where

$$B = \frac{b}{t}\sqrt{\frac{\sigma_y}{E}}$$

and

σ_{max} = absolute value of σ_{max}

If $\sigma_{max} = \sigma_y$ at failure, then Equation (3.13) reduces to

$$\left(\frac{b_e}{b}\right)_{failure} = \frac{2}{B} - \frac{1}{b^2} \qquad (3.15)$$

If σ_{cr} is replaced by its classical value

$$\sigma_{cr} = -\frac{k\,\pi^2\,E}{12(1-\nu^2)}\left(\frac{t}{b}\right)^2 = -\frac{3.62\,\sigma_y}{B^2} \qquad (3.16)$$

where

$$k = 4, \quad \nu = 0.3$$

then

$$\eta = \frac{\sigma_{max}}{\sigma_{cr}} = \frac{0.276 \left| \sigma_{max} \right| B^2}{\sigma_y} \tag{3.17}$$

and Equation (3.14) may then be rewritten as:

$$\frac{b_e}{b} = 1.052 \sqrt{\frac{\sigma_{cr}}{\sigma_{max}}} - \frac{\sigma_{cr}}{3.6\ \sigma_{max}} = \frac{1.052}{\sqrt{\eta}} -$$

$$- \frac{0.276}{\eta} \tag{3.18}$$

where

$$\eta \geq 0.276$$

Similarly, Winter's Equation (3.11) can be rewritten as

$$\frac{b_e}{b} = \frac{1.9}{B} \sqrt{\frac{\sigma_y}{\sigma_{max}}} - \frac{0.9}{b^2} \frac{\sigma_y}{\sigma_{max}} \tag{3.19}$$

Introducing η into Equation (3.19) gives

$$\frac{b_e}{b} = \frac{1}{\sqrt{\eta}} - \frac{0.25}{\eta} \tag{3.20}$$

where

$$\eta \geq 0.25$$

In the same manner, Von Karman's Equation (3.1) becomes

$$\frac{b_e}{b} = \frac{1.9}{B}\sqrt{\frac{\sigma_y}{\sigma_{max}}} \qquad (3.21)$$

or

$$\frac{b_e}{b} = \sqrt{\frac{\sigma_{cr}}{\sigma_{max}}} = \sqrt{\frac{1}{\eta}} \qquad (3.22)$$

After an examination of Sokolov's results [108], Papkovitch [108], derived the following Equations (3.23) and (3.24)

$$\frac{b_e}{b} = 0.44 + 0.56\,\frac{\sigma_{cr}}{\sigma_{max}} \qquad (3.23)$$

or

$$\frac{b_e}{b} = 0.44 + \frac{2.03\sigma_y}{\sigma_{max}\,B^2} = 0.44 + \frac{0.56}{\eta} \qquad (3.24)$$

Marguerre[109],[110]and Sechler[111] have respectively proposed Equations (3.25) and (3.26)

$$\frac{b_e}{b} = \sqrt{\frac{\sigma_{cr}}{\sigma_{max}}} \qquad (3.25)$$

$$\frac{b_e}{b} = \frac{1 + \beta^4}{3 + \beta^4} + \frac{2}{3 + \beta^4}\left(\frac{\sigma_{cr}}{\sigma_{max}}\right) \qquad (3.26)$$

Massonnet and Maquoi [64] have proposed Equation (3.27), as applied to an isotropic-perfectly plane plate. The equation is based upon the theory of first approximation.

$$\frac{b_e}{b} = \frac{1}{2}\left(1 + \frac{\sigma_{cr}}{\sigma_{max}}\right) = \frac{1}{2}\left(1 + \frac{1}{\eta}\right) \qquad (3.27)$$

Criticism is continually made on the proposed effective width formulas. Volmir [108] has shown that Equation (3.25) can be applied only for $\frac{\sigma_{cr}}{\sigma_{max}} > 0.2$, and Equation (3.21) is valid in the case of stiffeners whose relative rigidity is much less than that required to remain straight after plate failure (γ_ρ^* Massonnet's ultimate strength theory). Again, Massonnet [32] has shown, by a comparison based upon Dubas' [29] work that Equations (3.23) and (3.26) are the most satisfactory, and Equations (3.19) and (3.21) are substantially low.

Although in application a long time and found to be successful in design, the effective width concept is still an object of many discussions and its use is judged inadequate by some researchers. This is the case in the work by Dwight [26] who suggested that the strength of simple compression panels should be determined on a stress basis (σ_m), using Equations (3.28),(3.29),(3.30) and (3.31), and not by using the effective width approach. However, he added that the above remarks apply to the structural panels in the range $b/t < 80$, and it would be too safe, if applied to wider panels ($b/t \simeq 150$), for which it is desirable to account for edge restraints, both rotational and anti-pull-in.

For stress-free (unwelded) panels:

$$\sigma_m = \sigma_y \quad \text{if } b/t < (b/t)_1 \tag{3.28}$$

$$\sigma_m = \frac{(b/t)_1}{(b/t)}\sigma_y \quad \text{if } b/t > (b/t)_1 \tag{3.29}$$

For welded panels:

$$\sigma_m = \left[\frac{(b/t)_1\ \sigma_y}{(b/t)} - \frac{(b/t)_y\ \sigma_r}{(b/t)}\right] \leq \sigma_y \tag{3.30}$$

or

$$\sigma_m = \frac{(b/t)_y}{(b/t)}\left[\frac{0.85b - 3.7C}{b - 2C}\right]\sigma_y \tag{3.31}$$

For a plastic design:

To exhibit a plastic plateau, the following criteria should be met:

$$(b/t) \leq (b/t)_2 \tag{3.32}$$

where

$$(b/t)_1 = 0.85\ (b/t)_y = 1.6\sqrt{\frac{E}{\sigma_y}}$$

$(b/t)_y$ = (b/t) at which $\sigma_m = \sigma_y$

$$(b/t)_2 = 0.75\ (b/t)_1 = 0.64\ (b/t)_y = 1.2\sqrt{\frac{E}{\sigma_y}}$$

and

σ_r = residual stress

C = width of tension block at the edge of the panel (Figure 3.3).

For higher b/t ratios, an effective width method can be used. For panels in the region $(b/t) \simeq (b/t)_y$ the collapse is in a 'brittle' manner, and consequently, the effective width concept seems unsound. Dwight [26] has suggested that the strength of thin-walled beams and columns should be predicted on a simple elastic basis by replacing the true yield stress σ_y by a fictitious value equal to σ_m. This procedure will then tend to give lower loads than the effective width methos used in the case of beams and higher loads for columns. The strength of the box-columns could be made by using the Perry-Robertson formula (Equation (3.33)), for which pin-ended struts can allow the interaction between the yield and overall instability and the effect of the initial bow in both phenomena have great influence in the region of $(b/t) \leq 80$.

The column treatment can be extended to cover wide stiffened panels.

$$(\sigma_y-\sigma_m)(\sigma_I-\sigma_m) = \eta\, \sigma_I\, \sigma_m \qquad (3.33)$$

where

η = imperfection parameter and varies with b/t.

For columns, σ_I = Euler stress. For plates, since σ_m rises above σ_{cr} at high b/t, σ_I cannot be taken as the elastic buckling stress σ_{cr} of the plate. Instead, an expression is chosen for σ_I which corresponds for $b/t > (b/t)_y$, with

the theoretical predictions of the strength of the initial perfect plates. For $b/t < (b/t)_y$, and σ_I is taken as σ_{cr}. The failure stress σ_m is the lower root of the quadric Equation (3.33).

In using the effective width method for stiffened panels, several designers tend to neglect the interaction between the stiffeners. This means that the stiffener is considered individually, with an adjacent plate on its side and its strength evaluated as a pin-ended column between the transverse stiffeners. If a stiffened panel has N stiffeners, then its strength is simply equal to the sum of the strength of N stiffeners. In other words, each plate is considered as simply-supported. This treatment has been recently supported by Ratcliffe [35] in tests at Cambridge University [27] and it is thus used in the Merrison Appraisals Rules [14]. Massonnet [32],[64] claimed the above consideration would result in a non-economical design, because of the neglected stabilizing effect due to the membrane stresses.

For comparison purpose, the values of the effective width b_e, as proposed by different researchers, is computed in Table 3.1 for values of η from 0.2 to 2.0, and the results are plotted in Figure 3.4.

It may be observed in Figure 3.4 that:

a) Two separate tendencies exist. The first, comprising Equations (3.17) and (3.19), applies in both regions A and B for $0.2 \leq \eta \leq 2.0$. The second group comprises Equations (3.20), (3.23) and (3.26) apply only in the region B for $1.0 \leq \eta \leq 2.0$.

b) It may thus be concluded that in region B, if group I is considered as underestimating the effective width value b_e, then group II overestimates it. The difference between the two groups is of the order of 25%, which is too much for design consideration. Only by experimental tests may it be determined which group is the most accurate.

3.3.2 Consideration of the Participation of All Cross-Sectional Components

All the above-presented effective width methods are based mostly upon the behaviour of the plate between the stiffeners. However, some attempt is made to include the contribution of the stiffeners. Also, in the case of a steel box-girder, the contribution of the web plates, bottom flange and cantilever parts need to be accounted for. This attempt has been made by the Merrison Rules [14], Kondo [112], [113] and Abdel Sayed [114]. These proposed methods are reported in this section.

Using the results of the research program which was often initiated following the collapse of some large box-girder bridges [14], the Merrison Report [14] recommended the allowance for in-plane shear flexibility in flanges (shear lag), based upon elastic analysis by using the effective width of the flange in the calculations of stress and vertical deflections.

The effective width of each portion on each side of each web, is taken as βB and $0.85B_p$, respectively, for parts between the webs and those parts projecting beyond an outer web, Figure 3.5.

$$b_e = \beta B$$

or

$$b_e = 0.85\beta\, B_p \qquad (3.34)$$

where

β = effective width ratios

$B = B_T$ or B_B for top and bottom flanges, respectively

B_p = cantilever part of the flange

The stress computed as above, is the longitudinal stress at the edge of the web/flange. The stress distribution across the flange is given by Equations (3.35) and (3.36) for those parts between the webs and for projection, respectively.

$$\sigma_{1x} = \sigma_{1_{max}} \left[4\left(\frac{x}{3}\right)^2 + \left(\frac{3\beta-1}{2}\right)\left\{1 - 4\left(\frac{x}{B}\right)^2\right\}\right] \qquad (3.35)$$

$$\sigma_{1x} = \sigma_{1_{max}} \left[4\left(\frac{x}{B_p}\right)^2 + \left(\frac{3\beta-1}{2}\right)\left\{1 - 4\left(\frac{x}{B_p}\right)^2\right\}\right] \qquad (3.36)$$

where

x = distance measured from mid-point between the webs or from the free-edge of the flange for parts between the webs or projections, respectively.

Let

$$\frac{b_e}{2} = \frac{\int_0^{B/2} \sigma_{1_x}\, dx}{\sigma_{max}} \qquad (3.37)$$

Substituting σ_{1_x} by its value from Equations (3.35) or (3.36):

$$\frac{b_e}{2}\sigma_{1_{max}} = \int_0^{b/2} \frac{4x^2}{B^2}\, dx + \left(\frac{3\beta-1}{2}\right)\int dx - 4\left(\frac{3\beta-1}{2}\right)\int \frac{x^2}{B^2}\, dx \qquad (3.38)$$

After integration and simplification of Equation (3.38), the effective width is

$$\frac{b_e}{B} = \beta \qquad (3.39)$$

The effective width-ratio β is dependent upon three parameters:

1) The ratio of the cross-sectional area per unit width of a flange of longitudinal stiffeners A_s to that of the flange plate (A_s/bt).

2) The loading condition.

3) The ratio $\frac{B_T}{2L}$ or $\frac{B_B}{2L}$ or $\frac{B_p}{l}$, where

L = span length, B_B, B_T, B_p, as defined above.

An interesting and practical method for an effective width calculation was carried out by Japanese researchers [112],[113], by taking into consideration the static characteristics of the stiffened plate by longitudinal and transverse stiffeners. Their analytical expressions were proven to be in good agreement with the model results.

The following assumptions are made:

1) The axial displacements at both the deck plate and bottom plate vary parabolically over the transverse section, being linearly located at the web plates.

2) The distortions of any cross-section is sufficiently restricted by means of rigid stiffeners, as well as diaphragms.

3) The stiffness of the ribs can effectively prevent the steel deck plates from elongating in a transverse direction.

Using Galerkin's generalized method, a set of differential simultaneous equations was developed governing both the deflection $w(x)$ of the girder and the axial displacement $f_1(x)$, $f_2(x)$ at any point of the deck and bottom flange. From the above, an axial stress of the girder at any point can be calculated for a given load.

The effective width b_m is defined as

$$b_m = \frac{b_e}{2} = \frac{\int_0^b \sigma_x \, dy}{(\sigma_x)_{max}} \qquad (3.40a)$$

Equation (3.40a) was developed both for simply supported as well as continuous box girders with open or closed cross-sections under different loads. However, the effect of the initial imperfections is not included.

Equation (3.40b) gives the value of the effective width be in the case of an open cross-section (Figure 3.6), for a concentrated load P acting at its midspan and a uniformly distributed load q acting over the lengths for a simply-supported box-girder.

$$\frac{b_e}{b} = 1 - \frac{\sqrt{\frac{1.5\,w}{1.2-K}} \cdot \lambda + 2\frac{q}{p}L \cdot \frac{1}{(L/b)} \cdot w\,x}{(0.75+0.375\frac{q}{p}L)\frac{L}{b} + k\left(\sqrt{\frac{1.5\,w}{1.2-K}} \cdot \lambda + 2\frac{q}{p}L \cdot \frac{1}{(L/b)} w\,x\right)} \qquad (3.40b)$$

where

L = length of the span

$$w = \frac{1}{(1-\nu)} + \frac{K}{a \cdot t}(1 + \nu)$$

$$k = \frac{A}{F} + \frac{\bar{I}}{I}$$

$$\bar{I} = 2A\, h_u^2$$

$$A = b\left(\frac{t}{1-\nu^2} + \frac{A_s}{a}\right)$$

ν = Poisson's ratio

t = thickness of steel deck plate

A_s = cross-sectional area of a longitudinal stiffener

a = spacing of longitudinal stiffeners

I = total moment of inertia about the girder centroid

F = half of total cross-sectional area of main girder

h_u = distance between neutral axis of the girder and neutral plane of the stiffened deck plate

$2b$ = distance between the web plates

Two parameters λ and x are the function of three quantities L/b, w and k as follows:

$$\lambda = 1 \quad \ldots\ldots\ldots\ldots\ldots\ldots\ldots\ldots\ldots\ldots \quad L/b \geq 5$$

$$\lambda = \tanh \frac{L/b}{2\,w} \sqrt{\frac{1.5\,w}{1.2+k}} \quad \ldots\ldots\ldots\ldots\ldots\ldots \quad L/b < 5$$

$$x = 1 \quad \ldots\ldots\ldots\ldots\ldots\ldots\ldots\ldots\ldots\ldots \quad L/b \geq 10$$

$$= 1 - \operatorname{sech} \frac{L/b}{2\,w} \sqrt{\frac{1.5\,w}{1.2+k}} \quad \ldots\ldots\ldots\ldots\ldots \quad L/b < 10$$

The preceding effective width expressions for open cross-sections can be extended approximately to a single cell box, to a multi-cell box and to the cantilever, by decomposing the cross-section.

The above effective calculation, if supported by experimental tests, may be considered of great importance for design consideration in that it takes into account the contribution of all components comprising a steel box-girder. This is a great difference when compared with such methods accounting only for the behaviour of the plate between the stiffeners.

Again, Equation (3.40b) does not include the effect of initial geometrical imperfections, nor that of the welding residual stresses. It has been shown in Chapter II, that these two factors are of great importance.

Another method of calculating the effective width, accounting for the contribution of all cross-sectional components, has been proposed by Abdel Sayed [114] for an open

steel box-girder. He analyzed a stiffened deck plate loaded by in-plane shear forces along the junction deck/web (Figure 3.7b). The deck plate has been stiffened in both the longitudinal and transverse directions. The effect of the area and the spacing of the stiffeners has been accounted for, but he concluded that the influence of the area of the transverse stiffener on the longitudinal stress distribution in the deck could be neglected.

In his analysis, it is assumed that the deck plate is continuously welded to the stiffeners, so that the strains along their lines of connection are equal. The shear strain in the stiffeners is neglected, so that axial strains in the stiffeners are considered to be constant over their depths.

Figure 3.7c shows the typical element of a stiffened deck plate. He uses the differential equation of plane state stress and has derived an equation expressing the effective width.

At the longitudinal edges, two conditions have to be satisfied. First, the longitudinal strains of the deck plate $(\varepsilon_y)_{Dp}$ and the main girder $(\varepsilon_y)_w$ at their junction, have to be equal (Equation (3.41)). This is fulfilled if adequate shear connection is provided at the junction deck/web. Second, shear forces η_{xy} are acted upon between the web and the flange. For a simply-supported bridge, the longitudinal force in the flange $2P_y$ is equal to the sum of the edge

force η_{xy} between $y = o$ and $y = L/2$ (Figure 3.7(b)), Equation (3.42).

$$(\varepsilon_y)_{Dp} = (\varepsilon_y)_w \tag{3.41}$$

$$2P_y = 2\int_y^{L/2} (\eta_{xy})_{x=b/2}\, dy = 2\left[\sum_{m=1}^{\infty} \left(\frac{\partial X_m}{\partial x}\right) \cos\frac{m\pi}{\ell} y\right]_{x=b/2} \tag{3.42}$$

At a section y, $2P_y$ is considered to be equally distributed over the effective width b_e, defined as follows:

$$b_e = \frac{2P_y}{E(\varepsilon_y)_{Dp}\,(t+\frac{A_y}{a_y})} \tag{3.43}$$

where

$$(\varepsilon_y)_{Dp} = \frac{1}{RE}\left(D_x \frac{\partial^2 F}{\partial x^2} - \frac{\nu}{(1-\nu^2)} \frac{\partial^2 F}{\partial y^2}\right) \tag{3.44}$$

$$R = t\left[D_x D_y - \frac{\nu^2}{(1-\nu^2)^2}\right] \tag{3.45}$$

Equation (3.43) can be rewritten in a general manner as:

$$b_e = \frac{2\sum_{m=1}^{\infty} \left(\frac{\partial X_m}{\partial x}\right) \cos\frac{m\pi}{\ell} y}{\frac{1}{R}\left(1+\frac{A_y}{a_y}\right) \sum_{m=1}^{\infty} \left[D_x \left(\frac{\partial^2 X_m}{\partial x^2}\right) + \left(\frac{m\pi}{\ell}\right)^2 \frac{\nu}{(1-\nu^2)} X_m\right] \cos\frac{m\pi}{\ell} y} \tag{3.46}$$

Equation (3.46) is very general, and may be developed for each particular case of loading condition in a deck comprising two or more main girders; and it is interesting in that it accounts for the contribution of the stiffeners' spacing and rigidity. However, the effect of any initial imperfections is not included, nor is the basic small deflections theory equation. To account for any initial imperfections, Abdel Sayed [115] has used large deflections differential equations governing a plate loaded in its plane beyond its buckling limit, as established by Von Karman.

But, in the large deflections analysis, the participation of the stiffeners is not accounted for, only the plate elements between the stiffeners is considered.

Regarding the boundary conditions, he considered alternatively the usual cases:

a) The unloaded edges (longitudinal) remain straight in and perpendicular to the plane of the plate,(for example, a panel removed from a continuous plate over many longitudinal ribs.)

b) The unloaded edges are free to move in its plane (for example, no continuation over the longitudinal ribs.) In this case, Winter [71] has presented experimental results.

The initial deflection w_o is presented in a Fourier series

$$w_o = e_o \cos \frac{\pi}{b} x \cos \frac{\pi}{L} y \qquad (3.47)$$

He carried out the following equations for a theoretical flat plate (Equations 3.48 and 3.49) and for a plate with initial deflections (Equations (3.50), (3.51) and (3.52).

1) Flat Plate: Restrained straight longitudinal edges.

$$\frac{b_e}{b} = \frac{\eta_a}{(\eta_y)_{x=\pm b/2}} = \frac{1}{2}[1 + \frac{\eta_{cr}}{(\eta_y)_{x=\pm b/2}}] \qquad (3.48a)$$

or

$$\frac{b_e}{b} = \frac{1}{2}[1 + \frac{\eta_{cr}}{(\eta_y)_{x=\pm b/2}}]\frac{b}{t} \qquad (3.48b)$$

2) Flat Plate: Longitudinal edges free to move in.

$$\frac{b_e}{b} = \frac{\eta_a}{(\eta_y)_{max}} = \frac{1}{3.93}[1 + 2.93\frac{\eta_{cr}}{(\eta_y)_{max}}] \qquad (3.49a)$$

or

$$\frac{b_e}{b} = \frac{1}{3.93}[1 + 2.93 \frac{\eta_{cr}}{(\eta_y)_{max}}]\frac{b}{t} \qquad (3.49b)$$

Equations (3.49a) and (3.49b) are used when calculating the maximum stresses along the edges. In calculating the deflection, Equations (3.49c) and (3.49d) are adequate.

$$\frac{b_e}{b} = \frac{1}{2.465}\left(1 + 1.465\,\frac{\eta_{cr}}{\bar{\eta}_y}\right) \qquad (3.49c)$$

$$\frac{b_e}{t} = \frac{1}{2.465}\left(1 + 1.465\,\frac{\eta_{cr}}{\bar{\eta}_y}\right)\frac{b}{t} \qquad (3.49d)$$

3) Plate With Initial Deflection: The longitudinal edges are forced to stay straight in its plane.

$$\frac{b_e}{t} = \frac{1}{2}\left[1 + \frac{\eta_{cr}\left(\frac{e}{e+e_o}\right)}{(\eta_y)_{x=\pm b/2}}\right](b/t) \qquad (3.50)$$

4) Plate With Initial Deflection: Longitudinal edges free to move in its plane.

$$\frac{b_e}{t} = \frac{1}{5.93}\left[1 + 2.93\,\frac{\eta_{cr}}{(\eta_y)_{max}}\left(\frac{e}{e+e_o}\right)\right]\frac{b}{t} \qquad (3.51)$$

If the deformation along $x = \pm b/2$ is considered to govern, thus $b_e/b = \eta_a/\bar{\eta}_y$, and it follows that

$$\frac{b_e}{t} = \frac{1}{2.469}\left[1 + 1.465\,\frac{\eta_{cr}}{\bar{\eta}_y}\left(\frac{e}{e+e_o}\right)\right]\frac{b}{t} \qquad (3.52)$$

Abdel concluded that in the case of a flat plate with restrained straight edges, the equation giving b_e/t is considered reasonable, up to a b/t ratio, where the critical load is 1/8 of the maximum load. By considering the

flexible edges, the magnitude of the deflection is increased to about 21% when it buckles, compared to restrained straight edges. The effect of the boundary conditions is also shown by Dawson and Walker [67], (Figure 3.8).

For flat plates, the effective width b_e remains equal to the actual width b until η_a exceeds the buckling limit η_{cr}, then a sudden drop takes place.

Figure 3.9, shows the influence of initial imperfections on the effective width, and thus upon the ultimate strength.

3.4 TANGENT MODULUS APPROACH

The tangent modulus approach is frequently used in aircraft, and is conveniently found in Region A(Figure 3.1a). The method consists of treating the failure stress σ_m as an "inelastic buckling stress" by substituting the modulus E by a modified value E^1 in the formula for the elastic critical stress. The approach leads itself to aluminum, where E^1 can be related to the shape of the stress-strain curve. Bleich [116] suggests the use of $E^1 = \sqrt{E\ E_t}$ where E_t is the tangential modulus. But, the use of $E^1 = E_t$ is safe and convenient, in that it leads to the "equivalent slenderness ratio" approach in which the failing stress is obtained by entering the (tangential modulus) column curve with given L/r.

For structural steel that has an elastic/perfectly plastic stress-strain curve, the tangential modulus method needs some modification. This difficulty can be overcome by employing a fictitious value of E_t as carried out by Richmond [117], who worked back from the curve.

3.5 ANALYTICAL METHODS

The prediction of the failure stress σ_m by analytical methods, is much more difficult, due to the number and nature of factors involved.

For panels with b/t ratios that lie in Region A (Figure 3.1a), the calculation must take into account first, the interaction between the yield and buckling, and second, the remarkable effect of the initial geometrical imperfections and residual stresses.

For panels in Region B(Figure 3.1a), the reserved post-buckling strength must be accounted for.

Another problem is the assumption of suitable edge conditions, which may consist of:

a) Rotation: Here, for practical purposes, the panel is assumed as simply-supported.

b) The ability to pull-in: to straighten (plane section remain plane) for wide stiffened panels, and -

complete freedom to pull in, for example, an unstiffened box-column.

Figure 3.8, shows the effect of edge conditions on the stress distribution in a direction parallel to the applied compression upon longitudinal edges free to deform in-plane and edges held straight.

For stiffened panels, the contribution of the stiffener spacing and rigidity should be included. This involves many factors regarding the stress distribution, for both the plate and the stiffeners.

Due to the above difficulties, the analytical determination of the failure stress σ_m is possible only by an approximate approach..

Because the elastic linear buckling theory of plates is considered to be unsafe [14],[17],[18],[20],[27], when applied to stiffened plates which are used in steel box-girder bridges, the proposed alternative is the large-deflection (non-linear) theory.

3.5.1 Large-Deflection Theory

The large-deflection (non-linear) analysis of stiffened plates is an extension of the large-deflection theory of isotropic plates initiated by Von Karman [118],(1910).

In 1940, Rostovtsev [119] applied Von Karman's findings to the case of orthotropic plates and derived the following fundamental equations.

$$\frac{1}{E_y} \cdot \frac{\partial^4 F}{\partial x^4} + \left(\frac{1}{G} - \frac{2\nu_x}{E_x}\right) \frac{\partial^4 F}{\partial x^2 \partial y^2} + \frac{1}{E_x} \cdot \frac{\partial^4 F}{\partial y^4} =$$

$$= \left(\frac{\partial^2 w}{\partial x \partial y}\right)^2 - \frac{\partial^2 w}{\partial x^2} \cdot \frac{\partial^2 w}{\partial y^2} \qquad (3.53)$$

$$D_x \frac{\partial^4 w}{\partial x^4} + 2H \frac{\partial^4 w}{\partial x^2 \partial y^2} + D_y \frac{\partial^4 w}{\partial y^4} =$$

$$p + t\left(\frac{\partial^2 F}{\partial y^2} \frac{\partial^2 w}{\partial x^2} - 2\frac{\partial^2 F}{\partial x \partial y} \cdot \frac{\partial^2 w}{\partial x \partial y} + \frac{\partial^2 F}{\partial x^2} \cdot \frac{\partial^2 w}{\partial y^2}\right) \qquad (3.54)$$

Equations (3.53) and (3.54) were derived for a plate of natural orthotropy. For stiffened plates or structural orthotropy, some modifications are necessary and new terms are introduced.

In practice, a stiffened plate is substituted by an equivalent orthotropic plate. Different methods for this substitution exist and may be found in literature [120].

Historically, Pflüger [121], (1947), was the first to study the case of stiffened plates, but he considered the small deflection theory. His work was continued by such other researchers as Giencke [122], and Massonnet [123], and Soper [124]. Massonnet [123] introduced new terms to

account for the effect of eccentricity where the neutral plane of the stiffened plate does not coincide with that of the plate, itself.

Vogel [125], (1961), used energy methods for the solution of a plate stiffened in two orthogonal directions.

Abdel-Sayed [115], [126], used an equilibrium method for the solution of large-deflection equations. He was able to introduce the effect of initial geometrical imperfections.

The large-deflection theory was used by many investigators for the analysis of unstiffened plates. The case of stiffened plates was also considered, but only the behaviour of the plate between the stiffeners was studied. Since 1969, following the collapse of a few large steel box-girder bridges, both the plates and stiffened plates were investigated, especially in countries where those bridge collapses happened. In this section, some of the proposed solutions are reported.

3.5.1.1 Solution of the fundamental large-deflection equations

Various methods exist for the solution of the fundamental Equations (3.53) and (3.54). The results may be conservative or unsafe, depending upon the structural parameters involved, as well as on some basic assumptions made, such as, for example, boundary conditions. The widely used methods are:

1) Equilibrium method

2) Energy method
   - conservation of energy
   - the Rayleigh method
   - minimum potential energy
   - virtual displacement method

3) Lagrangian multiplier method

4) Finite difference method

5) Finite element method

The equilibrium method gives closed solutions for stiffened plates. However, it requires the integration of differential equations for buckled plates, and therefore, its use is a tedious operation.

Energy methods are especially useful in those cases where a rigiourous solution of the equations (3.53) and (3.54) is unknown and it is required to find only an approximate value of the critical load.

The Lagrangian multiplier method is often used to facilitate some of the difficulties encountered when using the Ritz method.

The finite difference method is useful when mixed boundary conditions may be considered.

The finite element method is based on forces and displacement matrix calculations, and is computer-oriented. It

is more advantageous when any of the boundary conditions and loading combinations may be considered.

Different authors have applied fundamental Equations (3.53) and (3.54) of the large deflection analysis of orthotropic plates to the case of stiffened plates. After a number of modifications and assumptions, some approximate solutions are found.

In this study, in using the energy method, the fundamentally large deflection Equations (3.53) and (3.54) have been developed for stiffened plates. The effect of any initial geometrical imperfections is accounted for. This development is given in Appendix B and compare closely with [127].

In this section, some solutions by the large-deflection theory are presented.

Graves Smith [128],[129] has developed a powerful energy method for predicting the strength of thin-walled columns which fail elastoplastically. He considered the case of a thin square tube and was able to account for the effect of slight initial imperfection of amplitude δ_o, assumed to be the same form as those buckles which develop in a perfect member. He used a computer program in his work. Figure 3.10, shows the results by Graves Smith upon the effect of initial imperfection δ_o on the critical stress of simply-supported webs.

He considered the local-flexural interaction problem. In his results, (Figure 3.11), the theoretical interaction curve for a perfect column meets the Euler curve at $\sigma_m^1 = \sigma_{cr}$, the failing load being unaffected by local instability at slenderness ratios above $\pi\sqrt{E/\sigma_{cr}}$ (= 1.65 b/t for a square tube). He was able to account for the effect of initial imperfection, as shown in Figure 3.11. These findings are deemed to be most interesting and could lead to greater economy. Similar findings for aluminium have been found by Bijlaard and Fisher [130].

The Abdel Sayed [115] solution of effective width, presented in Section 3.3 of this Chapter, is based upon the large-deflection Equations (3.53) and (3.54). The extension of the stability investigation to include the post-buckling range, begins by considering the buckled plate panel to the form

$$w = e_o \cos \frac{\pi}{b} x \cos \frac{\pi}{\ell} y \qquad (3.55)$$

The solution is given in Section 3.3.2.

In his discussion of the report by Dubas [29], Massonnet [32] reported the results carried out by Skaloud and Novotny regarding the effect of the initial deformation of a stiffened plate at its ultimate strength. They have used the Rayleigh-Ritz energy method. The results were found in the case of a stiffened plate with one median stiffener,

and for this, with two stiffeners each located at a third of the width. The edges are assumed to move freely in the plate's plane.

The shape of the initial deformation is expressed by

$$w_o = f_o \sin\frac{\pi x}{a} \sin\frac{\pi y}{b} \qquad (3.56)$$

Skaloud and Novotny [131] have established for various relative rigidity γ of the stiffener, charts (Figure 3.12) giving $\bar{\sigma}/\sigma_y$ as the function of relative thickness b/t and f_o/t for a plate with $\sigma_y = 31$ Kip/in^2.

Massonnet and Maquoi [64] presented the non-linear analysis of a stiffened box-girder, subject to pure bending. The deck is subject to compression. This analysis enables the calculation of the applied maximum stress σ_m at collapse and the required optimum rigidity of the stiffeners for those later to remain straight after buckling of the plate has taken place. The effect of the initial imperfections is included.

Sherbourne [36] has presented an energy method for the ultimate strength of a stiffened plate, which possesses different rigidities in two orthogonal directions, with its load applied in the stronger direction. This study covers the elastic behaviour of a stiffened plate, simply-supported along all sides. Unfortunately, the analysis does not account for the effect of initial imperfections.

The method is based on the following assumptions:

1) The plate possesses infinite elasticity, in terms of its stress-strain for the calculation of the loading line, and perfect plasticity for the purpose of its mechanism.

2) For the buckled plate, each half-wave can be considered as simply-supported.

3) The edges are assumed to remain straight.

4) The strains in post-buckling are accurately prescribed by first and second-order terms in the displacement.

5) The initial imperfections are neglected.

6) Loading is in uniaxial compression.

Regarding the (elastic) post-buckling behaviour, the energy method was used to derive the relationships between the load and central deflection of the plate, assumed to buckle in one-half wave, only. The deflected shape of the plate is given by

$$w = \delta \cos \frac{\pi x}{a} \cos \frac{\pi y}{b} \qquad (3.57)$$

where

δ = deflection at the centre of the plate.

The plastic post-buckling mechanism which takes place after the attainment of the ultimate load was also considered.

The energy method has also been used by Chapman and Falconer [132] for the determination of the critical load of initially largely deformed orthotropic plates simply-supported with unloaded edges free to pull-in. The elastic and post-buckling characteristics have been studied.

Dawson and Walker [67] have presented an analytical method of considering the post-buckling behaviour of imperfect plates.

They have derived what they called straightforward, explicit expressions for the ultimate load, end-shortening and stiffness of a simply-supported, uniformly-loaded square plate that undergoes elastic buckling. Figure 3.8 shows the effect of edge restraint upon the stress distribution. The shape of the initial deflection is given in Equation (2.7).

After neglecting some of the terms used in the equation derived by Coan [69], the analysis may be simplified as follows. The deflection parameter e at the centre of a panel having an initial imperfection parameter e_o, is given by

$$e^3 - e[e_o^2+4.25(\frac{\sigma_{av}}{\sigma_{cr}}-1)] - 4.25\, e_o = 0 \qquad (3.58)$$

The maximum and average edge membrane stresses are derived as:

$$\frac{\sigma_{e_{max}}}{\sigma_{cr}} = \frac{\sigma_{av}}{\sigma_{cr}} + 2.832\left(\frac{\sigma_{av}}{\sigma_{cr}}-1+\frac{e_o}{e}\right) + \left[0.515\left(\frac{\sigma_{av}}{\sigma_{cr}}-1\right)^2\right]_{(\sigma_{av}>\sigma_{cr})} \quad (3.59)$$

$$\frac{\sigma_{e_{av}}}{\sigma_{cr}} = \frac{\sigma_{av}}{\sigma_{cr}} + 1.449\left(\frac{\sigma_{av}}{\sigma_{cr}}-1+\frac{e_o}{e}\right) + \left[0.384\left(\frac{\sigma_{av}}{\sigma_{cr}}-1\right)^2\right]_{(\sigma_{av}>\sigma_{cr})} \quad (3.60)$$

A comparison with Yamaki's [133] results suggests that Equations (3.58), (3.59) and (3.60) are accurate for $\sigma_{av} \leq 4\sigma_{cr}$.

Referring to Graves Smith's results [129], it is shown that the plate fails at $P = P_{ult}$, when the mid-plane of the plate first starts yielding. That is, when $\sigma_{e_{max}} = \sigma_y$. Then, at $P = P_{ult}$, $\sigma_{av} = \sigma_{ult}$ and $e = e_{ult}$, the Equation (3.58) becomes

$$\frac{\sigma_y}{\sigma_{cr}} = \frac{\sigma_{ult}}{\sigma_{cr}} + 2.832\left(\frac{\sigma_{ult}}{\sigma_{cr}}-1+\frac{e_o}{e_{ult}}\right) + \left[0.515\left(\frac{\sigma_{ult}}{\sigma_{cr}}-1\right)^2\right]_{(\sigma_{ult}>\sigma_{cr})} \quad (3.61)$$

Tests also show that the initial imperfection parameter e_o is accurately given by Equation (2.12) for $(\sigma_y/\sigma_{cr}) \leq 50$ (that is, $b/t \leq 380$ for $\sigma_y = 36$ kip/in^2).

The behaviour of the plate is thus defined by Equations (3.57) to (3.61) with the initial imperfections given by Equation (2.12).

A comparison of Equation (3.61) with other works is shown in Figure 3.13.

Dawson and Walker [73] have used the results of their previous work above [67] to develop a simple method for the design of thin-walled beams which buckle locally. A comparison with the test results for lipped-channel beams shows that the proposed method is in good agreement with both the collapse moments and elastic deflections.

3.5.1.2 Numerical solution of elastic large-deflection equations

Williams and Walker [134] have presented explicit solutions for the design of initially deformed plates subject to compression. The solution is obtained by elastic large deflection analysis, based upon the perturbation approach and the results obtained by finite difference computer analysis. The method permits the calculation of deflections, stresses, in-plane effective stiffness, bending moment and twisting moment. Allowance is made for the non-linear behaviour in the large-

deflection regime, due to the interaction of the flexural and membrane effects. The interaction then becomes practically important for deflections exceeding t/4.

The approach used is a numerical method by finite difference, together with dynamic relaxation. The solutions are presented in tabular form, and are for rectangular plates, subjected to uniaxial and biaxial compression. Some results are intended to deal with non-uniform compression, shear, and a combination of shear and compression.

The magnitude of geometric imperfections used are those given by Merrison's Rules [14]. The residual stresses may be accounted for as a magnification of the geometric imperfection.

Regarding the boundary conditions: the plate used is assumed to be simply supported. (This is conservative since it assumes antisymmetric buckling across panel boundaries, and it completely ignores the torsional rigidity of plate stiffeners and the restraint afforded by the adjacent panels.) With regard to the membrane edge conditions, it is usual to assume that the edges of the interior panels remain straight in-plane, although free to displace, the exterior edges are assumed stress-free. The free-edge condition ignores the in-plane constraint due to edge members, which could be significant, in some cases.

The results given by explicit solutions have been found to be in good agreement with those given by the finite element elasto-plastic method carried out by Frieze [135]. Frieze found the factor against the collapse of 1.54 (1.52 allowing interaction) as compared to the membrane yield factor of 1.59, given by explicit solutions. However, Frieze considers that more improvements are needed for explicit solutions. There is some criticism by Parry [135] regarding the form of initial imperfections and also regarding the adoption of one-half sine-wave lateral deflections only, for aspect ratios greater than one, seems to be questionable.

3.5.1.3 Numerical solution of moment-curvature-twist relationships of the plate/stiffener inelastic column

Little [136] has presented a theoretical method for predicting the strength of stiffened plating loaded in uniaxial compression. The local buckling of the plate is allowed by using an average compressive 'stress-strain' curve appropriate to the plate elements. However, local buckling is not allowed in the stiffeners. Thus, if failure occurs in the stiffeners, it is assumed to occur through yielding with no associated local buckling. This implies that the stiffeners are of stocky cross-section (compact).

The stiffened plating is analysed as a column. Two cases are to be considered:

a) Pin-ended panels, and

b) The effect of longitudinal continuity in a multi-bay structure.

The study of pin-ended panels is restricted to a situation where the overall failure is triggered by a local failure of the plate. The following assumptions are made:

1) Failure of the stiffened flange occurs between cross-frames. (Cross-frames are flexurally stiff enough).

2) The flange is wide enough, compared with the cross-frame spacings to be analysed as a column (otherwise lateral deflections of a flange as whole, would produce transverse membrane stresses).

This type of approach was used in the past by Kondo [137], Vojata and Ostapenko [138].

a) Failure Analysis: no longitudinal continuity

A positive (toward the stiffener outstand) initial imperfection $\overset{\frown}{\Delta_o}$ of the column causes a strain in the plate to become magnified by the column action (with zero end eccentricity of loading) and a failure results from the interaction between the local buckling of the plate and the overall buckling of the completely stiffened panel.

This mode of failure is a plate failure, according to Murray [37] and Horne [39]. Little [136] does not consider the stiffener buckling mode because he assumes that the stiffeners are of compact sections, thus the mode of failure in which the overall failure is precipitated by local failure of the stiffener, is simply a column strength problem involving no local overall buckling.

The method of solution is a numerical solution of moment-curvature-twist (M-ψ-P) relationships. The column is treated as an assembly of equal-length elements, each having full cross-sections of the column and, each being approximately one of the plate buckles, that is, 0.875b, as carried out by Moxham [76], (b = longitudinal stiffener spacings). The M-ψ-P relationship for a one-plate-buckle-length is used in an iterative numerical method for inelastic column analysis.

The initial imperfections of the column were taken as L/800.

As a conclusion, the author has shown that for given imperfections, the strength of a stiffened panel depends primarily on b/t, L/r and σ_{sk} (residual stresses in skin plate) and secondly, at the ratios A_o/bt and Z_{sk}/r. An increase in b/t, L/r and σ_{sk} will result in a decrease in strength. A_o/bt (A_o = cross-sectional area of stiffener) increases the strength but seems to also increase Z_{sk}/r which has a weakening effect.

b) Effect of Longitudinal Continuity

Longitudinal continuity has a tendency to strengthen where failure occurs in a plate and weaken where it occurs in a stiffener. However, although an infinite number of spans is specified, the behaviour of the central span of a three-span column would probably be very similar to that of the central span of a much larger number of spans.

As there is not any numerical example illustrating its use, the proposed method seems to be more complex and purely theoretical.

3.5.1.4 Finite element solution of large-deflection elasto-plastic equations

Crisfield [82],[139] has presented an approximated method, based upon a finite element formulation for calculating the ultimate strength of plates and stiffened plates under uniaxial compression. This method is a large-deflection elasto-plastic analysis. The effect of initial imperfections and residual stresses is accounted for and it is possible to study the unloading stage following collapse.

The plates are assumed simply supported.

Regarding the plasticity, the author has adopted an unfamiliar criterion. In fact, a yield criterion is a direct function of the six generalized stress resultants N_x, N_y, N_{xy}, M_x, M_y, M_{xy}. This approach is similar to the criterion derived

by Ilyushin [140] but with a modified yield function F as:

$$F = \frac{\bar{N}}{t^2 \delta_o^2} + \frac{4|\bar{M}\bar{N}|}{\sqrt{3\alpha}\, t^3 \sigma_o^2} + \frac{16\, \bar{M}}{\alpha^2 t^4 \sigma_o^2} = 1 \qquad (3.62)$$

The results of the plate strengths were compared with those of Moxham [76] and were close to 10%. When compared with Little and Dwight [77], close agreement was found to exist between them. However, the case of stiffened plates seems not to have been studied too deeply, and needs more investigation.

This method by Crisfield, is discussed in Reference [141]. Little [141] considers that Ilyushin's modified criterion is safe for column analysis, thus, the proposed curves may be used for column design while some modifications are needed for plate analysis. Although Moxham, Frieze and Harding [141] seem to disagree on some points, the proposed method seems to be well-supported and so, of greater interest.

3.5.1.5 Finite difference solution of large-deflection elasto-plastic equations

Harding and Hobbs [142] have presented an elasto-plastic analysis of imperfect square plates under in-plane loading. The method is a finite difference formulation of large deflections solved by the dynamic relaxation technique. Load-deflection curves are presented which include the response following the attainment of the peak load. These curves

show the effects of axial and shear in-plane loading (acting alone or in combination), strain hardening, magnitude of out-of-plane imperfection, and uniaxial and biaxial residual stresses.

The analysis presented is for unstiffened plate panels, using a large deflection elasto-plastic dynamic relaxation program and the plasticity is treated by a multi-layer approach.

The following conclusions may be outlined from the analytical results:

a) The influence of the imperfection level on the effects of different boundary restraints is fairly complex. However, it seems that at an intermediate imperfection level, the effect of boundary restraint on the panel strength is relatively small.

b) The effects of uniaxial and biaxial residual stresses on compression panel behaviour were studied, and it was concluded that for the level of residual stresses investigated, there was no significant effect of the biaxial residual stresses, as compared the uniaxial stresses on any of the panels.

c) The effects of strain-hardening on compression panel behaviour. It was found that even a modest amount of hardening (H = 0.1) has considerable beneficial effects on the panels considered. The plateau is converted to the rising line and the falling path is converted to a plateau.

d) The effects of the imperfection level and boundary conditions on shear panel behaviour. It was concluded that for these loadings, the effect of initial imperfections on the ultimate collapse behaviour is small. The most interesting feature of these results is the influence of the boundary conditions. In fact, there is no difference for stocky panels. However, as the slenderness increases, the development of a tension field becomes more significant and the provision of the boundary restraint in accepting these forces becomes more important for the panel strength, that is, it is an important conclusion that the partial restraint case offers a significant increase in the design strength over an unrestrained case for a typical web panel which is supported by adjacent panels.

e) The interaction of the axial and shear loadings was also investigated, but extensive investigation is still needed. The presented method necessitates the use of a large capacity computer. As in most of all the suggested methods, its accuracy and use in practical design are discussable. It was discussed by Chaplin and Little [143].

3.5.2 Effective Yield Approach

Dwight and Little [144] have presented a method for calculating the strength of stiffened steel compression flanges. Similar to that work done by Little [136], the local buckling of the plating is allowed for, but not for the stiffeners, which are assumed to be compact sections.

The overall buckling between the cross-frames is covered by a column-type treatment. An essential feature is the use of an effective yield approach for dealing with the interaction between the local and overall buckling, as an alternative to that of the effective section method.

In the work by Little [136], the compression force P is the result of direct stress acting upon the column end. P is assumed not to vary over the length of the stiffener-plate column. This implies that the overall bending moment gradient effects, and hence the shear stresses are assumed negligible. In Reference [144], the loading consists of a

longitudinal direct stress decreasing along the length, together with associated shear which may contain a torsional component. The stress gradient from one end to the other is regarded as constant.

The basis for plate strength curves comes partly from tests conducted [83],[144] and partly from the ultimate load theory [77],[145]. Regarding the boundary conditions, the plates are assumed to be simply-supported and free to pull in. This method allows for the effects of the initial geometrical imperfections and of the residual stresses from welding.

From this proposed method, a set of curves is carried out which enables the designer to check both the unserviceability and the collapse criteria of a stiffened panel under uniaxial compression. The method is believed to be quicker and more reliable than the Merrison Rules procedure.

It may be pointed out that the collapse checks made by the proposed method just described, neglect the shear lag effect. Thus, the direct stresses at the ends of the considered column are factored mid-skin stresses averaging across the width of the flange. The reduction of the plate strength in the presence of shear has been assumed to be simply a function of the effective decrease in yield. The curves are defined by an empirical formula of the Perry type, containing an imperfection factor.

3.5.3 Elasto-Plastic Buckling Theory

Some attempts have been made [146] to determine the ultimate buckling strength of stiffened plates by using the elasto-plastic theory.

The principle is to analyze the failure mechanisms of a stiffened panel after reaching its load-carrying capacity. The shape of the plastic collapse curves determine such important properties as how sensitive a stiffened plate is, to its initial imperfections and also whether or not collapse will be sudden; otherwise, the ability to withstand a limited amount of overload. Figure 3.14, shows the drop of load-carrying capacity for two box-girder beams, while Figure 3.15 makes a comparison of elasto-plastic theory with other methods.

It is found that for both mild and high steel, when b/t is < 50 the elastic critical stress σ_{cr} exceeds yield stress. So, in this important practical range, the plastic effects obviously predominate.

The collapse-line may drop away rapidly, even when the deflections have very small values. Thus, even for b/t ratios which are considerably in excess of 50, it is the plastic effects which determine the collapse load and other important parameters.

According to the elasto-plastic theory, the total axial

load carried by the panel is given by Equations (3.63) and (3.64) for plate failure modes and for stiffener failure mode (Figure 1.16), respectively.

$$P = \sigma_y t (S-B)\left[\sqrt{\frac{4\delta^2}{t^2}+1} - \frac{2\delta}{t}\right] + \frac{\sigma_y t^2 B}{2\delta} \log\left(\frac{2\delta}{t} + \sqrt{\frac{4\delta^2}{t^2}+1}\right) \qquad (3.63)$$

$$P = 2\sigma_y S \left[\sqrt{A_1} + \frac{P_s}{2\sigma_y S} - \frac{t_1}{2} - \frac{\ell \Delta^2}{h_s^2 \tan \beta} - c\right] \qquad (3.64)$$

where

A_1 is given by:

$$A_1 = \left(\frac{F_s}{2\sigma_y S} - \frac{t_1}{2} - \frac{1\Delta}{h_s^2 \tan \beta} - c\right) - \left(\frac{t_1}{2} + \frac{P_s}{2\sigma_y S}\right)^2 \frac{t_1^2}{2} \frac{P_s t_1}{\sigma_y S} + \frac{M_s}{\sigma_y S}$$

$$M_s = \frac{\sigma_y t_s^3 h_s^3}{3\Delta^2}\left[\left(\frac{\Delta^2}{t_s^2}+1\right)^{3/2} - 1 - \frac{\Delta^2}{t_s^3}\right] \qquad (3.65)$$

The elasto-plastic buckling theory leads to very complicated equations. Tests made in References [37] and [147] led to the following conclusions.

1) The point of first yielding, which is often used as a failure criteria, may be a reliable method in those cases where the axial stresses are large, provided allowance is made in a logical way for loss of effec-

tive width, initial imperfections and eccentricity at collapse.

2) In cases where the axial stresses are small and buckling does not occur, it is shown that the use of the full plastic moment capacity of the section gives a more accurate estimate of the failure load.

Using the first conclusion and the Perry-Robertson formula, and assuming simply-supported conditions, the axial collapse load of a stiffened panel may be calculated as follows:

Collapse Load: axial loading

1) When $\sigma_c > \sigma_e$: Simple elasto-plastic column theory may be used.

σ_c = axial stress at which the plate buckles

σ_e = axial stress at which the panel buckles as a column

$= \pi^2 E(r/L)^2$

2) When $\sigma_c < \sigma_e$: The analysis is made as follows:

The eccentricity Δ^1 of the load when an effective column carries zero axial load

$$\Delta^1 = \Delta\left(1 - \frac{\sigma_c \, A/A^1}{\sigma_c^1}\right) \qquad (3.66)$$

The eccentricity Δ^1 is added to the initial imperfection δ_o including the load misalignment.

The total deflection δ at the centre of the column is:

a) $\sigma < \sigma_c$

$$\delta = \frac{\delta_o}{1 - \sigma/\sigma_e} \qquad (3.67)$$

where

σ = the applied axial stress.

b) $\sigma_c < \sigma < \sigma_f$

$$\delta = \frac{\delta_o + \Delta^1}{1 - \frac{\sigma}{\sigma_c^1}} \qquad (3.68)$$

where

$\delta_f = \sigma$ at failure.

From previous work, Walker and Murray [38] have demonstrated that the failure of a square plate occurs when the membrance stress at some point in the plate reaches the yield stress. At the point of failure, the effective width b_e is given by

$$b_e = \frac{\sigma_m}{\sigma_y} b \qquad (3.69)$$

(σ_m/σ_y) is read on a curve $(\sigma_y/\sigma_c)^{1/2}$ versus $(\sigma_m/\sigma_y)^{1/2}$.

Failure of the whole panel is now assumed to occur when the effective column so obtained, reaches a yield stress leading to the plate or to the stiffener buckling. The choice at which failure mechanism occurs depends only upon the sign of $\delta_o + \Delta^1$. If it is positive, the plate fails and if it is negative, the stiffener fails. At the collapse stress σ_f^1 the stress at the outer fibre is

$$\sigma_y = \sigma_f^1 + \frac{\sigma_f^1 A^1 y^1 (\delta_o + \Delta^1)}{I^1 (1 - \frac{\sigma_f^1}{\sigma_e^1})} \qquad (3.70)$$

The solution of this quadratic equation is the Perry-Robertson formulae (Equation 3.72) with the imperfection term η given by:

$$\eta = \frac{A^1 y^1 (\delta_o + \Delta^1)}{I^1} \qquad (3.71)$$

$$\frac{\sigma_f^1}{\sigma_y} = \frac{1}{2}\left[1 + (1+\eta)\frac{\sigma_e^1}{\sigma_y}\right] - \sqrt{\frac{1}{4}\left[1 + (1+\eta)\frac{\sigma_e^1}{\sigma_y}\right] - \frac{\sigma_e^1}{\sigma_y}} \qquad (3.72)$$

3.5.4 Secant Effective Width Method

A method of calculating the ultimate strength of stiffened plates was recently reported [39],[40],[74],[148] termed the "Secant Effective Width Method". This method allows for the reduction of plate stiffness with large values b/t, the effect of residual stresses and the initial geometrical imperfections.

The stiffeners are assumed to be of sufficiently stocky cross-section to be able to develop yield at their extreme fibers before collapsing by local torsional buckling.

Regarding the boundary conditions: the interactive moments between the plate and the web of the stiffener are neglected. This means a simply-supported plate. Also, the edges are restrained so as to remain straight (in-plane).

The method is based on the Perry-Robertson formulae (strut treatment), the criterion being the attainment of a longitudinal membrane stress at plate/stiffener boundary, equal to yield stress. The effective width is taken as constant along the panel length, while in reality, it varies, being greater at the ends where the mean stress is less in the plate than at mid-length. The stress distribution for simply-supported, edges restrained to remain straight in-plane are shown in Figure 3.8.

The ultimate strength is computed as follows:

Under a mean longitudinal stress σ_m, a plate with initial imperfection Δ_x will have a maximum displacement Δ_{max} expressed as

$$\Delta_{max} = m\Delta_x \tag{3.73}$$

where m is given by:

$$\frac{\sigma_m}{\sigma_{cr}} = \frac{m-1}{m}[1 + 2m(m+1)c \tag{3.74}$$

$$c = \frac{3}{16}(1-\nu^2)\left(\frac{\Delta_x}{t}\right)^2 \tag{3.75}$$

When thelongitudinal boundary stress has just reached the yield, the mean stress σ_m is computed as follows:

$$\sigma_m = K_{bs}\sigma_y \tag{3.76}$$

where

K_{bs} is defined as the secant effective width and is

$$K_{bs} = \frac{1 + 2m(m+1)c}{1 + 4m(m+1)c} \tag{3.77}$$

For given $\nu, \sigma_y, E, b/t, \Delta_x/t$, Equations (3.74) and (3.77) are simultaneous, and are easily solved to find m and K_{bs}.

For accurately calculating the effective width at collapse, allowance has to be made of - local plastic zones

which take place before the boundary stress reaches the yield stress, - transverse membrane stresses due to restraining of the edges to remain straight in-plane, - premature collapse of the panel before the boundary stress reaches the yield stress for panels with higher b/t ratios, - and finally, the effect of residual stress. To account for all these factors, if Δ_x is the measured imperfection, the initial imperfection has to be taken as given by Equation (3.80).

The stiffener and associated effective width so obtained constitute the effective column. The stiffened panel is then considered as an assembly of the effective columns. The load has an eccentricity e with report to centre of gravity of the effective column. The total eccentricity Δ, including the overall initial imperfection of the stiffened plate Δ_{sx} is given by:

$$\Delta = \Delta_{sx} + 1.2\ e \qquad (3.78)$$

Two modes of failure are analyzed, plate failure mode and stiffener failure mode. In each failure mode, the interaction of the overall column buckling for the entire panel is allowed for.

The criterion for the loss of stiffness of the plate is an attainment of a longitudinal membrane stress at the plate-stiffener boundary equal to the yield stress. The criterion for the stiffener initiated failure is either yield

(in compression or tension) or instability in the outstand.

This method is based on the Perry-Robertson formula and consists in analyzing the stiffened plates as a series of isolated struts, comprising the individual stiffeners and an associated effective width of plating.

The squash load is computed by adding the yield stress of stiffener, σ_{ys} times the area of the stiffener A_s, to a yield stress of the plate, σ_{yp}, times the area of the plate A_p. An ultimate load refers to the maximum load sustained by the stiffened panel.

Torsional buckling limiting stress σ_{yT} is the maximum allowable stress in the stiffener limited by lateral buckling.

Failure modes are treated in the following sections.

3.5.4.1 Plate failure criterion

It is assumed that the plate panel has initial imperfections similar in form to the buckled shape of an initially flat plate with simply-supported edges. In the analysis, the longitudinal edges (unloaded) are assumed to remain straight in-plane.

The effective plate stress is maximum at the mid-length of the stiffened panel, and is calculated by considering the behaviour of a strut with an initial equivalent sinusoidal imperfection Δ, so that the condition for the failure

of a stiffened panel of length L is given by Equation (3.79).

$$\sigma_y = \sigma_a^1 + \frac{\sigma_a^1}{\left(1-\frac{\sigma_a^1}{\sigma_e^1}\right)} \cdot \frac{a_o \Delta A^1}{I^1} \qquad (3.79)$$

where

a_o = distance between centroid of effective column and mid-plane of the plate

σ_e^1 = Euler stress $\pi^2 E I^1/(L^2 A^1)$

All primes refer to the effective columns (Figure 2.7a)

The solution of Equation (3.79) is the Perry-Robertson formula, Equation (3.83).

The collapse load of the panel for the plate failure criterion is computed as follows:

a) Compute the enhanced value of plate imperfection Δ_x^1, from the dimension of the panel and tolerance rules for the plate imperfection δ_{xm} (Equation (3.80)).

b) Compute the value of the secant effective width factor K_{bs} appropriate to Δ_x^1, by solving Equations (3.74) and (3.77).

and (3.77).

c) Compute the reduced value of the equivalent imperfection Δ (actual initial imperfection, Figure 2.4a, and eccentricity of end load) by Equations (3.81) and (3.82).

d) Compute the mean stress in effective column at collapse for plate failure, σ_a^1, by Equation (3.83).

e) The collapse load is given by Equation (3.84):

$$\Delta_x^1 = (\Delta_x + \frac{1}{2}\delta_{xm})\frac{b}{30t}\sqrt{\frac{\sigma_y}{245}} \qquad (3.80)$$

where

Δ_x = measured plate imperfection (Figure 2.4a)

δ_{xm} = fabrication tolerance (Merrison Rules)

$$\Delta = (\Delta_{sx} + 1.2e) - (\frac{L - L_o}{L}) \qquad (3.81)$$

$$L_o = 0.2\pi r\sqrt{E/\sigma_y}, \quad \text{when} \quad L > L_o \qquad (3.82)$$

$$= L \quad \text{when} \quad L \leq L_o$$

$$\frac{\sigma_a^1}{\sigma_y} = \frac{1}{2}\left[1 + (1+\eta)\frac{\sigma_e^1}{\sigma_y}\right] - \sqrt{\frac{1}{4}\left[1 + (1+\eta)\frac{\sigma_e^1}{\sigma_y}\right]^2 - \frac{\sigma_e^1}{\sigma_y}} \qquad (3.83)$$

where

$$\eta = A^1 a_o \Delta / I^1$$

and

$$P = \sigma_a^1 (K_{bs}\ bt + A_s) \qquad (3.84)$$

3.5.4.2 Stiffener failure

3.5.4.2.1 Tensile failure of stiffener

Failure may be initiated by tensile yield in stiffener outstands for panels with high slenderness (L/r) ratios. The condition for the maximum tensile fibre stress at the tip of a stiffener just reaching the yield strength, may be expressed as:

$$-\sigma_y = \sigma_a^{11} - \frac{\sigma_a^{11}}{(1-\frac{\sigma_a^{11}}{\sigma_e^{11}})} \cdot \frac{a_b\ \Delta\ A^1}{I^1} \qquad (3.85)$$

where

σ_a^{11} = mean stress in effective column at collapse for tensile failure in stiffener outstand

a_b = distance of tip of stiffener from centroid of effective section

σ_e^{11} = mean stress in effective column Euler stress.

3.5.4.2.2 Compressive failure of stiffener

This failure is the most critical because of the sudden collapse associated with it. In checking this failure mode, the secant effective width factor K_{bs} is taken as unity and the maximum compressive strength in the outstand is taken to be $\sigma_y^1 = 0.90\ \sigma_y$, or $\sigma_y^1 = 0.90\ \sigma_{yT}$, whichever is the lower. The reduction of 10% accounts for the excessively high residual stress.

The maximum compressive stress at the tip of the stiffener becomes equal to σ_y^1 when

$$\sigma_y^1 = \sigma_a - \frac{\sigma_a}{(1-\frac{\sigma_a}{\sigma_e})} \cdot \frac{a_b\ \Delta_1}{I} \qquad (3.86)$$

where

σ_a = mean stress at collapse of the cross column ($K_{bs} = 1$)

σ_e, A, a_b and I apply to the cross-column

$\Delta_1 = \Delta_{sx} + 1.2e$

a_b = distance of extreme fiber of tip of stiffener from centroid of effective section

The collapse load for this failure mode is given by

$$P = \sigma_a (bt + A_s) \qquad (3.87)$$

The above modified method has been compared with test and other theoretical results from other researchers, and it is deemed to have acceptable accuracy for stiffened panels containing plate panels with (b/t) ratios up to 70. For short fixed-ended columns, ($b/t \leq 70$ and $L/r \leq 20$), the modified "short column method" (Equation (3.88)), gives less conservative results, and may be used.

$$\sigma_{ult} = \frac{\sigma_{yp} A_p + \sigma_{ys} \Sigma A_s}{A_p + \Sigma A_s} \qquad (3.88)$$

where

σ_{ult} = failure stress for overall yield

A_p = plate area

ΣA_s = stiffeners area

σ_{yp} = mean stress in plate panel to cause plate failure

σ_{yo} = stress in stiffener to cause stiffener compression failure

3.6 MODEL ANALYSIS

As well as the considerable numbers of theoretical methods for ultimate strengths of box-girders, some research-

ers are considering the model analysis. This is the case of Parr and Maggard [149]. Their purpose was to formulate methematical relationships that would accurately predict load-displacement relationships gained from testing models, from which criteria may be proposed for ultimate strength analysis. Their models were unstiffened longitudinally, but with transverse diaphragms at various sections L/4, L/2, etc.

Although recognizing the influence of initial imperfections, the investigation did not account for them.

Regarding the buckling, the limit of elastic action was used as the upper bound for stability considerations. The simply-supported edge conditions were used during tests, but they also considered the possibility of partial restraint at the edges of an individual plate supplied by adjoining plates.

It was observed that the critical elastic buckling stress of the web plates was in excess of that of the yield point stress. Thus, the yield point stress would control if the limit of elastic action is taken as an upper bound. But, in many cases, the critical elastic buckling stress of the compression flanges was found to be below the yield point and in some cases, below the allowable working stresses. If simply-supported edge conditions are considered, it appears that the compression flange will buckle either below or near the yield point.

Care has to be taken for stability considerations. Premature buckling of the plates in both the flange and the web has to be prevented. The width-thickness ratios are of importance. In an allowable stress design, in order that buckling does not control the design, the plate elements are required to reach yield stress without buckling. In ultimate design, sufficient rotation for the realization of the highest possible ultimate load without premature buckling is required.

To develop the ultimate load, stiffeners subject to compression should possess sufficient b/t ratios and such required rigidity as that recommended by Massonnet [150] and Rockey [151]. Spacing of the longitudinal stiffeners is limited by the ratio width-thicknesses of $190/\sqrt{\sigma_y}$ and $412/\sqrt{\sigma_y}$ for the flange and web plates, respectively [99]. The vertical stiffeners subject to flexure may be designed as recommended by Cooper. It is observed that when the aspect ratios of the plates have a value greater than 1.5 to 2.0, their vertical stiffeners have little effect on the critical buckling stress of the plate.

Some factors which most affect the shear lag in a box section, have been considered. These are:

a) The span-width ratio of the flange elements

b) The width-thickness ratio of the flange elements

c) The external loading conditions, and

d) The boundary conditions at each end of the beam.

The ultimate flexural strength of a box-beam is given by

$$M_u = \frac{\sigma_y A}{2}(\bar{J}_1+\bar{J}_2) \qquad (3.89)$$

where

M_u = Ultimate resisting moment of the cross-section

A = cross sectional area (effective)

σ_y = yield stress

$\bar{J}_1, \bar{J}_2$ = distances from the neutral axis to the centroid of the area below and above the neutral axis, respectively

For the doubly symmetrical case, M_u is given as:

$$M_u = \sigma_y[\frac{bd^2}{4} - \frac{(b-t_w)(d-2t)^2}{4}] \qquad (3.90)$$

where

d = cross-sectional depth

b = flange width

t_w = web thickness

t = flange thickness

3.7 DISCUSSION OF THE SUGGESTED ULTIMATE STRENGTH METHODS

We have presented in this Chapter, a summary of about twenty suggested methods, based upon more than one hundred research works, in an attempt to carry out an accurate evaluation of the ultimate strength of plates and stiffened plates comprising steel box-girder bridges.

It is now well-established, that initial geometrical imperfections, welding residual stresses and construction imperfections, have a weakening effect on the buckling behaviour of plates, and also upon the ultimate strength of steel box-girder bridges. This weakening effect is greater in the practical range of width-to-thickness ratio (b/t) or slenderness (L/r), (Figure 2.1).

Due to the above reason, in evaluating ultimate strength, an account must be made of these weakening factors. This is a far from easy job for the researchers, and not less for the designer. Therefore, all theoretical and experimental works should be oriented to be as accurate as possible and their results should be then presented in a suitable form for use in design.

A careful analysis of all suggested methods herein presented, reveals that most methods are purely theoretical, and even well-elaborated ; their use in design seems to be

a tedious work. Some are computer-oriented solutions and would either be too expensive in computer time, or the capacity of most practical design engineering offices does not permit their use.

However, it may be pointed out that all these research works do constitute helpful means for the analysis of box-girder bridges. The problem is how safe all those presented approaches are, how economical and how they could be presented in a suitable and easy form for design. The form should be a set of curves or mathematical equations, set up in such a way as to enable the designer to understand either the structural behaviour of the bridge cross-section components, or the bridge structure, as a whole.

The elasto-plastic analysis given by Grave Smith [128], [129], is of great interest and could be extended to cover possibly greater ranges of practical width-to-thickness ratios or slenderness ratios.

The effective width method, as given by Abdel Sayed [115], could be extended to include such effects of residual stress and interaction between local plate buckling and overall panels, as to include stiffener participation.

The elastic large-deflection non-linear analysis of orthotropic plate shown by Massonnet and Maquoi [64], is of great importance for non-linear behaviour and could be used in

calculating the ultimate strength of steel box-girder bridges, such as that used to verify test results by Dubas [29] and the collapse of the Danube Bridge [64]. This method was proven to be accurate and could be extended to include the effect of residual stresses, and to clarify the failure mode (plate failure or stiffener failure), as pointed out by Little [136].

In evaluating the ultimate strength of a steel box-girder bridge, the boundary conditions of different components and interaction of local and overall buckling need to be considered, as outlined by Dwight [26].

The energy method by Sherbourne [36] could be of interest if it includes the effect of initial imperfection and residual stress, based upon careful test results.

The method by Dawson and Walker [67], based upon post-buckling behaviour of the imperfect plates, seems to be accurate, if used [73] to calculate the ultimate strength of a lipped channel with initial imperfection, subject to pure bending. This method could be extended to include residual stresses and other loading cases, as well as in dealing with stiffened plates.

The rigid-plastic mechanism method by Murray [37],[146] and continued later by Walker [147], was later extended [38] as an effective width method and could be deeply checked with

test results and recommended for use in design.

The secand effective width method by Horne and Narayanan [39],[40] could be regarded as an interesting design tool. The behaviour observed is similar to that by Murray [37],[38],[146]. This method has been checked with test results [39] and discussed in detail by a considerable number of researchers, and [159] specialists in this field. Following this criticism, some improvements have been made [40], but some modifications are still needed. The research by Horne and Narayanan are a part of an extensive research program undertaken in other English universities, following the Merrison Rules [14] with the purpose of carrying out design specifications for steel box-girder bridges.

This is the case in the numerical solution of moment-curvature-twist relationships given by Little [136], the effective yield method given by Dwight and Little [144], the finite element solution method given by Crisfield [82], and finite difference formulation given by Harding and Hobbs [142].

An empirical ultimate strengt.. method accounting for the effect of initial imperfection and interaction between local and overall buckling has been presented by Allen [95], but its use and accuracy is questionable.

Experimental results on a box-girder model have been reported by Parr and Maggard [149]. The model was stiffened transversally by an intermediate diaphragm but with unstiffened flanges and webs. The effect of initial imperfection and residual stress was not included. Therefore, further information is needed.

An observation of recent research works shows that most of them are being used in Great Britain, following the collapse of steel box-girder bridges which have caused a loss of human life [14],[20]. Others from Europe, are also from the failure of some bridges [17], such as, for example, the Koblenz Bridge, in West Germany and the Danube Bridge in Vienna. Another research program was undertaken in Australia, following the collapse of the West Gate Bridge [9].

A summary of these works, conducted in the United States, is given in Reference [18].

It may be concluded that more information is needed for the design of steel box-girder bridges. To our knowledge, little research works have been undertaken in this field in Canadian Universities. Some model studies on single-span composite box-girder bridges are being conducted at Waterloo University, and other results regarding the construction phase loadings have been presented by Green [152].

A considerable number of theoretical methods are proposed for investigating the structural behaviour of steel box-girder bridges. However, these methods mostly consider each component separately, as shown in the present study. It is also recognized that all those suggested methods need more experimental work before being recommended for design. It is for this reason, that the program of this research has been separated into two parts, analytical and experimental buckling behaviour of steel box-girder bridges.

For the analysis, it was considered necessary to proceed gradually as follows:

a) To collect available literature related to this topic,

b) To study these publications with the purpose of knowing what is to be done, and what needs complementary research,

c) To become familiar with typical structural characteristics of steel box-girder bridges,

d) To study and compare some design bridge standards [14],[22],[23].

For this analysis, four technical reports are provided [57], [153] - [155].

The experimental test is presented in Chapter IV, in which the buckling behaviour is investigated, considering the interaction between all the components comprising a cross-section, together with the effect of initial geometrical imperfections and the influence of the failure mode.

A comparison of analytical and experimental results is given in Chapter IV, and tentative design recommendations are given in Chapter V.

TABLE 3.1 EFFECTIVE WIDTH RATIO b_e/b AS GIVEN BY DIFFERENT AUTHORS

$$\eta = \frac{\sigma_{max}}{\sigma_{cr}}$$

η	EQUATIONS				
	(3.17)	(3.19)	(3.20)	(3.23)	(3.26)
0.2		0.986			
0.3	1.000	0.992			
0.4	0.973	0.956			
0.5	0.936	0.914			
0.6	0.898	0.874			
0.7	0.863	0.838			
0.8	0.831	0.806			
0.9	0.802	0.776			
1.0	0.776	0.750	1.000	1.000	1.000
1.1	0.752	0.726	0.953	0.949	0.955
1.2	0.730	0.705	0.913	0.907	0.917
1.3	0.710	0.685	0.877	0.871	0.885
1.4	0.692	0.667	0.845	0.840	0.857
1.5	0.675	0.650	0.816	0.813	0.833
1.6	0.659	0.634	0.791	0.790	0.813
1.7	0.644	0.620	0.767	0.769	0.794
1.8	0.631	0.606	0.745	0.751	0.778
1.9	0.618	0.594	0.725	0.735	0.763
2.0	0.606	0.582	0.707	0.720	0.750

The Effective Width Ratios b_e/b are plotted in Figure 3.4.

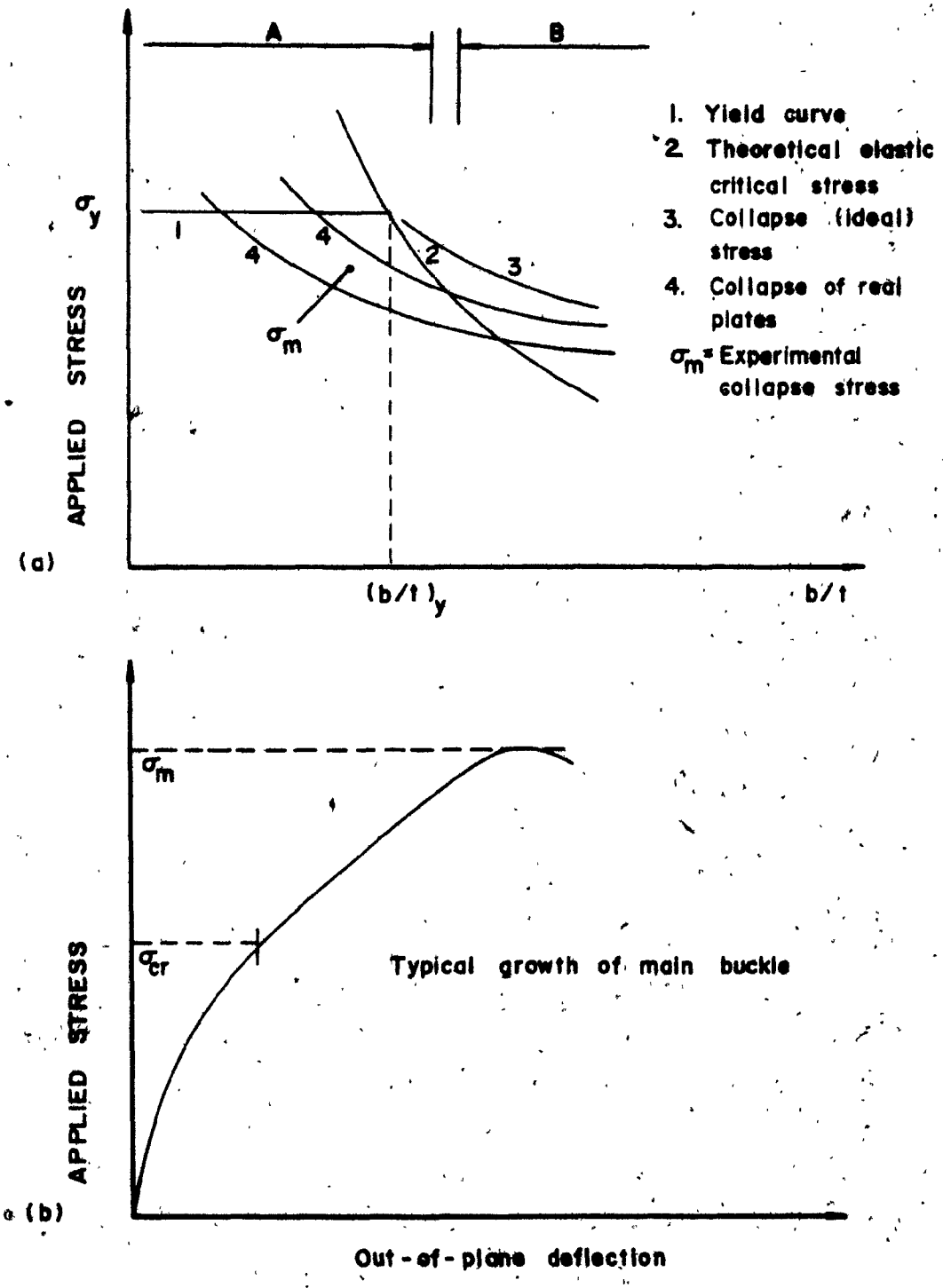

FIG. 3.1 INADEQUACY OF THE THEORETICAL ELASTIC CRITICAL STRESS σ_{cr} AS DESIGN CRITERION FOR SIMPLY SUPPORTED PLATE

a) APPLIED STRESS VERSUS (b/t)
b) APPLIED STRESS VERSUS OUT-OF-PLANE DEFLECTION

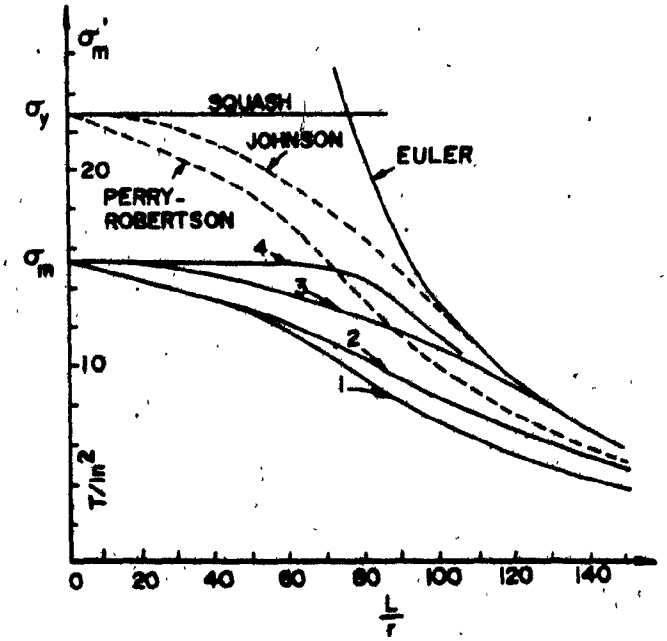

FIG. 3.2 VARIATION OF THE STRENGTH WITH LENGTH FOR A THIN-WALLED BOX COLUMN, $b/t = 60, \sigma_y = 23$ ton/in^2. CURVE 1 (BS 153), CURVE 2 (BS 449 (EQ.(3.5)), CURVE 3 (AISI (EQ.(3.5)), CURVE 4 (GRAVES SMITH[126] $\delta_o = b/500$)

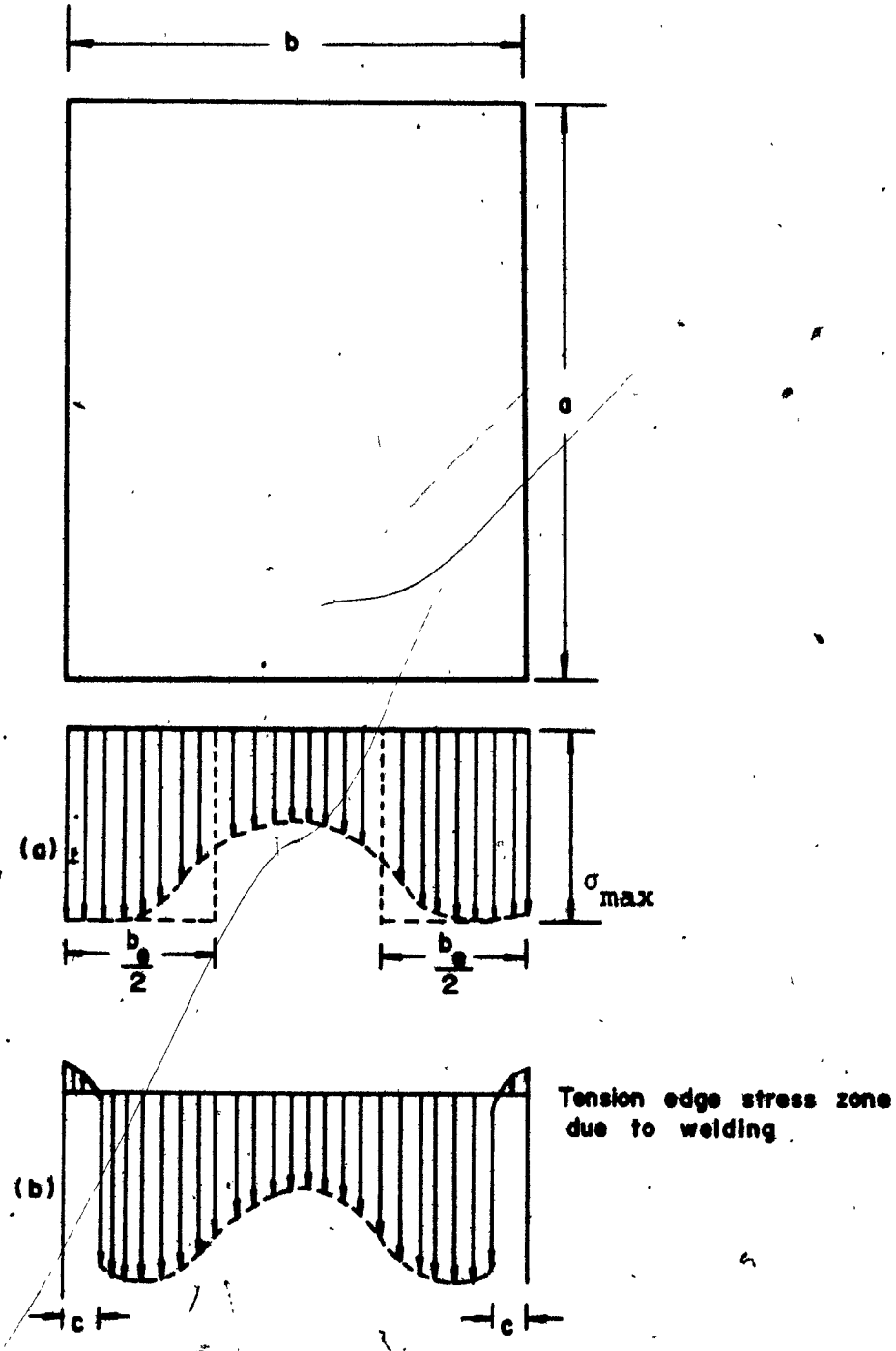

FIG. 3.3 EFFECTIVE WIDTH CONCEPT

a) EFFECTIVE WIDTH WITH TENSION WELDING EDGE STRESS NOT ACCOUNTED FOR; b) EFFECTIVE WIDTH WITH TENSION WELDING EDGE STRESS ACCOUNTED FOR

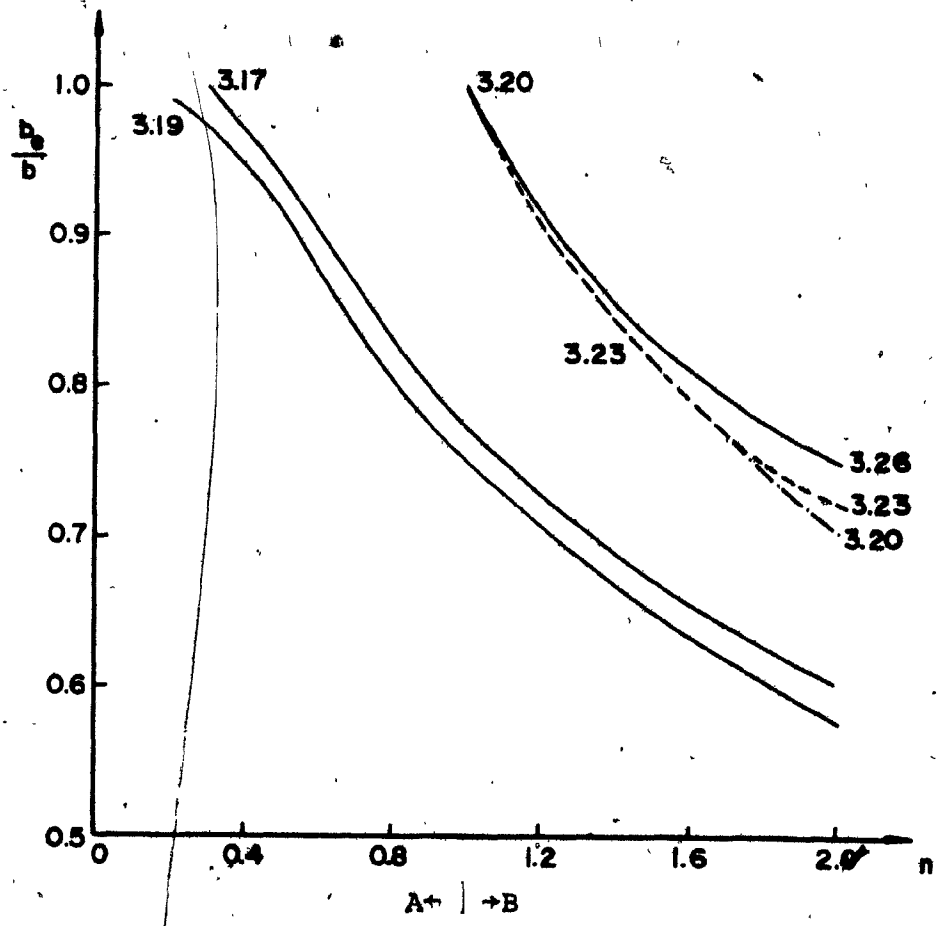

FIG. 3.4 COMPARISON OF EFFECTIVE WIDTH RATIOS be/b FROM DIFFERENT AUTHORS

FAULKNER (EQ.(3.17))
WINTER (EQ.(3.19))
KARMAN (EQ.(3.20))
PAPKOVITCH (EQ.(3.23))
MASSONNET (EQ.(3.26))

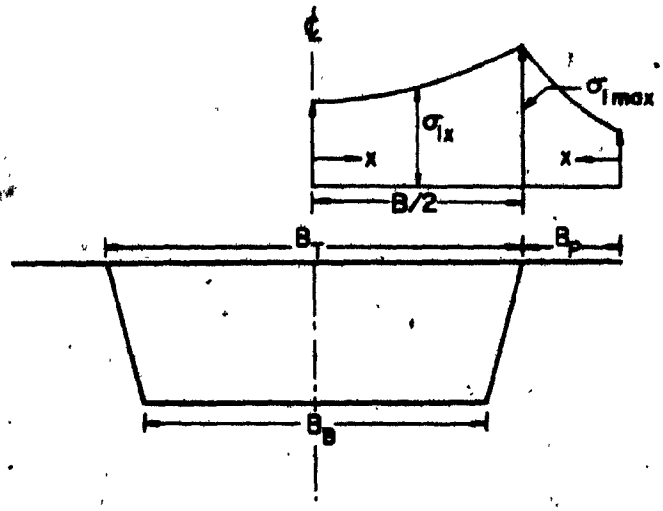

FIG. 3.5 DISTRIBUTION OF LONGITUDINAL STRESS σ_{1x} IN THE COMPRESSION FLANGE (EQS.(3.35) AND (3.36))

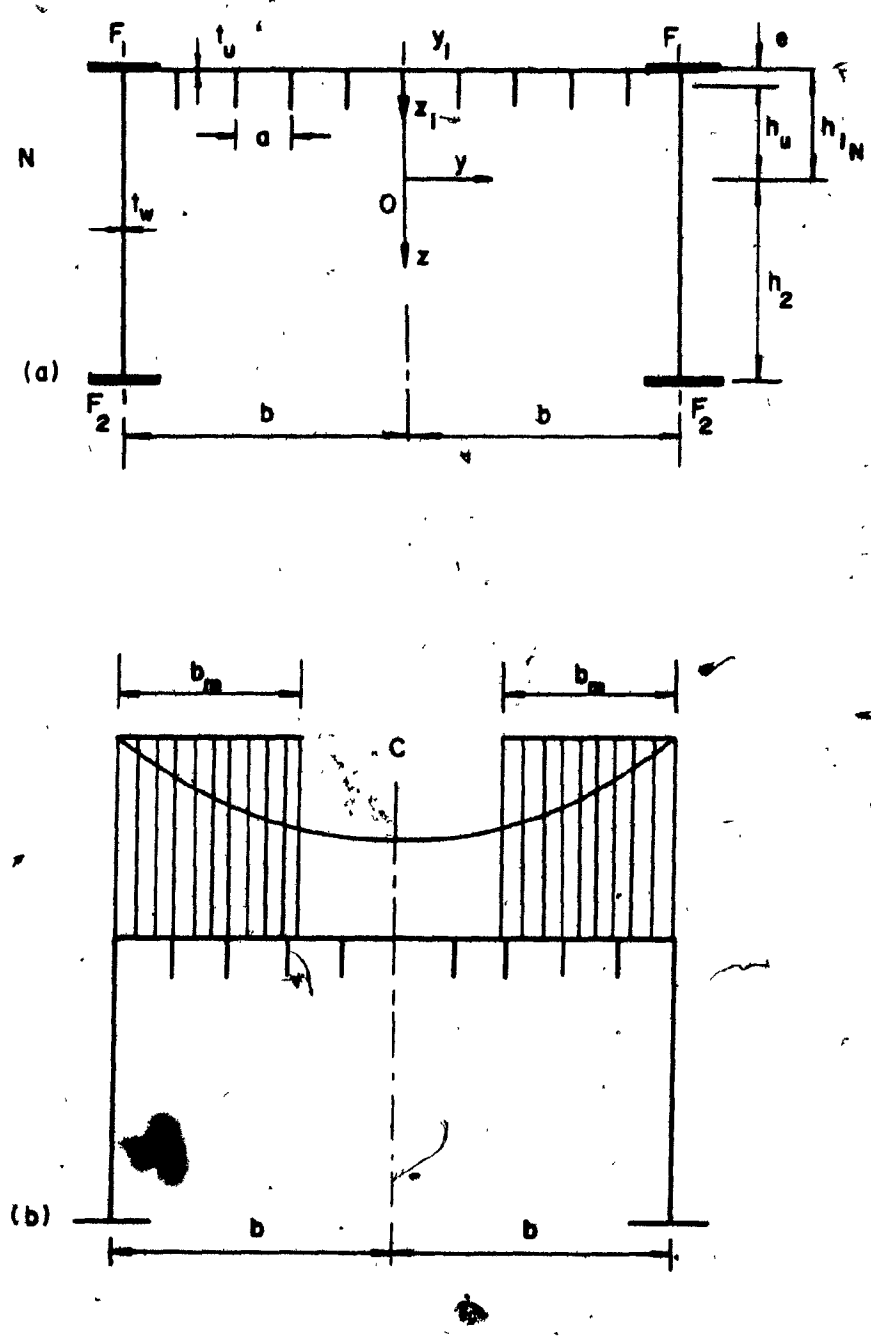

FIG. 3.6 EFFECTIVE WIDTH CALCULATION ACCOUNTING FOR ALL COMPONENTS OF THE CROSS-SECTION [112],[113]

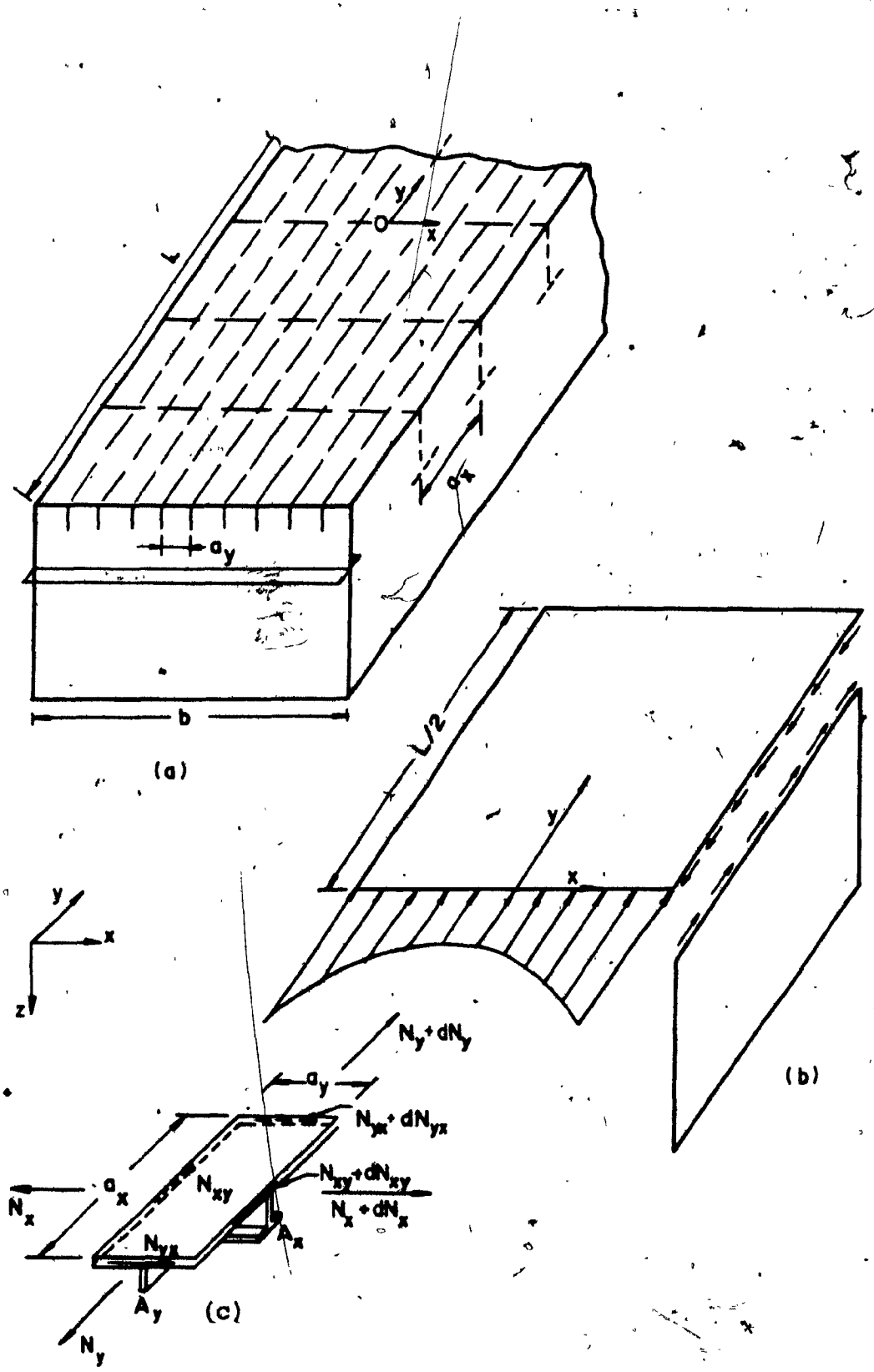

FIG. 3.7 BASIC ELEMENTS CONSIDERED BY ABDEL SAYED [114] FOR EFFECTIVE WIDTH CALCULATION

a) TYPICAL STEEL BOX-GIRDER, b) STRESS DISTRIBUTION ACROSS THE FLANGE AND AT FLANGE/WEB EDGE, c) EQUILIBRIUM CONDITION OF A BASIC ELEMENT

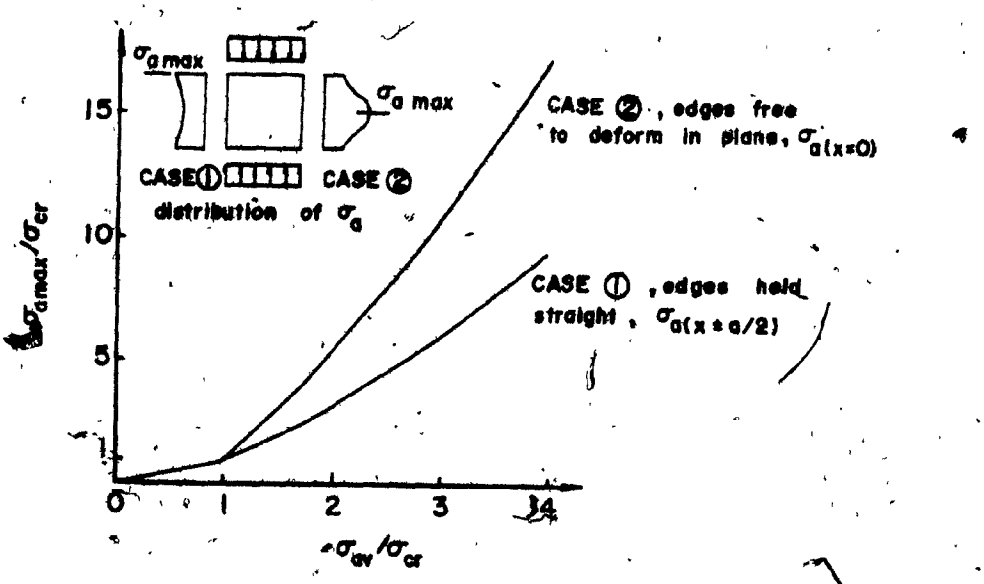

FIG. 3.8 EFFECT OF EDGE CONDITIONS ON THE MAXIMUM MEMBRANE STRESS FOR SQUARE PERFECT (NO INITIAL IMPERFECTIONS) PLATES

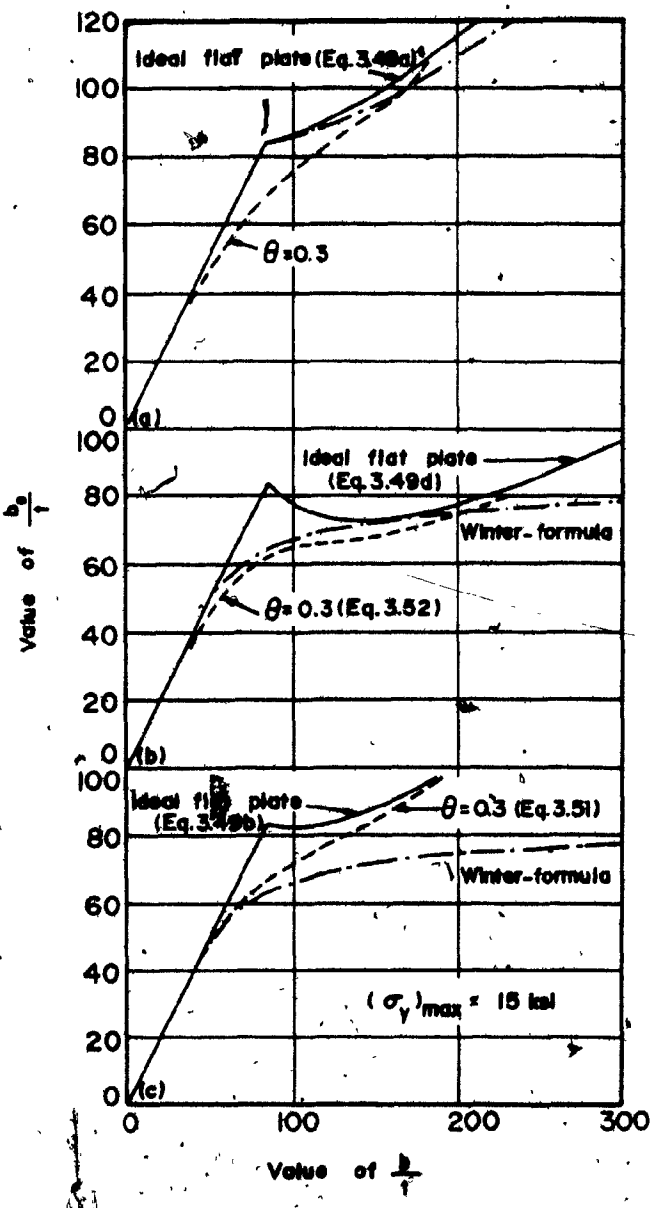

FIG. 3.9 EFFECT OF EDGE CONDITIONS ON EFFECTIVE WIDTH. COMPARISON OF RESULTS FROM DIFFERENT SOURCES be/t VERSUS b/t

a) LONGITUDINAL EDGES CONSTRAINED TO REMAIN STRAIGHT IN ITS PLANE, b) LONGITUDINAL EDGES FREE TO MOVE IN ITS PLANE (AVERAGE LONGITUDINAL STRESS AT EDGES ASSUMED TO BE GOVERNING), c) LONGITUDINAL EDGES FREE TO MOVE IN ITS PLANE (MAXIMUM LONGITUDINAL STRESS AT EDGES ASSUMED TO BE GOVERNING)

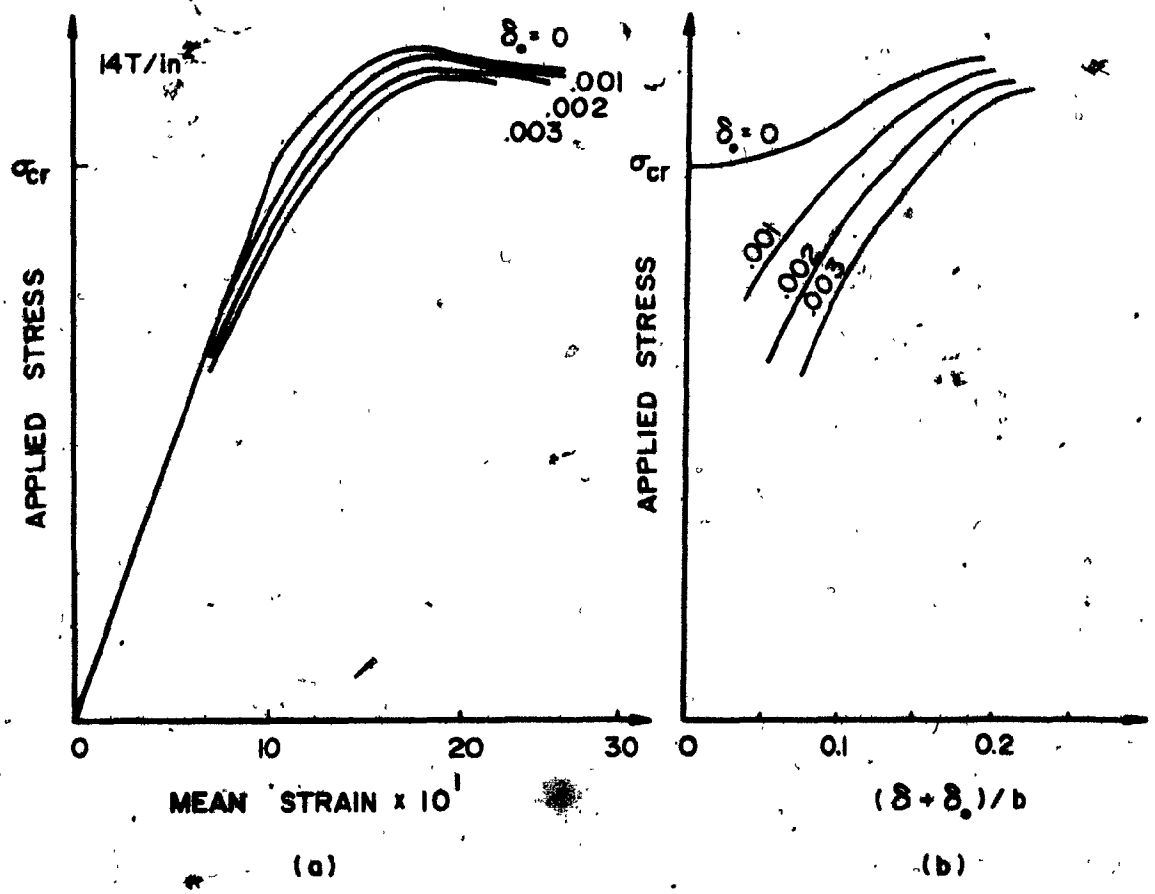

FIG. 3.10 EFFECT OF INITIAL IMPERFECTIONS ON THEORETICAL DEFORMATIONS OF A SIMPLY-SUPPORTED WEB [128], $b/t = 59$, $\sigma_y = 24$ ton/in^2

a) AXIAL SHORTENING, b) OUT-OF-PLANE DEFLECTION

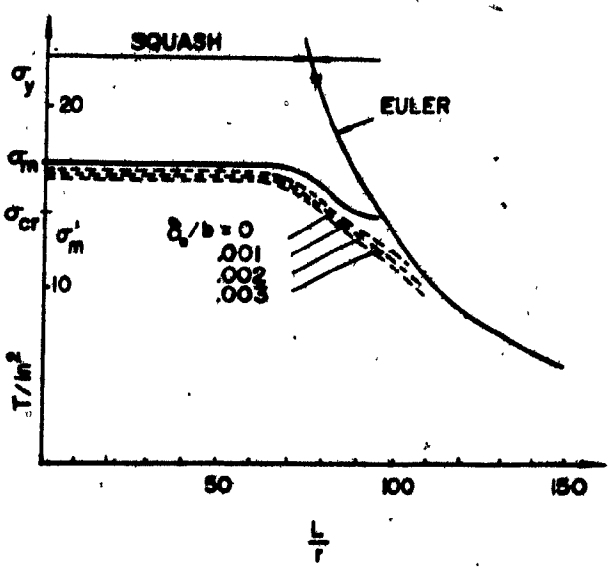

FIG. 3.11 THEORETICAL VARIATION OF STRENGTH WITH LENGTH FOR A SQUARE BOX-COLUMN [128] INCLUDING INITIAL IMPERFECTIONS, $b/t = 59, \sigma_y = 24$ ton/in^2

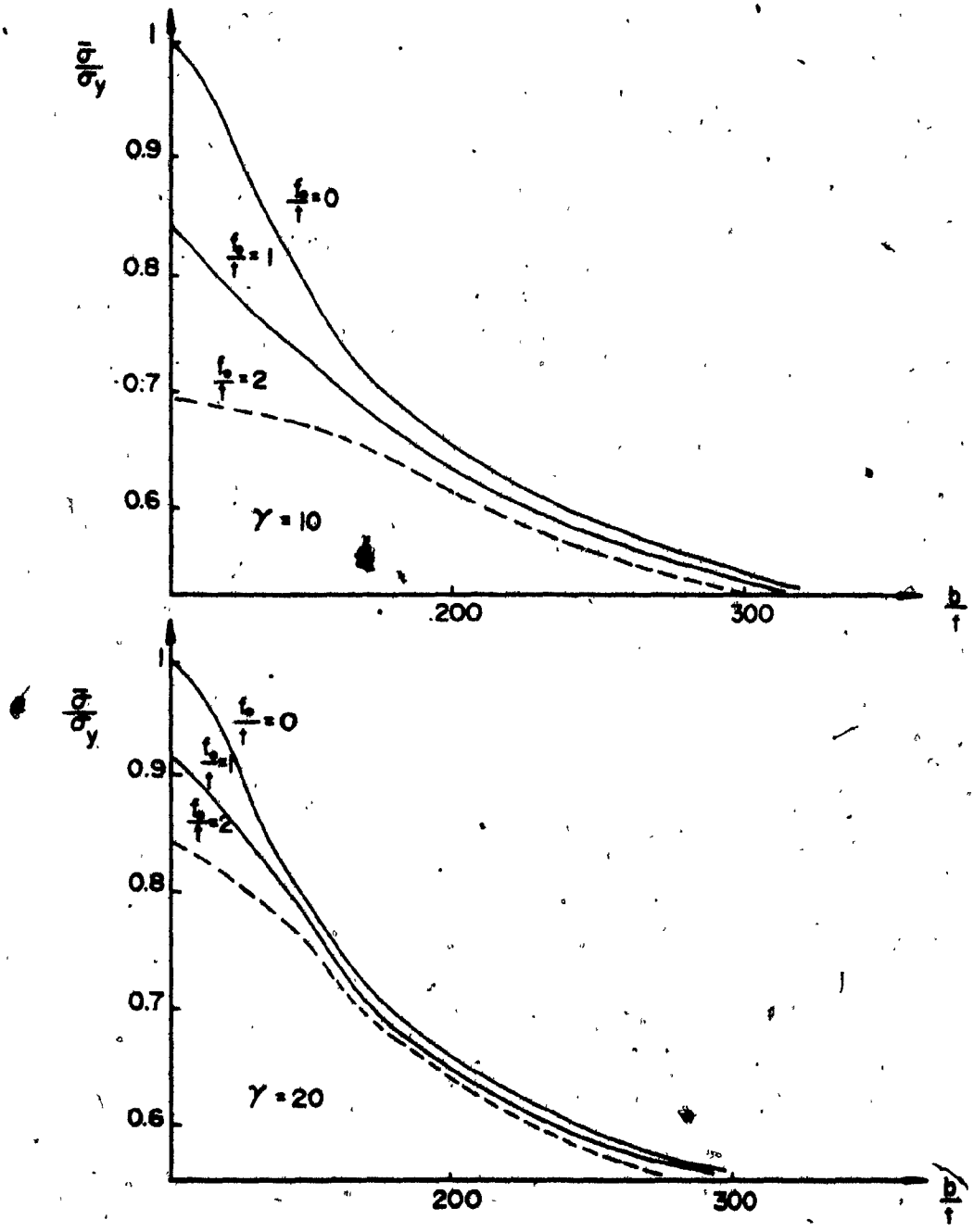

FIG. 3.12 CURVES GIVING THE ULTIMATE STRENGTH OF A STIFFENED PLATE WITH ONE MEDIAN LONGITUDINAL STIFFENER, INCLUDING THE EFFECT OF INITIAL IMPERFECTIONS [32].

a) STIFFENER RELATIVE RIGIDITY, $\gamma = 10$,
b) STIFFENER RELATIVE RIGIDITY, $\gamma = 20$.

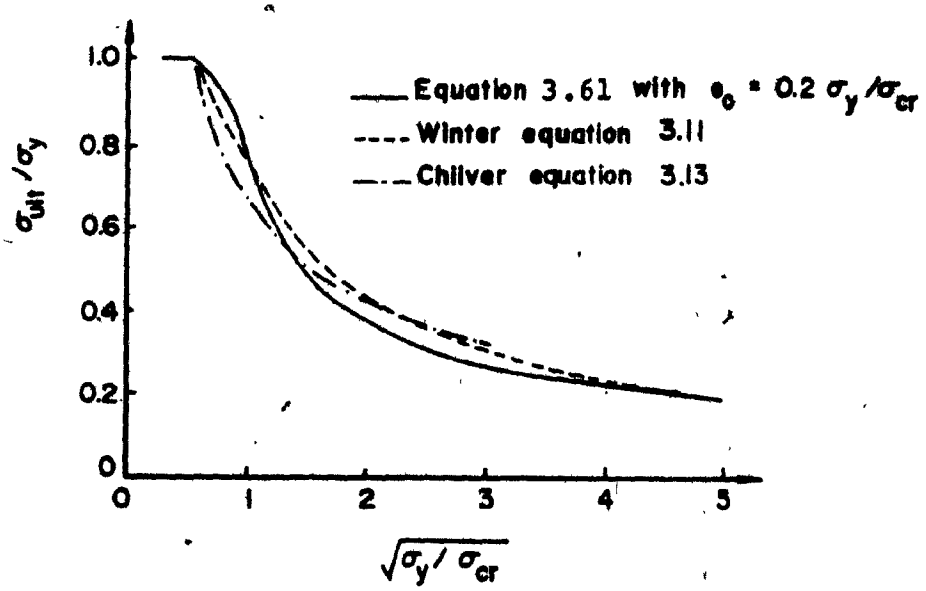

FIG. 3.13 COMPARISON OF GENERALIZED COLLAPSE CURVE USING RESULTS FROM DIFFERENT SOURCES

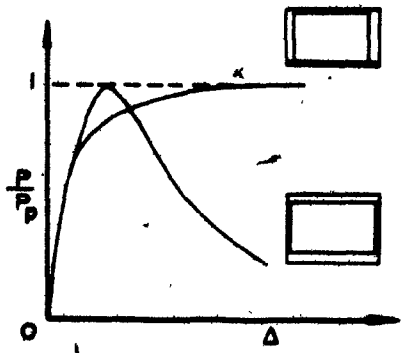

FIG. 3.14 VARIATION OF LOAD-CARRYING CAPACITY CURVES OF TWO BOX-GIRDER BEAMS [146]

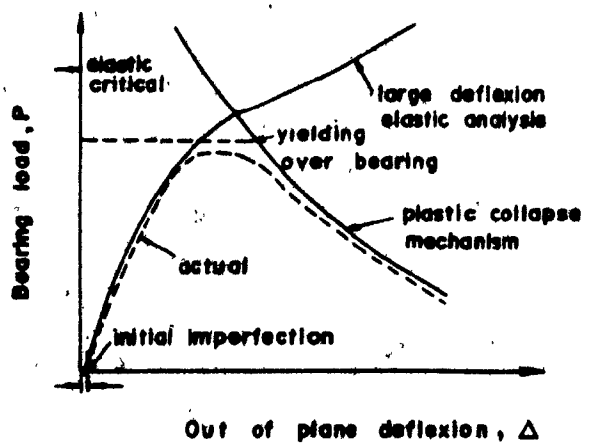

FIG. 3.15 COMPARISON OF ELASTO-PLASTIC THEORY WITH OTHER METHODS

CHAPTER IV

EXPERIMENTAL ANALYSIS OF BUCKLING BEHAVIOUR OF STEEL BOX-GIRDER BRIDGES

CHAPTER IV

EXPERIMENTAL ANALYSIS OF BUCKLING BEHAVIOUR OF STEEL BOX-GIRDER BRIDGES

4.1 INTRODUCTION

In Chapter I, a brief note on the deficiencies of the actual analysis methods in considering some important factors which may influence the buckling capacity of plates and stiffened panels has been outlined.

In Chapter II, the influence of initial geometrical imperfections, of residual welding stress and of the construction and erection imperfections on the buckling capacity of steel box-girder bridges has been explained.

In Chapter III, some theoretical analytical methods for the ultimate buckling strength including the effects of imperfections, have been reported and discussed.

In the present Chapter IV, a full investigation program of the experimental tests made upon three models of steel box-girder bridges is reported, and the experimental results are compared with the theoretical results from Chapter III.

As explained in Chapter I, a steel box-girder bridge is an assembly of thin plates and stiffened panels. Its

buckling behaviour may be analysed by first considering each component separately and, secondly, considering all components together.

Considering each component separately, may be reliable only if attention is taken in assuming suitable boundary conditions capable of providing existing interaction between adjacent components, for example, a plate and stiffener, a web and flange, a web - transverse diaphragm - flange.

Although more complex, considering all components together is more reliable in that it provides the real state of interaction between the components, and the influence of each may well be observed.

Following the collapse of various modern steel box-girder bridges [5] - [8], many theoretical research works have been reported, dealing with plates and stiffened panels. However, very limited experimental results are reported. It is recognized [18] that more experimental tests are needed before defining accurate design recommendations dealing with steel box-girder bridges. Such experimental tests should account for those special factors associated with steel box-girder bridges, mainly the interaction between the components, the influence of initial geometrical imperfections, and of welding residual stresses, which influence is deemed to be greater in the intermediate range (most practical) to b/t ratios. Also, post-buckling behaviour needs more experimental

tests. The program of this research deals with these recommendations.

It may be recalled here, that the objective of this research program has been to study the buckling behaviour of steel box-girder bridges, mainly the compression flange, considering the following parameters which are believed to influence its ultimate strength:

a) The influence of stiffener spacings and rigities, and the required rigidity for the stiffeners to remain rigid up to and after the buckling of the plate.

b) The influence of the initial geometrical imperfections of the plates, the stiffeners, as well as of their overall imperfections, and of residual welding stresses.

c) The interaction between the web and flange, as well as their influence on the overall failure mode.

d) The influence of the failure mode on the overall strength, post-buckling behaviour.

Three models have been tested. For each model, the initial geometrical imperfections have been measured for each component, and including their overall imperfections.

The loading was maintained even after reaching the collapse criteria. This enabled the development of the full

failure mechanism and important observations have been made for the post-buckling stage.

The experimental investigation can be logically divided into five steps: design, fabrication, preparation, testing and interpretation of the results. The contents of this Chapter are presented, according to this logic.

4.2 GEOMETRICAL PARAMETERS OF THE THREE MODELS

Three models have been designed in such a way as to cover the influence of each parameter explained in the preceding paragraph. The compression flange has been stiffened with three longitudinal stiffeners, spaced at 10-1/2 inches for Model A, and four longitudinal stiffeners have been spaced at 8-1/2 inches for Models B and C. This gives a ratio b/t of 56 for Model A and 45 for Models B and C. Then, the tests cover the intermediate range, where the influence of initial geometrical imperfections and residual welding stresses is critical (Figure 2.1b).

The rigidity of longitudinal stiffeners is the same for Models A and B, and is increased for Model C.

As a result, the comparison of Models A and B give the influence of stiffener spacings, while the comparison between Model B and Model C give the influence of stiffener rigidities.

The capacity of the stiffeners to remain straight up to the buckling of the plate will be demonstrated during loading.

Web plates are stiffened with vertical stiffeners on both sides, spaced 45 inches apart, and with a one-sided longitudinal stiffener located at 0.20d from the compression flange. The location of this longitudinal stiffener is the optimum location in preventing lateral buckling of the web plate due to bending stresses, and therefore, the premature vertical buckling of the compression flange.

In a plate girder, this longitudinal stiffener location increases the allowable maximum slenderness ratio required for the web to develop the yield stress moment capacity of the girder without buckling, from 170 to about 450.

The minimum thickness of the elements was chosen to permit the use of the minimum weld size of 3/16 inches, as specified in bridge design standards [22],[23]. Except for longitudinal stiffener spacings and rigidities in the compression flange, the remainder components are the same in the three models.

To permit access inside the model during loading, the tension flange (bottom flange) is concentrated toward the webs. To provide torsional stiffness of a closed section, transverse bracings have been provided. This substitution

was used by other researchers [21],[28],[29],[64] and is believed to be acceptable.

Some modifications have been made during testing, for example, in Models B and C, additional transverse stiffeners have been added to the web end panels to permit the full development of the post-buckling mechanism in the deck before collapse.

Figure 4.1 shows the geometrical arrangement of Model A, and Figure 4.2 for Models B and C. The dimensions of all components are given in Table 4.1, and Table 4.2 gives the structural properties of the three models.

Using the classical elastic plate buckling theory as design criteria, this geometrical arrangement gives a relative optimum rigidity for the compression flange longitudinal stiffeners of 1.3, 1.6 and 3.36 for Models A, B and C, respectively. Those ratios are 1.14, 1.05 and 1.9 for transverse stiffeners.

For the web end panels, the aspect ratio a/b is 3.13 for Model A and 1.04 for Models B and C. For the web middle panels, the aspect ratio a/b is 3.13 in all three models. Table 4.3 gives a summary of those relative structural parameters.

The three models have been designed in accordance with the analysis method given by the Canadian bridges Standards

[23] for composite girders, with regard to the compression flange and webs. The steel used for all components is G40.21 44W with a modulus of elasticity of 29,000 ksi.

4.3 FABRICATION

All three models were fabricated in a well-equipped steel shop for handling and assembling thin plates. Pieces have been cut and identified before assembling them together. Care was taken during all of the fabrication processes to keep the sequence of operations as currently used for the bridge components' shop fabrication. Welding was made by a licensed welder. All welds are continuous and are 3/16 inch in size, which is the minimum required by bridge design standards [22],[23].

All remarkable distortions or imperfections were identified and noted. For example, Figure 4.3 shows the distortion of longitudinal web stiffener plates.

Figure 4.4 to Figure 4.7 gives an idea of the fabrication process. Longitudinal deck stiffeners are cut at transverse stiffeners and are continuously welded at the plate and at the transverse stiffeners. Transverse stiffeners are also continuously welded at the plate, as are those for longitudinal and transverse web stiffeners.

4.4 MEASUREMENT OF INITIAL GEOMETRICAL IMPERFECTIONS

As already explained in Chapter II, it is important to measure the initial geometrical imperfections of all components to determine their effective magnitude and shape with the purpose of seeing how they may affect the buckling behaviour.

This has been accomplished by designing a special reading track, capable of moving in three directions and using a dial gauge with 1/1000 inch graduation. The reading track is shown in Appendix A. Figure 4.9 shows the track when taking the reading.

The results of the initial imperfection readings are plotted and compared with the deflections due to loading.

4.4.1 Deck (Compression Flange)

The compression flange is divided into a grid form with a 9 × 17 matrix (Figure 4.8a) for Model A, and an 11 × 17 matrix (Figure 4.8b) for Models B and C. This enables a reading of 153 and 187 points, respectively, on a surface of 42 × 90 inches. Such sub-division accurately shows the initial shape of the deck. Figure 4.9 shows a typical reading of initial imperfections of the deck.

4.4.2 Web Plates

As for the deck, the web plates have been sub-divided into a 9 × 17 matrix (Figure 4.8c) and the initial imperfections in the lateral direction are read on an 18 × 90 inch surface.

4.4.3 Longitudinal Stiffeners

Although initial geometrical imperfections Δ_{sx} in the vertical direction, are read when measuring those of the deck, it was also necessary to read the initial imperfections Δ_{sy} in the lateral direction. This has also required a special design tool, as shown in Figure A.3. Readings are at every 5-5/8 inches in the longitudinal direction.

The same was made for the longitudinal web stiffeners.

4.4.4 Overall Initial Imperfections

Overall initial imperfections in the transverse direction are measured when taking a reading for the deck, while those in the longitudinal direction are taken by reading both on the deck and on the tension flange.

4.4.5 Results of Initial Imperfections Measurement

The results of initial geometrical imperfection measurements are given in Appendix A, Tables A.1 to A.7. Figure 4.10 to Figure 4.17 are typical curves of those initial measured imperfections.

The comparison of Model A (Figures 4.10 and 4.11) and Model B, (Figures 4.12 and 4.13), lead to the conclusion that, in both the transverse and longitudinal directions, the local plate imperfections are less pronounced if the number of stiffeners is increased. The same result is obtained if the rigidity of the stiffener is increased as it is concluded, by comparing Model B and Model C (Figures 4.14 and 4.15), but this latter case is true only for panels having the same number of stiffeners. In the transverse direction, the peak values represent the local maximum plate imperfections between two longitudinal stiffeners. In Model A, those peak points are more pronounced than in Models B and C.

In the longitudinal direction, the local imperfections are almost negligible when compared with those of the overall imperfections. The influence of the middle transverse stiffener (point 9 in Figures 4.11, 4.13 and 4.15) on the overall imperfection in longitudinal directions, is well evident. This influence will again be predominant in the loading stage, as is demonstrated in Sections 4.6.3 and 4.6.5 for the buckling

behaviour of the compression flange and the overall buckling behaviour of the whole model.

Figure 4.16 is a typical curve of measured overall initial geometrical imperfections of the tension flange and web longitudinal stiffeners. Those overall imperfections of the tension flange, measured along the web lines, have been found to influence the overall deflection curve of the model due to loading. The web longitudinal stiffeners buckling, as explained in Section 4.6.4, is also influenced by the shape and direction of their initial imperfections.

Figure 4.17 shows typical initial lateral imperfections of the web panels and the lateral deformation due to loading. It may be observed that up to the beginning of the post-buckling stage, the shape and the direction of initial imperfections influence the lateral deformation.

The variation observed of the initial geometrical imperfections, Figures 4.10 to 4.16, lead to the conclusion that their average values may be computed only on the basis of numerical integration. This was accomplished by using the Simpson Rule method, and after numerous calculations, the following average values are given.

For plate between the longitudinal stiffeners, a local initial imperfection is of the order of b/170 in transverse direction (Δ_y) and a/340 in the longitudinal direc-

tion, (Δ_x). This may be compared, according to the Merrison Rules [14].

For longitudinal stiffeners, the initial imperfection in the vertical direction Δ_{sx} is of the order a/700 and that in the lateral direction Δ_{sy} is $t_s/7$, as compared to a/640 and $t_s/9$, according to the Merrison Rules [14].

Tables 4.4 and 4.5 give a complete comparison figure of the average initial imperfections measured and their expected values, according to the Merrison Rules [14].

Regarding the overall imperfections, it may be observed from Figures 4.10 to 4.16 that, in both the transverse and longitudinal directions, the initial imperfections may be represented by a trigonometric function, cosine or sinusoidal.

$$w_o = \delta_o \cos\frac{m\pi x}{a} \cos\frac{n\pi y}{b} \qquad (4.1)$$

However, the question is the number of waves to be used in each direction. For narrow box-girders, with the spacing of transverse stiffeners (cross-beam) equal to the spacing of the two webs, one-half wave may accurately be used in transverse direction. In general, the number of waves will be a function of transverse stiffener spacings as compared to that of the width between the webs, and is also a function of relative rigidity for both longitudinal and transverse stiffeners.

In longitudinal direction, if the spacing of transverse stiffeners is ± five times the spacing of the longitudinal stiffeners, one-half wave may be used. In general, the number of waves will again be a function of the spacing and relative rigidity of the longitudinal and transverse stiffeners.

The magnitude of the mean overall imperfection δ_o was found to be b/120 in transverse direction, and a/850 in longitudinal direction. They are compared with the values from the other sources described in Table 4.6.

4.5 LOADING

4.5.1 Loading Conditions

Loading Conditions are conducted in such a way as to produce compression in the deck and tension in the bottom flange. Figure 4.18 shows the idealisation of these loading conditions and Figure 4.19 shows the real testing ring arrangement. Figure 4.20 is overall view during testing.

Longitudinally, the model is divided into four equal panels. The load is applied at its ends (upward direction) with one jack at each end. The reactions are taken by transverse beams, located at quarter points from the ends of the model.

Those loading conditions produce pure bending in the two interior panels, and bending and shear in the two end panels.

All testing rings are shown in Appendix A.

4.5.2 Strain Gauges Location and Reading

For testing each model, one hundred strain gauges were used, 45° rosettes for the plate between the stiffeners and single gauges for the stiffeners and webs. The gauges were located at two transverse sections, 5 and 9, for Model A, and at three transverse sections, 5, 9 and 18, for Models B and C. Figures 4.21, 4.22 and 4.23 show the strain gauge location sectors of the three models.

With such strain gauge locations, the deformation mechanism of the model can be well recorded and plotted at each loading stage.

The strain gauges were located at the mid-span and at the tip of the outstand for longitudinal and transverse stiffeners of the deck, and at the mid-span and mid-width for longitudinal web stiffeners. All the results of the strain gauge readings are given in Appendix A, Tables A.41 to A.61.

The strains in the model were read with strain gauges connected to the strain-gauge Data Logger, Model B&F SY 161, (Figure ~~3.20~~), enabling a direct reading of the real strain in the model.

4.5.3 Deflection Readings

It was necessary to read at every loading step, the deflection and deformations of the model. Then, the deformation mechanism was defined at every stage.

For the deck and the webs, the same grids as those for the initial geometrical imperfection readings were used, as well as the same developed reading machines. Although the overall deflection in the longitudinal direction is read directly on the deck along the web lines, a check was made by using dial gauges located under the tension flange. Figure 4.24 shows the locations of these extra dial gauges. A reading of the course of the jack piston gives the displacement of the two ends of the model.

4.5.4 Observation of Deformation Lines

Identification of the deformation lines is important in that the initial deformations of the model can be identified and subsequent deformation mechanisms can be observed at every loading stage.

This has been kept in mind and care has been taken to place lime on the model (Figure 4.25) directly, before placing the model into the loading frame. Then, the initial deformation due to handling was noted, and further deformations under the load were easily identified. Figure 4.26 shows

how it was possible to identify the deformation mechanism in the deck and web panels.

4.5.5 Application of Load

As already mentioned in Section 4.5.1, the load is applied by two hydraulic jacks of 300.0 ton capacity, each located at the ends of the models. The jacks are double-acting and pressure is simultaneously provided in both by a pump connected to them, (Figure 4.20). The pressure was then equalized in both jacks at each loading step. It was possible to check this with a dial gauge located on each line, and also by the course of the jack's piston at each end.

Each jack has an effective area of 93.0 square inches and the pressure was increased by an increment of 100.0 psi; then the applied load was increased each time by 9.3 kips.

At each load increment, the reading of the strains was taken with the Data Acquisition System and the deflections read with the reading machine, and dial gauges.

The load was increased up to complete failure, until the pressure in the jacks did not increase any further. After this moment, the jack started to lose pressure. Any attempt to increase the pressure resulted in increasing the course of the jack's piston and continuous development of the failure mechanism.

4.6 RESULTS

In this section, a complete interpretation of the experimental results is made. Wherever possible, curves are plotted for easy understanding of the results. The analysis is made in such a way as to cover all points of the objective of this research. For the sake of clarity, we will proceed point-by-point.

The influence of initial geometrical imperfections is analysed by comparing their shape and direction to those deflections or deformations due to loading, from the local buckling stage to the overall post-buckling behaviour.

The influence of stiffener spacing in the compression flange is investigated by analysing the local plate buckling mechanism and the overall buckling mode in all three models. The influence of the stiffener rigidity is analysed, on the basis of strain (stress) distribution and on their performance, both in local and overall post-buckling stages.

The interaction between the web and compression flange is analysed on the basis of their reciprocal influence on the buckling behaviour of each, and on the overall failure mechanism. The influence of the failure mode on the ultimate strength is studied by considering the post-buckling behaviour, failure mechanism and abruptness or speed of their collapse. Finally, the ultimate strength is calculated by

some proposed analytical methods from Chapter III, and a comparison is made with the experimental results.

4.6.1 Comparison of Initial Geometrical Imperfections and Deflections Due to Loading

In the present study, special attention has been paid to the importance of considering the influence of initial geometrical imperfections on the buckling behaviour of steel box-girder bridges and upon their ultimate strength. This influence is summarized in Figure 2.1. As explained in Chapter II, initial imperfections produce internal eccentricities which add to the load eccentricities and the final effective eccentricity, which influences the mode of buckling, is the algebraic sum of these two eccentricities. Due to these internal eccentricities, the load deflection curves may be non-linear.

The influence of those initial imperfections may also be demonstrated by plotting them on the same curves as the deflections or deformations due to load. This shows, at every loading stage, the variation of the deformation mechanism and may be compared with the initial shape of the element. For the above reason, the deflections of all components have been recorded at every load increment. Then, the deformation mechanism can be plotted. Figures 4.27 to 4.32 are examples of the comparison of the overall initial geometrical

imperfections of the compression flange in both the transverse and longitudinal directions, with the deflections due to load. Their shape and directions may be compared.

It has been observed in all three models, that the local buckling of both plate and stiffeners have the shape and direction of their initial imperfections. This has an influence on the direction and mode of the overall buckling, except in some cases, where the overall buckling mode developed in the opposite direction.

Even in the overall buckling mode, the influence of initial imperfections is again evident. It may be observed in Figures 4.27 to 4.32, that deflections due to load have the same shape as initial imperfections, and their peak values are almost at the same locations, except when the overall buckling mode is more advanced (post-buckling stage); then, the deflections may change their shape and direction.

In the web panels, the weakening effect of initial imperfections is believed to be compensated by the post-buckling reserve strength due to the formation of the tension field action. But it can be observed in Figure 4.17, that the lateral deflection of the web panels is influenced by the shape and the direction of initial imperfections. As the post-buckling mode is, to a certain extent, influenced by the buckling mode, therefore, even for the web panels, the initial imperfections do have a weakening effect.

4.6.2 Distribution of Strains (Stresses)

The distribution of strains and, consequently, the distribution of stresses in both the longitudinal and transverse directions at different loading stages, is important in that the behaviour of the elements is shown, and it also serve as the basis for establishing design criteria, such as the effective width method, the equivalent thickness concept, the column treatment approach and the failure criteria, as explained in Chapter III.

Important observations may be made from the strain distribution. For example, the failure criteria of the compression flange is considered to be reached, once the longitudinal stress reaches the yield stress value at the web/flange edge. The effective column formed by the longitudinal stiffener and the associated plate on each side, is assumed to reach its maximum strength, once the stress at mid-length reaches the yield value.

The strain distribution may show the displacement of the neutral axis of the whole cross-section at every loading stage. This is used as the criteria for the participation of the stiffeners in the overall strength. When analysing stiffened panels, the location of the neutral axis of the plate stiffeners element is always a problem. Some designers consider the neutral axis of the plate element, itself. Others, the neutral axis of the plate and stiffener, together. This

disagreement may lead to different allowable limits. Only experimental tests may show the accuracy of each alternative.

In the present study, the strains in all the elements have been recorded, plotted and analysed to study the behaviour of each component. As explained in Section 4.5.2, the strains have been measured at two transverse sections of the compression flange and in the web panels, as shown in Figures 4.21, 4.22 and 4.23 for the three models.

In the compression flange, the two transverse sections are termed 9 and 5. Section 9 is at the mid-span of the model at the middle transverse stiffener location, and Section 5, is at the middle of the panel, between the two transverse stiffeners.

According to the loading conditions (Figure 4.18), transverse Sections 9 and 5 are located in the part subjected only to bending. For Models B and C, strains also have been measured at transverse section 18 (Figures 4.22 and 4.23), located in the compression flange end panel. This part is subjected both to bending and to shear.

In the following sections, strain (stress) distributions are analysed and commented upon for all three models. For discussion, the longitudinal strain ε_x (Figures 4.33 to 4.35) is used, although the same analysis may be based on both strains ε_x and ε_y (Figures 4.36 to 4.38).

4.6.2.1 Model A - Transverse distribution of longitudinal strain ε_x

A) At Section 9: (Figure 4.33a)

At 500 psi, the distribution of ε_x is already far from uniform. There are peak values at the centerline of the two middle sub-panels. It can be observed that, at every loading, the maximum strain ε_x is located at the web/flange edge and at the centerlines of the two middle sub-panels. Once the strain at the web/flange ε_{xe} has reached the yield strain, ε_{yi}, any increase in loading results in an increase of ε_{xe} with the diminution of ε_x within the plate. This is proof that once ε_{xe} reaches ε_{yi}, the plate has become a mechanism and does not sustain any load. This is a point of achievement of the ultimate strength criteria used by some designers such as Skaloud [158] and Massonnet [64].

It is interesting to note here that, at the location of the transverse stiffener, the distribution of longitudinal strain ε_x and, consequently, of the longitudinal stress σ_x is not maximum at the longitudinal stiffener locations, as it generally is expected for the longitudinal stiffeners to be considered as T-beams (stiffener and effective plate width on each side). The fact that the maximum or peak values are located at the centerlines of the two middle sub-panels, may be due to the influence of the web/flange boundary conditions,

which produce the maximum ε_{xe} at this location.

Using this strain distribution, it seems to suggest that, if the ultimate strength of a stiffened panel is to be calculated on the basis of stress distribution of the section at a transverse stiffener location, it may be more realistic to use the equivalent thickness method, rather than the T-beams (effective width) approach.

The equivalent thickness method is the one in which the whole stiffened panel cross-section is substituted by a plate that has the same cross-sectional area as that for the same given width, Equation (4.2).

$$bt_e = bt + nA_s \tag{4.2}$$

where

t_e = equivalent thickness of the plate, and

b = width of plate between the webs

t = plate thickness

n = number of stiffeners

A_s = area of stiffener cross-section

In general, the strain distribution shows a concentration at the flange/web edge with a pocket across the panel. Local pockets represent the loss of stiffness of plate elements, and the general pocket represents the loss of stiffness of the whole flange. This may lead to the effective

width concept and justify the use of the edge stress σ_{xe} equal to yield stress σ_y as failure criteria.

b) At Section 5: (Figure 4.33b)

The distribution of the longitudinal strain ε_x at this section is completely different to the one at Section 9. Up to 400 psi, the distribution seems to be uniform across the flange. At 500 psi, the distribution starts to show pockets at the middle of each flange sub-panel, resulting in a concentration at the longitudinal stiffener locations and at the flange/web edges. Up to the collapse pressure (1700 psi), the strain at each longitudinal stiffener location and at the flange/web edge is almost the same. It may be outlined here, that 1800 psi was the collapse pressure for this model, since there was no further pressure increase.

Due to this strain distribution, it seems that if the ultimate strength of a stiffened panel is to be calculated on the basis of stress at a section half-way between two transverse stiffeners, it may be realistic to consider each longitudinal stiffener as a T-shape column, using the effective width method in determining the portion of the flange associated with the longitudinal stiffener and the web panel, the failure criteria being the attainment of the yield stress. The ultimate capacity in this case, is the sum of capacity of those T-columns, and is given by Equation (4.3). This approach was also suggested

by some researchers

$$P_u = \sum_{i=1}^{n+1} b_{ei} t \sigma_y \qquad (4.3)$$

For equally spaced longitudinal stiffeners, Equation (4.3), reduce to

$$P_u = b_e (n+1) t \sigma_y \qquad (4.4)$$

Note that the number of stiffeners, n, is increased by one to account for the two web plates which are considered as one longitudinal stiffener.

4.6.2.2 Model B - Transverse distribution of longitudinal strain ϵ_x

a) At Section 9: (Figure 4.34a)

At this section, the strain distribution is similar to the corresponding section of Model A. The peak values are at the centerlines of the plate elements between the longitudinal stiffeners and also at the flange/web edges. However, the pockets are less pronounced, compared to the one in Model A. This fact is certainly due to the influence of longitudinal stiffener spacings. With four longitudinal stiffeners, the b/t ratio is 46, compared to 56 for Model A. The flange is then stiffer and results in a better distribution of stress.

For this model, there is an improvement, up to 500 psi. The strain distribution is almost uniform across the flange.

With an increase of the load, there is a concentration of stress at the flange/web edges and a little increase in the middle portion of the flange. In Model A, there was a decrease of stress for the middle portion of the flange once the yield stress was reached (at 1500 psi). In Model B, a decrease of stress was observed after 2000 psi for the middle portion of the flange, and after 2100 psi for the flange/web edges. This behaviour again confirms the influence of the number of longitudinal stiffeners and, consequently, of the b/t ratio.

Because the distribution of stress shows, in general, a less pronounced pocket across the flange, it may be suggested that if the ultimate buckling strength is to be calculated on the basis of maximum stress at this section, it appears reasonable to use the average stress σ_{am} of the whole flange; the failure criteria being the attainment of yield stress at the flange/web edge.

b) At Section 5: (Figure 4.34b)

As observed in Model A, at a similar section with an increase of load, there is a strain concentration at the longitudinal stiffener locations and at the flange/web edges. Up to 1700 psi, the peak values at the longitudinal stiffener locations are almost the same as the ones at the flange/web edges. After 1700 psi, there was a decrease of stress at the

centerlines of the plate elements. This decrease of stress, even resulted in tension stress at certain sections. There was not any decrease of stress at the flange/web edges. The edge strain ε_{xe} at 1700 psi is almost equal to ε_{yi}. This may be considered as the failure point, as suggested by Skaloud [158].

In general, it was again proven that by increasing the number of longitudinal stiffeners, and consequently, by reducing the b/t ratio, it has resulted in an increase of the capacity of the compression flange, the greater portion of the plate being effective.

Similar to that of Model A, if the ultimate buckling strength is to be calculated on the basis of stress distribution at this section, it may be advisable to use the concept of the T-shape column, considering the longitudinal stiffeners and associated effective plate width. The sum of the capacity of those T-shape columns including the flange/web L-shape columns will give the overall ultiamte strength, Equation (4.3).

4.6.2.3 Model C - Transverse distribution of longitudinal strain ε_x

a) At Section 9: (Figure 4.35a)

The performance of the stiffness is improved, when compared to both Models A and B, up to 700 psi, the strain distribu-

tion is almost uniform across the flange. After this pressure and with any increase of load, the peak values are at centerlines of the plate elements and at the flange/web edges. Those peak points seem to have the same value up to 1000 psi. After 1000 psi, there is a concentration of stress at the flange/web edges, resulting in general pockets in the middle portion of the flange. After 1700 psi, the pressure at which $\varepsilon_{xe} \simeq \varepsilon_y$, there is a decrease in stress at the longitudinal stiffener locations and in general, across the flange, resulting in a more pronounced pocket. There was no decrease of stress at the flange/web edges, up to 2000 psi.

The distribution of stress seems to be improved upon by comparison with Model B. This is the influence of the stiffener rigidities. In using this stress distribution, it may be recommended that the ultimate strength be calculated on the basis of the average stress σ_{am} of the whole flange, using the effective width b_e of the whole flange or using the concept of the equivalent thickness, Equation (4.2), the failure criteria being $\sigma_{xe} \simeq \sigma_y$.

b) <u>At Section 5:</u> (Figure 4.35b)

For this model, up to 1000 psi, the strain distribution is almost uniform across the flange. At 1200 psi, the distribution starts to show peak values at the longitudinal stiffener locations and at the flange/web edges. Even after the

failure point $\sigma_{xe} = \sigma_y$ (1700 psi) up to 2000 psi, those peak points seem to have the same value. The local pockets (between longitudinal stiffeners) generally remain less pronounced.

In general, it is clear that this stress distribution confirms the influence of stiffener rigidities when compared to Model B and of stiffener spacings when compared to Model A. The whole panel (plate and stiffeners) is effective in resisting the applied load.

If the ultimate buckling strength is to be calculated on the basis of this section, both the T-shaped column and the equivalent thickness approach could give the same value. The failure criteria may be $\sigma_{max} = \sigma_y$ for both methods.

4.6.3 Buckling Behaviour of the Compression Flange

It was outlined in Chapter I, that one of the deficiencies in the actual design methods dealing with the compression flange of steel box-girder bridges, is to be based upon the elastic buckling theory of ideal (no imperfections) plates, in which the plate is analysed in isolation of the stiffeners. Therefore, to be safe and economical, the theory should include the interaction between the plate and stiffeners, and needs to be based upon the post-buckling behaviour of the whole stiffened panel.

For the above reason, in the present experimental investigation, it was decided to load the models up to complete failure, care being taken to study the behaviour of both the plate and stiffeners, from the local buckling to the overall post-buckling stage, to note the failure mechanism and derive some tentative recommendations.

To facilitate an understanding of the text, the following definition needs to be kept in mind. According to the loading conditions, Section 4.5.1, Figure 4.18, each model is divided longitudinally into four sub-panels with a quarter span length each. The middle two, termed middle panels, are that part of the model subjected only to bending. The two extremes are sub-panels, termed end panels, and are located in that part of the model subjected to bending and shear.

4.6.3.1 Model A

It was already observed that, at 700 psi, the compression flange starts to buckle locally in the plate between the stiffeners. This buckling mode was oriented toward the stiffener outstands.

Considering first the two middle panels, Figure 4.39a, in the transverse direction, the plate buckling is a series of pockets between the longitudinal stiffeners, those latter being the point of contraflexure. In the longitudinal direction, the plate also buckles in a series of pockets between the trans-

verse stiffeners. In the transverse direction, the local buckling may be expressed mathematically by a cosine function with one half-wave for each plate element between the two longitudinal stiffeners. In the longitudinal direction, the number of half-waves may vary from two to four between the two transverse stiffeners.

It may be noted here, that in general, the local plate buckling is located in the direction of its initial geometrical imperfections. But, as the load was increased, the overall buckling mode took place and became predominant. The overall buckling mode was characterized by a one-half wave in the transverse direction and two half-waves in the longitudinal direction where one half of the middle panel buckled downward and the other half upward.

In the end panel, the behaviour was quite different. The local buckling of the plate began late (±1400 psi) compared to the middle panel, and very quickly resulted in an overall buckling mode. At 1700 psi, the end panel became almost a mechanism, as the web panel buckled at the same time. The two buckling lines met at the web/flange edge and formed a hinge (Figure 4.39b). From this moment, it was impossible to increase the load, although the middle panel seemed to be able to sustain some load increments.

This failure mode of the end panel is termed the: "plate failure mode", as explained in Chapter I, Figure 1.16,

the failure being initiated by excessively high compression stress in the plate elements. This failure mode was also observed by Murray [37] and Horne [40]. The above observations of the buckling behaviour led to the conclusion that, at the point of local plate buckling and, therefore, at the elastic plate buckling stress level, the behaviour of a stiffened panel cannot be thoroughly investigated, as shown in Figure 3.1. Consequently, the buckling behaviour may well be understood in considering both the local and overall buckling mode, and the ultimate strength as limited by the buckling performance will be determined by the post-buckling behaviour.

It may be recalled here, that for this model in the local buckling stage, there was some local lateral buckling of the stiffeners, although those latter have a relative rigidity of 1.3 times the optimum relative rigidity. According to the classical elastic plate-buckling theory, stiffeners having optimum relative rigidity are believed to remained straight up to and after the buckling of the plate elements.

4.6.3.2 Model B

As for Model A, local buckling of the plate between the stiffeners took place first, but at 1000 psi, compared to 700 psi for Model A. This is certainly due to the influence of the stiffener spacings. With four longitudinal stiffeners, the b/t ratio is 45, compared to 56 for Model A.

The mode of local buckling remained the same, but with less pronounced pockets when compared with that of Model A. With an increasing load, the overall buckling became more and more predominant. In general, the overall buckling mode was well developed for this model and better performance was achieved. In the middle panel, one-half buckled downward and the other upward, resulting in one half-wave in the transverse direction and two half-waves in the longitudinal direction, one half-wave located between the two transverse stiffeners. Figure 4.40a is an interior view of the overall buckling mode of the compression flange middle panel of Model B (bottom view); Figure 4.40b is a top view of each middle sub-panel. If the whole middle panel is to be analysed as a compressed panel, the shape of buckling may be expressed as:

$$w(x,y) = w_o \sin \frac{m\pi x}{a} \sin \frac{n\pi y}{b} \qquad (4.5)$$

where

n = 1, for the transverse direction, and

m = 3, for the longitudinal direction.

Three failure modes are possible for this middle panel. First, the plate failure mode may take place in the middle sub-panel bowing downward (Figure 4.40). Secondly, the stiffener failure mode may be initiated by yielding of the tip of the stiffener in the middle sub-panel, bowing downward and thirdly, the stiffener failure may be initiated by an

excessively high compression stress at the tip of the stiffener in the middle sub-panel bowing upward (Figure 4.40).

It is interesting to note that for this model, the stiffeners did not show any lateral local buckling during the local buckling mode of the plate. It is only when the overall buckling mode became more predominant that the longitudinal stiffeners began to buckle in the lateral direction. This lateral buckling took place mostly in the middle sub-panel bowing upward, with the top of the stiffeners being compressed (Figure 4.41). This lateral buckling was a half-wave in the vicinity of the transverse stiffener and two or three half-waves in the remainder of the stiffener span. In the middle sub-panel bowing downward, the longitudinal stiffeners buckled laterally only in the vicinity of the transverse stiffeners.

In general, the longitudinal stiffeners buckled laterally in the direction and shape of their initial geometrical imperfections. This fact confirms the influence of initial imperfections upon the buckling mode, and also upon the ultimate strength.

In the end panels, the mode of buckling was the same as that in Model A, the first local plate buckling mode being followed by the overall plate buckling mode. It buckled down and upward, resulting in a plate-failure mode.

The overall post-buckling shape of this model is shown in Figure 4.40a and may be expressed, in a general way, to that in Figure 4.42.

The overall failure mechanism for this model was different to that of Model A. This time, the overall failure occurred by the simultaneous formation of hinges (mechanism lines) at the center of the middle sub-panel bowing downward (plate failure mode) and in the end panel, failing again by the plate failure mode with the mechanism line meeting the one in the web end panel.

It is interesting to note here, that the influence of stiffener spacings was again well-demonstrated in Model B. It was possible to sustain more load with a 2300 failure pressure, compared to 1700 psi for Model A. The failure occurred by the overall buckling mode and not by local instability of the elements. In post-buckling behaviour, it is also able to learn more on the failure mode and ultimate strength of those characteristics which cannot be observed in the local buckling stage. The participation of both plate and stiffeners in a resisting load was demonstrated. On the whole, the overall performance was improved.

4.6.3.3 Model C

For Model C, local plate buckling started at almost the same load as that in Model B, however, the overall buckling mode

began at a higher load. This is the influence of stiffener rigidities. It may be recalled here, that a relative rigidity is 3.36 times the optimum rigidity, according to classical elastic linear buckling theory, as compared to 1.6 for Model B. This influence is demonstrated in that the overall buckling behaviour is similar to that in Model B, except that the mechanism is less pronounced and a higher applied load has been achieved.

Lateral buckling of the stiffeners was very small, even when the overall buckling mode was well advanced (Figure 4.43). One middle sub-panel buckled downward and the other upward, and both end panels buckled downward. Then, the middle panel developed both plate and stiffener failure modes, while the end panels developed only plate failure modes.

The overall failure was initiated by the formation of a hinge in the end panel (plate failure mode) such as that shown in Model A, while the middle panel was able to sustain some additional load. Again, the post-buckling stage shows the influence of stiffener rigidities and of the failure mode upon the ultimate strength.

The effect of initial imperfections was once more demonstrated in that the local buckling had the direction and shape of initial imperfections. As the overall buckling mode is affected by local and lateral buckling, therefore, in-

fluence is evident of initial imperfections on the ultimate buckling strength.

4.6.4 Web Plates Buckling Behaviour

One of the main objectives of the present study is to investigate the interaction between all components comprising the cross-section of a steel box-girder bridge, the influence of the buckling behaviour of each component on the overall buckling behaviour and, consequently, upon the ultimate strength.

In the present study, only the reciprocal influence of the compression flange and webs is considered. It has been explained in Chapter III that in evaluating the buckling strength of steel box-girder bridges, some design methods consider only the compression flange and analyse it as a stiffened panel, thus ignoring any interaction with the web panels. Such consideration is not realistic, and does not reflect the real behaviour of steel box-girders, as encountered in practice. Some designers consider that a web contributes only a small amount (10 to 15%) to the moment of inertia and therefore, does not influence the ultimate strength. But, in recent research, for example, the Merrison Rules [14] have demonstrated that web panels have an influence on the overall buckling strength. In fact, web/flange boundary conditions affect the compression stress at this location and

the shear lag effect due to the interaction of the web and flange, has a great influence on the stress distribution in the compression flange.

The main reason for which most designers treat the compression flange in isolation of the web panels is strictly due to the mathematical complexity of the problem. This is why it is recommended [18],[14] that many experimental tests are needed before formulating any design recommendations which account for the influence of the interaction of all components on the buckling strength of steel box-girder bridges.

The influence of web panels on the buckling behaviour of the compression flange was demonstrated even in the early years of buckling investigations of steel box-girder bridges. In fact, Hodgkinson [156] who is the first to study the buckling strength of compressed thin plates, had demonstrated by his experimental analysis of the Britannia Bridge, in 1845, that the web panels' behaviour had an influence on the buckling strength of the compression flange.

When the buckling strength of these compressed plates was investigated mathematically for the first time, by Brian [88], in 1891, the beginning of the classical elastic buckling theory, and even the participation of the stiffener, was neglected. As steel box-girder bridges are now in growing demand, the problem of web/flange interaction is of great importance and needs more experimental tests.

In the following sections, the observations made during such tests are reported for the three models.

4.6.4.1 Model A

Although the compression flange began to buckle first, it was the buckling of the web panels that influenced the mode of failure more, and even precipitated it. The lateral buckling of the web panels began directly when the overall buckling mode was initiated in the compression flange. Only the web end-panels buckled. It may be recalled here, that loading conditions (Figure 4.18) are such that they produce shear and bending in the end panels; the shear being zero in the middle panel.

The development of the web buckling was very rapid, compared to that of the compression flange. The buckling started at 1200 psi and at 1700 psi, the plastic stage (mechanism) was reached. It was observed that since the time the web began to buckle, the compression flange did not sustain enough load. As the overall plate buckling mode had started in the compression flange end panel, the web buckling contributed more to reduce the capacity of the end panel. The mechanism line (hinge) occurring in the compression flange end panel continued up to the web/flange edges, and from this moment, the model could not sustain any additional load. Any attempt

to increase the load contributed to the development of the failure mechanism, Figure 4.44.

The web plate buckled laterally inward and outward, following a diagonal line between the corner of the tension flange and the vertical stiffener, and the corner of the longitudinal stiffener and the end vertical stiffener, Figure 4.45. This was in the direction of the tension field zone as proposed by Rockey [46]. It is interesting to note here, that the diagonal did not go to the corner of the compression flange and end vertical stiffener. This confirms two points: first, that the web longitudinal stiffener, which is located at 0.20d, prevents the propagation of the tension field zone up to the compression flange; and secondly, that this location of the web longitudinal stiffener is the optimum for preventing lateral buckling due to flexural compressive stress. Strain gage readings show that the part of the web (0.20d) located between the longitudinal stiffener and the compression flange was under high compressive stresses.

The fact that the tension field line did not start exactly at the corner of the vertical stiffener and the tension flange, but a little bit further from the corner, confirms again the hypothesis that one part of the flange is part of the tension field. This could be similar to that of the compression flange, if there were no web longitudinal stiffeners. It may be recalled here, that the tension field is a mechanism which takes place in the web post-buckling stage.

That part of the flange which is part of the tension field zone could be determined, as was proposed by Rockey and Skaloud [58].

It may be outlined here, that the initial web lateral buckling mode was located in the direction of initial imperfections; although their weakening effect on the buckling strength of web panels is believed to be compensated by the tension field mechanism strength. But, as this latter is post-buckling behaviour, which is, to some extent, influenced by the direction of initial lateral buckling, it is clear that the initial imperfections have an influence on the ultimate buckling strength of web panels. As the load increased, the web plate buckled both inward and outward. The longitudinal stiffeners also buckled in the direction of their initial imperfections and the longitudinal stiffener buckling mode influenced the overall web-buckling mode more.

The deformation lines in the vicinity of the web end vertical bearing stiffener, Figure 4.46, is a proof that the bearing stiffener needs to be designed as a cross-shaped column, composed of vertical bearing stiffener plates and one portion of the web plate. Also, the deformation lines at the corner of the longitudinal and vertical bearing stiffeners through the tension flange, show the necessity of an additional vertical stiffener at a distance not more than 0.80d from the end-bearing stiffener.

It is interesting that the tension field diagonal, which began by a line at the beginning, becomes a series of lines when overall buckling is well advanced. This is a proof of the interaction between the flange and web.

4.6.4.2 Model B

Observations made on Model A lead to the conclusion that the buckling behaviour of web panels has influenced the overall buckling behaviour of the compression flange and contributed more to the failure mode. It was also noted that the compression flange, as well as the model, could sustain some additional load if the web panels were quite reinforced, especially the web end panels, which are subjected to shear and bending.

Due to the above remarks, for models B and C, the web end panels have been reinforced with two additional transverse sti-feners on both sides, spaced at 15 inches, Figure 4.2. The aspect ratio a/b became 1.04 as compared to 3.13 for Model A. This reinforcement shows a beneficial effect on the overall buckling mode. The failure pressure was extended from 1700 psi to 2300 psi. The buckling mode changed completely. In fact, the web plate did not show any local lateral buckling. It was only when the overall buckling mode of the compression flange was developed and the plate failure mode initiated in the compression flange end panels that the web end panel began to buckle.

The web deformation lines changed completely. Instead of a diagonal line such as that in Model A, (Figure 4.45), the deformation is a series of lines, almost uniformly distributed (Figure 4.47), on the whole part of the web plate below the longitudinal stiffener. These lines have the same distribution and inclination in all three end sub-panels. This inclination was 12 degrees from the horizontal plane.

The distribution of the deformation lines shows that the whole web plate was effective in sustaining the load.

The longitudinal web stiffener buckled almost the same way as that in Model A, but this was only in the end sub-panel close to the point of load application, or more precisely, where the mechanism line formed in the compression flange end panel meets the web. This section is subject to higher stresses due both to shear and flexural compression.

It is interesting to note that the compression flange buckling had a reciprocal influence on the web buckling. In fact, the middle web panel buckled laterally outward (Figure 4.48). This was purely due to the influence of the compression flange middle sub-panel that buckled downward. Also, the longitudinal web stiffener located in this sub-panel buckled also. The above remarks show that the interaction between the web and flange has a great influence on the overall buckling behaviour and also on the ultimate strength, and that this influence is reciprocal. Therefore, it is too conservative and

questionable to separately treat these two components, especially in the post-buckling stage, where this interaction is evident. This effect seems to be neglected only because of the mathematical complexity of the formulation. The best performance achieved by this model, compared to Model A, has led to the conclusion that during the design stage, care should be taken in the stiffening of all parts.

4.6.4.3 Model C

The web panels in Model C, have been reinforced axactly the same way as in Model B (Figure 4.2). In general, the buckling behaviour is the same up to the the maximum capacity of the web panels. In Model B, both the web and compression flanges show a reciprocal influence on their overall buckling stage; however, in Model C, since the compression flange is stronger, its overall buckling did not develop as simultaneously as that of the web, and this fact seems to have influenced the overall failure load.

The formation of a hinge in the web end panel contributed more to the development of the plate buckling failure mode in the compression flange end panel, and precipitated the overall failure, although the compression flange middle panels did not buckle much and could sustain some additional load.

The fact that it was the web buckling that influenced the overall failure load more, is a proof of the importance

in considering the interaction between the components and shows that even if the web panels do not contribute greatly to the moment of inertia of a cross-section (10 to 15%), they have a great influence on the overall strength. This is in agreement with Figure 3.14, where it may be seen that the box girders having strong webs perform better.

It has been shown in Chapter III, that in evaluating the ultimate buckling strength of box girders, as limited by the compression flange performance, some suggested methods such as those given by Kondo [112],[113] account for the full participation of the web panels. However, most of those methods such as that given by Massonnet [64] has a tendency to minimize, and even completely ignore, the web contribution.

It has been demonstrated in the present experimental investigation, that web panels may have a predominant role on the overall buckling behaviour of the failure mode and also upon the strength. During the design stage, this remark needs to be kept in mind and care taken for better consideration of the contribution of each component.

4.6.5 Overall Buckling Behaviour

It may be concluded from Sections 4.6.3 and 4.6.4, that the overall buckling behaviour is different for the three models and so is their overall failure load. This difference constitute the response to the main objectives of the present study, the influence of the stiffeners' spacing and

rigidity, the interaction between the web and compression flange and their reciprocal influence on the overall buckling behaviour, the influence of the failure mode on the ultimate strength, and finally, the influence of initial imperfections upon the buckling mode and strength. The comparison of Models A and B show the influence of the stiffener spacings, while the comparison of Models B and C gives the influence of the stiffener rigidities and permits an estimation of the required optimum rigidity of the stiffeners to remain straight and rigid up to and after the buckling of the plate. In each model, the interaction and reciprocal influence between the webs and compression flange is shown. The failure mode and its influence on the overall strength is explained.

In Model A, local buckling was more pronounced than in Models B and C. The plate aspect ratio b/t is 56 in the compression flange and the a/b ratio is 3.36 in the web end panels. These two ratios are respectively 45 and 1.04 in Models B and C. The overall buckling was almost simultaneous in both the web and compression flange. The overall failure mode was initiated by "plate failure mode" in the compression flange end panels and by lateral buckling of the web end panels.

It was observed that at the load which caused overall failure, the middle panels in both the compression flange and web did not develop their full capacity and could sustain some additional load.

For Model B, the local buckling was less premature and less pronounced. The overall buckling mode was well developed and was simultaneous in both the web and compression flange.

The overall performance was more improved and each component seems to have developed its fullest ultimate buckling strength. The overall failure mode occurred by the simultaneous formation of the "plate failure mode" in the compression flange end panel and in the middle sub-panel which buckled downward, accompanied by a formation of hinge in the web end panels.

The interaction as well as the reciprocal influence of the web and compression flange is well demonstrated, and has a great influence on the ultimate buckling strength.

It is interesting to note that in Model B, the compression flange has developed both "stiffener and plate failure modes". The stiffener failure mode is believed to be the most critical, as explained in Chapters I and III, because it is abrupt and premature. But, in this model, the fact that the overall failure occurred by plate failure mode is due to the influence of the laterally buckling in-web end panels. This is again, a proof of considering the interaction between those two components, and not to treat them separately, as is current practice.

For Model C, local plate buckling began at almost the same load as that in Model B. However, the overall buckling began at a higher load. This is certainly due to the influence of the stiffener rigidity. Even during the overall buckling stage, the compression flange longitudinal stiffeners did not show any lateral buckling mode, Figure 4.43.

It may be recalled here, that the relative rigidity of longitudinal stiffeners for Model C is 3.36 times that of the required optimum elastic buckling rigidity. This ratio is 1.6 for Model B. The optimum relative rigidity, according to elastic buckling theory, is the required rigidity for those stiffeners to remain straight and rigid up to and after the buckling of the plate. The elastic plate buckling theory assumes that the plate is of perfect flatness and that stiffeners cannot be out to be straight. These ideal conditions are not met in practice, as explained in Chapter I. These characteristics are termed initial geometrical imperfections, whose nature and influence are explained in Chapter II.

By assuming the stiffeners to be rigid and straight up to and after plate buckling, the elastic plate buckling theory considers the stiffeners only as nodal lines and ignores their participation. In Models A and B, the lateral buckling of stiffeners and local plate buckling are close; it is only in Model C, where the assumed stiffener performances is achieved. This is proof of how elastic classical plate

buckling theory may be found to be unsafe. This statement is also supported by Dubas [29] and Massonnet [30], who also worked on the problem. In fact, Dubas found the required stiffener rigidity to be five times the optimum elastic rigidity. He worked on models having the b/t ratio of 60 and 50.

The overall buckling mode was influenced by initial geometrical imperfections in that they have influenced the direction and shape of local buckling, and this latter has a great influence on the overall buckling mode, as well as upon the ultimate strength. The influence of initial imperfections is also evident by comparing their shape and direction to those of deflections due to load.

In general, the shape or surface function of compression flanges in the overall buckling stage, may be expressed mathematically by a cosine or sinusoidal function of that type given by Equation 4.1. The main question is the number of half-waves to be considered in both the longitudinal and transverse directions. Based upon these experimental results, it may be recommended that for narrow girders having widths between their webs of approximately the spacing of transverse stiffeners, and a relative longitudinal stiffener rigidity of about 3.5, one half-wave may be assumed in a transverse direction. In the longitudinal direction, one half-wave may be used if the transverse stiffener spacings do not exceed five times

that of the longitudinal stiffener spacings.

In general, for a wide girder, the number of half-waves in both the longitudinal and transverse direction will be the function of the stiffener spacings and rigidities. It is clear that, for post-buckling behaviour or ultimate buckling strength, due to the complexity of mathematical formulation, only an experimental investigation may give the appropriate results. This statement is supported in Reference [18], and the present study is of great contribution to the solution of the problem.

Tests have also shown, Figure 4.49 to Figure 4.51, that the resultant of the compression stresses can be accurately assumed to lie in the neutral plane of the stiffened panel and not in that of the plate, itself.

4.6.6 Ultimate Strength of Each Model

A steel box-girder bridge is an assembly of stiffened panels, its ultimate strength being computed by analysing the behaviour of those components constituting its cross-section. Different proposed analytical methods, from empirical expressions to the most complexly large deflection theory are reported in Chapter III.

In this section, the experimental results are compared to those from the analytical methods, with the purpose of making some tentative recommendations. Almost all those

proposed analytical methods treat the stiffened panel as a series of columns, joining each other. The so-called column is formed from the stiffener section, and a portion of the adjacent plate. The difference between these methods is due to the evaluation of this associated portion of the plate, the failure criteria, the boundary conditions, as well as the inclusion of some factors such as the effect of initial geometrical imperfections and residual welding stresses.

4.6.6.1 Effective width of the plate/stiffener column

As the plate/stiffener column is the basic element used, it is important first to evaluate its structural properties. Therefore, an exact evaluation of the associated effective plate is of first consideration. Table 4.7, gives the effective width ratio b_e/b for all three models, as computed from different proposed analytical methods in Chapter III. This Table may be divided into three groups:

1) Methods considering only the plate element between the stiffeners. The plate is assumed to be a perfect, plane plate.

2) Consideration of the plate element between the stiffeners only, but an account being made of the initial geometrical imperfections in both the plate and the stiffeners.

3) Tentative approximate methods that account for the participation of all components (flange and web) that compose the transverse cross-section. In this group, the Merrison Rules [14] account for both the initial imperfections and residual welding stresses.

The ultimate strength is directly proportional to the effective width ratio, Equation (4.6).

$$\frac{\sigma_{av}}{\sigma_y} = \frac{b_e}{b} \qquad (4.6)$$

$$\frac{\sigma_u}{\sigma_y} = \frac{b_e}{b} \qquad (4.7)$$

where

σ_{av} is the average applied stress,

σ_y is the yield stress, and

b and b_e are the cross and effective width of the plate.

At collapse $\sigma_{av} \simeq \sigma_u$ and Equation (4.6) becomes Equation (4.7) as above-noted.

It may be observed from Table 4.7 that in the range of b/t = 56 (Model A), Group 1 overestimates the ultimate strength and Group 2 may be considered safe.

For Model A, the difference between Group 1 and Group 2 may be explained by the fact that Group 2 accounts for the effect of initial imperfections and residual welding stresses. Those two factors have a weakening effect which is greatest in the range of b/t = 56, Figure 2.1. This difference confirms the analysis given in Chapter II. For Model B and Model C, with a b/t ratio of 45, Group 1 again overestimates the ultimate strength, and the same explanation as that for Model A can be given.

A comparison of the three models leads to the conclusion that in the plate/stiffener column approach, the effective width ratio is a function of only the stiffener spacings. The large deflection method given by Massonnet [64] gives two different values for Models B and C, because it is based upon the equivalent thickness principle. Therefore, the rigidity of the stiffener is accounted for. The stiffener rigidity is also accounted for in Group 3, as given in the Merrison Rules [14] and also given by Kondo [113],[114].

The secant stiffness method given by Horne et al [39], [40],[74] give the lowest effective width ratios. This method accounts for both initial imperfections and residual welding stresses and is now currently used.

For the calculation of the ultimate stress, the effective width ratios used and the computed structural properties of the plate/stiffener column, are given in Tables 4.8, 4.9

and 4.10, for Models A, B and C, respectively.

4.6.6.2 Critical buckling stress

Observed experimental critical buckling stresses are given in Table 4.11, for the three models. These critical stresses are due to the applied load, at which points local buckling was observed for the first time in the plate elements between the stiffeners in the compression flange. It may be observed that experimental stresses are well below those corresponding values given by the classical elastic plate buckling theory, especially for Models B and C, where the experimental values are one half those given by the classical method.

Also shown in Table 4.11, are the critical buckling stresses when a stiffened panel is substituted by an equivalent orthotropic plate, using the equivalent thickness principle, accounting for both stiffener spacings (b/t ratio) and rigidity. The small deflection theory given by Timoshenko and Gere [25], is a basis for present Canadian Bridge Standards [23]. When the small and large deflections theories results are compared, it may again be concluded that the effect of initial imperfections is evident.

The critical buckling stress, based only upon the behaviour of the plate element between the stiffeners, is well lower, when compared to those given by the methods accounting

for both stiffener spacings and rigidities, and consequently, the buckling performance of the entire stiffened panel. The use of the local plate buckling stress as a design criteria will result in an uneconomical structure, while consideration of that accounting for the overall performance may be unsafe. This leads to the conclusion that an economical and safe design is that in which both the local and overall critical buckling stresses will be reached at almost the same applied load. But, the difference between the two is so high, that any compromise may need a long and tedious trial-and-error process.

4.6.6.3 Failure Stress

Although the critical buckling stress is currently used as a design criteria, it does not constitute the failure stress. This latter is defined as the average applied stress at which failure of the structure is assumed to take place. The magnitude of the failure stress is a function of the failure criteria established. For almost all analytical methods based upon the plate/stiffener column behaviour, the failure level is assumed to be reached when the extreme fiber at midlength of the column reaches yield stress, leading to the "plate failure mode" or "stiffener failure mode", depending upon which fiber reaches the yield first, and upon the direction of the net eccentricity. This latter includes both the load misalignment and the initial imperfections, Figure 2.7.

For the large deflection theory, considering the performance of the stiffened panel, as a whole, the failure criteria is assumed to be reached when the longitudinal stress σ_x reaches the yield value at the flange/web edge, $\sigma_{xe} = \sigma_y$. This criteria was, for the first time, assumed by Skaloud [158], and is now known in technical literature as the Skaloud failure criteria for the compression flange of steel box-girder bridges. In some proposed analysis methods, failure criteria is assumed to be reached when any portion of the compressed element reaches a yield stress.

Table 4.12 summarizes the failure stress or ultimate strength of the three models, as given by different proposed analytical methods in Chapter III. Those values may be compared with those observed experimental stresses. For a comprehensive understanding of the results, failure stresses of Table 4.12, are given in Table 4.13, as portions of the classical elastic buckling stress corresponding to the b/t ratio of each model.

It may therefore be concluded from Table 4.13, that the classical elastic buckling theory using the approximate Karman post-critical buckling stress (rows 3 and 4), may overestimate the strength. The observed experimental results are close to those of the second-order column numerical analysis given by Little [136], in row 10, when the Skaloud failure criteria is used (row 1), and are close to those by

the secant stiffness method (row 6) when the Karman approximate method is used (row 2).

An empirical method used by Allen [95] (row 5), may be used for the quick evaluation of ultimate strength accounting for initial imperfections. On the whole, the large deflection method gives a consistent percentage for all three models. In general, all methods accounting for the effect of initial imperfections and residual welding stresses give lower results when compared to the classical elastic buckling theory, (rows 3 and 4).

The second-order column method given by Little [136] (row 10), is the one which will be proposed by the American Association of State Highway and Transportation Officials (AASHTO), [157].

4.7 SUMMARY OF CHAPTER IV

In this Chapter, a full range of experimental tests for three models of steel box-girder bridges is reported. The main purpose is to explain as much as possible, the buckling behaviour of steel box-girder bridges, mainly the compression flange, and interaction between the flange and web panels.

Buckling behaviour is analysed on the basis of the influence of stiffener spacings and rigidities, the influence of initial geometrical imperfections, of the interaction

between web and compression flange panels and their reciprocal influence on the overall buckling mode. Finally, the influence of the failure mode upon the overall strength is considered.

Curves are presented for easy understanding of the results. The effect of the shape and direction of initial imperfections (For example, Figures 4.11 to 4.17), may be explained by comparison to their curves with those of deflections of the structure due to loading, Figures 4.27 to 4.32.

The influence of interaction between the compression flange and web panels on their reciprocal buckling strength and also upon the overall buckling behaviour is observed during the loading stage, as is the influence of the failure mode on the buckling strength. Care has been taken to identify and analyse the deformation mechanism at every loading stage, (for example, Figures 4.26, 4.39 to 4.48).

The influence of stiffener spacings and rigidities is analysed on the basis of strain (stress) distributions in both longitudinal and transverse directions, (Figures 4.33 to 4.38) and upon their performance in resisting lateral buckling up to and after buckling of the plate elements, and finally, upon the overall load sustained by each model.

Tables 4.7, 4.11, 4.12 and 4.13, give a comparison of observed experimental results with those given by different

proposed analytical methods.

A survey of initial geometrical imperfections was performed on the three models for both plate and stiffeners and also for the entire model. The results of this survey is given in Section 4.4.5 and summarized in Tables 4.4, 4.5 and 4.6.

In general, a full interpretation of the results is made, from which it is possible to make some tentative recommendations.

TABLE 4.1 DIMENSIONS OF COMPONENTS OF THE THREE MODELS

(Unit Inches) Length 15.5 ft, Width 42 in., Depth 18-11/16 in.

MODEL	COMPRESSION FLANGE							TENSION FLANGE PLATES	WEBS					
	PLATE	LONGITUDINAL STIFFENERS		b/t	TRANSVERSE STIFFENERS				PLATE	TRANSVERSE STIFFENERS			LONGITUDINAL STIFFENERS	
		N	SIZE		N	SIZE	S			N	SIZE	S	N	SIZE
A	42×3/16	3	2¼×3/16	56	5	4×½	45	8×½	18×1/8	5	3-15/16×¼	45	1	3-15/16×3/16
B	42×3/16	4	2¼×3/16	45	5	4×½	45	8×½	18×1/8	5 4*	3-15/16×¼	45	1	3-15/16×3/16
C	42×3/16	4	2-5/8×¼	45	5	5×½	45	8×½	18×1/8	5 4*	3-15/16×¼	45	1	3-15/16×3/16

* See Figure 4.2.

s = stiffeners spacing

N = number of stiffeners

TABLE 4.2 STRUCTURAL PROPERTIES OF THE CROSS-SECTION OF THREE MODELS

MODEL	A_t in^2	A_c in^2	I in^4	G_{in}	S_t in^3	S_b in^3	G/d	s_t/S_b	I/I_A	C K-ft	T K-ft
A	23.328	9.351	1584.04	8.413	188.28	154.17	0.450	1.22	1.0	690.36	665.29
B	23.753	9.773	1606.34	8.286	193.87	154.43	0.443	1.256	1.014	710.85	566.24
C	24.690	10.710	1644.71	8.041	204.54	154.48	0.430	1.324	1.038	749.98	566.43

G = Distance of center of gravity to the top fiber of the compression flange.

d = Depth of the model, A_t (A_c) total area of the cross-sec tion (compression flange).

C(T) = Required bending moment to cause yield in the top fiber of the compression flange (tension flange), elastic beam theory, S_t(S_b) section modulus for compression (tension).

* I_A = Moment of inertia of Model A.

TABLE 4.3 STRUCTURAL PROPERTIES OF THE COMPRESSION FLANGE STIFFENERS AND WEB PANELS

Compression Flange Longitudinal Stiffener								Compression Flange Transverse Stiffener			Web Plate Aspect Ratio	
Model	Size	I_s	δ	γ	L	L/r	I_s/I_o	Size	I	I/I_o	End Panel	Middle Panel
A	$2\frac{1}{2}\times 3/16$	0.712	0.052	27.38	45	83.22	1.3	$4\times\frac{1}{2}$	2.67	1.14	3.13	3.13
B	$2\frac{1}{2}\times 3/16$	0.712	0.052	27.38	45	77.25	1.6	$4\times\frac{1}{2}$	2.67	1.05	3.13	1.04
C	$2-5/8\times\frac{1}{2}$	1.507	0.081	57.96	45	59.05	3.36	$5\times\frac{1}{2}$	5.2	1.9	3.13	1.04

I_o = rigidity as required by elastic linear buckling theory

$\delta = A_s/bt$

$\gamma = I_s/bD$

$D = t^3/12(1-\nu^2)$

t = compression flange plate thickness

b = compression flange width

A_s = area of the longitudinal stiffener

r = ratio of gyration

L = compression flange longitudinal stiffener length

TABLE 4.4 VALUES OF INITIAL GEOMETRICAL IMPERFECTIONS OF PLATE PANELS IN THE COMPRESSION FLANGE (Unit Inches)

		EXPECTED VALUES (MERRISON RULES 14)				MEASURED VALUES			
N	b	Δ_x	Δ_y	δ_{ox}	δ_{oy}	Δ_x	Δ_y	δ_{ox}	δ_{oy}
3	10.5	0.1547 ≈ a/290	0.0774 ≈ b/150	0.0587 ≈ a/750	0.0737 ≈ b/150	0.1285 ≈ a/350	0.0652 ≈ b/160	0.0486 ≈ a/920	0.0493 ≈ b/120
4	8.4	0.124 ≈ a/360	0.062 ≈ b/140	0.0435 ≈ a/1000	0.0569 ≈ b/150	0.1330 ≈ a/340	0.0475 ≈ b/180	0.0603 ≈ a/740	0.0436 ≈ b/190

N number of longitudinal stiffeners

N 3 is for Model A

n 4 for Models B and C

TABLE 4.5 VALUES OF INITIAL GEOMETRICAL IMPERFECTIONS OF THE STIFFENERS IN THE COMPRESSION FLANGE (Unit Inches)

	Longitudinal Stiffener				Transverse Stiffener
	Δsx		Δsy		Δcy
	Δsx(+)	Δsx(-)	Δsy A	Δsy B,C	
EXPECTED VALUES MERRISON	0.0787 ≃ a/570	0.0787 ≃ a/570	0.0260 ≃ ts/7	0.0240 ≃ ts/10	0.0208 ≃ tc/25
MEASURED	0.0642 ≃ a/700	0.0642 ≃ a/700	0.0313 ≃ ts/6	0.0313 ≃ ts/7	≃ tc/20 ≃ ℓc/1600

A,B,C = Models A,B and C, respectively

Δcy = initial imperfection of transverse stiffener in lateral direction

ts = thickness of longitudinal stiffener

tc = thickness of transverse stiffener

ℓc = length of transverse stiffener

TABLE 4.6 RECOMMENDED VALUES OF INITIAL GEOMETRICAL IMPERFECTIONS TO BE ASSUMED IN DESIGN OF THE COMPRESSION FLANGE

SOURCE	PLATE		LONGITUDINAL STIFFENERS		TRANSVERSE STIFFENER
	Δx	Δy	Δsx	Δsy	Δcy
MERRISON RULES [14]	$\frac{b}{125}\sqrt{\frac{\sigma_y}{245}}$	$\frac{b}{250}\sqrt{\frac{\sigma_y}{245}}$	$\geq a/900$ $a/900(+)$ $a/1200(-)$	ts/9	tc/25
PRESENT TESTS	a/300	b/150	a/700	ts/7	tc/20 or $\ell c/1600$
LEONHARDT AND HOMMEL [61]	a/300 or a/750 (local)		a/600 $a \geq 33$ ft a/300 $a \geq 6.5$ ft		$\ell c/1000$
HORNE AND FLINT [62]			a/600 → (a/900 a/1200)		$\frac{\ell c}{1200} \rightarrow \frac{\ell c}{900}$
STEINHARDT [21]	b/150		$\ell/700$ $(0.9\ \frac{1}{\ell})$ or $\ell/600 \rightarrow \ell/500$		
DWIGHT [26]					$\ell c/2000$ or tc/36
DWIGHT AND LITTLE [86]			$\ell c/1000$		
DOWLING AND LOE [47]			$\Delta sx(+) = a/400$ $\Delta sx(-) = a/600$		
CHATERJEE [63]					$\frac{\ell c}{300} \rightarrow \frac{\ell c}{400}$

TABLE 4.7 EFFECTIVE WIDTH RATIO b_e/b OF THE THREE MODELS AS GIVEN BY DIFFERENT METHODS, CHAPTER III

*Initial imperfections and residual stresses accounted for.

GROUP	REFERENCE	MODEL		
		A	B	C
1	MARGUERRE [109] Equation (3.25)	0.912	1.059	1.059
	MASSONNET [64] SECHLER [110]	0.880	1.094	1.094
	KARMAN [96] Equation (3.22)	0.872	1.09	1.09
	PAPCOVITCH [108] Equation (3.23)	0.865	1.05	1.05
	FAULKNER [106] Equation (3.14)	0.707	0.818	0.818
	WINTER [70],[71] Equation (3.19)	0.704	0.828	0.828
	AVERAGE 1	0.831	1.012	1.012
2	*MURRAY [38] Equation (3.69)	0.704	0.828	0.828
	*CHATTERJEE AND DOWLING [87]	0.750	0.857	0.857
	*HORNE ET AL [40] Equation (3.77)	0.566	0.643	0.643
	*MASSONNET [64]	0.536	0.832	0.819
3	*MERRISON RULES [14]	0.757	0.753	0.745
	KONDO [112],[113]	1.0	1.0	1.0

NOTE: Groups 1 and 2 consider only the plate ement between the stiffener. Group 3 considers also the contribution of the web plates and of the tension flange.

TABLE 4.8 MODEL A: PROPERTIES OF THE CROSS AND EFFECTIVE PLATE/STIFFENER COLUMN FOR DIFFERENT EFFECTIVE WIDTH VALUES

(Units: Inch, KSI)

b_e/b	A	A'	G	G'	I	I'	r	r'	σ_{cr}	σ_e	σ_e'
1.0	2.392		0.309		0.610		0.541		33.43	41.38	
0.912		2.217		0.326		0.690		0.558			44.0
0.880		2.154		0.332		0.687		0.565			45.1
0.872		2.140		0.334		0.682		0.565			45.1
0.865		2.125		0.336		0.685		0.568			45.6
0.707		1.814		0.377		0.660		0.603			51.4
0.704		1.810		0.378		0.660		0.604			51.5
0.831		2.057		0.343		0.681		0.575			46.8

(Continued)

TABLE 4.8 MODEL A: PROPERTIES OF THE CROSS AND EFFECTIVE PLATE/STIFFENER COLUMN FOR DIFFERENT EFFECTIVE WIDTH VALUES

(Units: Inch, KSI)

b_e/b	A	A'	G	G'	I	I'	r	r'	σ_{cr}	σ_e	σ_e
0.750		1.9		0.365		0.670		0.594			49.9
0.566		1.536		0.428		0.636		0.643			58.5

NOTE: The prime sign means the effective column.

TABLE 4.9 MODEL B: PROPERTIES OF THE CROSS AND EFFECTIVE PLATE/STIFFENER COLUMN FOR DIFFERENT EFFECTIVE WIDTH VALUES

(Units: Inch, KSI)

b_e/b	1	0.818	0.828	0.857	0.643
A	2.00				
A'		1.710	1.726	1.770	1.434
G	0.351				
G'		0.394	0.392	0.384	0.452
I	0.677				
I'		0.654	0.655	0.659	0.623
r	0.582				
r'		0.618	0.616	0.610	0.659
σ_{cr}	52.24				
σ_e	47.9				
σ'_e		54.02	53.7	52.6	61.4

NOTE: Prime sign means the effective column.

TABLE 4.10 MODEL C: PROPERTIES OF THE CROSS AND EFFECTIVE PLATE/STIFFENER COLUMN FOR DIFFERENT EFFECTIVE WIDTH VALUES

(Units: Inch, KSI)

b_e/b	1.00	0.818	0.828	0.857	0.643
A	2.231				
A'		1.110	1.960	2.01	1.67
G	0.507				
G'		0.568	0.565	0.554	0.647
I	1.298				
I'		1.240	1.244	1.254	1.647
r	0.763				
r'		0.799	0.797	0.791	0.836
σ_{cr}	52.24				
σ_e	82.2				
σ_e'		90.2	89.7	88.4	98.8

NOTE: Prime sign means the effective column.

TABLE 4.11 CRITICAL BUCKLING STRESS σ_{cr} (KSI) OF THE THREE MODELS

	MODEL		
	A	B	C
*Observed	22.23	26.0	26.0
*Classical elastic buckling theory Equation (3.1)	33.43	54.24	52.24
**Small deflection theory Timoshenko and Gere [25]	43.85	52.86	97.0
***Large deflections theory	42.94	49.44	83.89

* Consideration of the plate element between stiffeners only.

** Consideration of the entire stiffened panel and using the equivalent thickness principle.

*** Equivalent thickness principle including the effect of initial imperfections.

TABLE 4.12 ULTIMATE STRENGTH σ_u (KSI) OF THE THREE MODELS

	METHODS	MODEL		
		A	B	C
1	*Observed	22.75	27.55	30.0
2	**Observed	31.0	33.83	33.83
3	**Classical elastic buckling theory	38.35	47.94	47.94
4	***Timoshenko and Gere [25] Canadian Standards [23]	43.92	47.88	63.35
5	Empirical method Allen [95]	23.50	28.20	32.85
6	****Secant stiffness method Horne et al [40]	33.47	34.54	36.38
7	Chatterjee and Dowling [87]	29.04	33.44	33.44
8	Elasto-plastic method Murray [38]	27.3	31.83	34.17

(Continued)

TABLE 4.12 ULTIMATE STRENGTH σ_u (KSI) OF THE THREE MODELS

	METHODS	MODEL		
		A	B	C
9	Large deflections theory Massonnet [64]	24.26	36.0.	38.18
10	Numerical solution of an inelastic plate/stiffener column Little [136] and AASHTO [157]	22.0	24.2	27.43

*Use of the Skaloud failure criteria $\sigma_{xe} = \sigma_y$ and the secant stiffness method.

**Consideration of the plate element only and the Karman approximate method $\sigma_u = \sqrt{\sigma_{cr}\sigma_y}$.

***Equivalent thickness principle and the Karman method.

****With the plate failure mode governing.

TABLE 4.13 ULTIMATE STRENGTH AS FRACTION OF THE CRITICAL BUCKLING STRENGTH. σ_u/σ_{cr}

	METHODS	MODEL		
		A	B	C
1	*Observed	0.68	0.53	0.57
2	**Observed	0.93	0.65	0.65
3	**Classical elastic buckling theory	1.15	0.92	0.92
4	***Timoshenko and Gere [25] Canadian Standards [23]	1.31	0.92	1.21
5	Empirical method Allen [95]	0.70	0.54	0.63
6	****Secant stiffeners Method Horne et al [40]	1.00	0.66	0.70
7	Chatterjee and Dowling [87]	0.87	0.64	0.64
8	Elasto-plastic method Murray [38]	0.82	0.61	0.65

(Continued)

TABLE 4.13 ULTIMATE STRENGTH AS FRACTION OF THE CRITICAL BUCKLING STRENGTH. σ_u/σ_{cr}

	METHODS	MODEL		
		A	B	C
9	Large deflections theory Massonnet [64]	0.73	0.69	0.73
10	Numerical solution of inelastic plate/ stiffener column Little [136] and AASHTO [157]	0.66	0.46	0.53

*Use of the Skaloud failure criteria $\sigma_{xe} = \sigma_y$ and the secant stiffness method.

**Consideration of the plate element only and the Karman approximate method $\sigma_u = \sqrt{\sigma_{cr}\sigma_y}$.

***Equivalent thickness principle and the Karman method.

****With the plate failure mode governing.

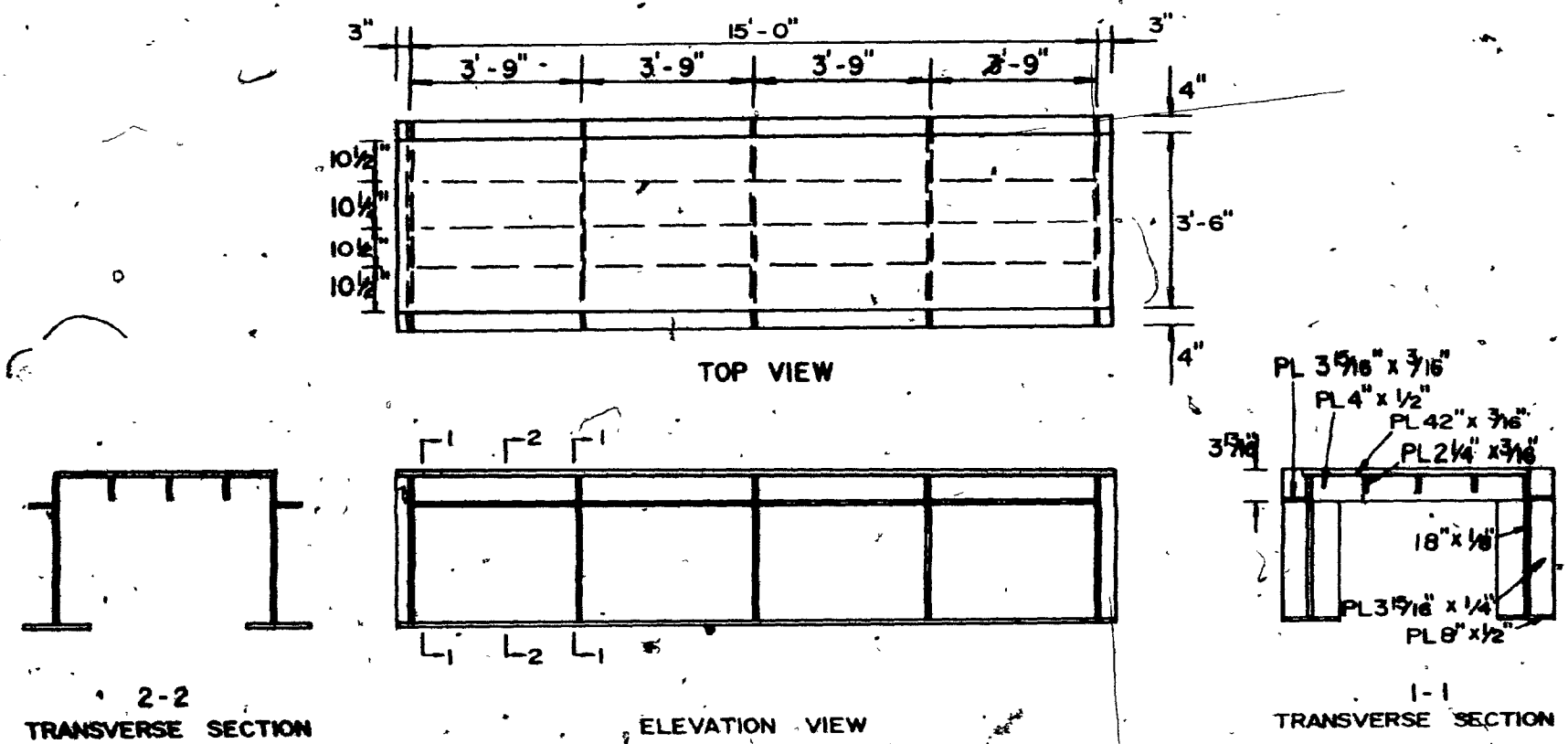

FIG. 4.1 GEOMETRICAL ARRANGEMENT OF MODEL A

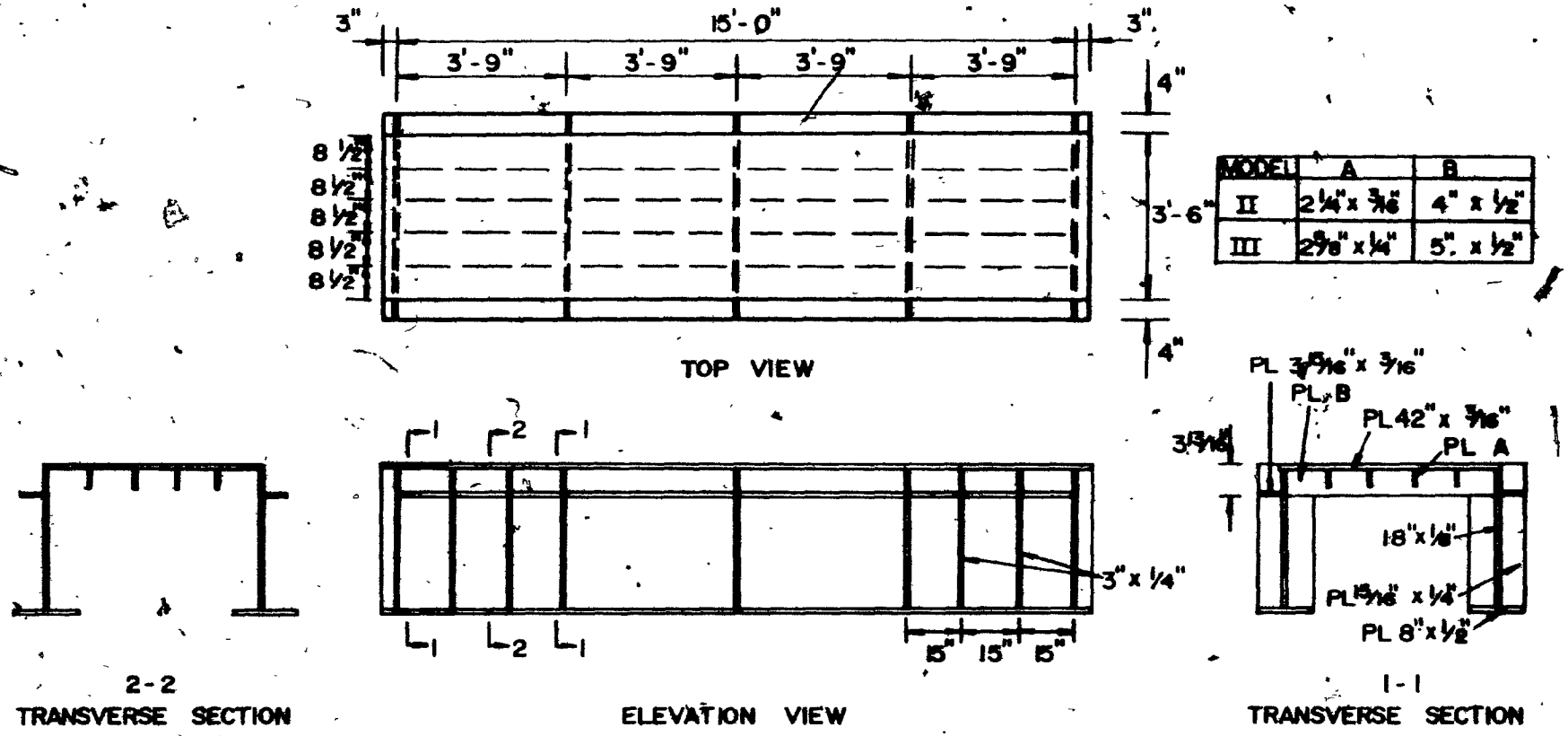

FIG. 4.2 GEOMETRICAL ARRANGEMENT OF MODELS B AND C

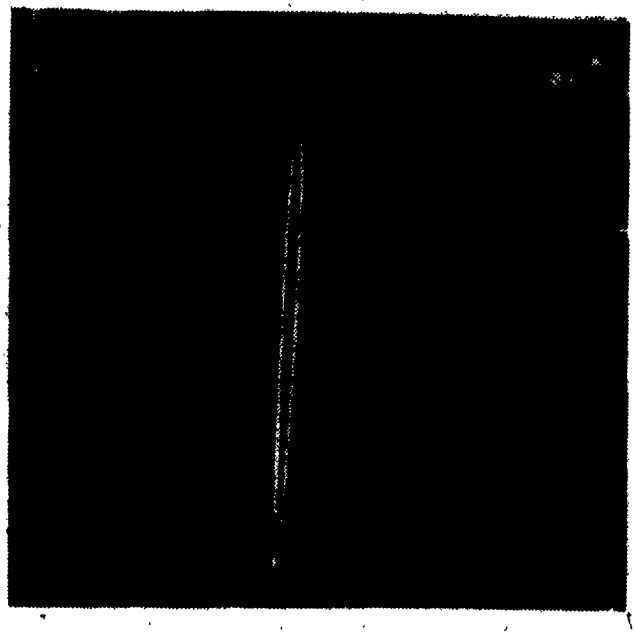

FIG. 4.3 DISTORTION OF WEB LONGITUDINAL STIFFENER PLATES BEFORE ASSEMBLING

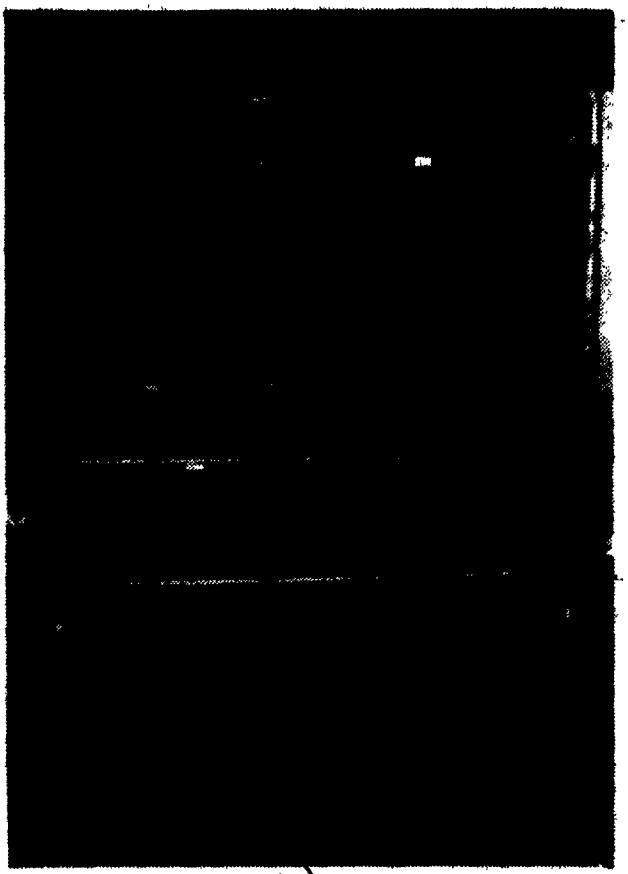

FIG. 4.4 FABRICATION STAGE: LOCATIONS OF DECK LONGITUDINAL AND TRANSVERSE
Stiffeners are marked for Model B.

(a)

(b)

FIG. 4.5 FABRICATION STAGE, (a) WEB COMPONENTS ARE TACK-WELDED TOGETHER, (b) FINAL ASSEMBLY BY CONTINUOUS WELDING

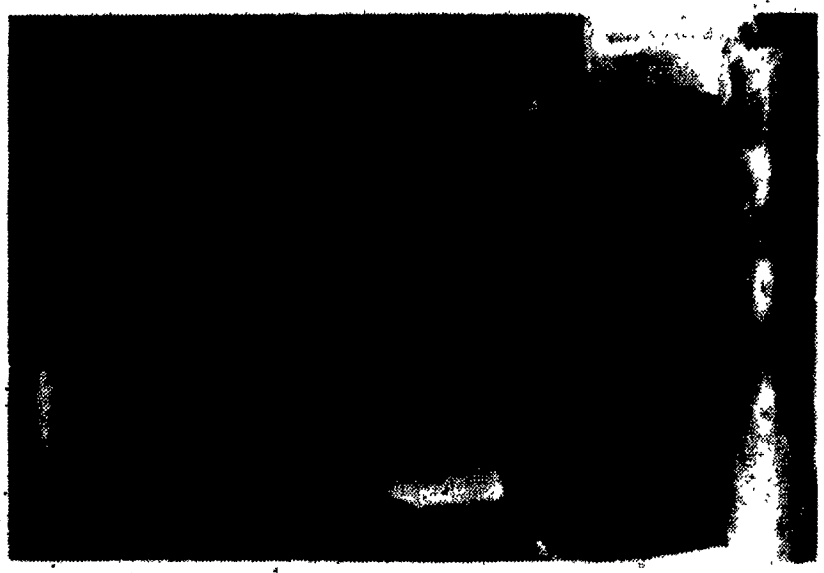

FIG. 4.6 INSIDE VIEW OF MODEL B

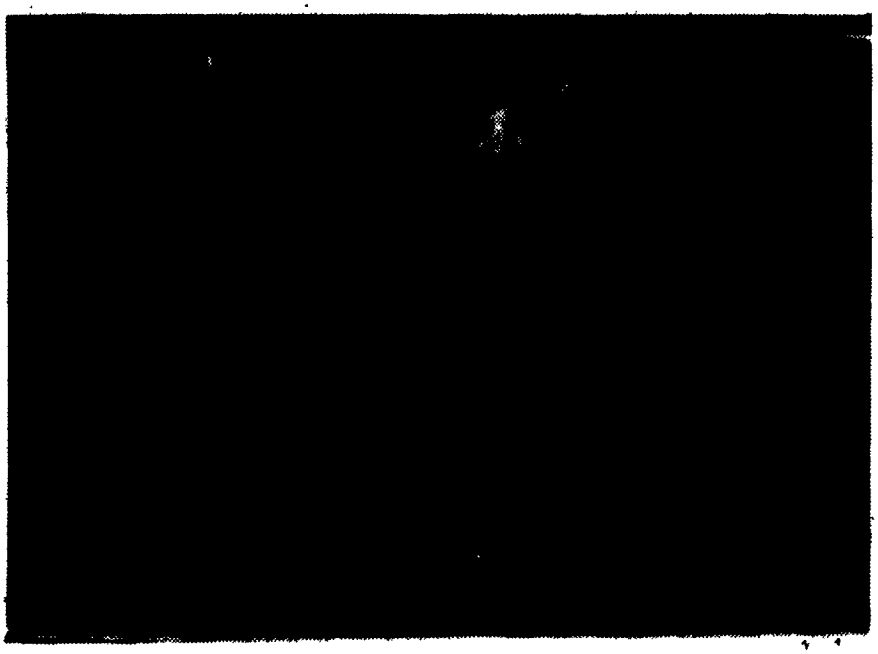

FIG. 4.7 VIEW OF THE COMPRESSION FLANGE TRANSVERSE AND LONGITUDINAL STIFFENERS AT THEIR INTERSECTION, AND THE CROSS-FRAME FORMED BY THE VERTICAL WEB STIFFENERS, COMPRESSION FLANGE TRANSVERSE STIFFENERS AND HORIZONTAL BRACING IN THE TENSION FLANGE

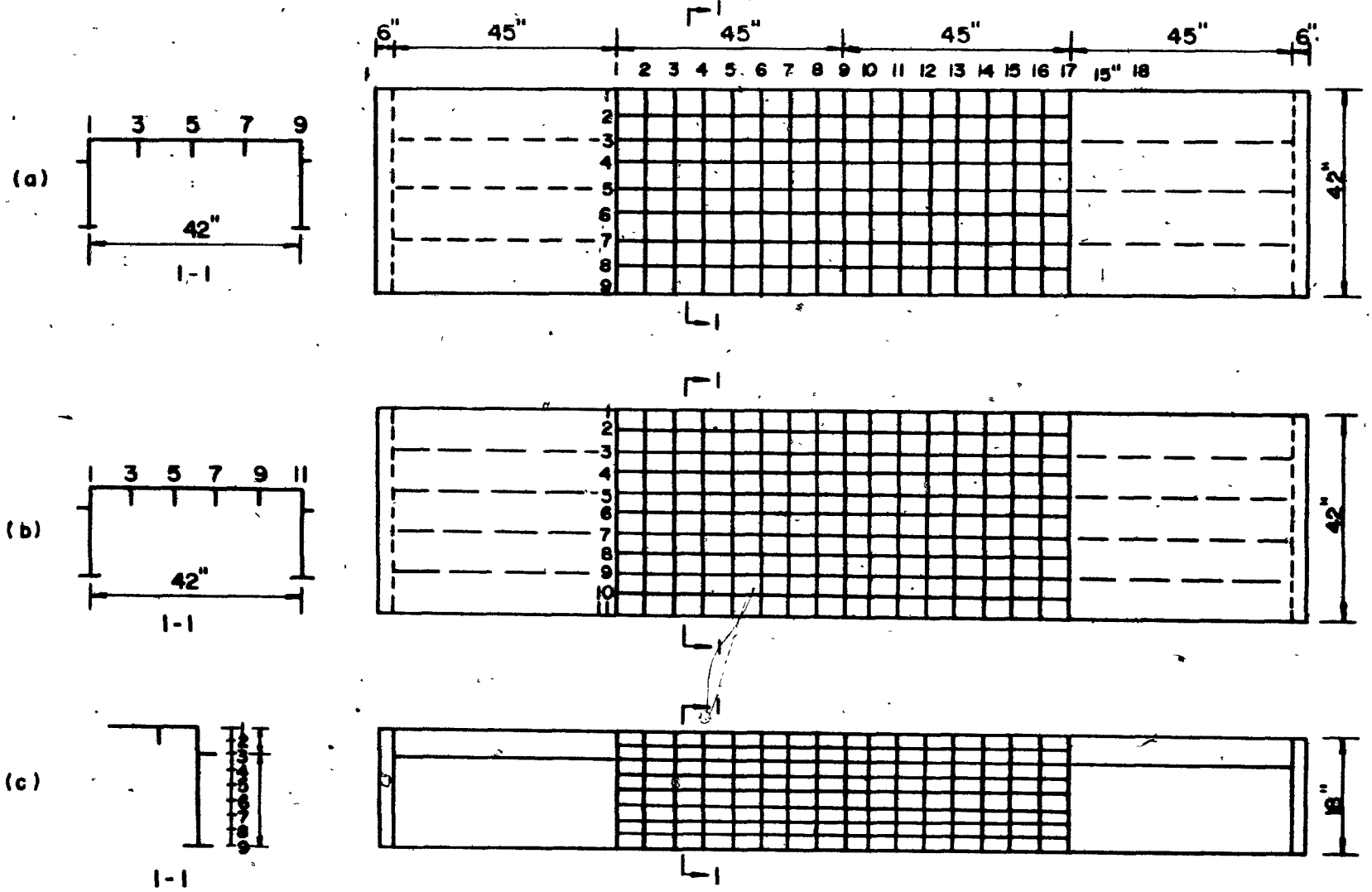

FIG. 4.8 GRID FOR MEASUREMENT OF INITIAL GEOMETRICAL IMPERFECTIONS. (a) DECK OF MODEL A, (b) DECK OF MODELS B AND C, (c) WEB PLATES OF EACH MODEL

FIG. 4.9 TYPICAL READING OF INITIAL GEOMETRICAL IMPERFECTIONS OF THE COMPRESSION FLANGE

At the top is a specially designed track capable of moving in three directions, carrying the dial gauge wherever needed.

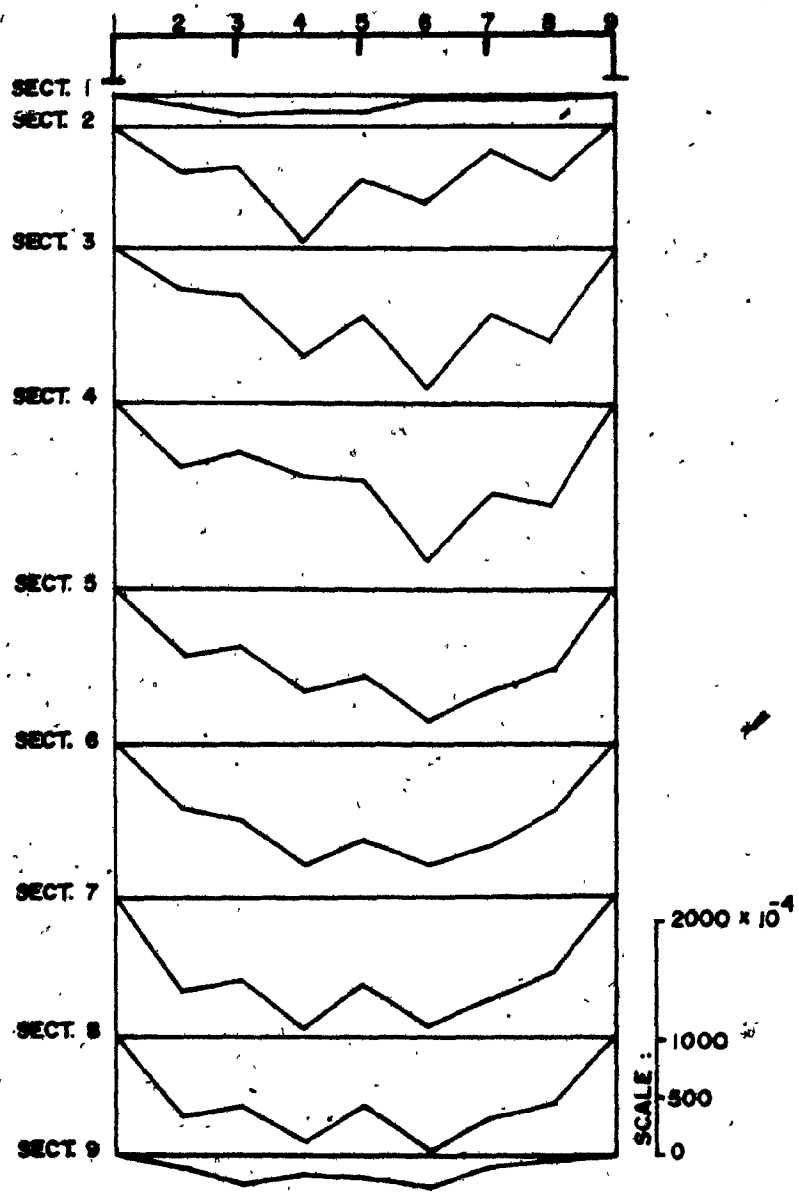

FIG. 4.10 MODEL A, OVERALL INITIAL IMPERFECTION (δ_{oy}) OF THE COMPRESSION FLANGE IN TRANSVERSE DIRECTION

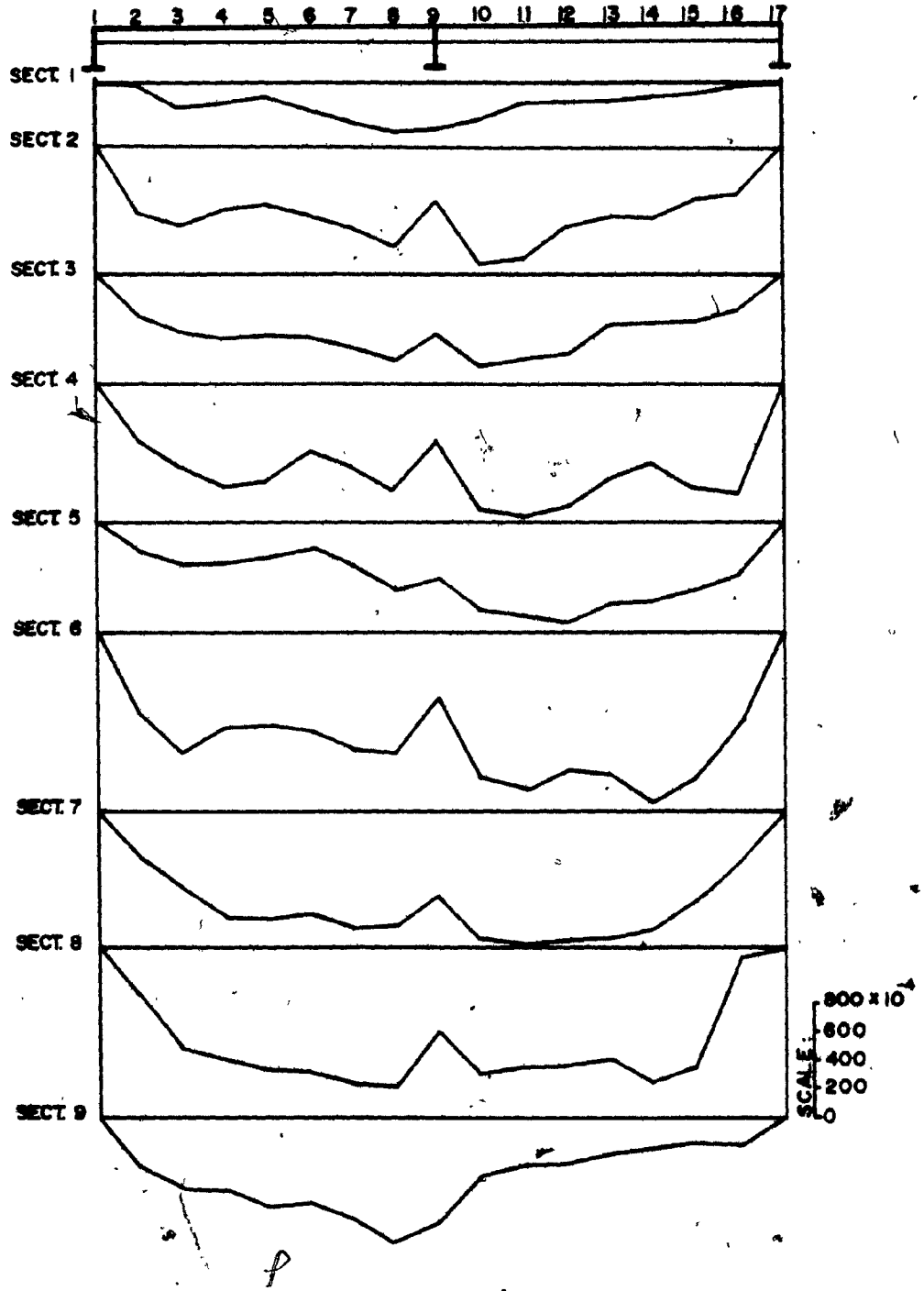

FIG. 4.11 MODEL A, OVERALL INITIAL IMPERFECTIONS (δ_{ox}) OF THE COMPRESSION IN LONGITUDINAL DIRECTION

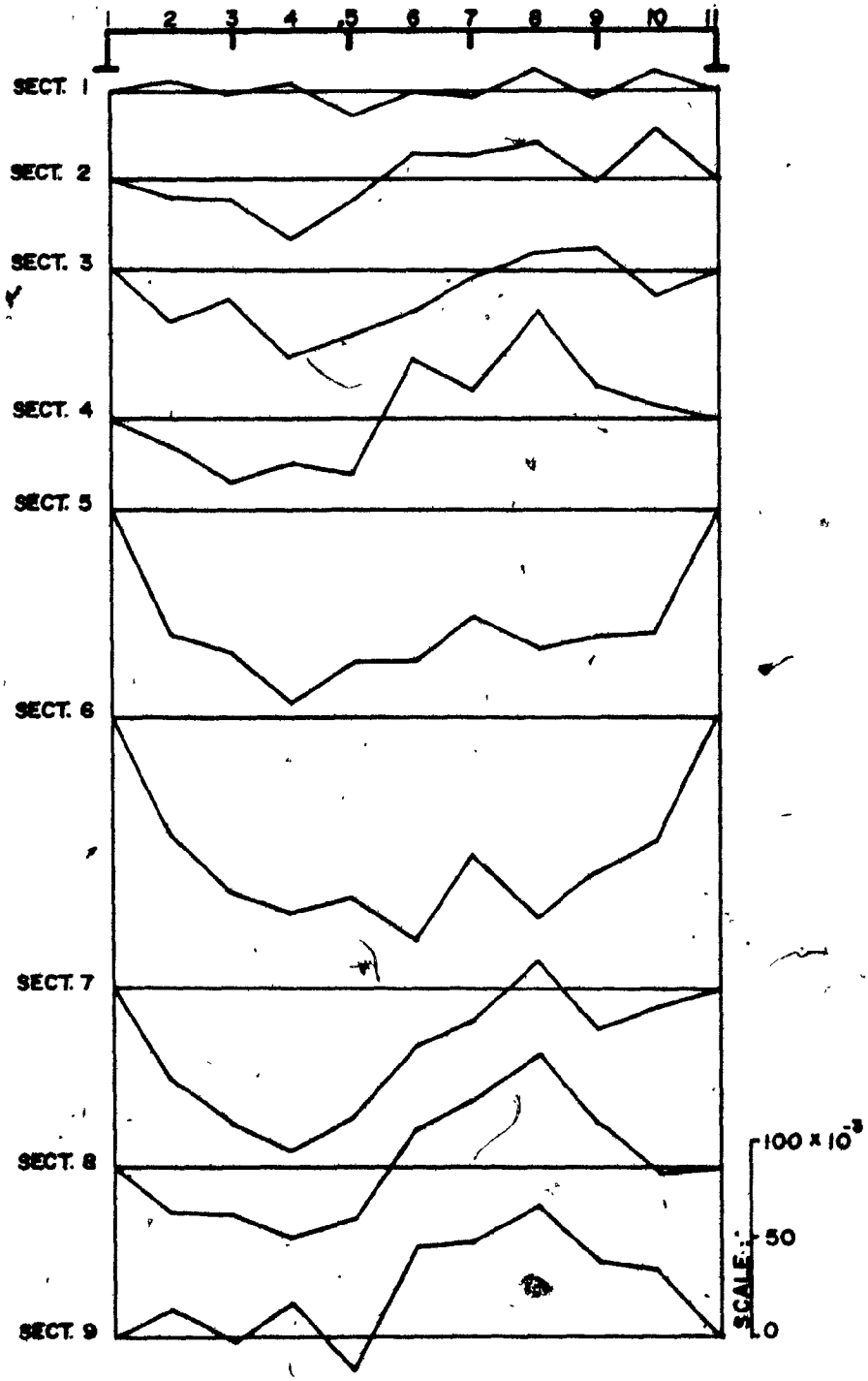

FIG. 4.12 MODEL B, OVERALL INITIAL IMPERFECTION (δ_{oy}) OF THE COMPRESSION FLANGE IN TRANSVERSE DIRECTION

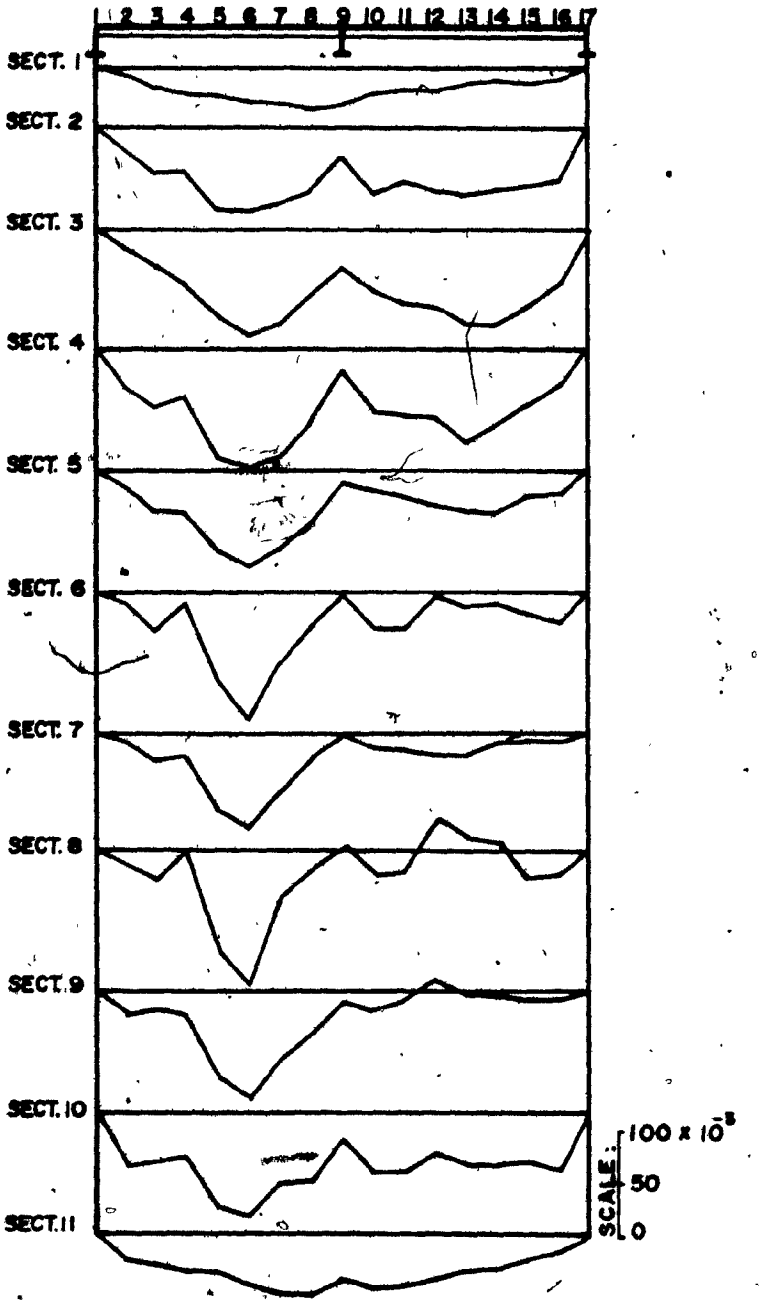

FIG. 4.13 MODEL B, OVERALL INITIAL IMPERFECTIONS (δ_{ox}) OF THE COMPRESSION FLANGE IN LONGITUDINAL DIRECTION

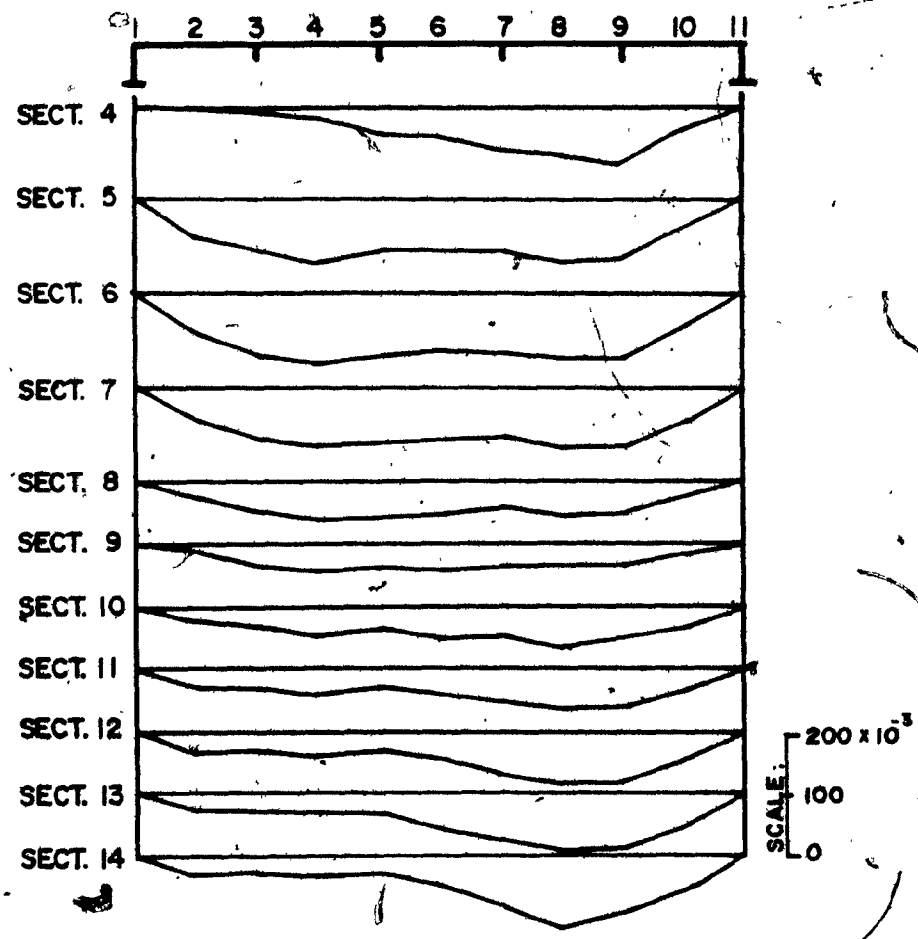

FIG. 4.14 MODEL C, OVERALL INITIAL IMPERFECTIONS (δ_{oi}) OF THE COMPRESSION FLANGE IN TRANSVERSE DIRECTION

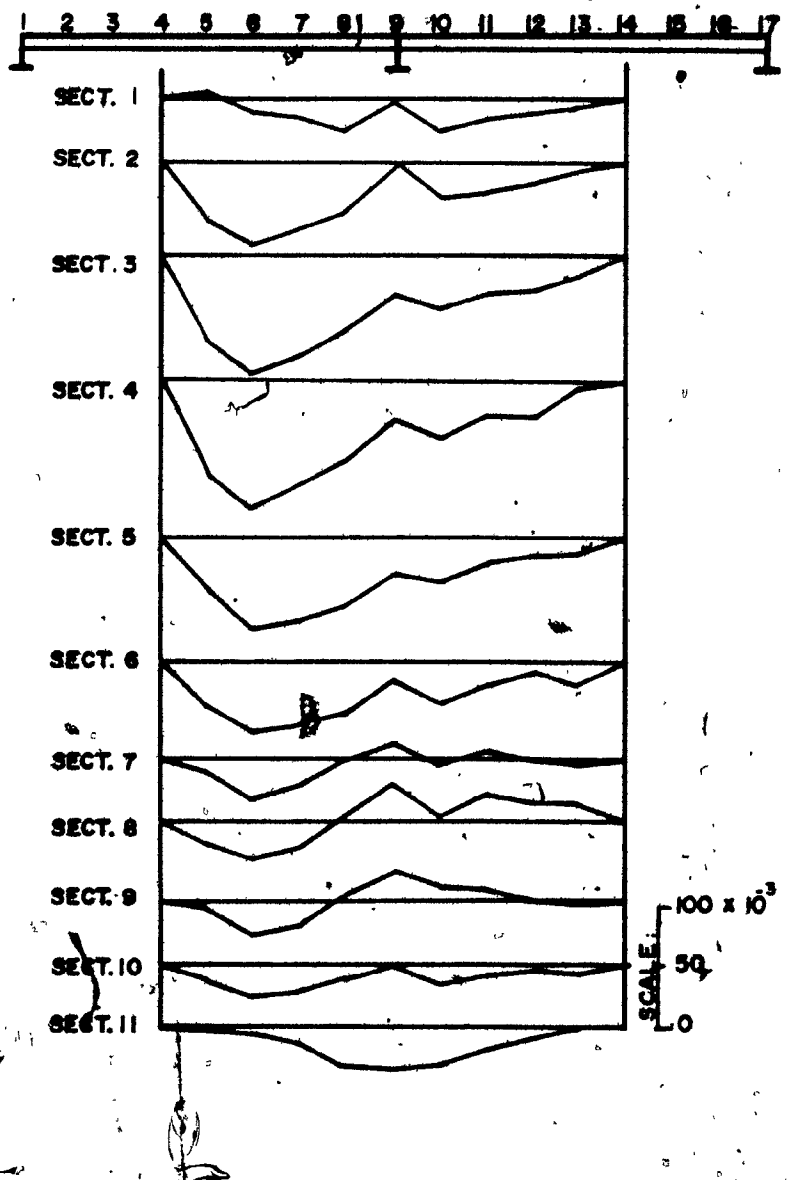

FIG. 4.15 . MODEL C, OVERALL INITIAL IMPERFECTIONS (δ_{ox}) OF THE COMPRESSION FLANGE IN LONGITUDINAL DIRECTION

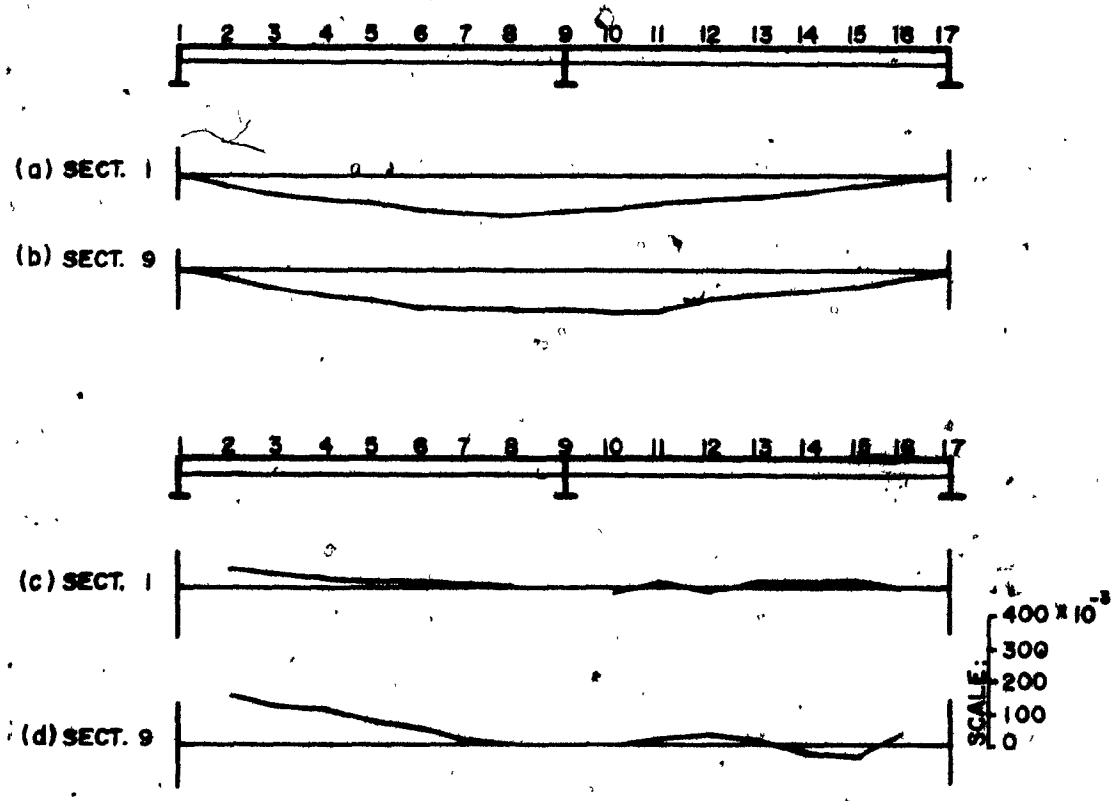

FIG. 4.16 MODEL A, OVERALL INITIAL IMPERFECTIONS, (a) AND (b) TENSION FLANGE ALONG WEBS 1 AND 2, (c) AND (d) LONGITUDINAL STIFFENERS OF WEBS 1 AND 2

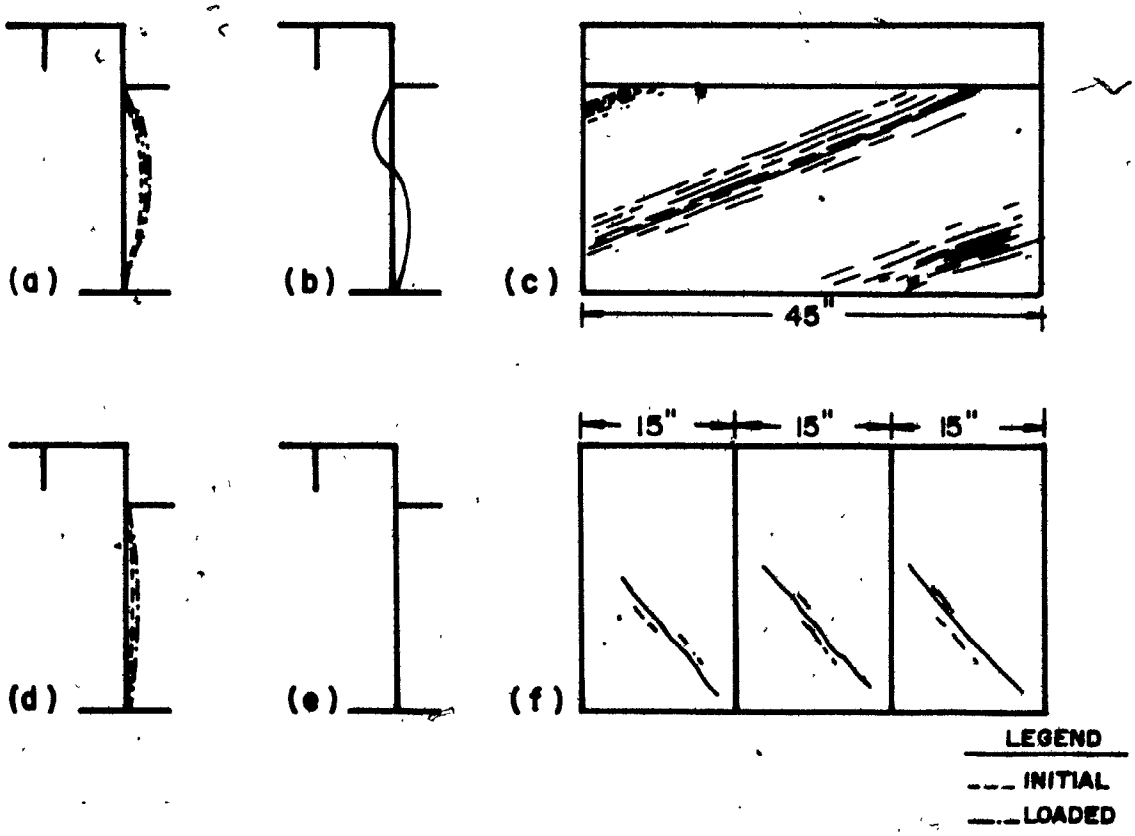

FIG. 4.17 INITIAL AND UNDER-LOAD LATERAL DEFORMATION OF WEB PANELS, (a),(b) AND (c) TYPICAL OF MODEL A, (d),(e) AND (f) TYPICAL OF MODELS B AND C, (b),(c),(e) AND (f) ARE IN THE POST-BUCKLING STAGE (TENSION FIELD)

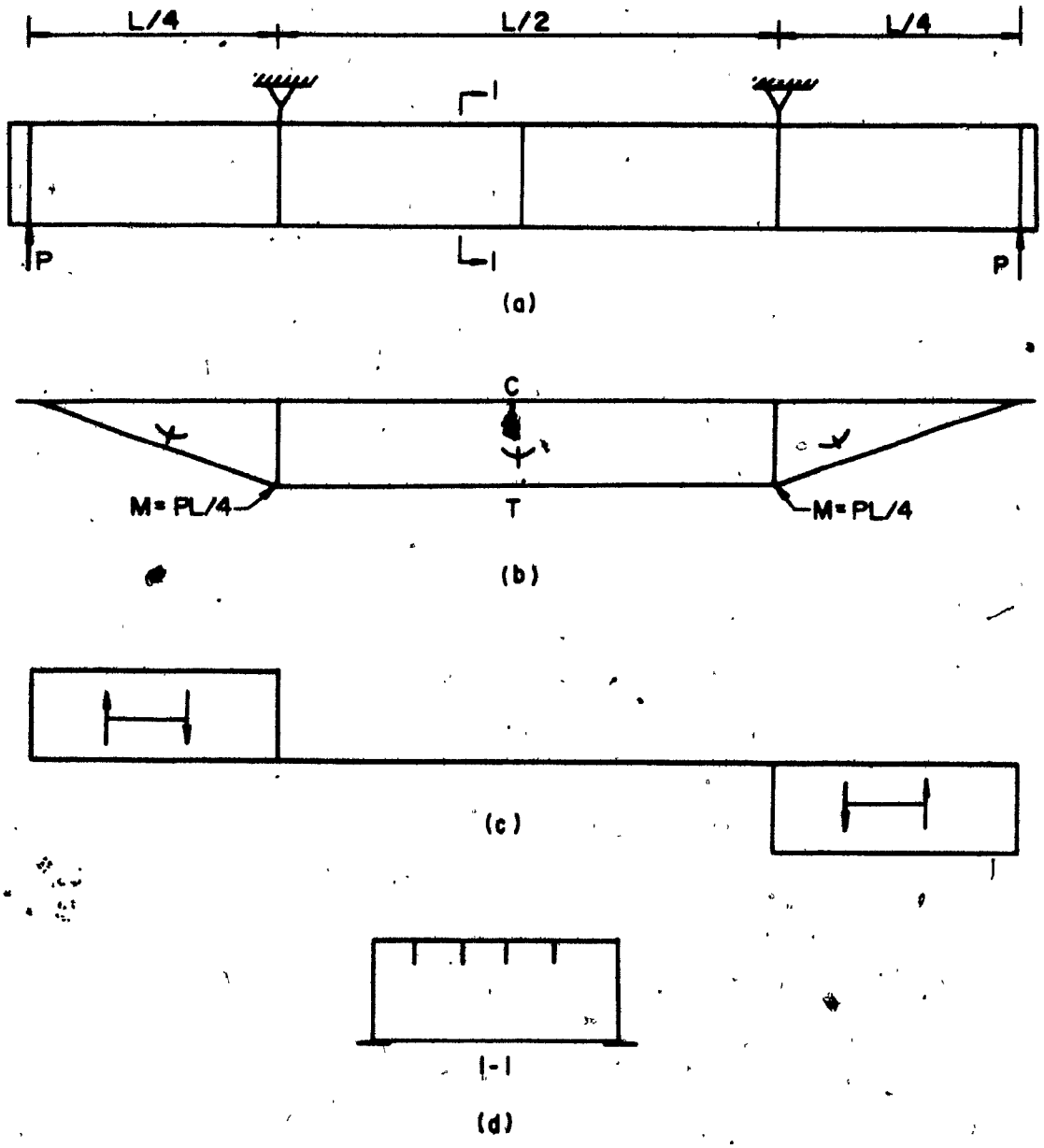

FIG. 4.18 LOADING CONDITIONS: (a) STRUCTURAL SYSTEM, (b) BENDING MOMENT DIAGRAM, (c) SHEAR DIAGRAM, (d) TYPICAL MODEL CROSS-SECTION

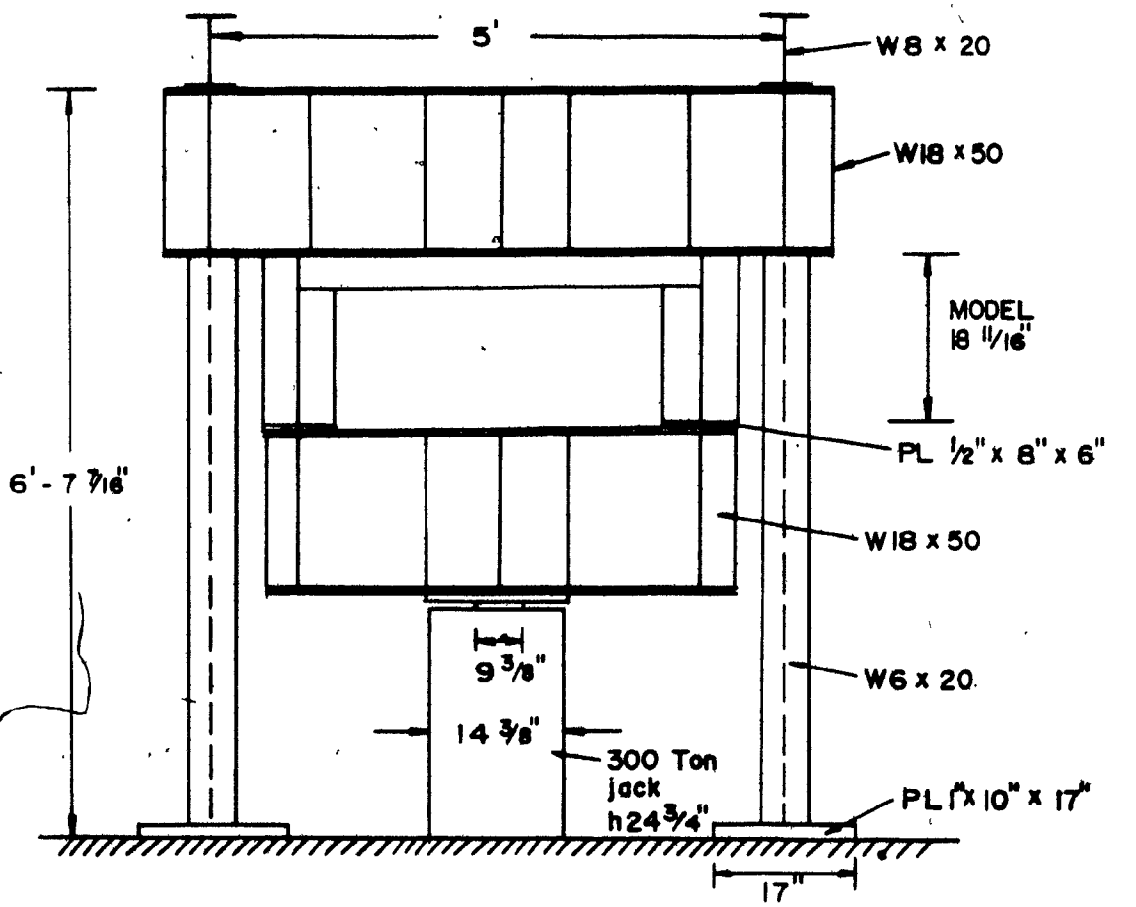

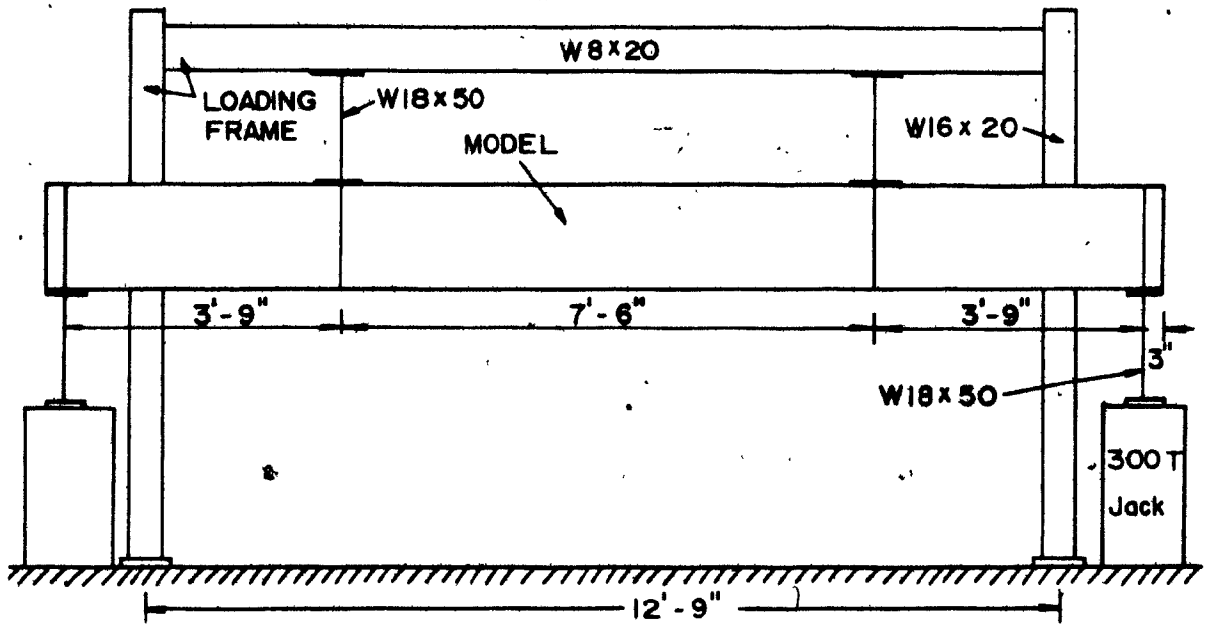

FIG. 4.1 TESTING RING ARRANGEMENT

FIG. 4.20 AN OVERALL VIEW OF THE TESTING RING

Model in the loading frame, one jack (below) at each end, the pump and strain gauges, and Data Logger (right corner). On top of the model is the track for reading of the compression flange deflections.

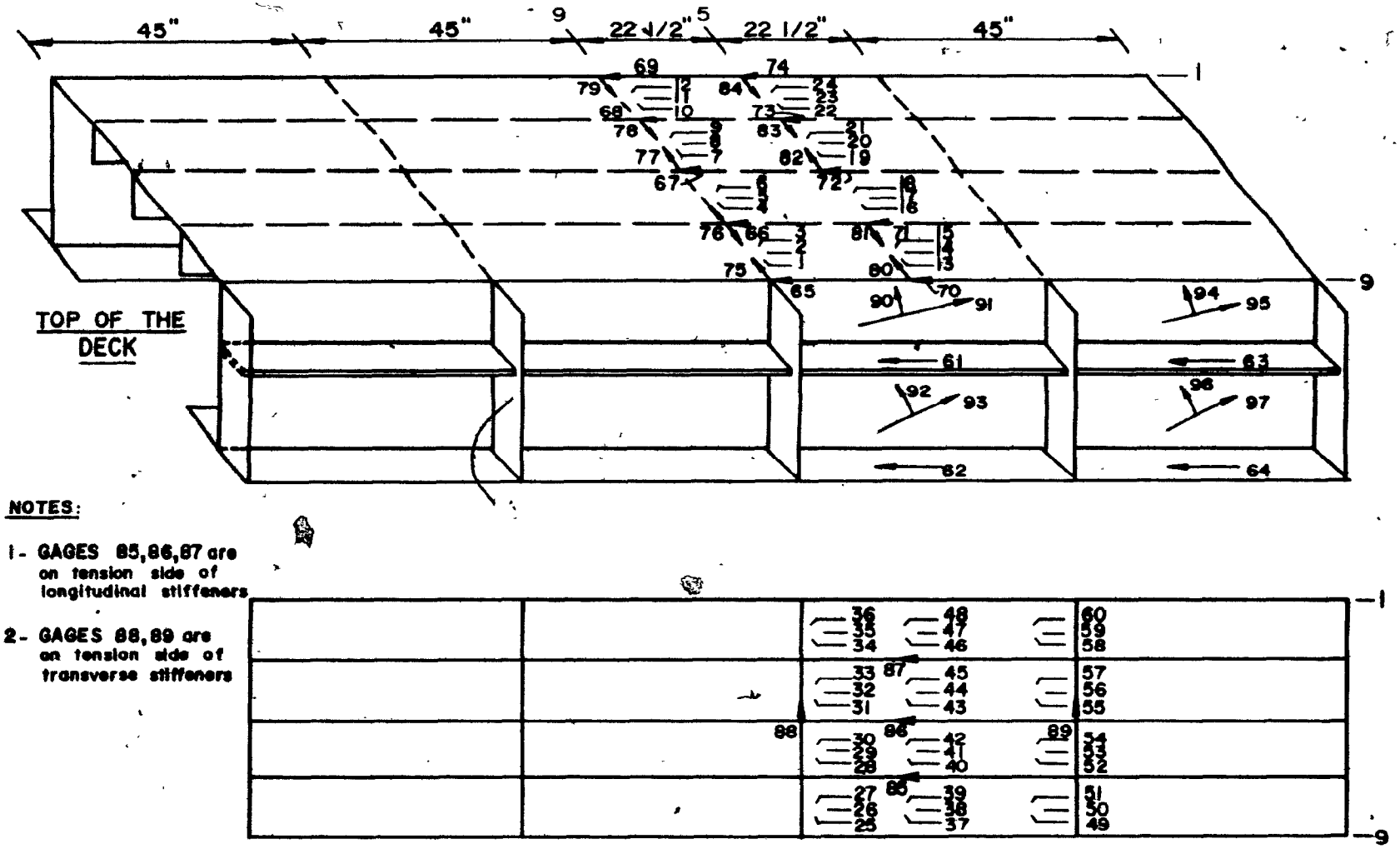

NOTES:

1- GAGES 85,86,87 are on tension side of longitudinal stiffeners

2- GAGES 88,89 are on tension side of transverse stiffeners

FIG. 4.21 STRAIN GAUGES LOCATION ON MODEL A

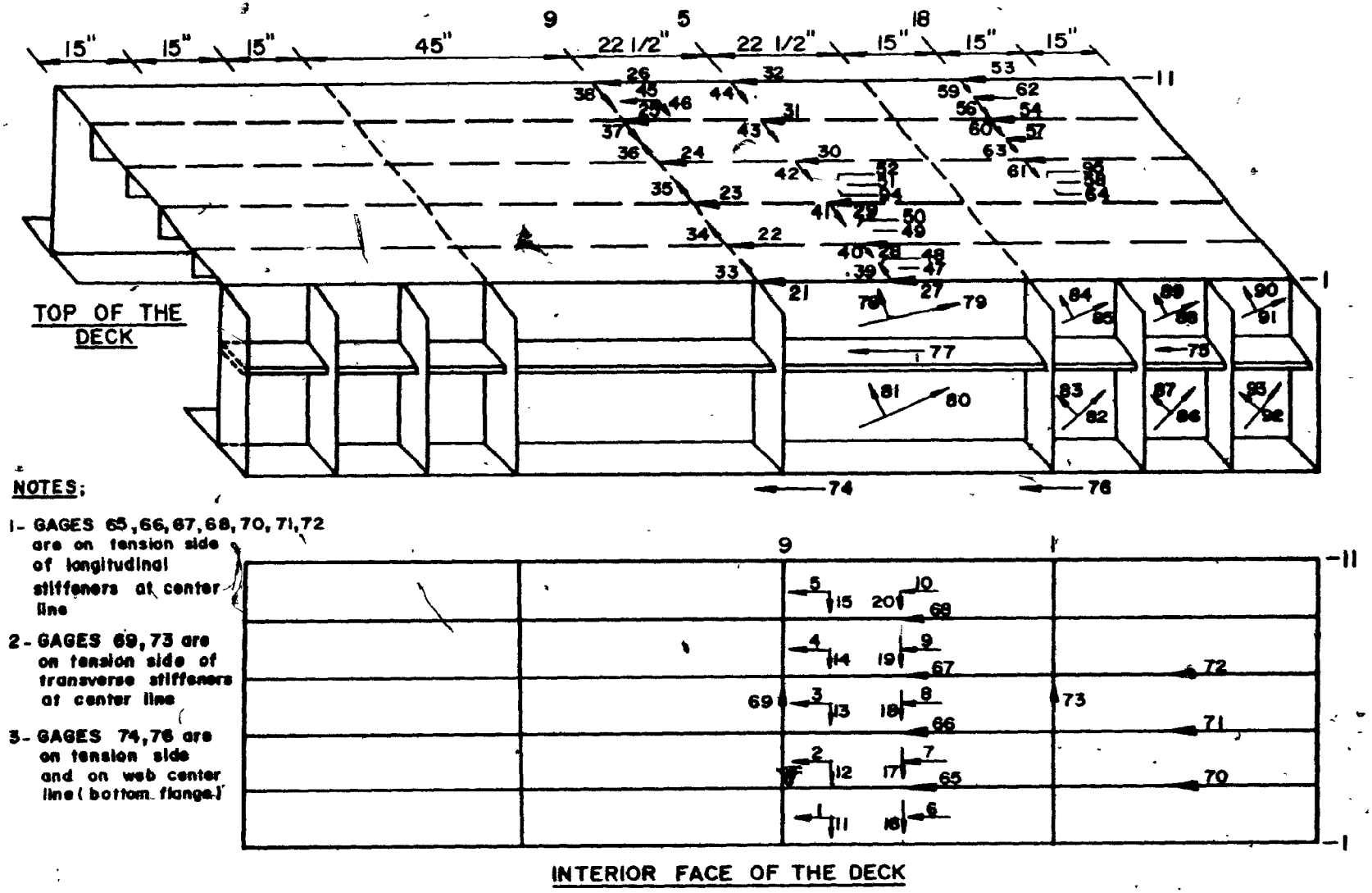

FIG. 4.22 STRAIN GAUGES LOCATION ON MODEL B

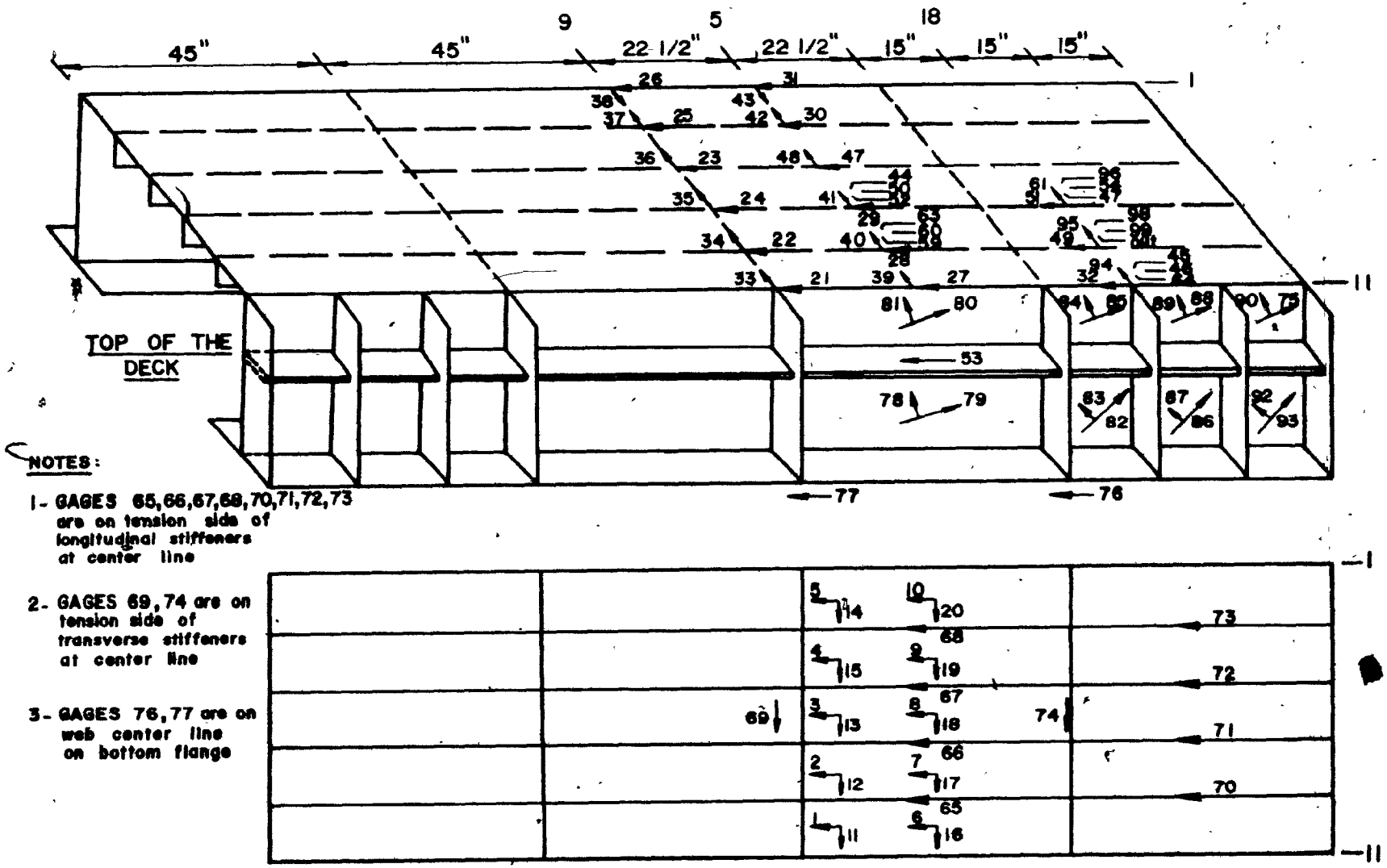

FIG. 4.23 STRAIN GAUGES LOCATION ON MODEL C

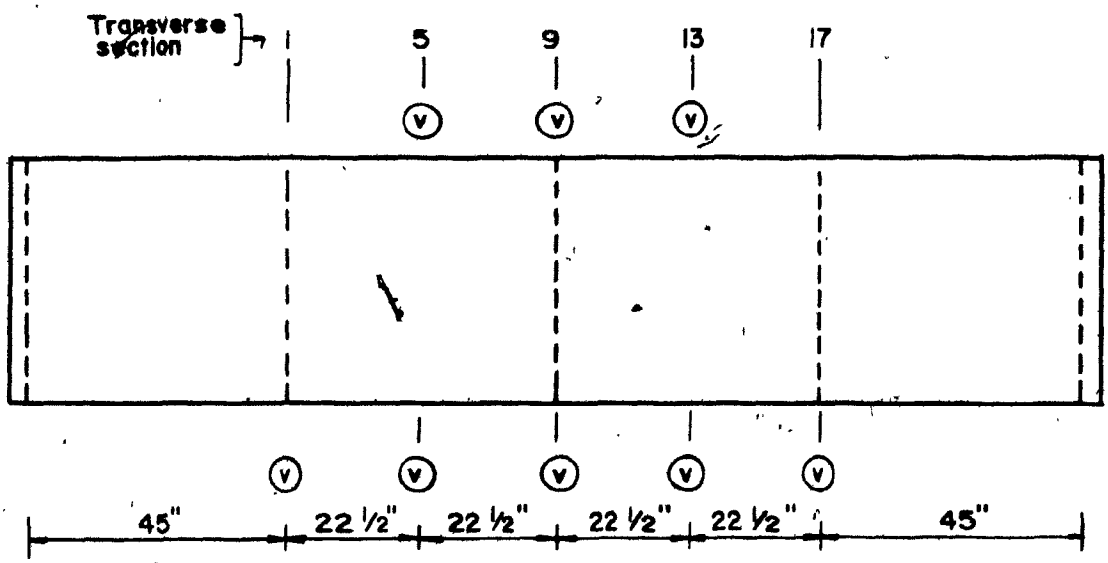

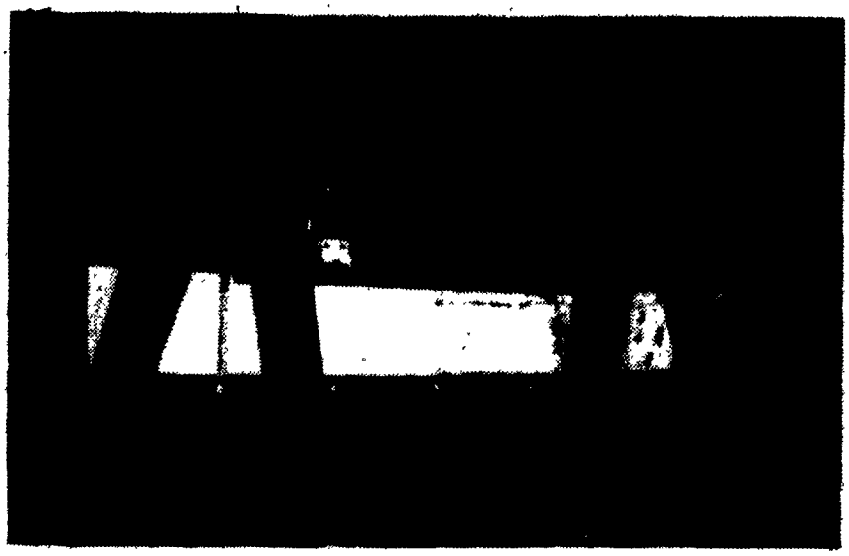

FIG. 4.24 LOCATION OF ADDITIONAL DIAL GAUGES FOR READING OF THE OVERALL DEFLECTION IN A LONGITUDINAL DIRECTION. (a) LOCATION PLAN, (b) VIEW OF THE MODEL

FIG. 4.25 LIME PLACED ON MODEL TO IDENTIFY DEFORMATION LINES

(a)

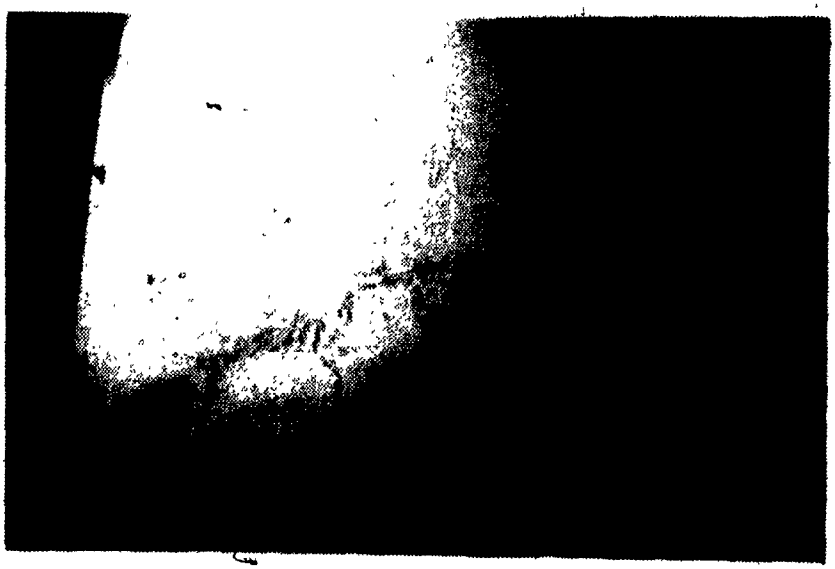

(b)

FIG. 4.26 DEFORMATION LINES. (a) IN THE COMPRESSION FLANGE, (b) IN THE WEB PANEL

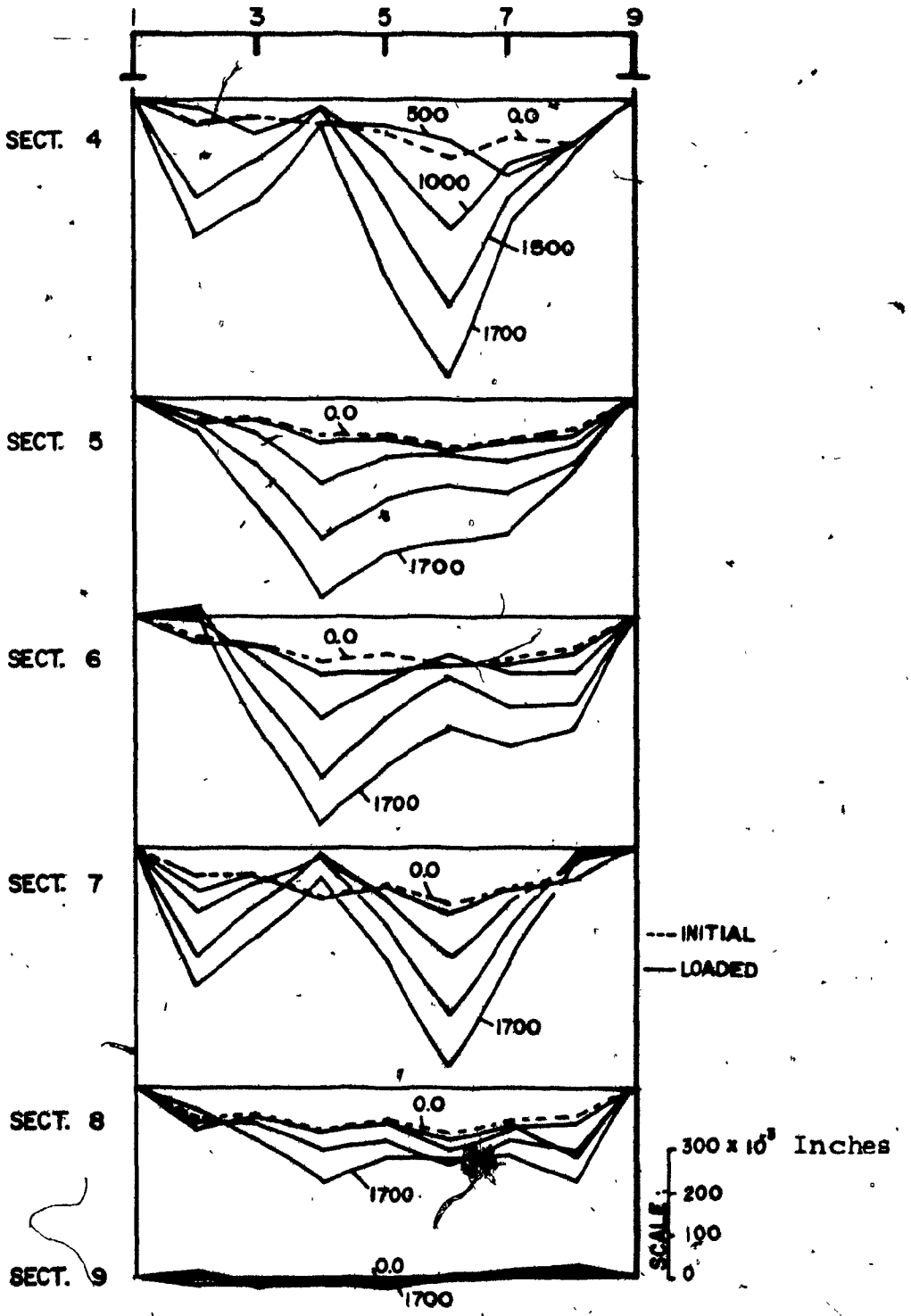

FIG. 4.27 MODEL A, COMPRESSION FLANGE: COMPARISON OF THE OVERALL INITIAL IMPERFECTIONS (δ_{oy}) AND DEFLECTIONS DUE TO LOADING

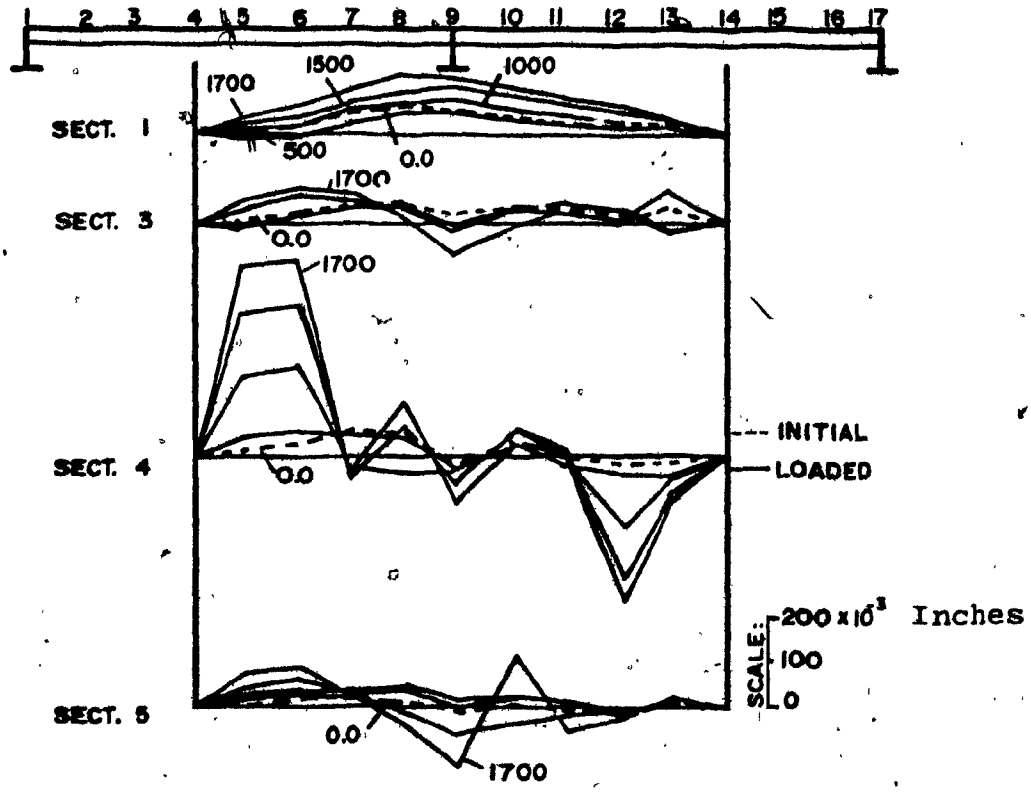

FIG. 4.28 MODEL A, COMPRESSION FLANGE: COMPARISON OF THE OVERALL INITIAL IMPERFECTION (δ_{ox}) AND DEFLECTIONS DUE TO LOADING

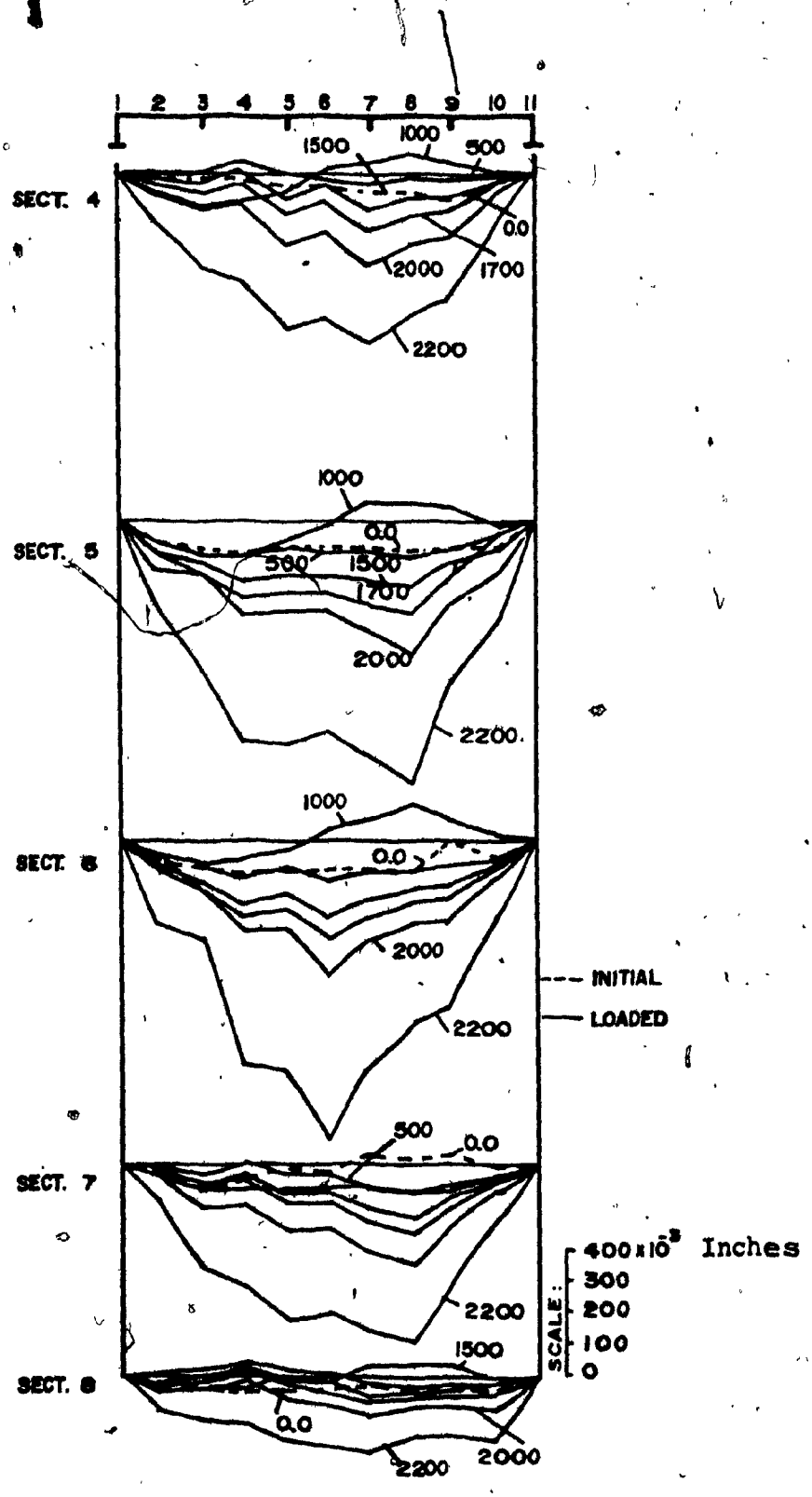

FIG. 4.29 MODEL B, COMPRESSION FLANGE: COMPARISON OF THE OVERALL INITIAL IMPERFECTION (δ_{oy}) AND DEFLECTIONS DUE TO LOADING

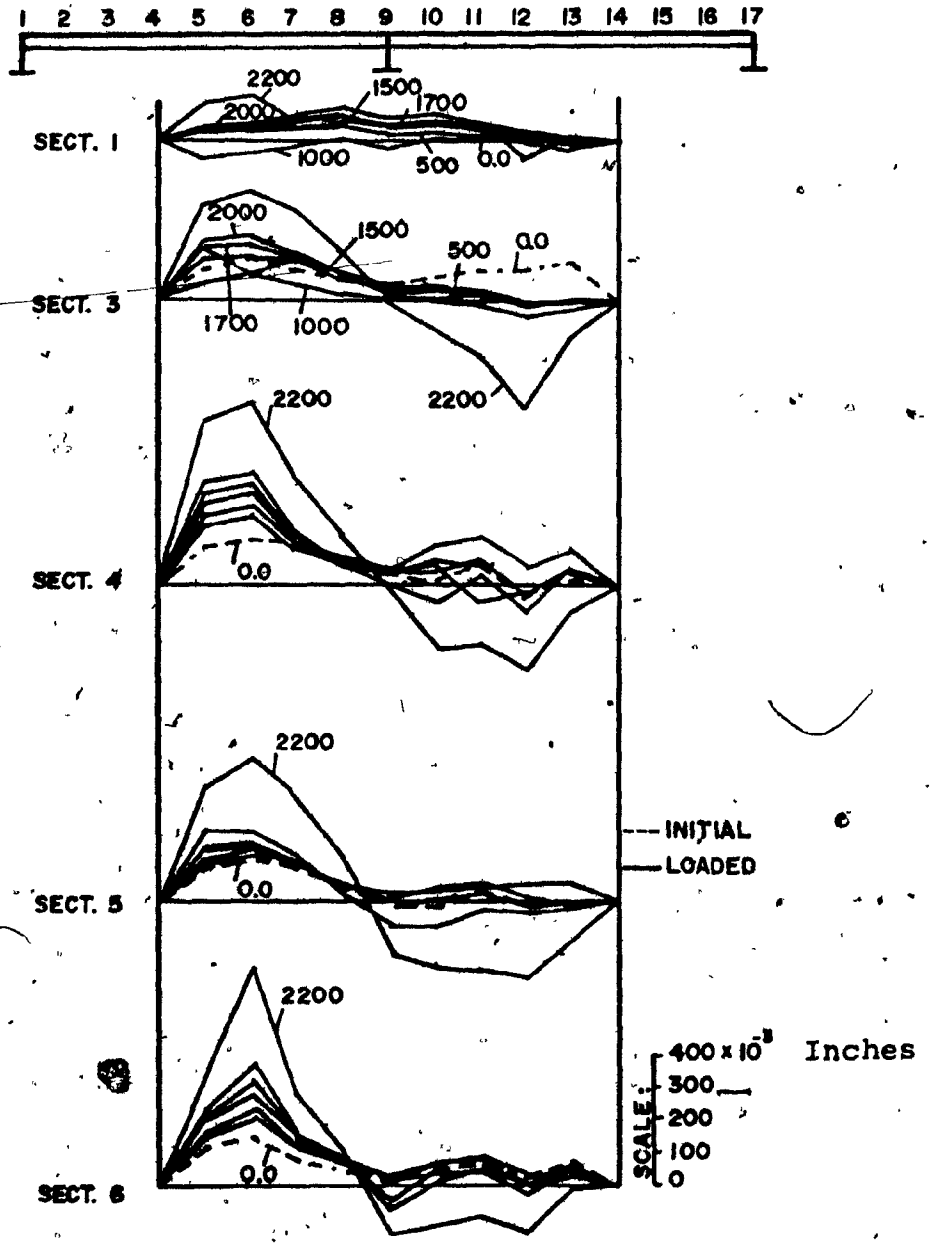

FIG. 4.30 MODEL B, COMPRESSION FLANGE:- COMPARISON OF THE INITIAL IMPERFECTIONS (δ_{ox}) AND DEFLECTIONS DUE TO LOADING

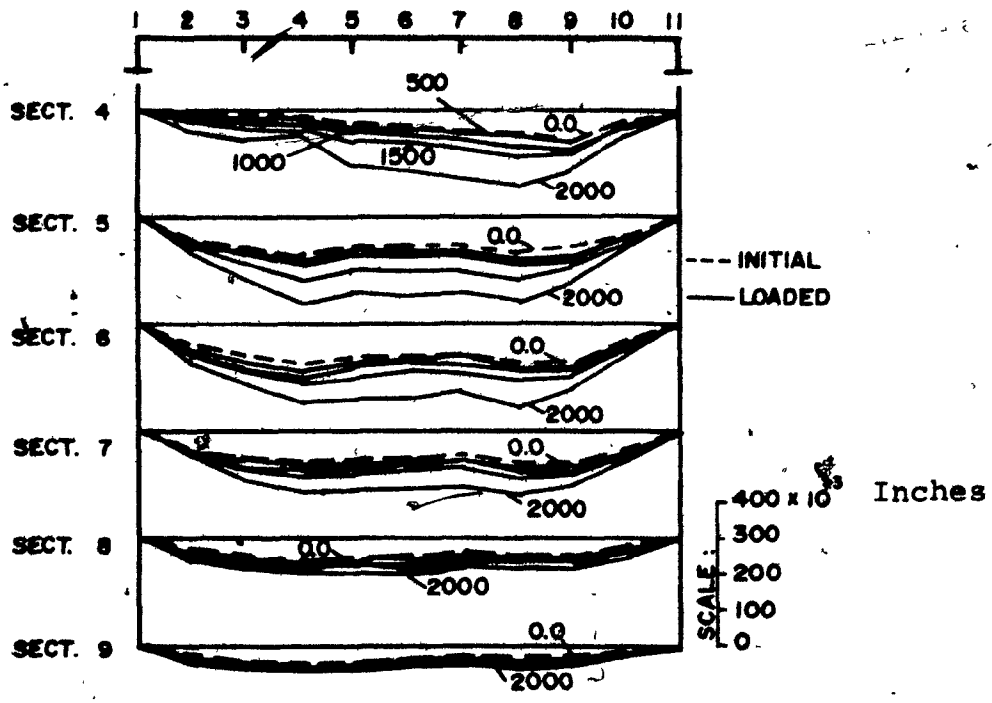

FIG. 4.31 MODEL C, COMPRESSION FLANGE: COMPARISON OF THE INITIAL IMPERFECTIONS (δ_{oy}) AND DEFLECTIONS DUE TO LOADING

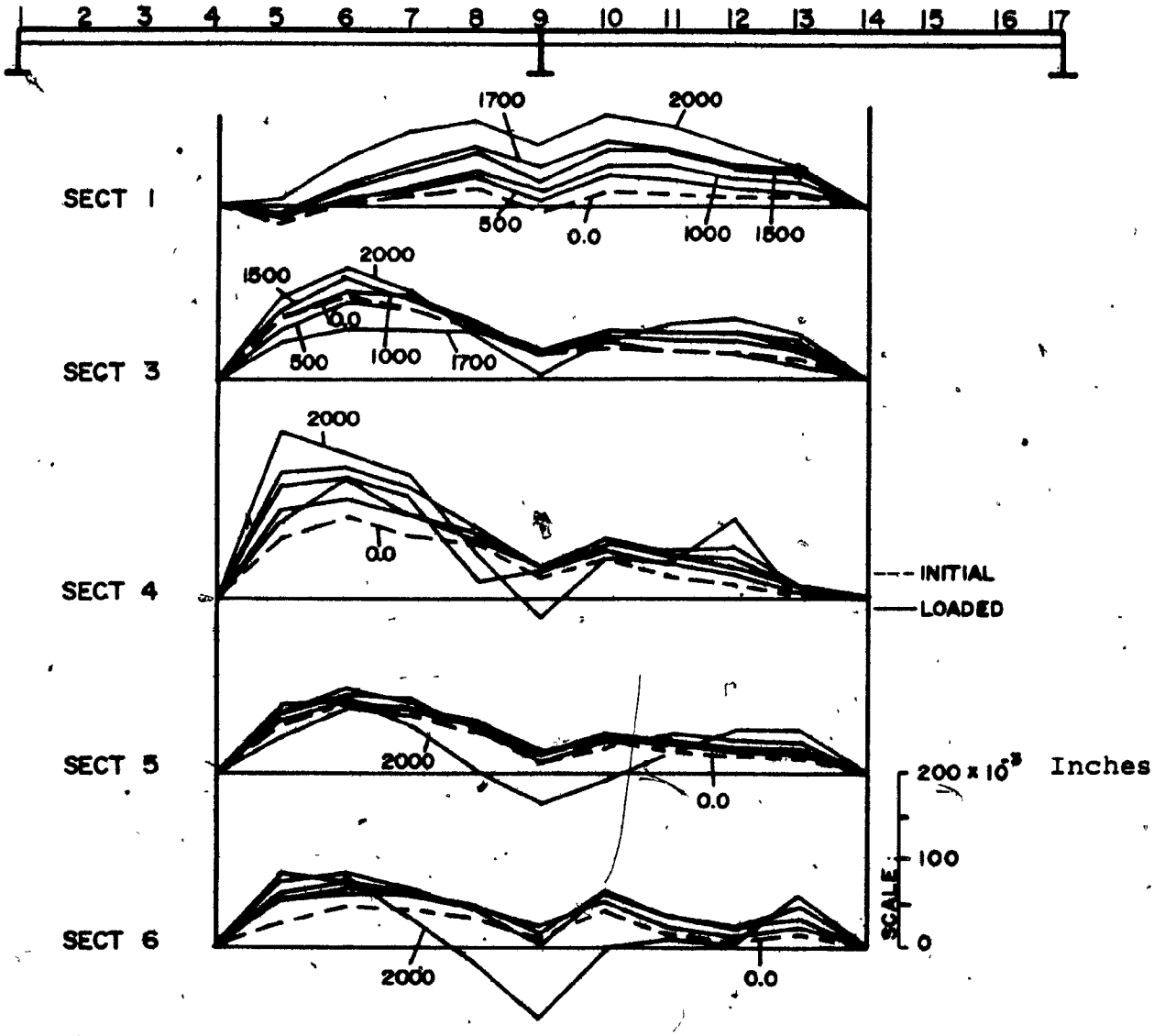

FIG. 4.32 MODEL C, COMPRESSION FLANGE: COMPARISON OF THE OVERALL INITIAL IMPERFECTIONS (δ_{ox}) AND DEFLECTIONS DUE TO LOADING

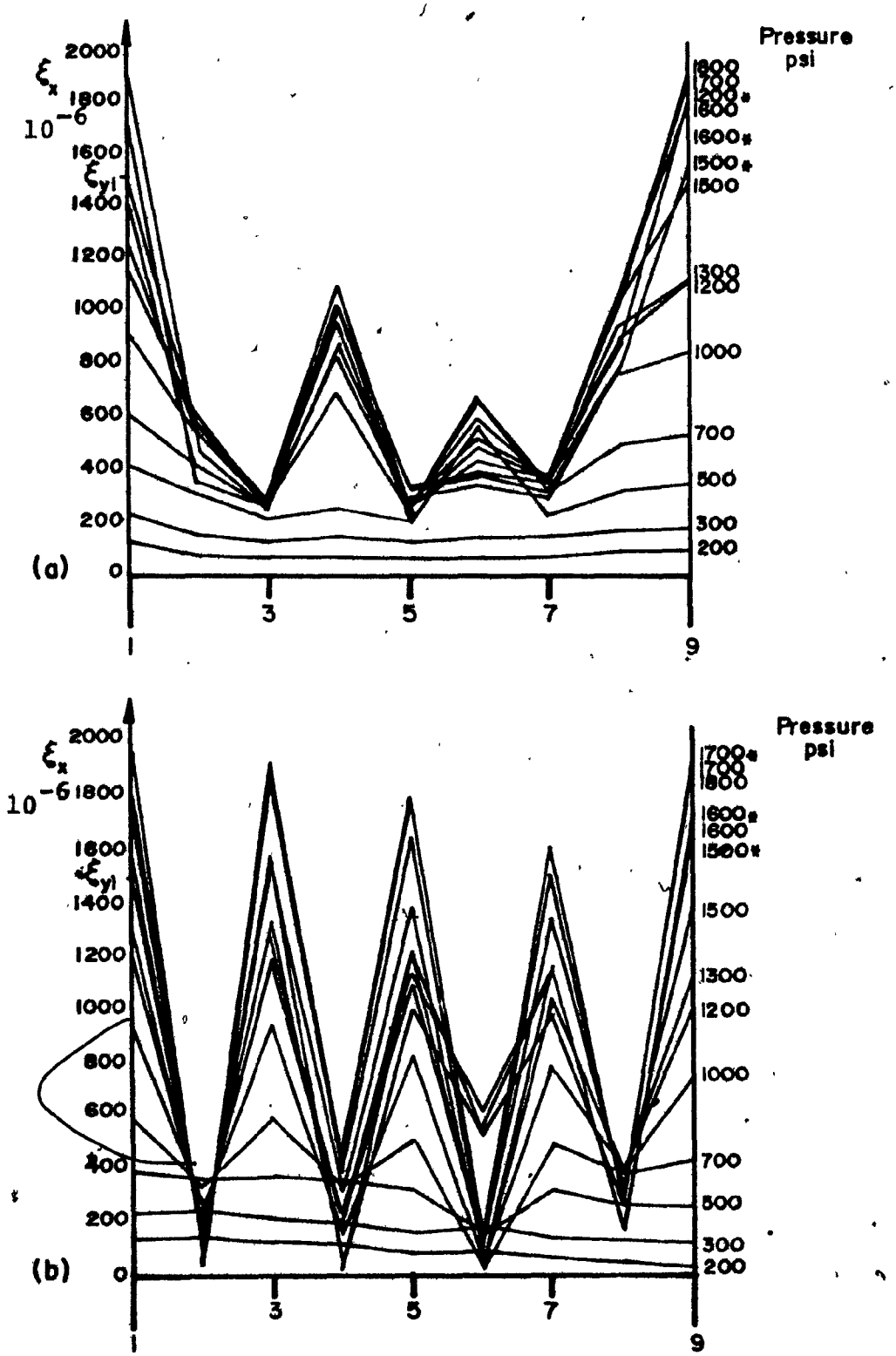

FIG. 4.33 MODEL A, COMPRESSION FLANGE: DISTRIBUTION OF THE LONGITUDINAL STRAIN ϵ_x IN TRANSVERSE DIRECTION AT (a) SECTION 9, (b) SECTION 5, * = AFTER FAILURE POINT

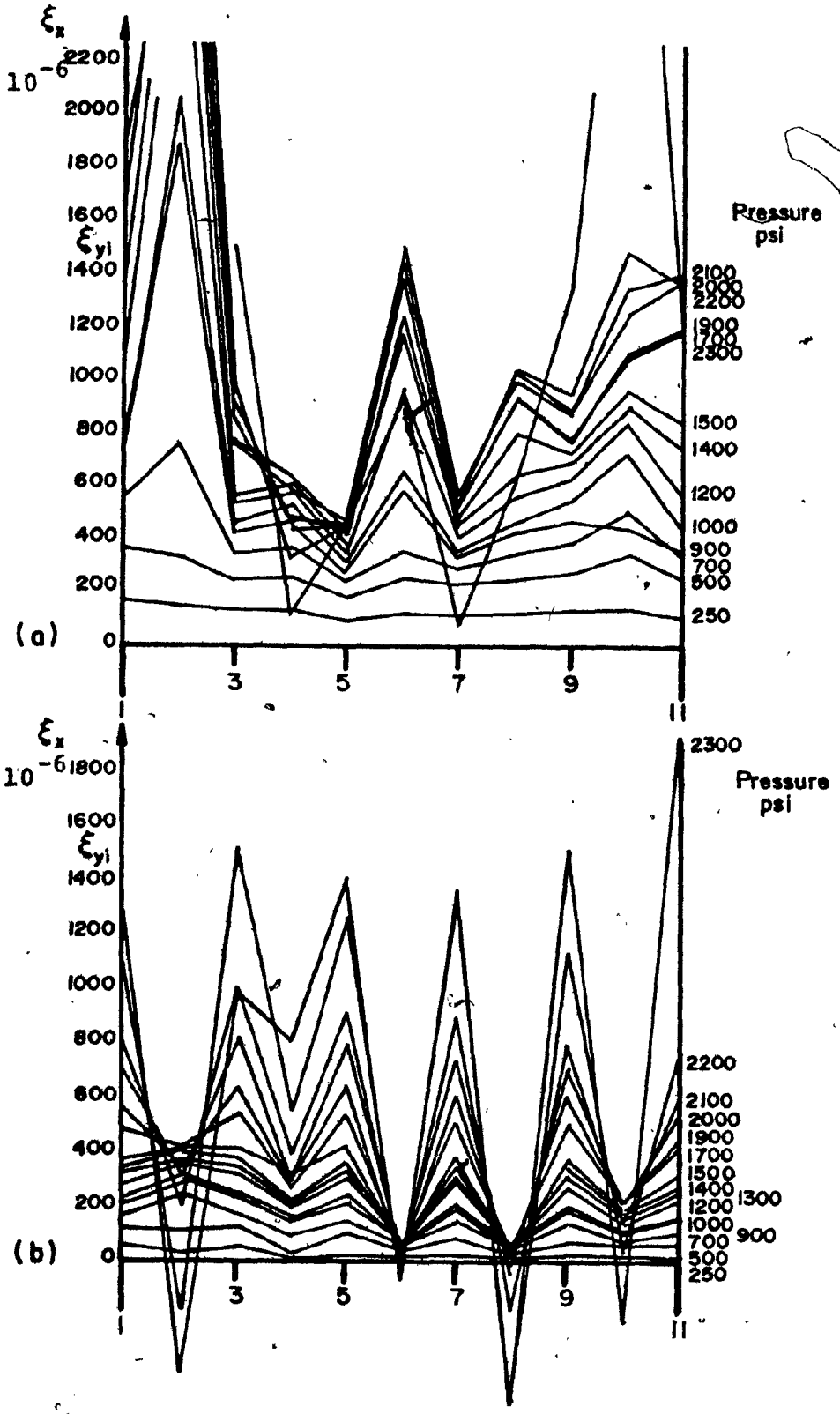

FIG. 4.34 MODEL B, COMPRESSION FLANGE: DISTRIBUTION OF THE LONGITUDINAL STRAIN ε_x IN A TRANSVERSE DIRECTION AT (a) SECTION 9, (b) SECTION 5.

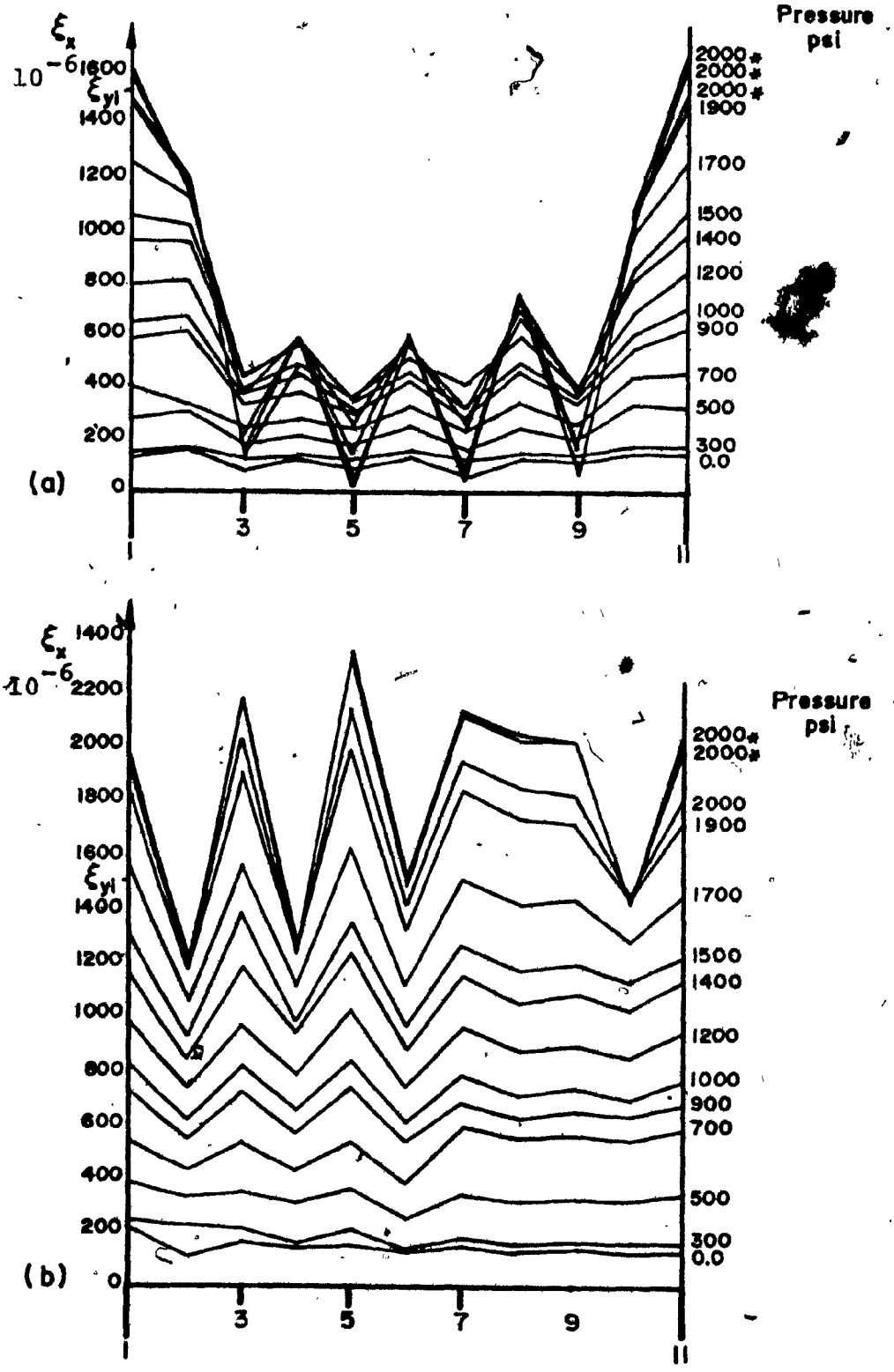

FIG. 4.35 MODEL C, COMPRESSION FLANGE: DISTRIBUTION OF LONGITUDINAL STRAIN ϵ_x IN A TRANSVERSE DIRECTION AT (a) SECTION 9, (b) SECTION 5, * = AFTER FAILURE POINT

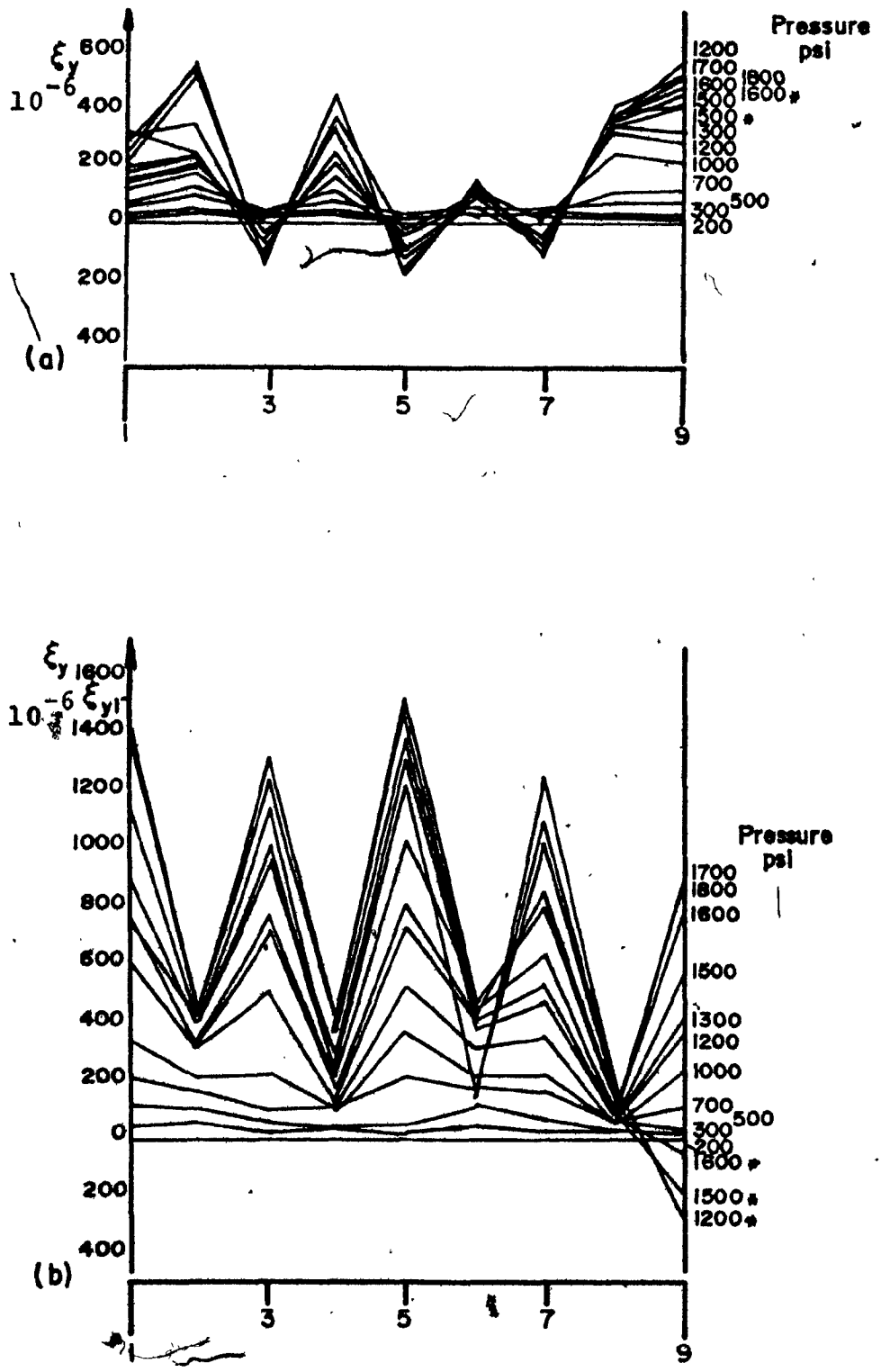

FIG. 4.36 MODEL A, COMPRESSION FLANGE: DISTRIBUTION OF THE TRANSVERSE STRAIN ε_y IN A TRANSVERSE DIRECTION AT (a) SECTION 9, (b) SECTION 5, * = AFTER FAILURE POINT

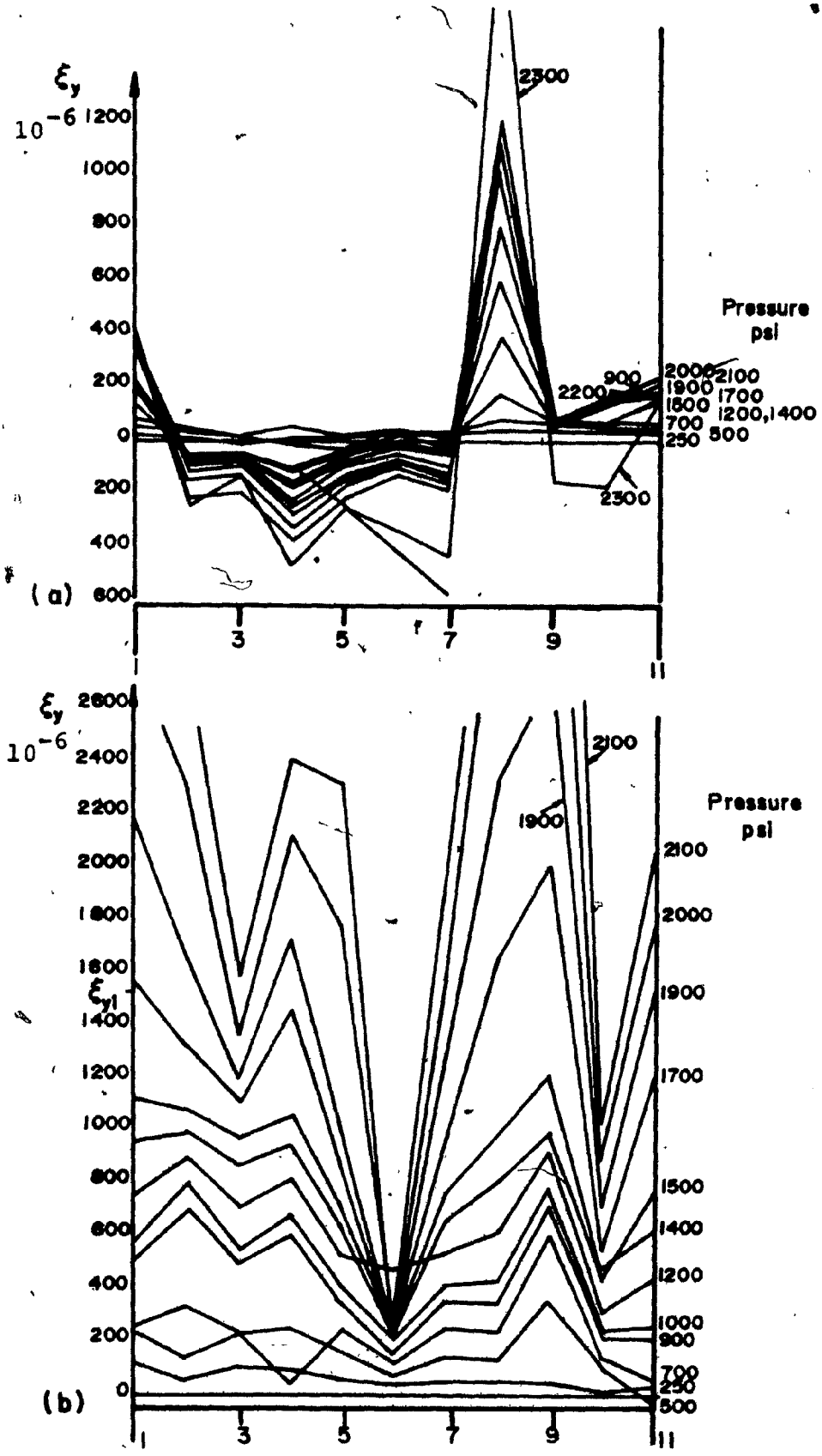

FIG. 4.37 MODEL B, COMPRESSION FLANGE: DISTRIBUTION OF THE TRANSVERSE STRAIN ε_y IN A TRANSVERSE DIRECTION AT (a) SECTION 9, (b) SECTION 5

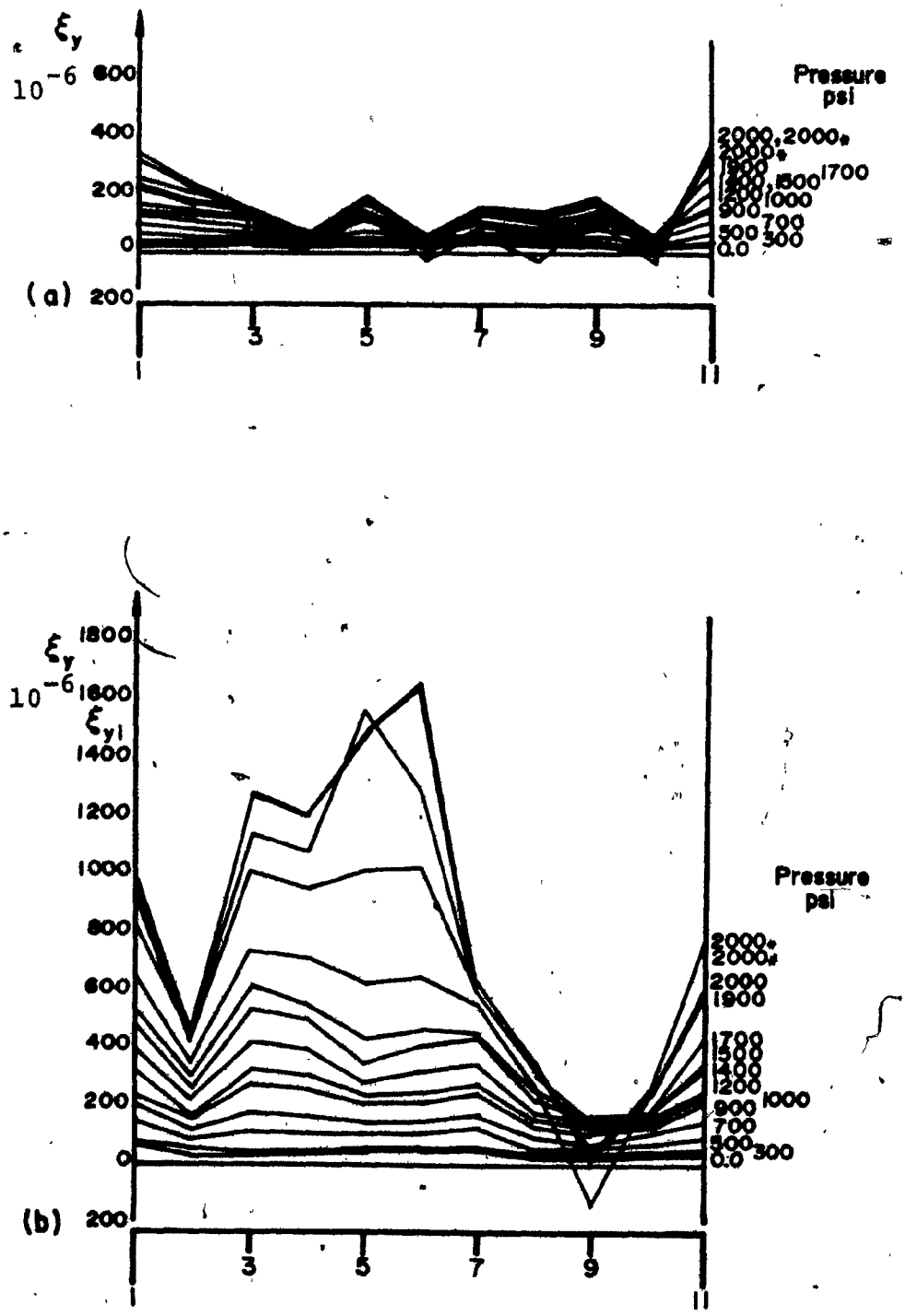

FIG. 4.38 MODEL C, COMPRESSION FLANGE: DISTRIBUTION OF THE TRANSVERSE STRAIN ε_y IN A TRANSVERSE DIRECTION AT. (a) SECTION 9, (b) SECTION 5,* = AFTER FAILURE POINT

(a)

(b)

FIG. 4.39 MODEL A: BUCKLING BEHAVIOUR OF THE COMPRESSION FLANGE. (a) MIDDLE PANEL D = DOWNWARD POCKET, (b) END PANEL (PLATE FAILURE MODE) ↓↓↓ DOWNWARD BOWING, ↑↑↑ UPWARD BOWING

(a)

(b)

FIG. 4.40 MODEL B - OVERALL BUCKLING BEHAVIOUR OF THE COMPRESSION FLANGE, (a) INSIDE VIEW, (b) TOP VIEW: UPWARD (left), DOWNWARD (right)

(a)

(b)

FIG. 4.41 MODEL B - LATERAL BUCKLING OF THE COMPRESSION FLANGE LONGITUDINAL STIFFENERS.
(a) IN THE MIDDLE SUB-PANEL BOWING UPWARD,
(b) IN THE VICINITY OF TRANSVERSE STIFFENERS.

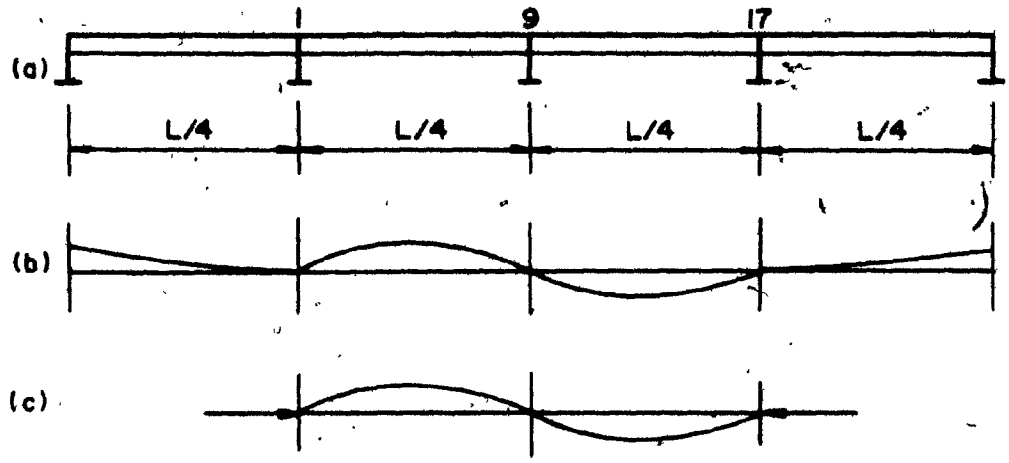

FIG. 4.42 GENERALIZED OVERALL MODE BUCKLING SHAPE OF THE COMPRESSION FLANGE

FIG. 4.43 MODEL C - A VIEW OF COMPRESSION FLANGE LONGITUDINAL STIFFENERS

The lateral buckling was very small, even in the overall buckling mode.

(a)

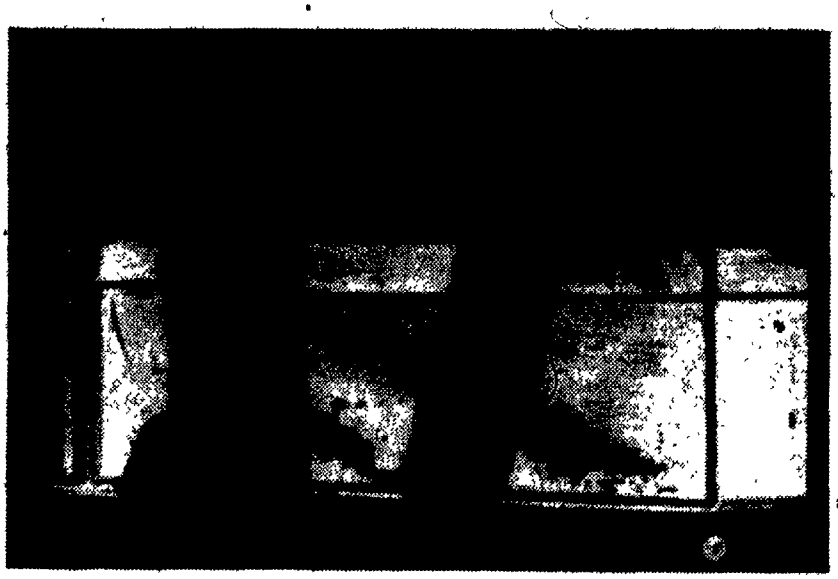

(b)

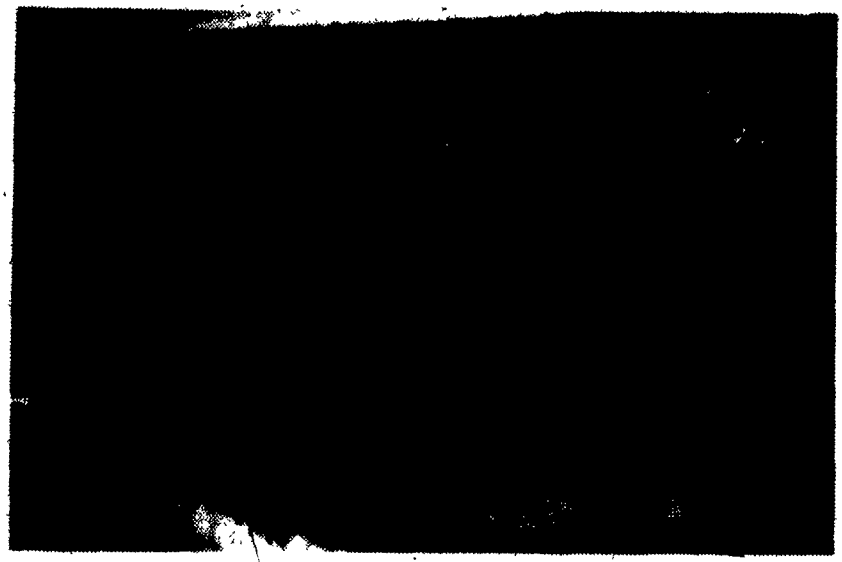

FIG. 4.44 MODEL A - WEB BUCKLING BEHAVIOUR FORMATION OF THE TENSION FIELD ACTION. (a) OUTSIDE VIEW, (b) INTERIOR VIEW

(a)

(b)

FIG. 4.45 MODEL A - WEB POST-BUCKLING BEHAVIOUR. (a) LATERAL BUCKLING OF LONGITUDINAL STIFFENER, (b) AT FAILURE, PARTIAL VIEW OF THE COMPRESSION FLANGE END PANEL (PLATE FAILURE MODE) AND WEB END PANEL (TENSION FIELD)

FIG. 4.46 DEFORMATION LINES IN THE VICINITY OF THE VERTICAL WEB BEARING STIFFENER, SHOWING THAT ONE PART OF THE WEB PLATE FORMS A CROSS-COLUMN SHAPE WITH THE BEARING STIFFENER

(a)

(b)

FIG. 4.47 MODEL C - WEB BUCKLING BEHAVIOUR. (a) OUTSIDE VIEW OF DEFORMATION LINES AND LATERAL BUCKLING OF LONGITUDINAL STIFFENER, (b) INSIDE VIEW OF TENSION FIELD DIAGONAL

FIG. 4.48 WEB BUCKLING IN THE MIDDLE SUB-PANEL DUE TO THE INFLUENCE OF THE OVERALL BUCKLING MODE OF THE COMPRESSION FLANGE

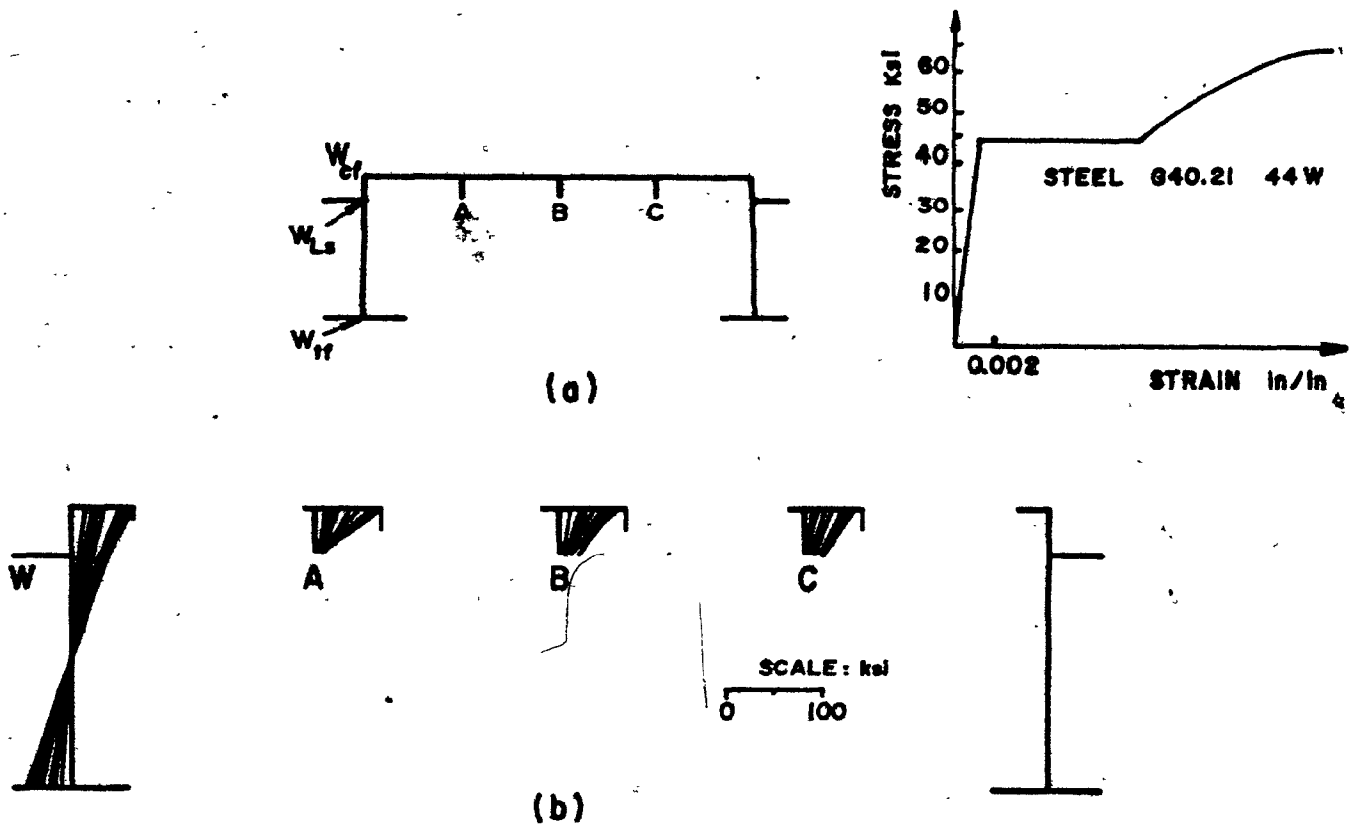

FIG. 4.49 MODEL A: DISTRIBUTION OF THE COMPRESSION STRESS (σ_x) IN COMPRESSION FLANGE LONGITUDINAL STIFFENERS AND IN WEB PANEL (AT TRANSVERSE SECTION 5)

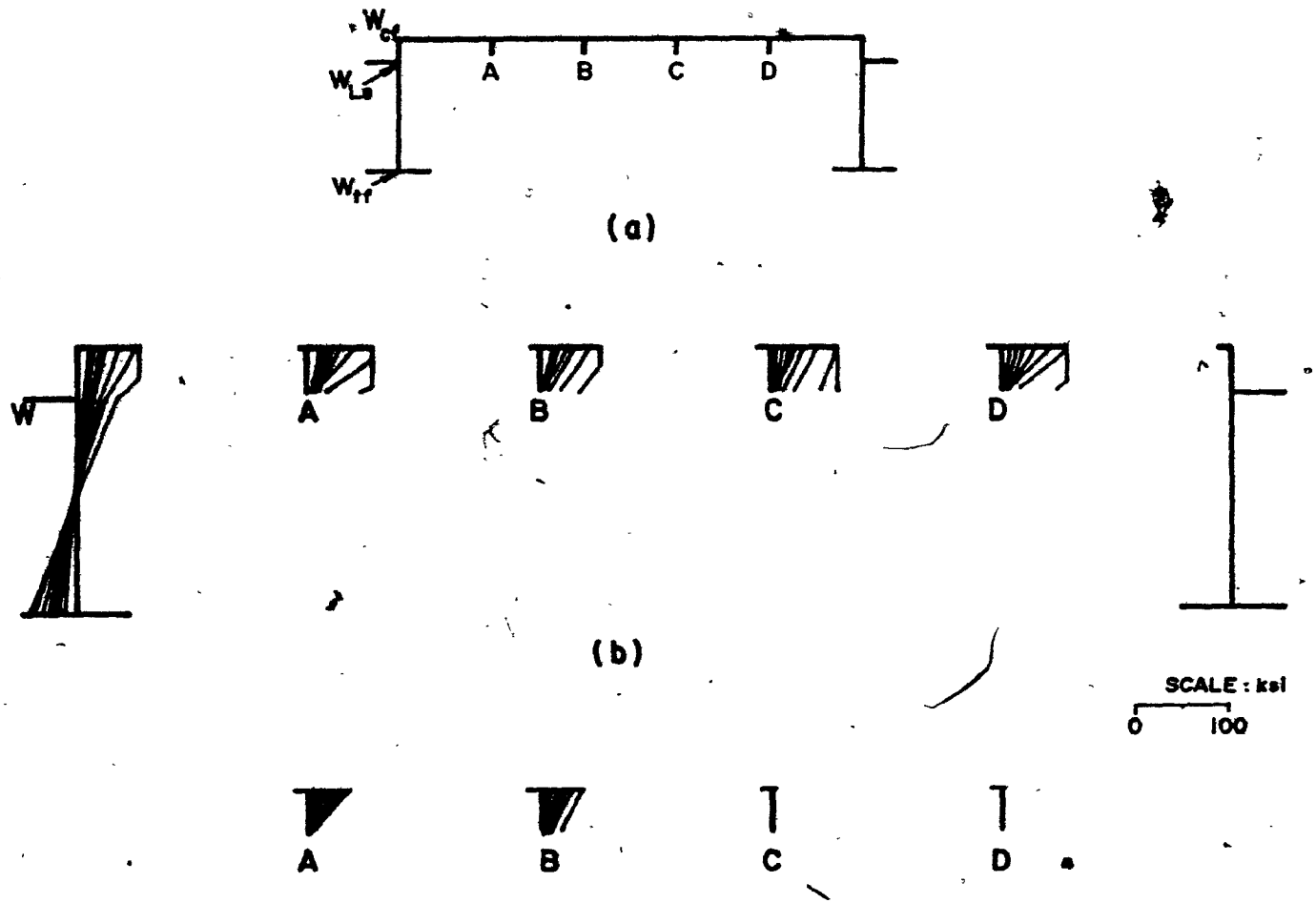

FIG. 4.50 MODEL B: DISTRIBUTION OF THE COMPRESSION STRESS (σ_x) IN THE COMPRESSION FLANGE LONGITUDINAL STIFFENERS AND IN THE WEB PANELS, (b) SECTION 5, AND (c) SECTION 18

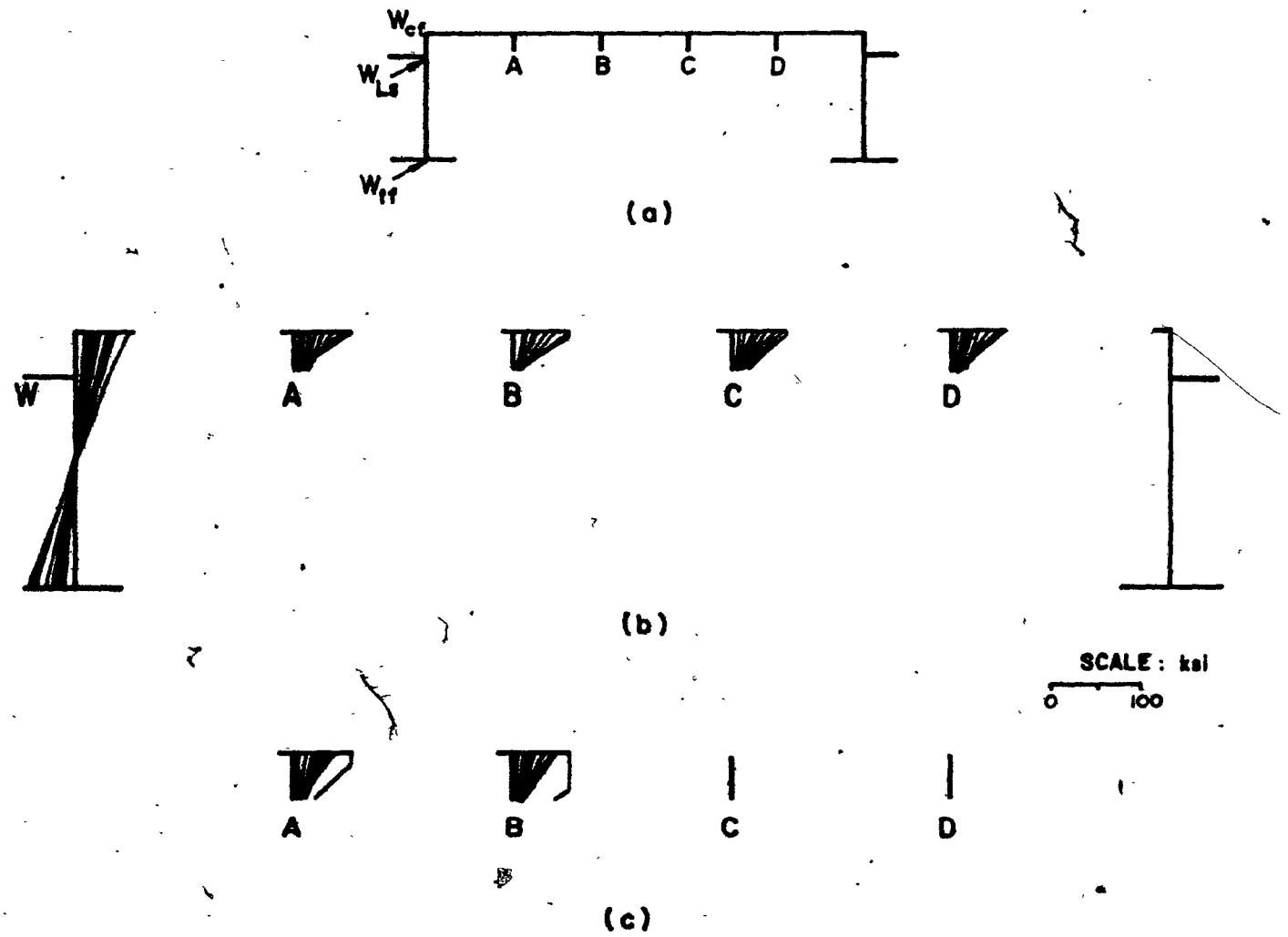

FIG. 4.51 MODEL C: DISTRIBUTION OF THE COMPRESSION STRESS (σ_x) IN THE COMPRESSION FLANGE LONGITUDINAL STIFFENERS AND IN THE WEB PANELS, (b) SECTION 5, AND (c) SECTION 18

CHAPTER V

CONCLUSIONS AND RECOMMENDATIONS

CHAPTER V

CONCLUSIONS AND RECOMMENDATIONS

5.1 CONCLUSIONS

The ultimate strength of steel box-girder bridges, as governed by their buckling performance is investigated, in particular, the compression flange. The main features considered are:

1) The influence of stiffener spacings and their rigidities.

2) The required optimum rigidity for a stiffener to remain rigid and straight up to and after the plate buckling.

3) The influence of any initial geometrical imperfections and residual welding stresses.

4) The influence of the interaction between the flange and web panels upon their reciprocal buckling behaviour, and also upon the overall buckling behaviour of the cross-section.

5) The influence of the buckling mode upon failure mechanism and upon the overall strength of the bridge.

It was first necessary to evaluate the up-to-date knowledge of the problem. For this, an extensive analysis of several bridge design standards [22],[23],[14] was made with the purpose of revealing any deficiencies that required further investigation. It was also necessary to evaluate how this problem had been treated, thus far, in the technical literature. This first step is treated in four technical reports [57],[153],[154],[155],and enables the definition of the main objectives of the present work, as listed above.

The second step is the evaluation of some factors to be considered, such as initial geometrical imperfections, residual welding stresses, fabrication and erection imperfections. It is important to evaluate their exact magnitudes to be included in analytical investigation.

It may be observed in Figure 4.5 (b), how heat due to the welding of longitudinal stiffeners (left part) to the flange plate affects the surrounding zone. Very high residual tension stresses are present in this zone, and the equilibrium condition creates residual compression stresses in the remaining section of the plate element, between the stiffeners.

The third step, is an analytical investigation of the buckling behaviour. Because a steel box-girder bridge is an assembly of plates and stiffened panels, its buckling strength can be better understood by first considering the stiffened panels that compose the cross-section, and secondly,

by considering all components together.

Some of the proposed analytical methods are reviewed and compared. From this study, it has been concluded that full-range extensive experimental tests are needed for a better understanding of the buckling behaviour of steel box-girder bridges.

In the present work, an extensive experimental investigation of the buckling behaviour has been performed. Three models of steel box-girder bridges have been designed in such a way as to cover all main factors considered at the beginning of this Chapter. Care has been taken from fabrication to loading stage, to identify all the initial geometrical imperfactions.

The results of this experimental investigation have led to the following conclusions:

1) The stiffener spacings and their rigidities do have an influence on the buckling strength, in that they affect the distribution of stresses in both longitudinal and transverse directions. Large stiffener spacings cause high losses of stiffness in the plate elements, resulting in a premature local buckling of the plate. Once the plate element starts to lose its stiffness, there occurs a concentration of stresses in the vicinity of the stiffeners. The overall buckling of the compression flange at this stage, depends upon the capacity

of the stiffeners and their associated plate elements in sustaining such high stresses. Therefore, the influence of the stiffener rigidities is evident.

Flanges with optimum stiffener spacings and rigidities will have almost uniform distributions of stresses in transverse directions and their critical buckling stresses may be reached simultaneously, in both the plate and the stiffener.

2) As the rigidity of the stiffener influences the overall buckling behaviour of the stiffened panels, it is important to establish the required optimum rigidity. In the classical elastic plates buckling theory, the optimum rigidity is defined as that required for the stiffener to remain straight and rigid up to and after local buckling of the plate, in other words, to avoid lateral buckling of the stiffener.

Tests have proven that, for the range of b/t ratios tested, 45 and 56, such stiffener performances are achieved only when the relative rigidity is about 3.5 times that of the required optimum rigidity of the classical elastic plates buckling theory, and when the slenderness ratio L/r is about 60.

3. Tests have shown that the influence of initial imperfections and residual welding stresses on the buckling behaviour is evident. Residual welding stresses are often released by reheating of the element after welding. As this correction

operation was not made upon the models, residual stresses are assumed to be present and their effect is accounted for by a magnification factor applied to their initial geometrical imperfections.

It was observed during the tests that almost all local buckling of the elements took plate in that direction, and had the shape of their initial geometrical imperfections. The fact that local buckling was observed at an earlier stage than that predicted by the classical elastic plates buckling theory, leads to the conclusion that there are initial eccentricities due to initial imperfections, with the consequence that the applied stress is higher than expected.

As the local buckling mode affects the overall buckling mode, therefore, the effect of initial imperfections is evident. It is only when the overall buckling mode of the entire flange is in a more advanced stage, that its direction is sometimes opposite to that of initial imperfections. The residual stress adds to the applied compression stresses. Therefore, it follows that the critical stress is less than expected.

The weakening effect of both the initial imperfections and residual stresses demonstrated by experimental results is in accordance with analytical investigation, where it is shown that the methods neglecting this effect overestimate the buckling strength.

4. The influence of the interaction between the flange and web panels needs to be considered in the design. Although the mathematical formulation of this interaction is complex, with the consequence that the flange and web are analytically treated separately, tests have shown that their interaction does have an influence on their respective buckling behaviour and also upon the overall buckling performance of the entire structure.

Although web panels do not contribute more than 10 to 15% to the moment of inertia of the entire cross-section, their behaviour affects the overall buckling strength. This finding is in accordance with tests made by Hodgkinson [156] for the Britannia Bridge. Tests conducted in the present work have shown that a longitudinal web stiffener located at 1/5 of the web depth from the compression flange, prevents the lateral buckling of the web panel due to high flexural compression stresses. This automatically prevents lateral buckling of the compression flange at the web/flange edge.

The stiffness of the connection element at the web/flange edge is of importance and needs special attention at its design stage. Lateral buckling of the web panel automatically affects the overall buckling of the entire structure. Tests have shown that by reducing the aspect ratio a/b of the web panels, by means of stiffeners, the buckling behaviour of the web is thus improved.

Webs capable of developing tension field action sustain more load. Tension field action is a post-buckling phenomena that takes place if the web panel has adequate stiffeners. Tension field produces vertical forces that need to be added to direct forces from the deck. The resulting vertical forces are supported by vertical stiffeners; longitudinal stiffeners reduce the aspect ratio a/b and are subjected to horizontal load due to flexural compression of the web panels.

In general, box-girders with strong webs and adequate flange/web connections will certainly sustain more load than those having weaker ones for the same compression flanges.

5) The buckling mode of the compression flange has an influence upon its overall buckling strength. Two overall buckling modes are identified during the tests:

a) First, the compression flange may deflect toward the stiffener outstand, with the plate being in compression and the stiffener free-edge under tension (Figure 4.40a, right-hand side). This mode of buckling may initiate two modes of failure.

(i) The "plate failure mode" due to the attainment of the critical buckling stress in the plate, and

(ii) The "stiffener failure mode" due to yielding of the extreme fiber in the stiffener free-edge.

b) The flange may deflect towards the plate element, with the plate being in tension and the stiffener free-edge with the compression (Figure 4.40a, left-hand side). This leads to the "stiffener failure mode" with lateral buckling of the outstand due to high compression stresses.

The stiffener failure mode in b) is the most critical because it is abrupt and a much lower load is associated with it. This is in agreement with analytical investigations. Plate failure modes are found to favour the formation of plastic mechanism in the compression flange. The plastic mechanism lines quickly become spine-lines (hinge) and cause failure. In each of these failure modes, the flange/web interaction has a non-negligible influence.

For a range of the overall aspect ratio a/b of the flange tested (a/b = 1.07), for the longitudinal stiffener spacings used (b/t = 45 and 56), and for the stiffener-relative rigidities provided, the overall buckling mode was characterized by one half-wave in both the longitudinal and transverse direction, with compression flange transverse stiffeners and web panels being nodal lines. This buckling mode may be expressed analytically by a sinusoidal function.

In general, for the overall buckling behaviour, the number of half-waves in each direction will be a function of the flange aspect ratio, both of the longitudinal and trans-

verse stiffener spacings and rigidities, and of the web/flange interaction.

As a general conclusion, tests have proven that the ultimate strength of steel box-girder bridges, as limited by their buckling performance, in particular the compression flange, cannot be treated accurately by the classical elastic plates buckling theory. The real behaviour cannot be well understood at the stage where the local buckling takes place. While some approximate analytical methods can be used for the quick evaluation of ultimate strength, the large deflection theory seems to be the most suitable. The effects of initial imperfections, of residual welding stresses, the interaction between components and the influence of the failure mode need to be considered during the design stage.

5.2 RECOMMENDATIONS

The present investigation is a contribution to the better understanding of the buckling behaviour of steel box-girder bridges, in particular, the compression flange. Such efforts could be extended to cover structural parameters not herein included, or to investigate steel box-girder bridge components, such as diaphragms.

There is considerable technical literature dealing with the buckling behaviour of stiffened panels, however, most of these publications are purely theoretical and their appli-

cation is complex. Some of them, such as those reviewed in the present work, could be found applicable to steel box-girder bridges if they were supplemented by extensive experimental test results, similar to those conducted in the present work. From both the analytical and experimental investigations, the following tentative recommendations can be made.

1) With regard to the analytical investigation, tests have shown that the classical elastic plate-buckling theory cannot accurately predict the buckling strength of wide stiffened panels such as those used in steel box-girder bridges, since it is based upon the behaviour of the plate element alone, and the overall buckling behaviour cannot be understood at the stage where local plate-buckling takes place. The buckling performance can be well understood through consideration of the overall behaviour of the structure, in particular, the post-buckling stage where the failure mechanism is well-developed.

It is only when the overall buckling mode is in a more advanced stage, that the influence of stiffener spacings and rigidities, the interaction between the components, for example flange and web panels, can be investigated and some important structural properties, such as the influence of the failure mode upon the ultimate strength can be observed.

It is shown that the initial geometrical imperfections and residual welding stresses have a weakening effect upon its

buckling strength, and this effect is greatest in the range of b/t and slenderness L/r ratios, currently used. These factors need to be included in the analytical investigation. As they could not be measured at the design stage, there is therefore, a need for bridge design standards to establish the values to be used; these could be done on the basis of fabrication and erection tolerances, such as that given in Reference [14].

Some approximate methods, based upon plate/stiffener column behaviour and accounting for those weaking factors, give acceptable results. But, as such considerations sometimes fail to consider the interaction between the components, those methods may, in some cases, lead to very conservative results or can be on the unsafe side. Although complex, the large deflection theory of stiffened panels, accounting for the effect of initial imperfections, of residual welding stresses and of the interaction between components, seems to be the most suitable.

2) Mathematical formulation of the overall buckling of steel box-girder bridges, accounting for the interaction between components, is too complex. A box-girder is different from the conventional plate-girder bridge type, where the stringer can be analysed separately with the floor beams and main girders.

A box-girder behaves as an integral structure and its buckling performance can be better understood by considering the whole cross-section. This is possible by experimental investigation, where the real behaviour of each element and the interaction between the different components can be observed from the early loading stage to the failure stage. Experimental test results are needed before formulating accurate specifications typical to those of steel box-girder bridges.

3) On the basis of experimental tests conducted in the present work and after comparison with those from other sources, the following tentative figures can be recommended for the design of a compression flange.

a) For plate elements between stiffeners, the initial imperfection may be assumed as $a/300$ in a longitudinal direction (Δ_x) and $b/150$ in a transverse direction (Δ_y), where a and b are the spacing of transverse and longitudinal stiffeners, respectively.

- For longitudinal stiffeners, the initial deflections in the longitudinal direction (Δ_{sx}) can be taken as $a/700$ and the initial lateral distortion (Δ_{sy}) as $t_s/7$, where t_s is the stiffener thickness.

- The overall initial imperfections of the entire flange may be assumed as $a/850$ and $b/120$ in longitudinal and transverse directions, respectively.

- The effect of residual welding stresses may be accounted for by a magnification factor on initial geometrical imperfections or by direct consideration of their magnitude as treated in the present thesis.

b) For the range of flange tested a/b_1 = 1.07, b/t = 45 and 56, L/r = 83, 77 and 59, the required optimum rigidity for the stiffener to remain rigid and straight up to and after the buckling of plate elements, is of the order of 3.5 times that given by the classical elastic buckling theory. The slenderness ratio L/r of such stiffener is about 60. This finding is in accordance with other test results given by Dubas [29] and Massonnet [30],[32] who found the optimum rigidity factor to be 5 for the range of models they tested, b/t = 62, L/r = 64 and the overall flange ratio a/b_1 = 1.125, b_1 being the width between the webs. Further tests covering other ranges of a/b_1, b/t and L/r would be useful.

c) The overall buckling mode in both the longitudinal and transverse directions can be expressed by a sinusoidal function. For the webs and transverse stiffener spacing ratios of about one, and transverse and longitudinal stiffener spacing ratios of about 5, for the range of both the longitudinal and transverse stiffener-relative rigidities used, one half-wave can

be used in both the longitudinal and transverse directions, the web lines and flange-transverse stiffeners being the nodal lines.

In general, the number of half-waves will be a function of both the transverse and longitudinal stiffener spacings and rigidities, as well as a function of the web/flange interaction at their common edge.

d) The critical failure mode needs to be investigated during the design stage. This is possibly only by consideration of the post-buckling behaviour.

e) Finally, for a better understanding of the buckling behaviour of steel box-girder bridges, more experimental tests are recommended to extend the range of those factors considered in the present work, or to investigate other components such as transverse diaphragms, web panel stiffeners, and interaction between the flanges, webs and diaphragms.

Steel box-girder bridges are widely used in intermediate and long-span ranges. This system provides many positive structural characteristics that justify their actual wide use. Therefore, a better understanding of their behaviour will lead to better efficiency, both economically and in providing better safety standards.

We conclude the present work as follows:

"Everything that is beautiful and noble, is the result of reason and calculation."

Beaudelaire

"...Therefore when we build, let us think that we build forever. Let it not be for present delight, nor for present use along..."

Ruskin

REFERENCES

REFERENCES

[1] Tyrrell, H.C., History of Bridge Engineering. The G.B. Williams Co., Printers, Chicago, Ill., 1911.

[2] Steinman, D.B., Watson, S.R. Bridges and Their Builders. Dover Publications Inc., New York, 1957.

[3] Shirley-Smith, H. The World's Great Bridges. Phoenix House, London, 1964.

[4] Hopinks, H.I. A Span of Bridges and Illustrated History. Praeger Publishers, New York, 1970.

[5] Heckel, R. "The Fourth Danube Bridge in Vienna, Damage and Repair." International Conference on Development in Bridge Design and Construction, University College, Cardiff Crosby Lockwood and Son Ltd., London, 1971. pp.588-598.

[6] Anonymous."Cantilever Box Grider Bridge Collapse During Construction." Engineering News Record, June 11, 1970. p.9.

[7] Anonymous. "Australian Box-Girder Span and Pier Collapse." Engineering News Record, October 22, 1970, p. 19.

[8] Anonymous. "Steel Box-Girder Bridge Collapses as Section is Hoisted From Barge," Engineering News Record, November 18, 1971, p.17.

[9] Riscon,C.R. Report of the Royal Commissions into the Failure of the West Gate Bridge. Government Printer, Melbourne, Australia.

[10] Anonymous. "West Gate Bridge Inquiry," Engineering News Record, November 12, 1970. p.11.

[11] Kozak, J.J., and Seim, C. "Poor Structural Design Brings West Gate Bridge Failure", Civil Engineering, ASCE, Vol. 42, No. 6, June 1972.

[12] Anonymous. "Rib Gaps Blamed for Bridge Failure," Engineering News Record, May 18, 1972, p. 25.

[13] Anonymous. "Bridge Collapse Report Faults Common Design Theory", Engineering News Record, November 23, 1972, p. 10.

[14] Department of the Environment, Merrison Committee. "Inquiry into the Basis of Design and Method of Erection of Steel Box Girder Bridges - Interim Report." HMSO, London, 1973.

[15] Anonymous. "Britain Restricts Traffic on Steel Box-Girder Spans," Engineering News Record, June 24, 1971, p. 11.

[16] Anonymous. "British Refine Steel Box-Girder Design Criteria," Engineering News Record, May 4, 1972, p. 9.

[17] Massonnet, C. and Maquoi, R. "Design of Steel Plate and Box-Girder Bridges". J. Struc.Div., ASCE, Vol.101, ST 11, November, 1975, pp.2477-2481.

[18] The Sub-committee on Ultimate Strength of Box-Girders of the ASCE-AASHTO Task Committee on Flexural Members of the Committee on Metals of Structural Division."Steel Box-Girder Bridges - Ultimate Strength Considerations." J.Struc.Div., ASCE, Vol. 100, ST 12, December 1974, pp. 2433-2448.

[19] The Institution of Civil Engineers. Informal Meeting on Steel Box-Girder Bridges, London, April, 1972.

[20] The Institution of Civil Engineers. "Steel Box-Girder Bridges." Proc. Internat. Conf., London, England, February 13-14, 1973.

[21] Steinhardt, O., "Recent Revisions to German Standard DIN 4114. Steel Box-Girder Bridges," Proc.Intl.Conf., ICE, London, February 1973, pp.203-208.

[22] The American Association of State Highway Officials. Standard Specifications for Highway Bridges, Eleventh Edition, 1973.

[23] Canadian Standards Association. Design of Highway Bridges, CSA - S6, 1974.

[24] Fountain, R.S., "Composite Steel-Concrete Multi-Base Girder Bridges." Paper presented at the Canadian Structural Engineering Conference, Toronto, 1968, pp.17-58.

[25] Timoshenko, S.P., and Gere, J.M. Theory of Elastic Stability. 2nd edition, McGraw-Hill Book Company, 1961, pp.394-404.

[26] Dwight, J.B. "Collapse of Steel Compression Panels." Development in Bridge Design and Construction Inter-National Conference. Crosby Lockwood and Son Ltd., London, 1971, pp.514-539.

[27] Dowling, P.J. "Strength of Steel Box-Girder Bridges - Recent British Research." Paper presented at ASCE/EIC/RTAC Joint Transportation Meeting, Montreal, July 15-19, 1974. See also J.Struc.Div., ASCE, Vol. 101, ST 9, September 1975. pp.1929-1946.

[28] Dowling,P.J., Harding,J.E., and Frieze, P.A. "Steel Plate Structures." An International Symposium. Crosby Lockwood Staples, London, 1977.

[29] Dubas, P. "Essais sue le comportement post-critique de pontes en caisson raidies." Seminar of International Association for Bridge and Structural Engineering (IABSE), Vol. 11, London, 1971, pp. 367-379.

[30] Massonnet, C. "Essais de voilement sur pontres à ames raidies." Memoires, AIPC, Vol.14, Zurich, 1954.pp.125-186.

[31] Massonnet, C., Más, E., and Maus, H. "Essais de voilement sur deux pontres à membrunes et raidisseurs tubulaires." Memoires, AIPC, Vol. 22, Zurich, 1962. pp. 183-228.

[32] Maquoi, R., and Massonnet, C. "Discussion of the Report by P. Dubas." Seminar of IABSE, Vol.11, London, 1971. pp.381-399.

[33] D'Aspice,M.A., and Cooper, P.B. "Static Bending Tests on Longitudinally Stiffened Plate-Girders." Fritz-Engineering Lab. Report No. 30#.5, Lehigh University, April 1965. pp.62.

[34] Owen, D.R.J., Rockey, K.C., and Skaloud, M. "Ultimate Load Behaviour of Longitudinally Reinforced Web-Plate Subjected to Pure Bending." Memoires. IABSE, Vol.18, Zurich, 1970, pp.113-148.

[35] Dwight, J.B., and Ractliffe, A.T. "The Strength of Plates in Compression."Thin-Walled Structures, Their Design and Use in Building (Symposium at University College of Swansea, 11-14, Sept. 1967). Crosby Lockwood and Sons, London, 1967.

[36] Sherbourne, A.N., Liaw, C.Y., and C. Marsh. "Stiffened Plates in Uniaxial Compression." Memoires, IABSE, Vol.31-I, October 1971, pp.145-176.

[37] Murray, N.W. "Buckling of Stiffened Panels Loaded Axially and in Bending." The Structural Engineer, Vol. 51, No. 8, August 1973, pp.285-300.

[38] Murray, N.W. "Analysis and Design of Stiffened Plates for Collapse Load," The Structural Engineer, Vol.53, No.3, March 1975, pp.153-158.

[39] Horne, M.R., and Narayanan, R. "Ultimate Capacity of Longitudinally Stiffened Plates Used in Box-Girders." Proc. ICE, Part 2, 61, June 1976, pp.253-280.

[40] Horne, M.R., and Narayanan, R. "Design of Axially Loaded Stiffened Plates." J. Struc. Div., ASCE, ST 11, November 1977, pp.2243-2257.

[41] Klöppel, E.K., and Scheer, J. Beulwerte ausgestefter Rechteckplatten, Vol.1, Ernst, Berlin, 1960.

[42] Klöppel, E.K., and Moller, K.H. Beulwerte ausgestefter Rechteckplatten, Vol. 2, Ernst, Berlin, 1968.

[43] Rockey, K.C. "An Ultimate Load Method of Design for Plate Girders," Proc. of Conf. on Developments in Bridge Design and Construction. Crosby Lockwood and Son, Ltd., London, 1971, pp.487-504.

[44] Chern, C., and Ostapenko, A. "Unsymmetrical Plate-Girders Under Shear and Moment." Fritz Engineering Laboratory, Report No. 328.9, Lehigh University, October 1970.

[45] Chern, C., and Ostapenko, A. "Strength of Longitudinally Stiffened Plate-Girders Under Combined Loads." Fritz Engineering Laboratory, Report No. 328.10, Lehigh University, December 1970.

[46] Rockey, K.C., Evans, H.R., and Porter, D.M. "Ultimate Load Capacity of Stiffened Webs Subjected to Shear and Bending." Proc. International Conf., ICE, London, 13-14 February 1973, pp.45-61.

[47] Dowling, P.J., Lee, J.A., and Dean, J.A. "The Behaviour up to Collapse of Load-Bearing Diaphragms in Rectangular and Trapezoidal Stiffened Steel Box-Girders." Proc. International Conf., ICE, London, 13-14 February, 1973, pp.95-117.

[48] Rockey, K.C. "The Design of Web Plates for Plate and Box-Girders - A State of the Art Report". Proc.Intl. Conf. on Steel Plated Structures. Imperial College, London, July 1976, pp.459-477.

[49] O'Connor, Colin. Design of Bridge Superstructures. John Wiley and Sons,Inc., 1971.

[50] Argyris, J.H. and Dunne, P.C. "The General Theory of Cylindrical and Conical Tubes Under Torsion and Bending Loads." J.Roy., Aeronaut.Soc. I-IV, February 1947, V, September 1947 and November 1947, VI, May 1949 and June 1949.

[51] Timoshenko, S., "Theory of Bending, Torsion and Buckling of Thin-Walled Members of Open Cross-Section." J. Franklin Institute, Nos. 3,4, and 5. 1945.

[52] Vlasov, V.Z. Thin-Walled Elastic Beams, 2nd edition. National Science Foundation, Department of Commerce, Washington, D.C., U.S.A. 1961.

[53] Rockey, K.C. and El-Gaaby, M.A. "Stability of Load-Bearing Trapezoidal Diaphragms." Int. Assoc. for Bridge and Struc. Engrg., (IABSE), Vol. 32-II,Oct.1972. pp.155-172.

[54] El-Gaaby, M.A. "Stability of Orthogonally Stiffened Load-Bearing Diaphragms." Intl. Assoc. for Bridge and Struc. Engrg., Vol. 34-II,Sept. 1974, pp.72-89.

[55] Wittrick, W.H. "Stress Singularities at Diaphragm-Web-Flange Junctions in Box-Girders", Proc. Inst.Civ. Engrs., Part 2, 59, 1975, (March) pp.79-89.

[56] Wood, J.G.M., and Flint, A.D. "The Design of Box-Girder Diaphragms." Steel Plated Structures, An International Symposium. Edited by Dowling,P.J., Harding, J.E. and Fieze, P.A., Crosby Lockwood Staples, London, pp.429-458.

[57] Tupula, Y.F., and Troitsky, M.S. "Buckling Behaviour of Steel Box-Girder Bridges," Report No. 1, Department of Civil Engineering, Concordia University, November 1976.

[58] Rockey, K.C. and Skaloud, M. "The Ultimate Behaviour of Plate Girders Loaded in Shear," Proc.Colloquium Int. Assoc. Bridge Struc. Engrg., Vol. II, London, 1971, pp.1-19.

[59] Department of the Environment. Committee of Investigation into the Design and Erection of Steel Box-Girder Bridges. Appendix A - Interim Design Appraisal Rules, London, Sept.1971.

[60] Beer, H. and Schulz, G. "Die Traglast des planmässig mittig gedrückten stabes mit Imperfektionen," VDI Journal, 11, Nos. 21,23 and 24, 1969.

[61] Leonhardt, F., and Hommel, D. "The Necessity of Quantifying Imperfections of All Structural Members for the Stability of Box Girders," Proc.Intl.Conf. Steel Box-Girder Bridges, Inst. Civ.Engrs., London, 1973, pp.11-19.

[62] Horne, M.R. Discussion on Session A. Proc.Intl.Conf. Steel Box-Girder Bridges, Inst. Civ.Engrs., London, 1973,pp.37-40.

[63] Chartterje, S. Discussion on Session A. Proc.Intl.Conf. Steel Box-Girder Bridges, Inst. Civ.Engrs., London, 1973, p.38.

[64] Maquoi, R. and Massonnet, C. "Theorie non-linéaire de la résistance post-critique des grandes poutres en Caisson raidies," Intl.Assoc. for Bridge and Structural Engineering, Vol.31-II, March 1971, p.91-140.

[65] Maquoi, R. "Essais de détermination des flèches initiales des panneaux raidis des grands ponts en Caisson," Intl. Assoc. for Bridge and Structural Engineering, Vol.31-II, March 1971, pp.141-151.

[66] Flint, R., and HOrne, R. "Conclusions of Research Program and Summary of Geometric Studies," Proc.Intl.Conf. Steel Box-Girder Bridges, Inst.Civ.Engrs., London, 1973, pp.173-191.

[67] Walker, A.C. "The Post-Buckling Behaviour of Simply-Supported Plates," Aeronautical Quarterly, Vol.20, 1969, pp.203-222.

[68] Walker, A.C. and Dawson, R.G., "Post-Buckling of Geometrically IMperfect Plates," J.Struc.Div., ASCE, ST 1,Vol.98, January 1972, pp.75-94.

[69] Coan, J.N. "Large Deflection Theory of Plates With Small Initial Curvature Loaded in Edge Compression," J. of Applied Mechanics, Vol.18, 1951, pp.143-151.

[70] Winter, G. "Strength of Thin Steel Compression Flanges," Trans. ASCE, Vol.112, 1947, pp.527-576.

[71] Winter, G. "Performance of Thin Steel Compression Flanges," IABSE Preliminary Publications, Third Congress, Liege, 1948, p.137.

[72] Chilver, A.H. "The Stability and Strength of Thin-Walled Steel Struts," The Engineer, Vol.7, August 1953, pp.180-183.

[73] Dawson, R.G. and Walker, A.C. "A Proposed Method for the Design of Thin-Walled Beams Which Buckle Locally," The Structural Engineer, No.2, Vol.50, February 1972, pp.95-105.

[74] Horne, M.R. and Narayanan, R. "An Approximative Method for the Design of Stiffened Steel Compression Panels," Proc.Inst.Civ.Engrs., Part 2, 59, September 1975, pp. 501-514.

[75] Horne, M.R. and Narayanan, R. "Strength of Axially Loaded Stiffened Panels," Simon Engineering Laboratories, University of Manchester, 1974.

[76] Moxham, K.E. "Theoretical Prediction of the Strength of Welded Steel Plates in Compression, CUED/C Report - Struct/TR2, Cambridge University, 1971.

[77] Dwight, J.B. and Little, G.H. "Compressive Tests on Plates With Transverse Welds," CUED/C - Struct/TR31, Cambridge University, 1972.

[78] Frieze, P.A. "Strength of Steel Box-Girder Bridges," Discussion. J. Struct.Div. ASCE, ST 10,Vol.102, October 1976, pp.2086-2088.

[79] Chapman, J.C. Discussion C146,Session C. Proc.Intl. Conf. Steel Box-Girder Bridges, Inst.Civ.Engrs., London, 1973, p.226.

[80] Flint and Horne. Discussion C132, Session C. Steel Box-Girder Bridges, Proc.Intl. Conf. Inst.Civ.Engrs., London, 1973, p.225.

[81] Young, B.W., Elliot, P. and Bowers, G. "Residual Stresses and Measurement of Tolerances," Proc.Intl.Conf., Steel Box-Girder Bridges, Inst. Civ.Engrs., London, 1973, pp.231-240.

[82] Crisfield, M.A. "Full-Range Analysis of Steel Plates and Stiffened Plating Under Uniaxial Compression," Proc. Inst. Civ. Engrs., Part 2, 59, December 1975, pp.595-624.

[83] Dwight, J.B. and Moxham, K.E. "Welded Steel Plates in Compression," The Structural Engineer, No.2, Vol.47, February 1969, pp.49-66.

[84] Nishiro, F., Ueda, Y. and Tall, L. "Experimental Investigation of Buckling of Plates With Residual Stresses, Test Methods for Compression Members," ASTM, STP 419, p.12.

[85] Frieze, P.A., Dowling, P.J. and Hobbs, R.E. "Steel Box-Girders. A Parametric Study on Plates in Compression," CESLIC Report, BG 39, Engineering Structures Laboratories, Civil Engineering Department, Imperial College, London, England, January 1975.

[86] Dwight, J.B. and Little, G.H. "Stiffened Steel Compression Flanges - A Simpler Approach," The Structural Engineer, No. 12, Vol. 54, December 1976, pp.501-509.

[87] Chatterjee, S., and Dowling, P.J. "The Design of Box-Girder Compression Flange," Steel Plated Structures, An International Symposium. Edited by P.J. Dowling, J.E. Harding, P.A. Frieze. Crosby Lockwood Staples, London, 1976. pp.196-228.

[88] Bryan, G.H. Proc.London Math.Soc., Vol.22, 1891.

[89] Gerard, G. Handbook of Structural Stability,Part IV - Failure of Plates and Composite Elements. NACA T.N.3784. August,1957.

[90] Cox, T.A. "A Practical Treatise on the Strength of Materials," Spon, London, 1883.

[91] Gerard, G. Introduction to Structural Stability Theory. McGraw-Hill, 1962.

[92] Chilver, A.H. "The Maximum Strength of the Thin-Walled Cham Strut," Civ.England Pub.Wks Rev., Vol.48, No. 570, December, 1953.

[93] Bulson, P.S. "Local Instability Problems of Light Alloy Struts," Research Report No.29, The Aluminium Development Association, December, 1955.

[94] American Iron and Steel Institute. Light Gauge Cold-for-Med Steel Design Manual. 1962.

[95] Allen, D. "Correspondence on Analysis and Design of Stiffened Plates for Collapse Load," The Structural Engineer, 53, No.9,1975, pp.381-382.

[96] Von Karman, T., Sechler, E.E., and Donnel, L.H. "The Strength of Thin Plates in Compression," Trans. ASME, Applied Mechanics,Vol.54,No.2,Jahuary 1932.

[97] Winter, G. "Light-Gage (Thin-Walled) Steel Structures for Buildings in the USA," IABSE, Fourth Congress, Cambridge - London. Preliminary publishing. 1952, p.522.

[98] Winter, G. "Cold-Formed, Light-Gage Steel Construction," Proc. J.Struc.Div. ASME, Vol. 85, No. ST 9, November 1959.

[99] American Iron and Steel Institute. Specification for the Design of Cold-Formed Steel Structural Members, 1968 ed., New York. Also, Commentary on the 1968 Edition, by G. Winter, New York, 1970.

[100] Winter, G.; and Johnson, A.L. "Stainless Steel Structural Members: Strength and Behaviour-" IABSE, Publ. Vol.26, 1966, p.593.

[101] Skaloud. "Grenzzustand Gedruckter Grutplatten Dunnwandiger Trager," Acta Technica CSAV (Prague) G, 1965, p.724.

[102] Winter, G. "Thin-Walled Structures: Theoretical Solutions and Test Results," IABSE, Prel.Pub., 8th Congress, New York, 9-14 Sept. 1968, pp.101-112.

[103] British Standards Institution, Specification for the Use of Cold-Formed Steel Sections in Buildings - PD 4064, Addendum No. 1 (1961) to B.S. 499. 1959.

[104] Frankland. E.M.B: Report 469, May 1940.

[105] Conley, Becker and Allnutt. David Taylor Model Basin Report 1682, May 1963.

[106] Faulkner, D. "A Review of Effective Plating to be Used in the Analysis of Stiffened Plating in Bending and Compression," Report No. MITSG 73-11, Mass.Inst. of Tech., Cambridge, U.S.A. 1973.

[107] Faulkner, D., "A Review of Effective Plating to be Used in the Analysis of Stiffened Plating in Bending and Compression," J. Ship Res., Vol.19,No.1, March 1975, pp.1-17.

[108] Wolmir, A.S., "Biegsame Platten und Schalen," V.E.B., Verlag für Bausvesen, Berlin, 1962.

[109] Marguerre, K., "The Apparent Width of Plates in Compression," NACA Technical Memoranda, No.833, 1937.

[110] Marguerre, K. Proceedings of the Fifth International Congress of Applied Mechanics, Cambridge, Mass.,U.S.A., 1938, p.93.

[111] Sechler, E.E., "The Ultimate Strength of Thin Flat Sheet in Compression," Publ. No.27, Guggenheim Aeronautics Lab., Calif. Inst. Tech., 1933.

[112] Kondo, K., Komatsu, S. and Nakai, H. "Theoretical and Experimental Researchs on the Effective Width of Girder Bridge With Steel Deck Plate," Civil Engineering in Japan, 1962-1963, pp.104-106.

[113] Kondo, K., Komatsu, S. and Nakai, H. "Theoretical and Experimental Researchs on the Effective Width of Girder Bridge With Steel Deck Plate," Trans. Japan Soc. Civ.Engrs.,Vol.86, October 1962, pp.1-19.

[114] Abdel-Sayed, G., "Effective Width of Steel Deck-Plate Bridge," J. Struct. Div.,ASCE, No. ST 7, Paper No.6673, July 1969, pp.1459-1474.

[115] Abdel-Sayed, G., "Effective Width of Thin Plates in Compression," J. Struct.Div., ASCE, Vol.95, No. ST 10, October 1969, pp.2183-2203.

[116] Bleich, H., Buckling Strength of Metal Structures, McGraw-Hill, 1952.

[117] Richmond, B. "Discussion on Forth Road Bridge," Proc. Inst.Civ.Eng.,Vol.36,January 1967,pp.156-158.

[118] Th. Von Karman. "Festigkeitsprobleme in Mechinenbau," Encyklopadie der mathematischen Wissenschaften, Vol.4, B.G. Tenboner, Leipzig, 1910, p.349.

[119] Rostovtsev, G.G., "Calculation of Thin Plane Sheeting Supported by Ribs," Trudy Leningr. Inst.Inzhenerov Grazhdanskogo Vosdushnogo Flota (in Russian), No.20, 1940, pp.3-108.

[120] Troitsky, M.S. Stiffened Plates Bending, Stability and Vibrations, Elsevier Scientific Publishing Company, New York, 1976.

[121] Pflüger, A., "Zum Beulproblem der anisotropen Rencht-eckplatte," Ingenieur-Archiv.,Vol.6, 1947,pp.111-120.

[122] Giencke, E. "Die Berechnung von Hohbrippenplatten," Der Stahlbau. Vol.29, 1960,pp.1-11,47-59.

[123] Massonnet, C.H. "Plaques et loque cylindriques ortho-tropes a nervunes dissymetriques," Memoires de l'AIPC, Vol.19, 1959, pp.202-230.

[124] Soper, W.G. J.Applied Mechanics, Vol. 25, 1958, pp.444-448.

[125] Vogel, V., "Approximate Determination of Bending and Membrane Stresses of the Rectangular Orthotropic Plate With Large Deflection Under Uniformly Distributed Load of Navier's Boundary Conditions," Dissertation Technische Hochschule Stuttgart (in German), 1961.

[126] Abdel-Sayed, G. "Zur Berechnung von Flachblechgurten bei gleichzeitigen Berucksichtigung der Platten - Membran-und Scheibenwirkung," Dissertation der Technis-chen Hochschule Karslsruhe, 1963.

[127] Yamaki, N., "Post-Buckling Behaviour of Rectangular Plates With Small Initial Curvature Loaded in Edge Compression," J. Applied Mechanics, Vol.26, 1959, pp.407-414.

[128] Graves Smith, T.R., "The Ultimate Strength of Locally Buckled Columns of Arbitrary Length," Cantab Ph.D. Thesis, September, 1966.

[129] Graves Smith, T.R., "The Ultimate Strength of Locally Buckled Columns of Arbitrary Length," Thin Walled Steel Structures, Their Design and Use in Building (Symposium at Univ. Coll. of Swansea, 11-14 September 1967) Crosby Lockwood and Sons, London, 1967, p.3.

[130] Builaard, P.P., and Fisher, G.P., "Interaction of Column and Local Buckling in Compression Members," NACA, TN 2640,1952.

[131] Skaloud, M., and Navotny,K., "Uberkritisches Verhalten einer anfärglich gekrummter gleinchförming gedrückten, in der mittemit einen längsrippe versteiften platte," Acta Technica CSAV, No.2, 1965.

[132] Falconer, B.H., and Chapman, J.C., "Compressive Buckling of Stiffened Plates," The Engineer, Vol.195, 1953, p.789.

[133] Yamaki, N., "Post-Buckling of Rectangular Plates With Small Initial Curvature Loaded in Edge Compression - (continued)", J. Applied Mechanics, Vol.27,1960,pp.335-342.

[134] Williams, D.G. and Walker, A.C. "Explicit Solutions for the Design of Initially Deformed Plates Subject to Compression," Proc.Inst. Civ.Engrs., Part 2, 59, December 1975, pp.763-787.

[135] Williams, D.G., and Walker, A.C., "Explicit Solutions for the Design of Initially Deformed Plates Subject to Compression," Paper Published. Proc.ICE, Part 2, 59, December 1975, pp.763-787.

[136] Little, G.H., "Stiffened Steel Compression Panels - Theoretical Failure Analysis," The Structural Engineer, Vol. 54, No.12, December 1976, pp.489-500.

[137] Kondo, J., "Ultimate Strength of Longitudinally Stiffened Plate Panels Subjected to Combined Axial and Lateral Loading," Lehigh Univ., Fritz Eng. Laboratory, Report No.248.13, August, 1965.

[138] Vojata, J.F. and Ostapenko, A., "Ultimate Strength Design of Longitudinally Stiffened Plate Panels With Large b/t," Fritz Eng. Laboratory, Report No.248.18, Lehigh Univ., August, 1967.

[139] Crisfield, M.A., "Collapse Analysis of Box Girder Components Using Finite Elements," Symposium on Non-Linear Techniques and Behaviour in Structural Analysis. Transport and Road Research Laboratory, Crowthorne, SR164UC, 1974.

[140] Ilyushin, A.A. Plasticité. Editions Eyrolles, Paris, 1956.

[141] Crisfield, M.A. "Full-Range Analysis of Steel Plates and Stiffened Plating Under Uniaxial Compression," Paper published. Proc. ICE, Part 2, 59, December, 1975, pp.595-624. Discussion by K.E.Moxham, G.H.Little, P.A.Frieze and J.E.Harding, Proc.ICE, Part 2, 61, June 1976, pp.445-452.

[142] Harding, J.E. and Hobbs, R.E., "The Elasto-Plastic Analysis of Imperfect Square Plates Under In-Plane Loading," Proc.ICE, Part 2, 63, March, 1977, pp.137-158.

[143] Harding, J.E. and Hobbs, R.E., "The Elasto-Plastic Analysis of Imperfect Square Plates Under In-Plane Loading," Discussion by: T.K.Chaplin and G.H.Little. Proc.ICE, Part 2, 63, September, 1977, pp.753-756.

[144] Dwight, J.B. and Little, G.H. "Stiffened Steel Compression Flanges - A Simpler Approach," The Structural Engineer, Vol.54, December, 1976, pp.501-509.

[145] Crisfield, M.A. "Large Deflection Elasto-Plastic Buckling Analysis of Plate Using Finite Elements," Transport and Road Research Laboratory, Report No.LR 593, 1973.

[146] Murray, N.W. "The Behaviour of Thin Stiffened Steel Plates," IABSE, Memoires, Vol.33-I, March 1973, pp.191-201.

[147] Walker, A.C. and Murray, N.W. "A Plastic Collapse Mechanism for Compressed Plates," IABSE, Memoires, Vol.35-I, April, 1975, pp.217-235.

[148] Horne, M.R. and Narayanan, R. "Strength of Axially Loaded Stiffened Panels," IABSE, Memoires, Vol.36-I, March,1976, pp.125-157.

[149] Parr, D.H. and Maggard, P.S., "Ultimate Design of Hollow Thin-Walled Box-Girders," J.Struct.Div.,ASCE, ST 7, July, 1972, pp.1427-1442.

[150] Massonnet, C., "Experimental Research on the Buckling Strength of the Webs of Solid Girders," Preliminary Publication, 4th Congress, IABSE, 1952, pp.539-555.

[151] Rockey,K.C. "Web Buckling and Design of Web Plates," Research Report No.36, British Aluminium Development Association, September, 1953.

[152] Green, R. "Composite Box-Girder Bridges - The Construction Phase," Paper presented at the Canadian Structural Engineering Conference, Toronto, March, 1978.

[153] Tupula, Y.F., and Troitsky,M.S., "Buckling Behaviour of Steel Box-Girder Bridges: Maximum Applied Stress at Collapse for Plate in Compression," Report No.2, Department of Civil Engineering, Concordia University, August 1977.

[154] Tupula, Y.F., and M.S. Troitsky, "Buckling Behaviour of Steel Box-Girder Bridges: Influence of Imperfections on the Buckling Strength," Report No. 3, Department of Civil Engineering, Concordia University, November 1977.

[155] Tupula, Y.F., and Troitsky, M.S. "Buckling Behaviour of Steel Box-Girder Bridges: Influence of Imperfections on the Ultimate Strength," Report No.4, Department of Civil Engineering, Concordia University, May, 1978.

[156] Rosenberg, N., and Vincenti, W.S., The Britannia Bridge. MIT Press, Cambridge, Mass., U.S.A., 1978.

[157] Wolchuck, R., "Proposed Specifications for Steel Box-Girder Bridges," J. Struct.Div., ASCE, Vol.106, No. ST 12, Proc. Paper 15942, December, 1980, pp.2463-2474.

[158] Skaloud, M., "Post-Buckled Behaviour of Stiffened Webs," Academia Nakladatelstai, Ceskoslovenske Academie VED, Prague, 1970.

[159] Horne, M.R. and Narayan, R., "An Approximate Method for Design of Stiffened Steel Compression Panels," Discussion by Allen, D., et al. Proc.Inst.Civ.Engrs., Part 2, 61, June, 1976, pp.453-474.

APPENDIX A

TESTS OF THE THREE MODELS

APPENDIX A

TESTS OF THE THREE MODELS

A.1 INTRODUCTION

The purpose of this section is to provide additional information to various stages of the experimental investigation. The conception and setting up of such full-range experiments cannot be accomplished without difficulties. It is a long process requiring, at every step, the spirit of courage and imagination, of patience and creativity. It is a tedious operation where everything requires special attention, and to which many modifications are necessary. Such work cannot be realized without motivation and discipline.

The experimental investigation is divided into five steps: design, fabrication, preparation, testing and interpretation of the results.

This logic is used in the presentation of Chapter IV.

A.2 FABRICATION OF THE MODELS

All models have been fabricated by a licensed steel shop. The parts have been cut and identified before their assembly. Care was taken to follow that sequence of operations normally used for bridge-component shop fabrications. Figures 4.4 to 4.7 give an idea of the fabrication process.

Figure A.1 shows how the heating due to welding of the stiffeners to the plate affect their surrounding zone and cause residual stresses, as explained in Section 2.4.

A.3 INITIAL GEOMETRICAL IMPERFECTION MEASUREMENTS

As initial geometrical imperfections are one of the main factors considered in the present work, their accurate measurement is important. This has required special attention, great imagination and creativity. Care was taken during the complete fabrication processes to note all remarkable distortions before and after the assembly of the elements. The models have been transported from the fabrication shop to the laboratory.

before testing the models, it was necessary to measure all initial imperfections. This required a design of the appropriate tools. Figure A.2 shows a specially designed track, capable of moving in three directions. This tool was used for the reading of the flange and web panels, in locating any initial imperfections. For the lateral imperfections of longitudinal stiffeners of the compression flange, Figure A.3 shows another specially designed instrument.

Grids used for reading the initial imperfections are given in the main part of Figure 4.8. Figure A.2 is a typical reading of the initial imperfections of the compression flange.

Selected results of the initial imperfection measurements are given in Tables A.1 to A.7.

A.4 STRAIN GAUGES

Deformations due to loading have been read by means of electrical strain gauges, single gauges for the stiffeners, and 45° rosettes for the plate elements. So, the behaviour of each element during loading was recorded. Figures 4.21, 4.22 and 4.23 are strain gauge locations for Models A,B and C, respectively. The reading of the strain gauges was made possible with a strain gauge logger system, Figure 4.20, enabling the direct reading of the real deformation.

A.5 LOADING

The dimensions of the models, the loading conditions, and the intensity of the load to be applied, required many modifications of the existing loading frame. It could be recalled here, that the models had to be loaded up to their complete failure.

Figure A.4 is an overall view of the loading frame with one 300-ton hydraulic jack at each end. Figure A.5 shows the model being placed inside the loading frame and ready for testing. At each end is the jack and the transverse beam, through which the load is transmitted to the model. On top of the model are two transverse beams located at quarter points, acting as supports, and through them the load

is transmitted to the loading frame.

The jacks, of double-acting action, are loaded with one pump. The pressure is transmitted simultaneously to both jacks. Therefore, the load in both is the same at all times. Figure 4.20 is an overall view of the testing ring, loading frame, model, jacks, pump and the strain gauge Data Logger System.

The loading conditions shown in Figure 4.18 produce pure bending in the middlepart of the model and bending plus shear in the two end parts.

The bending moment M at any transverse section and the compression force P per unit width of the compression flange are given respectively by Equations (A.1) and (A.2).

$$M = PR \times A \times x \qquad (A.1)$$

$$P = \frac{PR \times A \times x}{bd} \qquad (A.2)$$

where

PR = pressure in the jack

A = effective area of the jack (93.0 in^2)

x = distance measured from end of the model to the section considered

b = width of the compression flange between webs (42.0 in)

d = distance between middle planes of both the compression and the tension flange plates (18.34 in)

The applied stresses are computed from measured strains by using the Hooke's law in the elastic range. In the elasto-plastic range the stresses are expressed by relations similar to Hooke's law. Those relations involve the use of the secant modulus E_s and the von Mises yield criterion, as explained by Massonnet in Reference [20].

Selected test results are given in Tables A.8 to A.61. Table A.8 to A.40 contain the deflections, from which the deformation mechanism of the models can be plotted at each loading stage. Grids used for the deflections measurement are the same as those for the initial imperfections, Figure 4.8. The unit deformations are given in Tables A.41 to A.61, from which the stresses can be calculated. Figure A.6, shows the location of the deformations given in the Tables.

FIGURE A.1 VIEW OF THE EFFECT OF WELDING HEAT (LEFT-HAND SIDE) IN THE ZONE OF PLATE AND STIFFENER JUNCTION. CREATION OF TENSILE AND COMPRESSIVE RESIDUAL STRESSES.

FIGURE A.2 SPECIALLY DESIGNED TRACK FOR READING OF INITIAL GEOMETRICAL IMPERFECTIONS

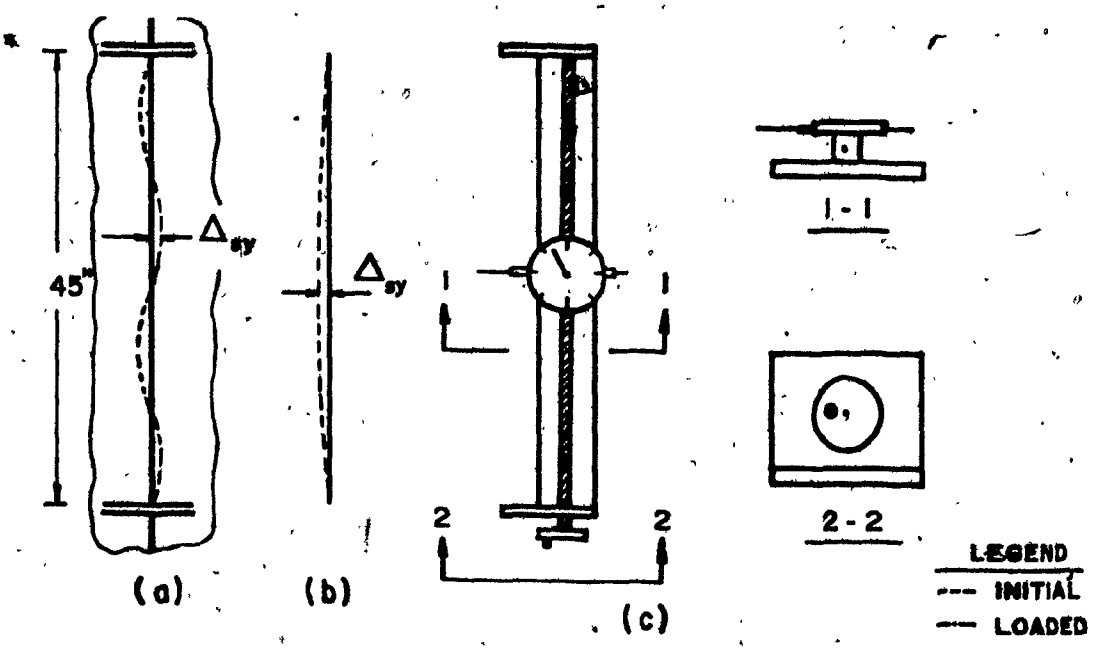

FIGURE A.3 SPECIALLY DESIGNED TOOL FOR READING OF STIFFENERS' INITIAL IMPERFECTIONS IN LATERAL DIRECTION (Δ_{sy}). a) AND b) ARE TYPICAL SHAPES OF Δ_{sy} INITIAL IMPERFECTIONS. c) TOOL USED.

FIGURE A.4 OVERALL VIEW OF THE LOADING FRAME AND THE LOCATION OF THE TWO JACKS

FIGURE A. 5 VIEW OF THE MODEL BEING PLACED INTO THE LOADING FRAME AND READY FOR TESTING

There is no page 348.

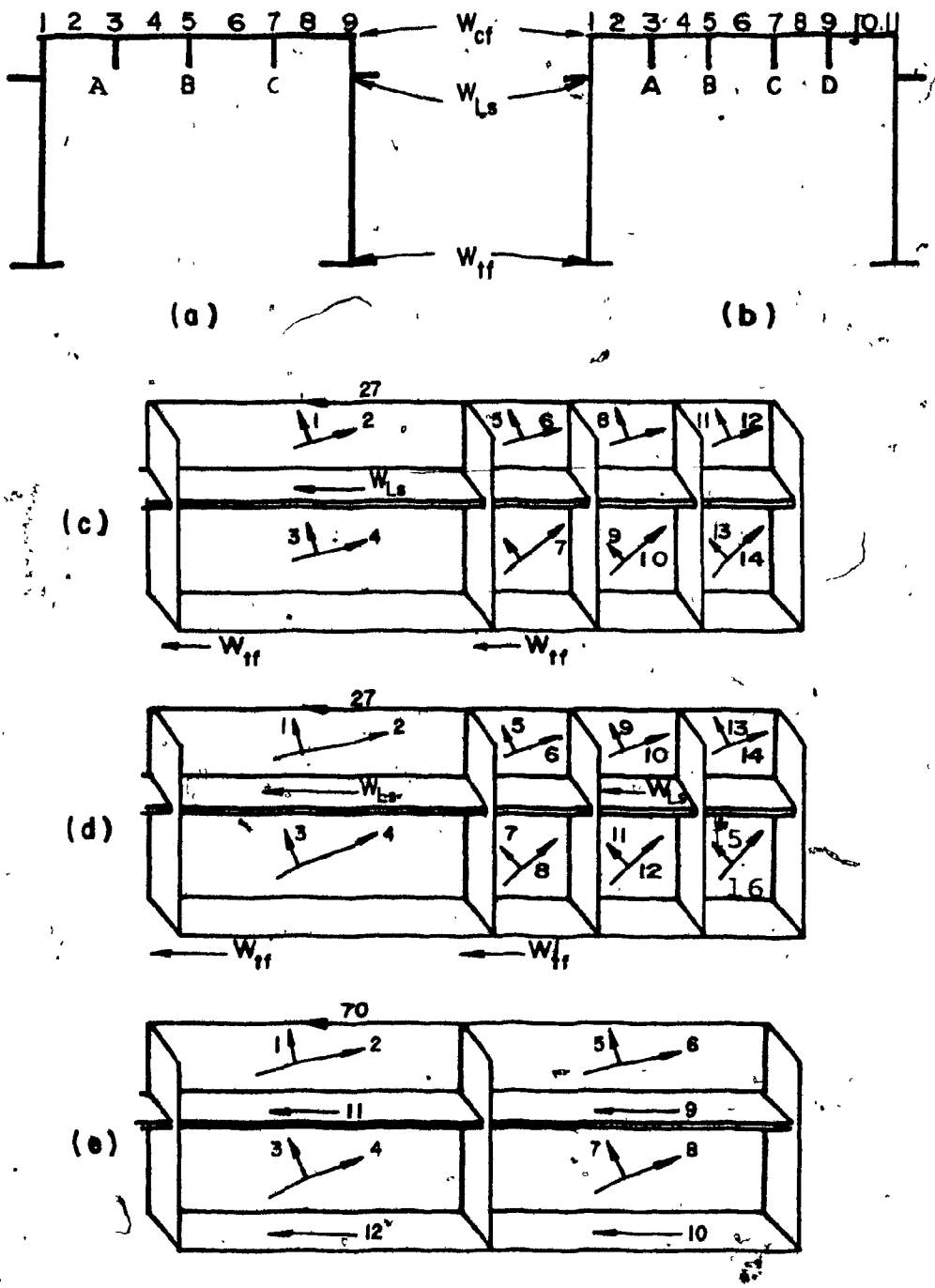

FIGURE A.6 LOCATION OF THE TABULATED DEFORMATION TABLE A-41 TO A-61 MODEL A, a) AND e), MODEL B, b) AND c), MODEL C, b) AND d).

APPENDIX A

TABLES

TABLE A-1 MODEL A, INITIAL GEOMETRICAL IMPERFECTIONS OF THE COMPRESSION FLANGE

$\Delta \times 10^3$ (Inch)

Line / Col.	1	2	3	4	5	6	7	8	9
1	281	283	279	285	288	303	314	325	332
2	265	233	240	174	231	212	262	244	302
3	243	220	220	172	209	152	219	202	300
4	239	195	208	188	190	125	188	185	287
5	237	193	200	165	180	142	172	200	280
6	220	175	167	130	152	136	162	188	265
7	200	137	150	111	149	113	153	180	259
8	184	126	136	110	144	114	149	169	243
9	179	173	160	165	167	180	184	200	190
10	181	125	124	107	146	120	150	143	169
11	188	136	129	123	160	118	140	140	188
12	185	140	131	128	165	128	149	146	195
13	175	137	125	92	150	123	135	143	198
14	170	128	115	80	133	114	130	145	197

(continued)

TABLE A-1 MODEL A, INITIAL GEOMETRICAL IMPERFECTIONS OF THE COMPRESSION FLANGE

$\Delta \times 10^3$ (Inch)

Line / Col.	1	2	3	4	5	6	7	8	9
15	166	106	110	87	124	82	150	150	191
16	161	108	114	103	125	110	165	191	205
17	161	164	145	145	146	175	206	230	247

TABLE A-2 MODEL B, INITIAL GEOMETRICAL IMPERFECTIONS OF THE COMPRESSION FLANGE

$\Delta \times 10^3$ (Inch)

Line / Col.	1	2	3	4	5	6	7	8	9	10	11
1	284	286	278	281	263	273	268	281	264	275	264
2	263	251	247	224	239	258	255	256	234	206	228
3	237	209	219	191	199	212	228	239	241	215	227
4	220	206	188	198	192	248	233	274	234	222	218
5	209	147	140	115	138	138	162	147	156	158	221
6	193	137	108	98	108	89	133	101	128	145	208
7	182	138	117	106	125	162	178	209	175	188	200
8	164	144	146	141	153	201	218	243	211	190	196
9	160	182	170	196	200	235	244	266	244	246	219
10	165	124	134	137	184	185	224	231	233	200	209
11	163	131	112	127	169	180	220	230	244	204	211
12	152	112	102	121	151	224	262	301	274	226	220
13	152	98	70	77	140	203	262	270	260	216	230
14	143	95	62	91	132	203	241	263	253	215	235

(Continued)

TABLE A-2 MODEL B, INITIAL GEOMETRICAL IMPERFECTIONS OF THE COMPRESSION FLANGE

$\Delta \times 10^3$ (Inch)

Line / Col.	1	2	3	4	5	6	7	8	9	10	11
15	132	91	78	112	148	184	220	216	245	218	248
16	124	89	100	127	145	168	215	218	247	207	260
17	131	146	161	166	166	203	222	246	255	280	282

TABLE A-3 MODEL A, AVERAGE OVERALL INITIAL IMPERFECTIONS δ_{ox} OF THE MODEL MEASURED ALONG THE WEB LINES

$\delta \times 10^3$ (Inch)

Line / Col.	Web 1	Web 2
1	0.0	0.0
2	37	27
3	55	52
4	67	70
5	87	88
6	101	108
7	110	113
8	112	119
9	105	113
10	105	121
11	92	117
12	75	94
13	63	76
14	46	67

(Continued)

TABLE A-3 MODEL A, AVERAGE OVERALL INITIAL IMPERFECTIONS δ_{ox} OF THE MODEL MEASURED ALONG THE WEB LINES

$\delta \times 10^3$ (Inch)

Line / Col.	Web 1	Web 2
15	27	53
16	14	21
17	0.0	0.0

TABLE A-4 AVERAGE OVERALL INITIAL IMPERFECTIONS δ_{ox} MEASURED ALONG WEB LINES FOR MODELS B AND C

$\delta \times 10^3$ (Inch)

Col.	Web 1	Web 2
1	0	0
2	41	37
3	71	58
4	93	90
5	121	105
6	137	119
7	149	135
8	151	126
9	174	117
10	157	122
11	154	122
12	142	111
13	125	102
14	104	82

(Continued)

TABLE A-4 AVERAGE OVERALL INITIAL IMPERFECTIONS δ_{ox} MEASURED ALONG WEB LINES FOR MODELS B AND C

$\delta \times 10^3$ (Inch)

Col.	Web 1	Web 2
15	66	57
16	36	37
17	0	0

TABLE A-5 AVERAGE OVERALL INITIAL IMPERFECTIONS δ_{ox} OF THE WEB LONGITUDINAL STIFFENER

$\delta_{ox} \times 10^3$ (Inch)

Col.	Web 1	Web 2
1	x	x
2	52	152
3	47	137
4	44	119
5	33	84
6	12	60
7	2	7
8	0	0
9	x	x
10	-9	0
11	9	14
12	-5	23
13	-3	7
14	-3	-19

(Continued)

TABLE A-5 AVERAGE OVERALL INITIAL IMPERFECTIONS δ_{ox} OF THE WEB LONGITUDINAL STIFFENER

$\delta_{ox} \times 10^3$ (Inch)

Col.	Web 1	Web 2
15	15	-29
16	0	25
17	x	x

TABLE A-6 TYPICAL INITIAL IMPERFECTIONS OF THE WEB PANEL IN THE LATERAL DIRECTION

$\Delta \times 10^3$ (Inch)

Col. / Line	1	2	3	4	5	6	7	8	9
1	0	0	0	0	0	0	0	0	0
2	0	x	1	11	27	37	35	9	0
3	0	x	x	x	x	x	x	x	0
4	0	x	56	65	66	60	43	33	0
5	0	x	23	14	27	35	30	21	0
6	0	x	15	7	19	18	21	15	0
7	0	x	8	3	6	8	4	2	0
8	0	x	0	0	2	0	0	0	0
9	0	0	0	0	0	0	0	0	0

0 = Point in plane of reference.

x = point not read because of obstacle.

TABLE A-7 TYPICAL INITIAL IMPERFECTIONS OF THE COMPRESSION FLANGE LONGITUDINAL STIFFENERS IN THE LATERAL DIRECTION (Δ_{sy})

$\Delta \times 10^3$ (Inch)

St. / Pt.	A	B	C
1	0	0	0
2	0	0	0
3	12	37	25
4	2	42	-58
5	12	46	-2
6	19	66	22
7	13	33	28
8	0	0	0
9	0	0	0

0 = Point in-plane of reference.

TABLE A-8 · MODEL A, DEFLECTION OF THE COMPRESSION FLANGE AT 0.0 PSI

$\delta \times 10^3$ (Inch)

Line / Col.	1	2	3	4	5	6	7	8	9
4	690	648	666	649	648	592	652	649	751
5	685	649	665	632	650	618	648	679	761
6	675	635	631	603	628	615	644	677	758
7	652	597	610	575	618	582	632	665	750
8	637	588	598	572	609	584	625	649	727
9	639 640	629	625	631 635	637	657	663	689	658
10	656	598	600	582	618	598	624	623	659
11	670	616	605	602	637	598	619	623	674
12	677	632	619	609	695	614	628	629	682
13	681 652	622	586	596 638	621	607	615	650	685
14	693	641	619	579	626	608	625	637	693

TABLE A-9 MODEL A, DEFLECTION OF THE COMPRESSION FLANGE AT 300 PSI

$\delta \times 10^3$ (Inch)

Line / Col.	1	2	3	4	5	6	7	8	9
4	623	683	705	688	680	612	683	680	788
5	736	696	606	661	675	636	667	702	775
6	745	700	687	641	664	646	666	694	770
7	735	662	676	631	665	619	662	695	765
8	731	667	670	636	665	625	651	674	742
9	742 739	718	704	701 699	695	704	701	710	672
10	771	692	691	660	689	648	669	654	678
11	699	727	708	689	707	649	660	652	692
12	719	754	725	708	725	671	676	666	708
13	839 799	752	693	685 721	698	668	657	682	713
14	858	790	748	687	721	690	679	678	721

TABLE A-10 MODEL A, DEFLECTION OF THE COMPRESSION FLANGE AT 500 PSI

$\delta \times 10^3$ (Inch)

Line / Col.	1	2	3	4	5	6	7	8	9
4	710	665	693	689	692	670	596	695	801
5	735	699	702	648	670	638	663	697	785
6	746	709	689	629	665	654	668	697	781
7	736	659	676	639	663	603	666	699	768
8	730	655	673	641	662	619	652	678	750
9	741	740 720	706	703 697	697	701	703	713	679
10	774	620	692	650	692	654	670	652	676
11	801	730	703	697	710	652	664	656	700
12	821	757	726	717	726	663	676	672	712
13	837	807 758	683	678 719	704	672	655	683	718
14	870	806	754	669	725	737	682	675	731

TABLE A-11 MODEL A, DEFLECTION OF THE COMPRESSION FLANGE AT 700 PSI

$\delta \times 10^3$ (Inch)

Line / Col.	1	2	3	4	5	6	7	8	9
4	715	651	684	706	655	645	662	677	790
5	741	602	690	617	650	628	685	669	761
6	741	712	672	584	643	654	646	669	766
7	730	633	665	655	648	654	647	694	763
8	722	641	660	636	650	596	640	663	736
9	733	730	710	695	693 688 686	691	691	704	672
10	765	684	680	621	678	662	662	631	669
11	793	725	694	665	697	665	649	619	690
12	815	735	712	721	709	612	657	688	700
13	833	802	753	665	660 705 690	655	639	673	714
14	868	815	747	633	714	762	670	647	730

TABLE A-12 MODEL A, DEFLECTION OF THE COMPRESSION FLANGE AT 900 PSI

$\delta \times 10^3$ (Inch)

Line / Col.	1	2	3	4	5	6	7	8	9
4	733	628	674	725	662	471	622	648	754
5	733	700	670	570	620	620	610	645	750
6	726	718	650	524	610	646	618	625	747
7	718	584	645	684	621	500	616	700	748
8	710	621	645	624	631	570	627	638	721
9	717	715	695	681	676 668 668	675	673	685	657
10	750	668	664	582	660	668	646	599	654
11	780	752	675	618	676	695	629	563	675
12	805	693	693	732	689	547	633	708	688
13	821	793	742	642	663 685 669	684	617	658	707
14	865	838	730	587	695	780	654	610	725

TABLE A-13 MODEL A, DEFLECTION OF THE COMPRESSION FLANGE AT 1000 PSI

$\delta \times 10^3$ (Inch)

Line / Col.	1	2	3	4	5	6	7	8	9
4	720	595	648	715	593	415	589	629	731
5	719	684	643	530	585	594	578	621	730
6	715	716	628	485	587	632	597	602	737
7	702	517	624	685	594	450	595	697	733
8	695	607	627	600	616	550	600	610	705
9	703	700	677	664	657 652 651	656	658	668	638
10	735	646	643	554	646	661	628	572	637
11	765	750	654	592	656	688	610	535	659
12	793	663	677	734	666	510	615	710	678
13	820	780	728	615	610 662 646	611	595	640	692
14	855	842	715	552	676	780	646	582	713

TABLE A-14 MODEL A, DEFLECTION OF THE COMPRESSION FLANGE AT 1400 PSI

$\delta \times 10^3$ (Inch)

Line / Col.	1	2	3	4	5	6	7	8	9
4	662	475	565	695	515	290	543	650	761
5	691	652	569	406	491	516	500	576	707
6	687	712	552	355	485	561	505	510	692
7	673	456	561	672	518	325	531	689	700
8	665	580	580	538	558	498	555	536	671
9	675	672	650	634	624 618 621	604	624	631	602
10	712	600	612	504	613	663	591	518	600
11	742	768	615	522	614	672	559	462	631
12	770	588	636	745	611	399	552	718	650
13	804	763	700	568	557 611 585	545	545	607	674
14	846	869	689	470	631	778	591	520	698

TABLE A-15 MODEL A, DEFLECTION OF THE COMPRESSION FLANGE AT 1500 PSI

$\delta \times 10^3$ (Inch)

Line / Col.	1	2	3	4	5	6	7	8	9
4	685	465	556	683	480	238	508	625	731
5	688	640	540	361	453	478	460	540	681
6	680	708	520	311	447	535	473	483	682
7	665	427	539	658	488	285	486	680	690
8	657	580	572	514	544	490	541	518	665
9	662	660	635	620	614 604 607	607	610	620	589
10	695	571	593	474	590	658	574	487	590
11	728	768	592	490	589	653	530	427	616
12	757	551	610	744	598	348	519	712	641
13	795	746	677	540	527 577 541	500	517	585	663
14	840	875	665	430	605	717	563	485	692

TABLE A-16 MODEL A, DEFLECTION OF THE COMPRESSION FLANGE

AT 1600 PSI

$\delta \times 10^3$ (Inch)

Line / Col.	1	2	3	4	5	6	7	8	9
4	629	345	438	613	367	071	419	604	747
5	667	603	454	243	348	385	385	514	700
6	665	682	448	190	348	430	377	410	653
7	647	355	466	598	400	168	415	651	661
8	640	580	527	435	484	455	488	442	632
9	650	645	620	605	594 585 590	592	595	600	570
10	683	555	580	460	585	660	558	467	571
11	720	770	577	466	570	644	512	392	597
12	750	519	593	740	559	300	485	706	618
13	800	743	666	515	507 553 511	467	487	568	648
14	840	880	656	403	585	756	547	461	685

TABLE A-17 MODEL A, DEFLECTION OF THE COMPRESSION FLANGE AT 1700 PSI

$\delta \times 10^3$ (Inch)

Line / Col.	1	2	3	4	5	6	7	8	9
4	689	371	450	613	337	021	374	555	666
5	670	593	420	193	295	327	330	468	652
6	656	668	410	152	300	395	343	380	643
7	644	327	445	585	380	140	393	635	655
8	625	580	510	408	467	457	475	420	628
9	642	638	616	597	590 580 580	580	582	592	558
10	678	540	570	440	574	656	542	455	564
11	711	775	564	440	555	638	488	375	590
12	742	505	580	736	544	266	465	708	615
13	785	730	655	500	483 534 485	444	469	561	642
14	838	890	645	370	565	758	522	438	677

TABLE A-18 MODEL A, DEFLECTION OF THE COMPRESSION FLANGE AT 1800 PSI

$\delta \times 10^3$ (Inch)

Line / Col.	1	2	3	4	5	6	7	8	9
4	695	335	414	600	265	254	285	532	685
5	680	590	384	137	228	330	260	435	661
6	664	655	378	128	254	111	300	372	654
7	649	322	428	553	340	436	369	622	668
8	639	578	504	395	449	590	455	410	630
9	648	645	620	602	594 575 590	678	585	600	568
10	685	557	588	475	603	674	570	478	574
11	718	787	585	465	589	320	530	402	597
12	748	528	610	767	580	495	515	723	625
13	790	740	678	538	530 579 540	800	511	583	650
14	836	900	666	405	608		570	478	682

TABLE A-19 MODEL B, DEFLECTION OF THE COMPRESSION FLANGE AT 250.0 PSI

(Inch)

Line / Col.	1	2	3	4	5	6	7	8	9	10	11
4	1.680	1.680	1.690	1.727	1.675	1.695	1.640	1.650	1.639	1.644	1.653
5	1.646	1.570	1.554	1.534	1.554	1.528	1.535	1.516	1.540	1.552	1.625
6	1.623	1.555	1.538	1.504	1.537	1.493	1.520	1.515	1.522	1.552	1.612
7	1.593	1.580	1.562	1.598	1.565	1.556	1.523	1.510	1.525	1.552	1.600
8	1.562	1.557	1.582	1.615	1.595	1.585	1.545	1.536	1.548	1.555	1.582
9	1.562			1.632		1.615		1.595		1.602	1.600
10	1.545	1.542	1.587	1.595	1.600	1.566	1.572	1.542	1.551	1.551	1.607
11	1.543	1.440	1.592	1.592	1.593	1.562	1.565	1.538	1.535	1.569	1.617

(Continued)

TABLE A-19 MODEL B, DEFLECTION OF THE COMPRESSION FLANGE

AT 250.0 PSI

(Inch)

Line / Col.	1	2	3	4	5	6	7	8	9	10	11
12	1.537	1.554	1.620	1.661	1.633	1.610	1.550	1.536	1.528	1.559	1.620
13	1.536	1.539	1.600	1.628	1.633	1.584	1.540	1.497	1.511	1.558	1.633
14	1.531	1.535	1.595	1.620	1.615	1.592	1.545	1.525	1.518	1.572	1.645

TABLE A-20 MODEL B, DEFLECTION OF THE COMPRESSION FLANGE

AT 500.0 PSI

(Inch)

Line / Col.	1	2	3	4	5	6	7	8	9	10	11
4	1.670	1.670	1.670	1.708	1.652	1.675	1.612	1.628	1.611	1.627	1.633
5	1.618	1.547	1.526	1.502	1.525	1.500	1.503	1.480	1.513	1.523	1.602
6	1.598	1.528	1.506	1.467	1.502	1.454	1.486	1.486	1.495	1.526	1.590
7	1.568	1.556	1.538	1.572	1.538	1.533	1.495	1.480	1.500	1.529	1.576
8	1.541	1.535	1.560	1.597	1.574	1.566	1.523	1.518	1.532	1.537	1.563
9	1.550	1.572		1.618		1.602		1.581		1.587	1.581
10	1.523	1.523	1.570	1.580	1.584	1.552	1.563	1.527	1.534	1.533	1.590
11	1.513	1.515	1.575	1.570	1.578	1.547	1.549	1.525	1.523	1.554	1.603

(Continued)

TABLE A-20 MODEL B, DEFLECTION OF THE COMPRESSION FLANGE

AT 500.0 PSI

(Inch)

Line / Col.	1	2	3	4	5	6	7	8	9	10	11
12	1.510	1.534	1.600	1.648	1.612	1.591	1.525	1.512	1.505	1.531	1.587
13	1.508	1.513	1.578	1.600	1.608	1.556	1.508	1.463	1.475	1.521	1.593
14	1.483	1.498	1.562	1.600	1.592	1.581	1.533	1.519	1.517	1.577	1.654

TABLE A-21 MODEL B, DEFLECTION OF THE COMPRESSION FLANGE AT 700.0 PSI

(Inch)

Line / Col.	1	2	3	4	5	6	7	8	0	10	11
4	1.675	1.672	1.672	1.710	1.650	1.676	1.604	1.627	1.610	1.628	1.633
5	1.611	1.535	1.512	1.483	1.505	1.480	1.488	1.462	1.504	1.515	1.600
6	1.595	1.521	1.495	1.450	1.488	1.435	1.473	1.478	1.487	1.519	1.582
7	1.562	1.550	1.525	1.564	1.525	1.523	1.480	1.465	1.490	1.522	1.570
8	1.540	1.530	1.556	1.592	1.568	1.560	1.520	1.513	1.527	1.532	1.560
9	1.550	1.565		1.610		1.597		1.575		1.578	1.575
10	1.515	1.515	1.563	1.573	1.575	1.545	1.557	1.520	1.527	1.524	1.582
11	1.508	1.512	1.574	1.565	1.575	1.539	1.550	1.522	1.521	1.549	1.593

(Continued)

TABLE A-21 MODEL B, DEFLECTION OF THE COMPRESSION FLANGE

AT 700.0 PSI

(Inch)

Line / Col.	1	2	3	4	5	6	7	8	9	10	11
12	1.508	1.530	1.595	1.647	1.608	1.584	1.514	1.502	1.491	1.522	1.581
13	1.513	1.520	1.585	1.603	1.615	1.559	1.514	1.469	1.485	1.533	1.605
14	1.488	1.503	1.570	1.608	1.603	1.590	1.535	1.523	1.523	1.585	1.661

TABLE A-22 MODEL B, DEFLECTION OF THE COMPRESSION FLANGE

AT 900.0 PSI

(Inch)

Line / Col.	1	2	3	4	5	6	7	8	9	10	11
4	1.668	1.662	1.647	1.696	1.627	1.660	1.586	1.610	1.596	1.620	1.628
5	1.608	1.525	1.498	1.465	1.486	1.465	1.470	1.447	1.491	1.603	1.596
6	1.588	1.510	1.482	1.430	1.470	1.411	1.455	1.466	1.469	1.510	1.576
7	1.555	1.545	1.514	1.552	1.510	1.510	1.463	1.445	1.476	1.511	1.562
8	1.525	1.515	1.544	1.578	1.552	1.544	1.503	1.498	1.512	1.516	1.549
9	1.530	1.558		1.603		1.588		1.565		1.570	1.565
10	1.508	1.503	1.555	1.567	1.567	1.533	1.545	1.510	1.514	1.511	1.572
11	1.498	1.500	1.558	1.546	1.560	1.515	1.526	1.498	1.495	1.531	1.578

(Continued)

TABLE A-22 MODEL B, DEFLECTION OF THE COMPRESSION FLANGE AT 900.0 PSI

(Inch)

Line / Col.	1	2	3	4	5	6	7	8	9	10	11
12	1.495	1.418	1.480	1.538	1.593	1.570	1.497	1.485	1.480	1.508	1.569
13	1.500	1.508	1.575	1.590	1.602	1.543	1.502	1.452	1.472	1.520	1.598
14	1.475	1.490	1.558	1.595	1.590	1.575	1.521	1.505	1.505	1.571	1.650

TABLE A-23 MODEL B , DEFLECTION OF THE COMPRESSION FLANGE

AT 1,000.0 PSI

(Inch)

Line / Col.	1	2	3	4	5	6	7	8	9	10	11
4	1.570	1.560	1.555	1.695	1.622	1.655	1.578	1.607	1.590	1.622	1.630
5	1.611	1.528	1.500	1.461	1.485	1.462	1.470	1.438	1.485	1500	1.591
6	1.583	1.507	1.475	1.420	1.460	1.400	1.445	1.460	1.467	1.505	1.574
7	1.550	1.542	1.508	1.547	1.500	1.505	1.460	1.437	1.473	1.510	1.560
8	1.528	1.515	1.542	1.578	1.552	1.544	1.495	1.498	1.512	1.517	1.550
9	1.537	1.555		1.600		1.585		1.563		1.567	1.567
10	1.506	1.500	1.555	1.570	1.565	1.528	1.540	1.505	1.514	1.510	1.570
11	1.494	1.498	1.545	1.543	1.555	1.510	1.524	1.495	1.492	1.530	1.575

(Continued)

TABLE A-23 MODEL B, DEFLECTION OF THE COMPRESSION FLANGE AT 1,000.0 PSI

(Inch)

Line / Col.	1	2	3	4	5	6	7	8	9	10	11
12	1.495	1.517	1.580	1.640	1.592	1.568	1.495	1.482	1.475	1.506	1.567
13	1.503	1.506	1.572	1.586	1.604	1.537	1.496	1.445	1.468	1.518	1.595
14	1.476	1.492	1.558	1.596	1.588	1.575	1.517	1.504	1.508	1.576	1.655

TABLE A-24 MODEL B, DEFLECTION OF THE COMPRESSION FLANGE

AT 1,300.0 PSI
(Inch)

Line / Col.	1	2	3	4	5	6	7	8	9	10	11
4	1.660	1.647	1.632	1.673	1.586	1.623	1.542	1.577	1.565	1.613	1.625
5	1.592	1.500	1.463	1.408	1.433	1.415	1.411	1.386	1.450	1.475	1.579
6	1.570	1.488	1.443	1.373	1.414	1.342	1.396	1.428	1.434	1.487	1.560
7	1.535	1.521	1.478	1.520	1.464	1.470	1.418	1.388	1.443	1.492	1.543
8	1.505	1.486	1.515	1.550	1.520	1.508	1.461	1.472	1.482	1.483	1.526
9	1.515	1.535		1.580		1.565		1.543		1.548	1.544
10	1.485	1.472	1.535	1.560	1.547	1.498	1.523	1.487	1.494	1.481	1.553
11	1.476	1.480	1.536	1.520	1.530	1.472	1.493	1.467	1.466	1.510	1.555

(Continued)

TABLE A-24 MODEL B, DEFLECTION OF THE COMPRESSION FLANGE AT 1,300.0 PSI

(Inch)

Line / Col.	1	2	3	4	5	6	7	8	9	10	11
12	1.480	1.500	1.565	1.626	1.568	1.544	1.460	1.453	1.453	1.485	1.554
13	1.480	1.482	1.550	1.552	1.570	1.492	1.450	1.395	1.428	1.483	1.563
14	1.458	1.470	1.538	1.577	1.562	1.547	1.480	1.468	1.477	1.552	1.637

TABLE A-25 MODEL B, DEFLECTION OF THE COMPRESSION FLANGE

AT 1,500.0 PSI

(Inch)

Line / Col.	1	2	3	4	5	6	7	8	9	10	11
4	1.653	1.632	1.610	1.648	1.550	1.590	1.500	1.541	1.537	1.600	1.617
5	1.584	1.482	1.435	1.370	1.390	1.378	1.365	1.335	1.417	1.458	1.571
6	1.560	1.472	1.415	1.335	1.372	1.286	1.350	1.395	1.398	1.467	1.551
7	1.525	1.510	1.454	1.495	1.428	1.438	1.371	1.346	1.415	1.475	1.533
8	1.492	1.470	1.495	1.533	1.495	1.480	1.435	1.452	1.460	1.460	1.515
9	1.500	1.522		1.566		1.552		1.530		1.533	1.532
10	1.470	1.452	1.522	1.560	1.535	1.473	1.505	1.480	1.478	1.460	1.540
11	1.465	1.470	1.530	1.510	1.520	1.450	1.475	1.452	1.451	1.503	1.548

(Continued)

TABLE A-25 MODEL B, DEFLECTION OF THE COMPRESSION FLANGE AT 1,500.0 PSI

(Inch)

Line / Col.	1	2	3	4	5	6	7	8	9	10	11
12	1.465	1.490	1.552	1.615	1.548	1.515	1.433	1.422	1.425	1.460	1.534
13	1.475	1.475	1.543	1.538	1.550	1.460	1.420	1.368	1.409	1.472	1.556
14	1.450	1.462	1.533	1.568	1.547	1.525	1.457	1.446	1.460	1.545	1.631

TABLE A-26 MODEL B, DEFLECTION OF THE COMPRESSION FLANGE

AT 1,700.0 PSI

(Inch)

Line / Col.	1	2	3	4	5	6	7	8	9	10	11
4	1.633	1.596	1.563	1.595	1.480	1.524	1.424	1.475	1.487	1.578	1.615
5	1.572	1.455	1.390	1.300	1.320	1.318	1.285	1.248	1.362	1.527	1.571
6	1.550	1.450	1.378	1.275	1.306	1.200	1.278	1.338	1.346	1.444	1.549
7	1.510	1.490	1.415	1.460	1.370	1.385	1.315	1.273	1.369	1.453	1.522
8	1.478	1.445	1.466	1.507	1.458	1.438	1.400	1.422	1.427	1.432	1.504
9	1.483	1.510		1.555		1.553		1.516		1.522	1.520
10	1.458	1.430	1.515	1.570	1.528	1.444	1.495	1.485	1.462	1.437	1.530
11	1.450	1.462	1.520	1.495	1.497	1.410	1.440	1.416	1.421	1.485	1.531

(Continued)

TABLE A-26 MODEL B , DEFLECTION OF THE COMPRESSION FLANGE AT 1,700.0 PSI

(Inch)

Line / Col.	1	2	3	4	5	6	7	8	9	10	11
12	1.460	1.490	1.555	1.619	1.540	1.500	1.409	1.405	1.415	1.461	1.542
13	1.467	1.470	1.538	1.520	1.532	1.422	1.387	1.329	1.386	1.461	1.555
14	1.455	1.465	1.533	1.565	1.533	1.500	1.430	1.421	1.444	1.536	1.630

TABLE A-27 MODEL B, DEFLECTION OF THE COMPRESSION FLANGE

AT 1,800.0 PSI

(Inch)

Line / Col.	1	2	3	4	5	6	7	8	9	10	11
4	1.630	1.585	1.548	1.575	1.455	1.495	1.395	1.450	1.463	1.573	1.612
5	1.570	1.447	1.370	1.270	1.293	1.290	1.255	1.210	1.336	1.410	1.564
6	1.454	1.438	1.360	1.246	1.375	1.140	1.246	1.312	1.320	1.433	1.542
7	1.505	1.480	1.398	1.430	1.348	1.360	1.288	1.244	1.348	1.443	1.516
8	1.470	1.437	1.460	1.492	1.443	1.422	1.383	1.410	1.415	1.414	1.495
9	1.480	1.503		1.553		1.532		1.510		1.517	1.512
10	1.452	1.422	1.512	1.570	1.522	1.436	1.490	1.486	1.455	1.426	1.522
11	1.445	1.458	1.520	1.490	1.495	1.398	1.434	1.405	1.417	1.485	1.529

(Continued)

TABLE A-27 MODEL B, DEFLECTION OF THE COMPRESSION FLANGE AT 1,800.0 PSI

(Inch)

Line / Col.	1	2	3	4	5	6	7	8	9	10	11
12	1.455	1.485	1.556	1.616	1.530	1.488	1.390	1.390	1.400	1.450	1.538
13	1.465	1.470	1.540	1.517	1.525	1.412	1.373	1.317	1.379	1.459	1.555
14	1.450	1.465	1.530	1.560	1.522	1.485	1.410	1.307	1.432	1.525	1.625

TABLE A-28 MODEL B, DEFLECTION OF THE COMPRESSION FLANGE AT 1,900.0 PSI

(Inch)

Line / Col.	1	2	3	4	5	6	7	8	9	10	11
4	1.625	1.570	1.518	1.543	1.408	1.448	1.342	1.405	1.423	1.553	1.605
5	1.550	1.425	1.338	1.220	1.240	1.243	1.196	1.140	1.286	1.383	1.555
6	1.540	1.420	1.320	1.200	1.225	1.087	1.187	1.263	1.277	1.410	1.530
7	1.498	1.470	1.370	1.385	1.305	1.320	1.240	1.193	1.311	1.419	1.505
8	1.465	1.422	1.438	1.470	1.415	1.390	1.358	1.386	I.390	1.385	1.483
9	1.470	1.495		1.538		1.520		1.495		1.500	1.498
10	1.446	1.412	1.510	1.577	1.520	1.425	1.480	1.486	1.440	1.503	1.508
11	1.443	1.463	1.528	1.500	1.495	1.390	1.408	1.375	1.390	1.461	1.507

(Continued)

TABLE A-28 MODEL B, DEFLECTION OF THE COMPRESSION FLANGE

AT 1,900.0 PSI

(Inch)

Line / Col.	1	2	3	4	5	6	7	8	9	10	11
12	1.448	1.485	1.558	1.615	1.515	1.467	1.362	1.361	1.377	1.427	1.520
13	1.460	1.470	1.540	1.510	1.510	1.390	1.348	1.287	1.357	1.445	1.545
14	1.447	1.465	1.530	1.555	1.510	1.465	1.390	1.388	1.412	1.515	1.617

TABLE A-29 MODEL B, DEFLECTION OF THE COMPRESSION FLANGE

AT 2,000.0 PSI

(Inch)

Line / Col.	1	2	3	4	5	6	7	8	9	10	11
4	1.615	1.545	1.480	1.492	1.353	1.393	1.286	1.355	1.379	1.534	1.597
5	1.458	1.306	1.297	1.160	1.180	1.187	1.135	1.065	1.240	1.357	1.547
6	1.435	1.395	1.283	1.145	1.165	1.015	1.130	1.213	1.230	1.387	1.520
7	1.493	1.458	1.338	1.352	1.255	1.275	1.193	1.141	1.269	1.394	1.493
8	1.460	1.410	1.422	1.445	1.388	1.360	1.322	1.362	1.362	1.358	1.473
9	1.470	1.490		1.530		1.508		1.484		1.488	1.485
10	1.440	1.408	1.512	1.586	1.522	1.420	1.478	1.487	1.430	1.388	1.496
11	1.435	1.460	1.530	1.503	1.487	1.372	1.403	1.367	1.383	1.455	1.503

(Continued)

TABLE A-29 MODEL B, DEFLECTION OF THE COMPRESSION FLANGE

AT 2,000.0 PSI

(Inch)

Line / Col.	1	2	3	4	5	6	7	8	9	10	11
12	1.442	1.487	1.563	1.620	1.513	1.459	1.344	1.343	1.360	1.412	1.512
13	1.455	1.470	1.544	1.508	1.508	1.375	1.327	1.265	1.340	1.430	1.537
14	1.440	1.463	1.527	1.553	1.502	1.450	1.370	1.367	1.395	1.502	1.612

TABLE A-30 MODEL B, DEFLECTION OF THE COMPRESSION FLANGE

AT 2,200.0 PSI

(Inch)

Line / Col.	1	2	3	4	5	6	7	8	9	10	11
4	1.583	1.400	1.242	1.195	1.025	1.057	.970	1.060	1.123	1.387	1.547
5	1.517	1.223	.983	.740	.726	.763	.685	.590	.910	1.135	1.480
6	1.490	1.194	.970	.720	.700	.462	.695	.855	.907	1.204	1.454
7	1.450	1.322	1.080	1.020	.905	.926	.862	.815	1.010	1.225	1.427
8	1.420	1.295	1.265	1.253	1.188	1.160	1.136	1.195	1.195	1.181	1.402
9	1.425	1.460		1.490		1.475		1.428		1.420	1.415
10	1.405	1.400	1.595	1.718	1.640	1.504	1.517	1.515	1.393	1.315	1.430
11	1.405	1.530	1.720	1.765	1.707	1.515	1.444	1.325	1.323	1.396	1.439

(Continued)

TABLE A-30 MODEL B, DEFLECTION OF THE COMPRESSION FLANGE

AT 2,200.0 PSI

(Inch)

Line / Col.	1	2	3	4	5	6	7	8	9	10	11
12	1.512	1.693	1.895	1.907	1.795	1.620	1.370	1.282	1.265	1.305	1.442
13	1.435	1.540	1.735	1.767	1.746	1.520	1.348	1.195	1.248	1.348	1.480
14	1.425	1.508	1.670	1.750	1.690	1.570	1.395	1.325	1.325	1.429	1.585

TABLE A-31 MODEL B, DEFLECTION OF THE COMPRESSION FLANGE

AT 2,100.0 - 2,300.0 PSI
(Inch)

Line / Col.	1	2	3	4	5	6	7	8	9	10	11
4	1.980	1.682	1.370	1.275	1.080	1.062	.937	.983	1.030	1.490	1.978
5	1.925	1.425	.018	.562	1.478	.453	.323	.175	.563	1.057	1.868
6	1.988	1.263	.855	.455	.371	.072	.300	.475	.640	1.277	1.848
7	1.950	1.560	1.100	.972	.803	.773	.710	.677	.948	1.342	1.847
8	.650 1.928	.378 1.560	.338 1.520	.202 1.480	1.378 .098	1.323 .045	1.287 .010	.082 1.358	.112 1.390	.131 1.434	.588 1.862
9	.658	.712		.710		.683		.627		.604	.573
10	.645	.765	1.040	1.195	1.140	1.060	1.073	1.035	.818	.574	.595
11	.648	1.132	1.430	1.530	1.522	1.430	1.363	1.175	.960	.762	.637

(Continued)

TABLE A-31 MODEL B, DEFLECTION OF THE COMPRESSION FLANGE AT 2,100.0 - 2,300.0 PSI

(Inch)

Line / Col.	1	2	3	4	5	6	7	8	9	10	11
12	.670	1.252	1.644	1.844	1.845	1.774	1.592	1.403	1.103	.781	.681
13	.710	1.125	1.552	1.745	1.840	1.746	1.600	1.308	1.026	.807	.745
14	.762	1.088	1.486	1.722	1.760	1.700	1.503	1.288	1.010	.837	.835

TABLE A-32 MODEL C, DEFLECTION OF THE COMPRESSION FLANGE

INITIAL OF THE RAISING

(Inch)

Line / Col.	1	2	3	4	5	6	7	8	9	10	11
4	1.317	1.317	1.329	1.333	1.323	1.333	1.321	1.330	1.317	1.382	1.432
5	1.315	1.288	1.280	1.270	1.298	1.310	1.320	1.313	1.330	1.388	1.447
6	1.336	1.278	1.260	1.252	1.280	1.299	1.310	1.308	1.418	1.384	1.451
7	1.345	1.305	1.275	1.280	1.295	1.310	1.328	1.316	1.327	1.377	1.442
8	1.340	1.320	1.310	1.300	1.311	1.322	1.343	1.342	1.349	1.388	1.419
9	1.383	1.365	1.347	1.345	x	1.355	1.362	1.365	1.372	1.393	1.411
10	1.365	1.345	1.314	1.333	1.348	1.330	1.348	1.335	1.355	1.377	1.415
11	1.385	1.357	1.362	1.356	1.370	1.362	1.357	1.352	1.356	1.385	1.428

(Continued)

TABLE A-32 MODEL C, DEFLECTION OF THE COMPRESSION FLANGE

INITIAL OF THE RAISING

(Inch)

Line / Col.	1	2	3	4	5	6	7	8	9	10	11
12	1.403	1.372	1.371	1.372	1.388	1.377	1.354	1.345	1.348	1.387	1.436
13	1.412	1.392	1.390	1.395	1.395	1.374	1.357	1.342	1.348	1.384	1.445
14	1.440	1.410	1.420	1.406	1.417	1.396	1.365	1.326	1.350	1.388	1.442

TABLE A-33 DEFLECTION OF THE COMPRESSION FLANGE

UNIT INCHES INITIAL NO BRIDGE RAISED

(Inch)

Line / Col.	1	2	3	4	5	6	7	8	9	10	11
4	.555	.558	.562	.560	.547	.548	.533	.534	.527	.588	.634
5	.565	.510	.495	.485	.508	.516	.523	.513	.524	.578	.634
6	.552	.493	.470	.462	.485	.500	.505	.500	.507	.565	.632
7	.553	.510	.488	.482	.495	.508	.518	.508	.517	.568	.627
8	.548	.525	.512	.502	.513	.522	.542	.536	.544	.580	.610
9	.575	.565	.543	.540	x	.550	.538	.560	.565	.590	.610
10	.558	.538	.536	.528	.542	.536	.543	.533	.554	.577	.615
11	.570	.546	.552	.548	.562	.557	.554	.550	.556	.585	.630
12	.580	.553	.555	.560	.574	.570	.550	.542	.548	.590	.641

(Continued)

TABLE A-33 DEFLECTION OF THE COMPRESSION FLANGE

UNIT INCHES INITIAL NO BRIDGE/RAISED
(Inch)

Line / Col.	1	2	3	4	5	6	7	8	9	10	11
13	.586	.564	.570	.575	.580	.564	.550	.540	.550	.588	.652
14	.600	.575	.590	.585	.600	.585	.557	.525	.554	.597	.654

TABLE A-34 MODEL C, DEFLECTION OF THE COMPRESSION FLANGE AT 300 PSI

(Inch)

Line / Col.	1	2	3	4	5	6	7	8	9	10	11
4	1.330	1.338	1.342	1.347	1.333	1.342	1.332	1.337	1.337	1.405	1.455
5	1.345	1.238	1.278	1.266	1.295	1.306	1.318	1.310	1.328	1.385	1.442
6	1.338	1.278	1.258	1.252	1.280	1.300	1.310	1.308	1.320	1.385	1.452
7	1.340	1.305	1.280	1.278	1.292	1.306	1.320	1.314	1.328	1.377	1.443
8	1.340	1.320	1.310	1.300	1.312	1.323	1.343	1.343	1.351	1.388	1.420
9	1.382	1.365	1.345	1.344	x	1.352	1.362	1.365	1.370	1.394	1.412
10	1.365	1.344	1.342	1.332	1.346	1.330	1.340	1.335	1.354	1.377	1.416
11	1.382	1.355	1.360	1.353	1.366	1.360	1.356	1.350	1.355	1.383	1.428

(Continued)

TABLE A-34 MODEL C, DEFLECTION OF THE COMPRESSION FLANGE AT 300 PSI

(Inch)

Line / Col.	1	2	3	4	5	6	7	8	9	10	11
13	1.403	1.372	1.370	1.370	1.384	1.377	1.355	1.343	1.347	1.386	1.435
13	1.415	1.392	1.390	1.394	1.393	1.373	1.356	1.342	1.348	1.384	1.446
14	1.440	1.410	1.415	1.405	1.415	1.394	1.362	1.324	1.348	1.388	1.441

TABLE A-35 MODEL C, DEFLECTION OF THE COMPRESSION FLANGE AT 500 PSI (Inch)

Line / Col.	1	2	3	4	5	6	7	8	9	10	11
4	1.315	1.323	1.326	1.340	1.328	1.342	1.332	1.340	1.316	1.417	1.471
5	1.337	1.275	1.265	1.252	1.280	1.272	1.305	1.295	1.314	1.376	1.437
6	1.330	1.268	1.248	1.241	1.271	1.290	1.305	1.300	1.311	1.378	1.448
7	1.330	1.290	1.268	1.265	1.280	1.295	1.310	1.305	1.317	1.371	1.436
8	1.330	1.310	1.300	1.290	1.304	1.313	1.336	1.355	1.343	1.380	1.413
9	1.370	1.355	1.336	1.335	x	1.345	1.355	1.350	1.365	1.387	1.402
10	1.355	1.335	1.332	1.321	1.340	1.320	1.338	1.326	1.348	1.369	1.408
11	1.375	1.348	1.354	1.347	1.360	1.354	1.349	1.344	1.348	1.375	1.421

(Continued)

TABLE A-35 MODEL C, DEFLECTION OF THE COMPRESSION FLANGE AT 500 PSI

(Inch)

Line / Col.	1	2	3	4	5	6	7	8	9	10	11
12	1.396	1.365	1.362	1.362	1.377	1.370	1.348	1.334	1.338	1.380	1.430
13	1.408	1.386	1.380	1.388	1.388	1.365	1.348	1.330	1.342	1.380	1.442
14	1.440	1.406	1.411	1.400	1.412	1.392	1.358	1.317	1.344	1.385	1.439

TABLE A-36 MODEL C , DEFLECTION OF THE COMPRESSION FLANGE

AT 700 PSI

(Inch)

Line / Col.	1	2	3	4	5	6	7	8	9	10	11
4	1.298	1.305	1.312	1.324	1.314	1.326	1.322	1.329	1.338	1.418	1.474
5	1.330	1.268	1.360	1.244	1.278	1.287	1.300	1.288	1.311	1.373	1.438
6	1.314	1.256	1.230	1.225	1.255	1.274	1.288	1.282	1.296	1.364	1.434
7	1.320	1.280	1.248	1.253	1.270	1.285	1.300	1.293	1.307	1.363	1.428
8	1.320	1.290	1.288	1.280	1.293	1.305	1.330	1.325	1.334	1.370	1.404
9	1.362	1.347	1.325	1.325	x	1.335	1.346	1.350	1.352	1.377	1.394
10	1.346	1.324	1.322	1.311	1.330	1.310	1.328	1.316	1.338	1.362	1.398
11	1.365	1.334	1.338	1.334	1.348	1.343	1.337	1.332	1.337	1.367	1.412

(Continued)

TABLE A-36 MODEL C, DEFLECTION OF THE COMPRESSION FLANGE AT 700 PSI

(Inch)

Line / Col.	1	2	3	4	5	6	7	8	9	10	11
12	1.390	1.355	1.352	1.352	1.365	1.360	1.337	1.322	1.330	1.372	1.423
13	1.407	1.382	1.373	1.380	1.380	1.357	1.340	1.321	1.333	1.372	1.437
14	1.438	1.402	1.408	1.393	1.410	1.387	1.353	1.310	1.338	1.381	1.436

TABLE A-37 MODEL C , DEFLECTION OF THE COMPRESSION FLANGE AT 1000 PSI (CRACK STARTS IN WEB SUB-PANEL)

(Inch)

Line / Col.	1	2	3	4	5	6	7	8	9	10	11
4	1.278	1.283	1.288	1.303	1.288	1.303	1.302	1.305	1.315	1.400	1.463
5	1.3.2	1.345	1.228	1.270	1.242	1.252	1.262	1.248	1.274	1.342	1.409
6	1.303	1.236	1.210	1.200	1.230	1.249	1.259	1.255	1.274	1.345	1.416
7	1.303	1.261	1.225	1.230	1.247	1.263	1.281	1.270	1.286	1.342	1.412
8	1.300	1.276	1.268	1.260	1.274	1.283	1.305	1.306	1.314	1.352	1.386
9	1.343	1.326	1.308	1.307	x	1.317	1.326	1.330	1.338	1.360	1.376
10	1.225	1.303	1.303	1.288	1.310	1.285	1.308	1.297	1.318	1.340	1.380
11	1.345	1.310	1.316	1.312	1.325	1.320	1.314	1.310	1.314	1.350	1.396

(Continued)

TABLE A-37 MODEL C, DEFLECTION OF THE COMPRESSION FLANGE

CROCK START IN WEB SUBPAD AT 1000 PSI

(Inch)

Line / Col.	1	2	3	4	5	6	7	8	9	10	11
12	1.372	1.337	1.330	1.330	1.345	1.340	1.312	1.297	1.308	1.354	1.407
13	1.392	1.365	1.353	1.360	1.358	1.336	1.317	1.297	1.312	1.355	1.426
14	1.432	1.390	1.395	1.377	1.395	1.374	1.340	1.290	1.324	1.375	1.430

TABLE A-38 MODEL C, DEFLECTION OF THE COMPRESSION FLANGE AT 1500 PSI

Line	1	2	3	4	5	6	7	8	9	10	11
4	1.260	1.250	1.250	1.270	1.242	1.257	1.253	1.256	1.277	1.377	1.445
5	1.288	1.212	1.153	1.152	1.188	1.197	1.208	1.190	1.228	1.303	1.386
6	1.273	1.195	1.160	1.145	1.175	1.195	1.210	1.198	1.223	1.310	1.387
7	1.266	1.228	1.186	1.174	1.195	1.210	1.232	1.218	1.240	1.300	1.377
8	1.265	1.235	1.226	1.275	1.230	1.237	1.263	1.266	1.272	1.308	1.351
9	1.310	1.288	1.268	1.268	x	1.278	1.290	1.292	1.297	1.323	1.340
10	1.290	1.263	1.262	1.240	1.268	1.237	1.264	1.253	1.284	1.300	1.345
11	1.370	1.266	1.270	1.262	1.275	1.270	1.297	1.264	1.270	1.311	1.361

(Continued)

TABLE A-38 MODEL C , DEFLECTION OF THE COMPRESSION FLANGE AT 1500 PSI

(Inch)

Line / Col.	1	2	3	4	5	6	7	8	9	10	11
12	1.345	1.300	1.283	1.270	1.292	1.292	1.261	1.243	1.261	1.318	1.378
13	1.365	1.338	1.310	1.310	1.310	1.281	1.267	1.244	1.267	1.322	1.400
14	1.418	1.362	1.358	1.330	1.352	1.332	1.300	1.240	1.287	1.353	1.413

TABLE A-39 MODEL C, DEFLECTION OF THE COMPRESSION FLANGE

AT 1700 PSI
(Inch)

Line / Col.	1	2	3	4	5	6	7	8	9	10	11
4	1.252	1.240	1.230	1.255	1.215	1.227	1.224	1.227	1.252	1.363	1.437
5	1.275	1.198	1.158	1.118	1.155	1.160	1.173	1.152	1.200	1.287	1.371
6	1.257	1.172	1.134	1.113	1.140	1.157	1.172	1.162	1.195	1.290	1.370
7	1.250	1.210	1.163	1.140	1.165	1.180	1.200	1.186	1.214	1.280	1.360
8	1.247	1.214	1.205	1.190	1.205	1.721	1.238	1.244	1.250	1.285	1.332
9	1.287	1.270	1.250	1.250	x	1.260	1.270	1.272	1.278	1.303	1.327
10	1.273	1.245	1.238	1.215	1.243	1.212	1.242	1.229	1.256	1.280	1.327
11	1.294	1.240	1.245	1.232	1.246	1.240	1.234	1.237	1.243	1.292	1.343

(Continued)

TABLE A-39 MODEL C, DEFLECTION OF THE COMPRESSION FLANGE AT 1700 PSI (Inch)

Line / Col.	1	2	3	4	5	6	7	8	9	10	11
12	1.330	1.278	1.255	1.230	1.260	1.260	1.227	1.257	1.230	1.297	1.362
13	1.350	1.318	1.280	1.280	1.273	1.245	1.233	1.203	1.240	1.302	1.388
14	1.407	1.342	1.332	1.295	1.320	1.298	1.266	1.206	1.262	1.340	1.403

TABLE A-40 MODEL C , DEFLECTION OF THE COMPRESSION FLANGE

AT 2000 PSI

(Inch)

Line / Col.	1	2	3	4	5	6	7	8	9	10	11
4	1.242	1.208	1.190	1.222	1.158	1.163	1.157	1.163	1.205	1.336	1.425
5	1.260	1.170	1.108	1.055	1.087	1.087	1.105	1.080	1.143	1.244	1.351
6	1.236	1.135	1.084	1.055	1.075	1.084	1.105	1.093	1.140	1.254	1.347
7	1.228	1.184	1.118	1.085	1.115	1.125	1.146	1.130	1.167	1.240	1.337
8	1.220	1.176	1.165	1.153	1.163	1.170	1.198	1.208	1.212	1.248	1.307
9	1.258	1.240	1.220	1.216	x	1.227	1.237	1.242	1.250	1.276	1.298
10	1.242	1.205	1.188	1.155	1.184	1.153	1.188	1.178	1.214	1.250	1.302
11	1.265	1.185	1.175	1.153	1.160	1.153	1.158	1.168	1.184	1.252	1.317

(Continued)

TABLE A-40 MODEL C, DEFLECTION OF THE COMPRESSION FLANGE AT 2000 PSI

(Inch)

Line / Col.	1	2	3	4	5	6	7	8	9	10	11
12	1.303	1.225	1.172	1.110	1.150	1.160	1.132	1.150	1.158	1.247	1.337
13	1.330	1.270	1.196	1.180	1.160	1.122	1.134	1.198	1.168	1.262	1.371
14	1.390	1.290	1.255	1.183	1.215	1.184	1.170	1.105	1.196	1.318	1.392

TABLE A-41 MODEL A, COMPRESSION FLANGE, DISTRIBUTION OF LONGITUDINAL STRAIN (ε_x) AT TRANSVERSE SECTION 9

$\varepsilon \times 10^6$ in/in

$\frac{Lo}{PR}$	1	2	3	4	5	6	7	8	9
200	-132	- 88	- 73	- 77	- 71	- 73	- 74	- 93	- 95
300	-230	-166	-128	-149	-132	-145	-141	-170	-181
400	-326	-241	-174	-214	-178	-221	-199	-245	-262
500	-412	-303	-207	-266	-200	-552	-236	-314	-342
600	-517	-369	-238	-599	-224	-630	-280	-398	-441
700	-609	-414	-251	-681	-234	-643	-309	-481	-528
800	-705	-457	-261	-759	-244	-652	-332	-586	-623
900	-820	-500	-264	-796	-250	-658	-345	-670	-737
1000	-914	-536	-264	-830	-254	-658	-354	-741	-829
1100	-1068	-574	-260	-879	-260	-652	-358	-828	-990
1200	-1161	-594	-253	-902	-255	-647	-349	-873	-1087
1300	-1269	-546	-252	-926	-259	-634	-350	-930	-1198
1500	-1514	-577	-242	-986	-255	-590	-342	-1001	-1447

(Continued)

TABLE A-41 MODEL A, COMPRESSION FLANGE, DISTRIBUTION OF LONGITUDINAL STRAIN (ϵ_x) AT TRANSVERSE SECTION 9

$\epsilon \times 10^6$ in/in

Lo/PR	1	2	3	4	5	6	7	8	9
1600	-1837	-577	-277	-1055	-283	-509	-367	-1041	-1719
1700	-1972	-568	-281	-1082	-278	-471	-366	-1032	-1831
1800	-1953	-492	-250	-1006	-245	-425	-344	-990	-1853
1600	-1748	-378	-268	-956	-334	-387	-344	-858	-1719
1500	-1463	-352	-277	-860	-285	-347	-286	-772	-1502
1200	-1746	-361	-267	-979	-325	-371	-322	-870	-1767

TABLE A-42 MODEL A, COMPRESSION FLANGE, DISTRIBUTION OF TRANSVERSE STRAIN ϵ_y AT TRANSVERSE SECTION 9

$\epsilon \times 10^6$ in/in

LO/PR	1	2	3	4	5	6	7	8	9
200	13	32	18	25	11	33	25	23	28
300	24	56	31	46	21	43	41	44	47
400	36	80	43	66	27	52	53	64	66
500	47	98	49	80	28	72	56	83	85
600	60	118	54	114	18	83	48	106	111
700	73	135	45	122	12	96	46	126	131
800	86	148	33	136	1	106	43	188	155
900	103	162	15	151	-14	113	32	232	185
1000	114	171	1	168	-26	119	25	259	209
1100	128	186	-22	195	-50	127	7	294	255
1200	139	196	-37	210	-63	129	-2	311	284
1300	154	199	-43	226	-67	127	-2	340	326
1500	178	219	-79	262	-91	123	-17	374	404

(Continued)

TABLE A-42 MODEL A, COMPRESSION FLANGE, DISTRIBUTION OF TRANSVERSE STRAIN ε_y AT TRANSVERSE SECTION 9

$\varepsilon \times 10^6$ in/in

Lo / PR	1	2	3	4	5	6	7	8	9
1600	193	234	-113	304	-114	105	-35	395	487
1700	302	236	-123	320	-119	95	-44	400	517
1800	297	334	-126	297	-122	81	-56	393	514
1600	283	535	-122	409	-45	119	-47	370	447
1500	227	501	-103	373	-36	104	-44	338	398
1200	263	543	-139	433	-65	126	-70	375	470

TABLE A-43 MODEL A , COMPRESSION FLANGE, DISTRIBUTION OF LONGITUDINAL STRAIN (ϵ_x) AT TRANSVERSE SECTION 5

$\epsilon \times 10^6$ in/in

Lo / PR	1	2	3	4	5	6	7	8	9
200	-142	-148	-121	-113	-82	-94	-60	-48	-34
300	-229	-247	-207	-193	-160	-187	-139	-120	-107
400	-311	-334	-288	-259	-234	-268	-221	-189	-178
500	-392	-368	-372	-361	-315	-158	-305	-255	-249
600	-477	-378	-473	-404	-406	-94	-390	-330	-330
700	-585	-336	-591	-328	-501	-20	-478	-377	-414
800	-704	-315	-713	-233	-602	22	-577	-381	-516
900	-832	-276	-842	-175	-715	55	-688	-375	-636
1000	-932	-259	-941	-162	-804	53	-776	-387	-730
1100	-1087	-220	-1097	-169	-951	50	-920	-398	-881
1200	-1189	-191	-1191	-194	-1083	57	-1007	-395	-975
1300	-1297	-166	-1266	-224	-1193	63	-1099	-379	-1078
1500	-1569	-117	-1533	-303	-1373	87	-1304	-331	-1334

(Continued)

TABLE A-43 MODEL A, COMPRESSION FLANGE, DISTRIBUTION OF LONGITUDINAL STRAIN (ϵ_x) AT TRANSVERSE SECTION 5

$\epsilon \times 10^6$ in/in

$\frac{Lo}{PR}$	1	2	3	4	5	6	7	8	9
1600	-1834	105	-1776	-393	-1635	101	-1477	-287	-1626
1700	-1975	-98	-1908	-454	-1781	138	-1619	-271	-1826
1800	-1857	-24	-1840	-423	-1746	191	-1587	-255	-1811
1600	-1712	100	-1542	10	-1177	550	-1132	-153	-1685
1500	-1510	90	-1335	19	-979	521	-949	-150	-1504
1200	-1767	89	-1570	38	-1128	601	-1105	-286	-1876

TABLE A-44 MODEL A, DISTRIBUTION OF TRANSVERSE STRAIN ϵ_y AT TRANSVERSE SECTION 5

$\epsilon \times 10^6$ in/in

LO/PR	1	2	3	4	5	6	7	8	9
200	65	66	32	46	38	65	41	23	-7
300	114	112	52	67	73	125	83	41	15
400	173	157	69	72	120	190	144	59	32
500	219	181	108	121	237	197	176	70	47
600	284	203	152	133	336	226	210	70	65
700	362	218	248	102	395	235	235	73	104
800	448	251	353	86	439	249	267	67	166
900	538	278	447	83	503	278	318	62	216
1000	613	301	515	100	560	314	363	68	254
1100	751	339	638	136	680	370	441	72	321
1200	838	354	720	161	761	391	490	78	373
1300	928	367	787	188	847	412	544	80	427
1500	1157	407	993	259	1089	453	674	98	601

(Continued)

TABLE A-44 MODEL A, DISTRIBUTION OF TRANSVERSE STRAIN ε_y AT TRANSVERSE SECTION 5

$\varepsilon \times 10^6$ in/in

$\frac{Lo}{PR}$	1	2	3	4	5	6	7	8	9
1600	1390	456	1232	380	1394	490	805	109	800
1700	1496	482	1383	432	1580	491	882	135	941
1800	1400	407	1326	396	1559	441	865	137	913
1600	903	370	1146	139	1350	471	1118	80	-66
1500	798	320	1035	118	1278	146	1068	79	-195
1200	784	424	1120	130	1417	158	1243	161	-298

TABLE A-45 MODEL A, DISTRIBUTION OF LONGITUDINAL STRAIN ε_x IN LONGITUDINAL STIFFENERS OF THE COMPRESSION FLANGE AND OF THE WEB

$\varepsilon \times 10^6$ in/in

$\frac{Lo}{PR}$	A_t	A_b	B_t	B_b	C_t	C_b	W_{cf}	W_{cf}	W_{tf}
200	-121	-62	-82	-43	-60	-29	-142	-1	113
300	-207	-99	-160	-80	-139	-70	-229	-43	212
400	-288	-140	-234	-115	-221	-102	-311	-85	301
500	-372	-199	-315	-113	-305	-123	-392	-128	385
600	-473	-244	-406	-124	-390	-165	-477	-179	476
700	-591	-252	-501	-120	-478	-204	-585	-228	556
800	-713	-256	-602	-118	-577	-246	-704	-286	657
900	-842	-276	-715	-127	-688	-306	-832	-362	768
1000	-941	-289	-804	-134	-776	-359	-932	-425	853
1100	-1097	-291	-951	-124	-920	-442	-1087	-538	990
1200	-1191	-275	-1083	-95	-1007	-482	-1189	-603	1077
1300	-1266	-250	-1193	-56	-1099	-522	-1297	-674	1156
1500	-1533	-134	-1373	115	-1304	-575	-1569	-848	1348

(Continued)

TABLE A-45 MODEL A, DISTRIBUTION OF LONGITUDINAL STRAIN ε_x IN LONGITUDINAL STIFFENERS OF THE COMPRESSION FLANGE AND OF THE WEB

$\varepsilon \times 10^6$ in/in

$\frac{L_o}{PR}$	A_t	A_b	B_t	B_b	C_t	C_b	W_{cf}	W_{cf}	W_{tf}
1600	-1776	62	-1634	350	-1477	-621	-1834	-1040	1520
1700	-1908	165	-1781	496	-1619	-612	-1975	-1130	1600
1800	-1840	44	-1746	396	-1587	-700	-1857	-1103	1568

TABLE A-46 MODEL A, STRAIN IN THE WEB PANELS AT DIFFERENT LOADINGS

$\varepsilon \times 10^6$ in/in

PR/Lo	200	300	400	500	600	700	800	900	1000
1	-14	65	-115	-164	-223	-282	-358	-463	-557
2	5	20	35	49	71	87	108	133	151
3	56	77	101	117	134	149	163	174	182
4	-52	-59	-66	-70	-72	-75	-77	-79	-81
5	14	13	36	55	76	95	116	146	174
6	-8	-18	-28	-38	-46	-57	-71	-85	-96
7	38	91	140	181	225	266	308	354	390
8	-17	-47	-75	-100	-121	-143	-165	-185	-200
9	13	-13	-37	-57	-78	-100	-124	-155	-185
10	53	104	146	179	219	258	296	340	375
11	-1	-43	-85	-126	-179	-228	-286	-361	-425
12	113	212	301	385	476	566	651	768	853

(Continued)

TABLE A-46 MODEL A, STRAIN IN THE WEB PANELS AT DIFFERENT LOADINGS

$\varepsilon \times 10^6$ in/in

PR / LO	1100	1200	1300	1500	1600	1700	1800
1	-729	-844	-979	-1319	-1662	-1846	-1851
2	187	205	225	287	357	402	401
3	193	198	198	194	188	174	173
4	-73	-73	377	1666	1606	1605	1615
5	-217	-246	-286	-373	-408	-559	-557
6	-112	-121	-132	-146	-108	45	55
7	451	490	539	699	1108	2384	2474
8	-218	-224	-219	-169	116	1516	1667
9	-230	-259	-294	-378	-487	-623	-629
10	427	458	506	576	634	719	725
11	-538	-603	-674	-848	-1040	-1130	-1103
12	990	1077	1156	1348	1520	1600	1568

TABLE A-47 MODEL B, COMPRESSION FLANGE, DISTRIBUTION OF LONGITUDINAL STRAIN $-\varepsilon_x$ AT TRANSVERSE SECTION 9

$\varepsilon \times 10^6$ in/in

LO PR	1	2	3	4	5	6	7	8	9	10	11
250	-167	-147	-122	-123	-98	-115	-112	-113	-125	-146	-109
500	-360	-322	-243	-255	-189	-249	-218	-248	-269	-329	-253
600	-447	-537	-296	-319	-219	-303	-256	-300	-333	-412	-303
700	-517	-738	-335	-362	-244	-354	-285	-345	-381	-490	-330
800	-609	-1202	-384	-438	-271	-421	-316	-393	-438	-574	-355
900	-702	-1847	-412	-455	-273	-579	-321	-414	-468	-632	-366
1000	-789	-2018	-454	-512	-303	-649	-358	-469	-520	-705	-432
1100	-882	-2377	-488	-534	-322	-801	-378	-500	-562	-745	-488
1200	-1003	-2702	-317	-569	-340	-947	-397	-547	-608	-815	-562

(Continued)

TABLE A-47 MODEL B', COMPRESSION FLANGE, DISTRIBUTION OF LONGITUDINAL STRAIN ε_x AT TRANSVERSE SECTION 9'

$\varepsilon \times 10^6$ in/in

LO / PR	1	2	3	4	5	6	7	8	9	10	11
1300	-1104	-2920	-543	-590	-364	-1057	-420	-589	-645	-836	-632
1400	-1204	-3246	-567	-599	-389	-1141	-441	-627	-675	-882	-712
1500	-1337	-3607	-741	-604	-419	-1207	-477	-792	-706	-943	-834
1600	-1480	-3652	-670	-590	-436	-1269	-496	-847	-730	-989	-1009
1700	-1037	-3683	-747	-580	-458	-1341	-520	-905	-766	-1052	-1156
1800	-1776	-3708	-799	-555	-471	-1386	-534	-931	-792	-1090	-1226
1900	-1881	-3526	-829	-487	-424	-1361	-497	-913	-751	-1077	-1180
2000	-2222	-3756	-899	-477	-470	-1465	-566	-987	-848	-1219	-1351

(Continued)

TABLE A-47 MODEL B, COMPRESSION FLANGE, DISTRIBUTION OF LONGITUDINAL STRAIN ϵ_x AT TRANSVERSE SECTION 9

$\epsilon \times 10^6$ in/in

LO/PR	1	2	3	4	5	6	7	8	9	10	11
2100	-2475	-3763	-924	-420	-463	-1477	-577	-1006	-873	-1305	-1383
2200	-2937	-3845	-949	-329	-452	-1416	-561	-1009	-921	-1456	-1340
2300	-3601	*	-1477	-102	-443	-913	-87	-594	-1337	-4668	-112

TABLE A-48 MODEL B, COMPRESSION FLANGE, DISTRIBUTION OF TRANSVERSE STRAIN ε_y ACROSS TRANSVERSE SECTION 9

$+\varepsilon \times 10^6$ in/in

$\frac{Lo}{PR}$	1	2	3	4	5	6	7	8	9	10	11
250	24	9	3	10	10	19	20	47	43	34	17
500	59	35	9	44	6	38	22	91	72	58	44
600	76	49	7	18	3	33	18	110	81	65	73
700	90	36	4	-8	-13	39	7	198	89	72	85
800	108	-15	3	-40	-21	52	6	276	93	80	110
900	129	-65	-24	-100	-35	10	-8	413	86	79	140
1000	147	-63	-24	-101	-35	15	-7	617	95	86	152
1100	168	-71	-38	-116	-44	8	-16	717	96	119	143
1200	193	-69	-53	-146	-50	-3	-22	832	97	152	164

(Continued)

TABLE A-48 MODEL B, COMPRESSION FLANGE, DISTRIBUTION OF TRANSVERSE STRAIN ϵ_y ACROSS TRANSVERSE SECTION 9

$\epsilon \times 10^6$ in/in

$\frac{Lo}{PR}$	1	2	3	4	5	6	7	8	9	10	11
1300	214	-14	-60	-164	-58	-15	-28	921	96	164	175
1400	233	-72	-66	-171	-65	-12	-38	976	96	172	185
1500	268	-69	-62	-181	-72	-8	-47	1021	93	195	197
1600	299	-71	-60	-198	-83	-17	-63	1066	87	193	216
1700	331	-69	-58	-216	-97	-33	-82	1130	82	185	217
1800	357	-72	-60	-233	-108	-47	-101	1161	82	179	218
1900	378	-86	-72	-246	-126	-59	-114	1095	80	157	211
2000	420	-105	-97	-290	-156	-79	-130	1213	86	173	223

(Continued)

TABLE A-48 MODEL B, COMPRESSION FLANGE, DISTRIBUTION OF TRANSVERSE STRAIN ε_y ACROSS TRANSVERSE SECTION 9

$\varepsilon \times 10^6$ in/in

$\frac{Lo}{PR}$	1	2	3	4	5	6	7	8	9	10	11
2100	439	141	-131	-330	-183	-92	-142	1204	82	165	219
2200	451	-215	-199	-396	-221	-119	-163	1267	72	138	213
2300	425	-267	-136	-491	-248	-369	-442	2207	-149	-187	185

TABLE A-49 MODEL B, COMPRESSION FLANGE, DISTRIBUTION OF LONGITUDINAL STRAIN ϵ_x AT TRANSVERSE SECTION 5

$\epsilon \times 10^6$ in/in

Lo/PR	1	2	3	4	5	6	7	8	9	10	11
250	-240	-146	-220	-41	-168	-81	-136	-52	-93	-48	-40
500	-434	-397	-429	-129	-366	-152	-334	-101	-296	-189	-215
600	-522	-750	-528	-210	-463	-165	-427	-110	-389	-249	-296
700	-591	-849	-606	-312	-541	-186	-502	-125	-462	-294	-361
800	-679	-955	-707	-415	-644	-198	-599	-136	-561	-328	-446
900	-761	-1045	-799	-509	-738	-182	-687	-135	-661	-347	-529
1000	-840	-1103	-889	-552	-831	-216	-775	-147	-751	-388	-608
1100	-922	-1180	-988	-615	-935	-217	-874	-146	-854	-438	-697
1200	-1031	-1264	-1118	-682	-1071	-206	-1000	-134	-987	-480	-809

(Continued)

TABLE A-49 MODEL B, COMPRESSION FLANGE, DISTRIBUTION OF LONGITUDINAL STRAIN ϵ_x AT TRANSVERSE SECTION 5

$\epsilon \times 10^6$ in/in

$\frac{Lo}{PR}$	1	2	3	4	5	6	7	8	9	10	11
1300	-1121	-1338	-1227	-721	-1185	-199	-1107	-123	-1098	-537	-902
1400	-1213	-1412	-1339	-866	-1300	-187	-1216	-99	-1210	-592	-994
1500	-1343	-1475	-1500	-803	-1457	-172	-1366	-74	-1365	-667	-1108
1600	-1481	-1485	-1684	-860	-1642	-138	-1540	-118	-1547	-712	-1249
1700	-1642	-1469	-1907	-905	-1865	-121	-1750	-117	-1763	-779	-1416
1800	-1799	-1423	-2115	-931	-2078	-98	-1941	-88	-1935	-795	-1535
1900	-1926	-1238	-2229	-974	-2249	-67	-2137	9	-2080	-746	-1616
2000	-2332	-1094	-2889	-1132	-2776	-65	-2629	219	-2472	-712	-1847

(Continued)

TABLE A-49 MODEL B, COMPRESSION FLANGE, DISTRIBUTION OF LONGITUDINAL STRAIN ϵ_x AT TRANSVERSE SECTION 5

$\epsilon \times 10^6$ in/in

$\frac{Lo}{PR}$	1	2	3	4	5	6	7	8	9	10	11
2100	-2647	-791	-3584	-1349	-3225	-60	-3160	599	-2841	-581	-2065
2200	-3476	621	-5290	-1949	-4447	-28	-4628	1689	-3965	-157	-2653
2300	-4229	1425	-3479	-2806	-4856	246	-4699	1779	-5389	801	-6580

TABLE A-50 MODEL B, COMPRESSION FLANGE, DISTRIBUTION OF TRANSVERSE STRAIN ε_y ACROSS TRANSVERSE SECTION 5

$\varepsilon \times 10^6$ in/in

$\frac{Lo}{PR}$	1	2	3	4	5	6	7	8	9	10	11
250	130	88	107	101	82	48	65	58	54	15	33
500	261	135	246	277	190	92	173	156	383	101	-10
600	326	284	314	381	242	115	227	206	290	139	42
700	386	451	371	49	286	139	273	251	639	167	84
800	462	591	445	543	340	168	331	316	621	200	148
900	536	733	510	628	383	182	384	383	740	225	225
1000	606	807	584	705	435	208	437	454	821	260	288
1100	685	874	658	786	485	221	497	531	836	288	364
1200	800	936	759	857	549	227	572	645	969	327	474

(Continued)

TABLE A-50 MODEL B, COMPRESSION FLANGE, DISTRIBUTION OF TRANSVERSE STRAIN ε_y ACROSS TRANSVERSE SECTION 5

$\varepsilon \times 10^6$ in/in

$\frac{Lo}{PR}$	1	2	3	4	5	6	7	8	9	10	11
1300	899	987	835	929	601	232	634	734	1111	357	562
1400	1008	1038	909	999	658	235	699	834	1111	396	660
1500	1181	1117	1010	1109	751	249	798	1025	1389	467	805
1600	1387	1227	1096	1233	860	250	904	1392	1529	522	1101
1700	1634	1347	1164	1525	1015	258	1034	1723	2096	577	1275
1800	1897	1503	1198	1729	1187	262	1155	2038	2327	622	1430
1900	2293	1699	1240	1799	1457	245	1323	2418	2826	720	1592
2000	2920	2373	1423	2235	1889	280	1628	3292	3735	911	1866

(Continued)

TABLE A-50 MODEL B, COMPRESSION FLANGE, DISTRIBUTION OF TRANSVERSE STRAIN ϵ_y ACROSS TRANSVERSE SECTION 5

$\epsilon \times 10^6$ in/in

Lo/PR	1	2	3	4	5	6	7	8	9	10	11
2100	3803	2973	1603	2537	2405	285	1983	4096	4371	1023	2145
2200	7066	4611	3021	3225	3377	255	2941	5843	6293	1375	3174
2300	*	*	9028	4264	3933	695	3186	8163	7343	3126	7648

TABLE A-51 MODEL B, COMPRESSION FLANGE, DISTRIBUTION OF LONGITUDINAL STRAIN ε_x, AND TRANSVERSE STRAIN ε_y AT TRANSVERSE SECTION 18 (IN END PANEL)

$\varepsilon \times 10^6$ in/in

$\frac{Lo}{PR}$	1x	3x	4x	5x	6x	1y	2y	3y	4y	5y
250	-15	-24	-42	-64	-145	4	-10	-8	17	-31
500	-212	-152	-193	-181	-761	38	-180	8	47	-28
600	-303	-210	-256	-225	-874	49	-251	10	60	-33
700	-400	-264	-334	-265	-1028	54	-436	13	70	-31
800	-481	-330	-431	-314	-1206	58	-832	20	79	-27
900	-549	-393	-551	-360	-1455	50	-1128	31	79	-11
1000	-614	-444	-602	-396	-1553	55	-1234	33	88	-15
1100	-680	-504	-702	-441	-1770	52	-1400	43	88	-4

(Continued)

TABLE A-51 MODEL B, COMPRESSION FLANGE, DISTRIBUTION OF LONGITUDINAL STRAIN ε_x AND TRANSVERSE STRAIN ε_y AT TRANSVERSE SECTION 18 (IN END PANEL)

$\varepsilon \times 10^6$ in/in

$\frac{Lo}{PR}$	1x	3x	4x	5x	6x	1y	2y	3y	4y	5y
1200	-746	-570	-798	-491	-1994	49	-1565	56	88	9
1300	-800	-625	-896	-534	-2241	43	-1696	65	86	23
1400	-842	-676	-992	-574	-2476	37	-1795	75	85	40
1500	-885	-738	-1123	-623	-2774	32	-1901	83	83	62
1600	-906	-793	-1211	-675	-3071	18	-1942	92	80	91
1700	-942	-862	-1355	-742	-3483	2	-2021	87	65	124
1800	-946	-903	-1509	-796	-3894	-7	-2077	81	43	159
1900	-919	-933	-1567	-860	-4618	-19	-2069	63	10	213

(Continued)

TABLE A-51 MODEL B, COMPRESSION FLANGE, DISTRIBUTION OF LONGITUDINAL STRAIN ε_x AND TRANSVERSE STRAIN ε_y AT TRANSVERSE SECTION 1 (IN END PANEL)

$\varepsilon \times 10^6$ in/in

Lo/PR	1x	3x	4x	5x	6x	1y	2y	3y	4y	5y
2000	-948	-1023	-1787	-969	-5364	-26	-2190	45	-28	258
2100	-949	-1098	-1879	-1094	-6601	-44	-2200	7	-74	345
2200	-951	-1312	-1985	-1553	-7322	-83	-2094	-171	-82	884
2300	-676	-1205	-1774	-1793	*	-211	-1781	-460	0	1638

TABLE A-52 MODEL B, LONGITUDINAL STRAIN ε_x IN LONGITUDINAL STIFFENERS OF THE COMPRESSION FLANGE AND OF THE WEB AT TRANSVERSE SECTION 5

$\varepsilon \times 10^6$ in/in

$\frac{Lo}{PR}$	A_t	A_b	B_t	B_b	C_t	C_b	D_t	D_b	W_{cf}	W_{Ls}	W_{tf}
250	-220	-101	-168	-40	-136	-5	-93	-15	-240	-164	190
500	-429	-187	-366	-78	-334	-8	-296	-57	-434	-270	384
600	-528	-179	-463	-87	-427	-2	-389	-76	-522	-318	461
700	-606	-214	-541	-88	-502	9	-462	-89	-591	-358	521
800	-707	-251	-644	-87	-599	29	-561	-103	-679	-407	593
900	-799	-226	-738	-85	-687	49	-661	-116	-761	-455	638
1000	-889	-256	-831	-73	-775	82	-751	-121	-840	-500	716
1100	-998	-265	-935	-57	-874	123	-854	-138	-922	-549	777

(Continued)

TABLE A-52 MODEL B, LONGITUDINAL STRAIN ϵ_x IN LONGITUDINAL STIFFENERS OF THE COMPRESSION FLANGE AND OF THE WEB AT TRANSVERSE SECTION 5

$\epsilon \times 10^6$ in/in

$\frac{Lo}{PR}$	A_t	A_b	B_t	B_b	C_t	C_b	D_t	D_b	W_{cf}	W_{Ls}	W_{tf}
1200	-1118	-241	-1071	-16	-1000	193	-987	-133	-1031	-611	852
1300	-1227	-250	-1185	34	-1107	263	-1098	-128	-1121	-664	913
1400	-1339	-223	-1300	103	-1216	348	-1210	-116	-1213	-716	971
1500	-1500	-110	-1457	229	-1366	490	-1365	-90	-1343	-790	1059
1600	-1684	-40	-1642	394	-1540	670	-1547	-47	-1481	-863	1138
1700	-1907	116	-1865	619	-1750	921	-1763	36	-1642	-946	1220
1800	-2115	215	-2078	829	-1941	1158	-1935	133	-1799	-1029	1290
1900	-2229	418	-2249	1150	-2137	1510	-2080	299	-1926	-1143	1366

(Continued)

TABLE A-52 MODEL B, LONGITUDINAL STRAIN ϵ_x IN LONGITUDINAL STIFFENERS OF THE COMPRESSION FLANGE AND OF THE WEB AT TRANSVERSE SECTION 5

$\epsilon \times 10^6$ in/in

$\frac{Lo}{PR}$	A_t	A_b	B_t	B_b	C_t	C_b	D_t	D_b	W_{cf}	W_{Ls}	W_{tf}
2000	-2889	695	-2776	1589	-2629	1957	-2472	513	-2332	-1305	1498
2100	-3584	977	-3225	2207	-3160	2523	-2841	808	-2647	-1448	1615
2200	-5290	1872	-4447	4465	-4628	4214	-3965	1987	-3476	-1509	1775
2300	*	*	-4856	*	-4699	9412	-5389	7119	*	-1896	1752

TABLE A-53 MODEL B, STRAIN IN WEB PANELS AT DIFFERENT LOADINGS

$\varepsilon \times 10^6$ in/in

PR/LO	250	500	600	700	800	900	1000	1100	1200	1300
1	75	124	145	164	187	208	229	251	283	310
2	-203	-354	-424	-479	-549	-613	-676	-743	-828	-900
3	51	55	52	53	51	50	48	45	45	42
4	-29	14	34	49	69	83	99	113	131	142
5	4	-33	-50	-61	-74	-81	-95	-111	-125	-106
6	-201	-328	-385	-431	-486	-539	-577	-609	-628	-787
7	-180	-316	-369	-413	-461	-488	-535	-577	-636	-663
8	164	326	394	451	518	573	644	723	866	968
9	-12	-37	-50	-59	-72	-83	-96	-107	-120	-132

(Continued)

TABLE A-53 MODEL B, STRAIN IN WEB PANELS AT DIFFERENT LOADINGS

$\epsilon \times 10^6$ in/in

PR / Lo	250	500	600	700	800	900	1000	1100	1200	1300
10	-100	-145	-168	-186	-205	-229	-241	-264	-284	-305
11	-180	-323	-379	-424	-476	-507	-556	-608	-651	-683
13	-55	-97	-114	-127	-140	-125	-139	-144	-150	-149
14	7	-4	-12	-17	-17	-5	5	-607	-714	-768
15	-195	-364	-433	-487	-551	-598	-656	-713	-776	-828
16	182	342	406	459	520	566	625	675	735	781

(Continued).

TABLE A-53 MODEL B, STRAIN IN WEB PANELS AT DIFFERENT LOADINGS

$\epsilon \times 10^6$ in/in

PR LO.	1400	1500	1600	1700	1800	1900	2000	2100	2200	2300
1	339	385	438	502	559	623	721	819	1767	4809
2	-973	-1076	-1183	-1300	-1396	-1405	-1604	-1639	-2077	-9333
3	39	36	35	34	39	47	47	48	70	1291
4	152	166	176	184	184	176	177	180	218	-34
5	-94	-117	-121	-72	-19	102	150	60	-240	-211
6	-851	-822	-871	-862	-835	-843	-888	-732	-591	-788
7	-679	-685	-716	-756	-892	-988	-1081	-1162	-874	-3208
8	1066	1158	1221	1268	1280	1250	1264	1296	2265	5664

(Continued)

TABLE A-53 MODEL B, STRAIN IN WEB PANELS AT DIFFERENT LOADINGS

$\varepsilon \times 10^6$ in/in

PR/LO	1400	1500	1600	1700	1800	1900	2000	2100	2200	2300
9	-142	-146	-154	-162	-155	-136	-154	-157	-170	-24
10	-321	-349	-371	-370	-392	-416	-475	-470	-437	-388
11	-709	-741	-780	-813	-850	-894	-1069	-1174	-1084	-893
13	-142	-145	-125	-110	-103	-89	-94	-82	-22	52
14	-805	-832	-741	-741	-686	-653	-663	-665	-686	-704
15	-877	-942	-1008	-1063	-1119	-1169	-1259	-1325	-1391	-1184
16	825	890	946	977	1050	1106	1193	1245	1340	1134

TABLE A-54 MODEL C, COMPRESSION FLANGE DISTRIBUTION OF LONGITUDINAL STRAIN ϵ_x AT TRANSVERSE SECTION 9

$\epsilon \times 10^6$ in/in

$\frac{Lo}{PR}$	1	2	3	4	5	6	7	8	9	10	11
Initial	-118	-144	-89	-116	-98	-130	-89	-116	-104	-146	-148
300	-147	-176	-108	-133	-116	-149	-105	-137	-124	-181	-180
500	-278	-300	-187	-205	-186	-250	-172	-240	-200	-322	-319
700	-399	-431	-250	-280	-242	-329	-225	-332	-261	-425	-446
800	-473	-508	-280	-316	-262	-348	-244	-372	-284	-466	-521
900	-552	-594	-319	-379	-297	-409	-279	-440	-325	-537	-602
1000	-625	-666	-354	-423	-321	-440	-302	-484	-351	-589	-675
1100	-689	-726	-370	-460	-333	-471	-312	-528	-368	-638	-739
1200	-766	-794	-389	-492	-339	-494	-314	-573	-381	-689	-815

(Continued)

TABLE A-54 MODEL C, COMPRESSION FLANGE DISTRIBUTION OF LONGITUDINAL STRAIN ϵ_x AT TRANSVERSE SECTION 9

$\epsilon \times 10^6$ in/in

$\frac{Lo}{PR}$	1	2	3	4	5	6	7	8	9	10	11
1300	-851	-862	-405	-519	-343	-515	-313	-612	-393	-741	-898
1400	-920	-919	-416	-540	-341	-531	-307	-644	-397	-780	-964
1500	-1010	-983	-416	-561	-325	-552	-286	-676	-389	-835	-1052
1600	-1113	-1049	-404	-475	-295	-568	-250	-699	-366	-893	-1151
1700	-1204	-1097	-375	-582	-254	-580	-217	-713	-332	-941	-1237
1800	-1293	-1132	-326	-581	-211	-583	-182	-717	-284	-976	-1318
1900	-1411	-1170	-225	-576	-121	-583	-93	-720	-198	-1017	-1431
2000	-1458	-1164	-165	-553	-58	-562	-28	-710	-142	-1029	-1489

(Continued)

TABLE A-54 MODEL C, COMPRESSION FLANGE DISTRIBUTION OF LONGITUDINAL STRAIN ϵ_x AT TRANSVERSE SECTION 9

$\epsilon \times 10^6$ in/in

LO / PR	1	2	3	4	5	6	7	8	9	10	11
2000Y	-1558	-1126	-149	-529	2	-563	46	-714	-80	-1014	-1609
2000Y	-1544	-1112	-143	-519	10	-555	54	-694	-69	-992	-1591
0.0	-1549	-1111	-143	-515	13	-549	57	-691	-66	-992	-1596

2000Y = plastic zone.

TABLE A-55 MODEL C, COMPRESSION OF DISTRIBUTION OF TRANSVERSE STRAIN (ϵ_y) AT TRANSVERSE SECTION 9

$\epsilon \times 10^6$ in/in

$\frac{Lo}{PR}$	1	2	3	4	5	6	7	8	9	10	11
Initial	32	29	31	18	27	21	30	27	29	14	33
300	39	36	37	21	34	24	35	32	35	15	40
500	72	68	65	31	65	34	59	53	66	23	75
700	104	94	85	42	94	44	80	68	94	31	110
800	122	110	93	44	112	45	92	73	110	33	131
900	142	124	105	52	127	52	102	84	126	41	153
1000	163	140	114	58	142	53	111	93	142	45	174
1100	177	150	122	63	153	57	118	99	153	50	191
1200	194	161	128	67	164	58	124	105	164	52	211

(Continued)

TABLE A-55 MODEL C, COMPRESSION OF DISTRIBUTION OF TRANSVERSE STRAIN (ϵ_y) AT TRANSVERSE SECTION 9.

$\epsilon \times 10^6$ in/in

$\frac{Lo}{PR}$	1	2	3	4	5	6	7	8	9	10	11
1300	212	174	133	71	174	60	129	114	176	55	235
1400	227	183	137	75	182	59	132	119	184	56	254
1500	245	194	140	77	190	60	136	125	191	56	279
1600	267	206	142	78	203	56	137	130	197	54	308
1700	284	214	142	76	202	53	136	134	199	51	332
1800	302	218	141	70	207	45	131	131	195	43	352
1900	335	228	144	60	203	30	118	123	183	26	381
2000	342	224	139	45	177	12	100	110	168	8	390

(Continued)

TABLE A-55 MODEL C, COMPRESSION OF DISTRIBUTION OF TRANSVERSE STRAIN (ϵ_y) AT TRANSVERSE SECTION 9

$\epsilon \times 10^6$ in/in

$\frac{Lo}{PR}$	1	2	3	4	5	6	7	8	9	10	11
2000Y	365	226	157	33	168	-9	84	-9	126	-25	396
2000Y	364	223	155	32	168	-9	85	52	124	-26	393
0.0	366	-223	156	31	168	-11	85	51	124	-26	395

2000Y = plastic zone

TABLE A-56 MODEL C, COMPRESSION DISTRIBUTION OF LONGITUDINAL STRAIN (ϵ_x) AT TRANSVERSE SECTION 5

$\epsilon \times 10^6$ in/in

LO / PR	1	2	3	4	5	6	7	8	9	10	11
Initial	-204	-192	-175	-142	-167	-112	-148	-127	-129	-123	-123
300	-240	-220	-209	-169	-205	-139	-183	-159	-164	-160	-162
500	-398	-339	-369	-304	-375	-267	-344	-305	-316	-311	-331
700	-546	-435	-522	-433	-536	-386	-497	-446	-461	-442	-490
800	-637	-480	-615	-507	-636	-454	-591	-525	-546	-520	-584
900	-735	-556	-713	-588	-741	-534	-690	-622	-641	-613	-683
1000	-824	-609	-805	-661	-840	-600	-781	-700	-727	-695	-774
1100	-901	-666	-883	-727	-926	-667	-861	-781	-803	-772	-851

(Continued)

TABLE A-56 MODEL C / COMPRESSION DISTRIBUTION OF LONGITUDINAL STRAIN (ε_x) AT TRANSVERSE SECTION 5

$\varepsilon \times 10^6$ in/in

$\frac{Lo}{PR}$	1	2	3	4	5	6	7	8	9	10	11
1200	-998	-731	-981	-796	-1032	-741	-959	-873	-897	-858	-945
1300	-1104	-797	-1087	-861	-1147	-812	-1065	-969	-1000	-945	-1048
1400	-1188	-852	-1174	-916	-1239	-873	-1151	-1050	-1081	-1017	-1130
1500	-1302	-923	-1291	-985	-1363	-952	-1266	-1162	-1192	-1111	-1238
1600	-1432	-996	-1429	-1060	-1506	-1038	-1399	-1291	-1316	-1208	-1359
1700	-1546	-1056	-1551	-1118	-1632	-1109	-1514	-1410	-1423	-1284	-1462
1800	-1665	-1109	-1684	-1172	-1769	-1191	-1634	-1532	-1533	-1348	-1565
1900	-1836	-1171	-1898	-1230	-1997	-1302	-1827	-1733	-1711	-1421	-1725

(Continued)

TABLE A-56 MODEL C, COMPRESSION DISTRIBUTION OF LONGITUDINAL STRAIN (ϵ_x) AT TRANSVERSE SECTION 5

$\epsilon \times 10^6$ in/in

Lo / PR	1	2	3	4	5	6	7	8	9	10	11
2000	-1895	-1190	-2019	-1257	-2152	-1408	-1953	-1850	-1828	-1450	-1820
2000Y	-1992	-1201	-2190	-1265	-2364	-1502	-2130	-2048	-2046	-1416	-2085
2000Y	-1976	-1187	-2171	-1253	-2342	-1497	-2107	-2023	-2025	-1400	-2067
0.0	-1981	-1186	-2176	-1254	-2347	-1500	-2112	-2023	-2031	-1400	-2073

2000Y = plastic zone

TABLE A-57 MODEL C, COMPRESSION FLANGE DISTRIBUTION OF TRANSVERSE STRAIN (ϵ_y) AT TRANSVERSE SECTION 5

$\epsilon \times 10^6$ in/in

LO/PR	1	2	3	4	5	6	7	8	9	10	11
Initial	75	46	44	43	47	48	51	26	21	30	42
300	88	55	56	52	58	59	63	32	26	40	54
500	150	91	123	114	105	108	121	60	52	78	98
700	211	123	193	180	152	152	180	91	77	103	151
800	250	139	243	227	180	179	220	109	93	112	184
900	292	161	287	270	214	214	256	130	107	128	217
1000	330	180	336	312	235	245	291	150	120	139	248
1100	365	199	378	354	261	278	323	167	129	147	254
1200	409	223	433	406	291	320	363	189	139	156	282

(Continued)

TABLE A-57 MODEL C, COMPRESSION FLANGE DISTRIBUTION OF TRANSVERSE STRAIN (ϵ_y) AT TRANSVERSE SECTION 5

$\epsilon \times 10^6$ in/in

LG / PR	1	2	3	4	5	6	7	8	9	10	11
1300	459	251	495	463	333	370	407	213	149	165	319
1400	500	274	547	511	373	413	441	233	155	172	348
1500	557	305	619	578	439	481	486	259	161	179	388
1600	623	342	705	658	527	573	531	284	159	186	435
1700	683	376	786	735	631	669	564	302	149	192	478
1800	746	410	877	822	763	790	588	313	125	197	524
1900	856	462	1048	985	1034	1060	611	319	51	219	616
2000	931	470	1156	1107	1225	1317	626	339	4	240	686

(Continued)

TABLE A-57 MODEL C, COMPRESSION FLANGE DISTRIBUTION OF TRANSVERSE STRAIN (ε_y) AT TRANSVERSE SECTION 5

$\varepsilon \times 10^6$ in/in

Lo/PR	1	2	3	4	5	6	7	8	9	10	11
56 525/32 521/32	1041	462	1333	1236	1564	1709	555	287	-143	252	826
60 2000Y	1034	457	1327	1232	1551	1700	553	287	-141	250	821
Last 0.0	1037	457	1332	1235	1554	1704	554	287	-141	250	824

TABLE A-58 MODEL C, DISTRIBUTION OF LONGITUDINAL STRAIN (ε_x) IN COMPRESSION FLANGE LONGITUDINAL STIFFENERS AND IN WEB PANELS

$\varepsilon \times 10^6$ in/in

$\frac{Lo}{PR}$	A_t	A_b	B_t	B_b	C_t	C_b	D_t	D_b	W_{cf}	W_{LS}	W_{tf}
Initial	-175	-84	-167	-73	-148	-67	-129	-76	-204	-130	227
300	-209	-104	-205	-88	-183	-82	-164	-94	-240	-153	270
500	-369	-176	-375	-150	-344	-146	-316	-172	-398	-248	445
700	-522	-235	-536	-203	-497	-199	-461	-240	-546	-341	591
800	-615	-271	-636	-231	-591	-228	-546	-279	-637	-399	662
900	-713	-308	-741	-260	-690	-257	-641	-321	-735	-460	761
1000	-805	-341	-840	-282	-781	-279	-727	-356	-824	-521	845
1100	-883	-366	-926	-301	-861	-294	-803	-383	-901	-571	911
1200	-981	-395	-1032	-319	-959	-308	-897	-414	-998	-632	990

(Continued)

TABLE A-58 MODEL C, DISTRIBUTION OF LONGITUDINAL STRAIN (ε_x) IN COMPRESSION FLANGE LONGITUDINAL STIFFENERS AND IN WEB PANELS

$\varepsilon \times 10^6$ in/in

$\frac{Lo}{PR}$	A_t	A_b	B_t	B_b	C_t	C_b	D_t	D_b	W_{cf}	W_{LS}	W_{tf}
1300	-1087	-425	-1147	-334	-1065	-317	-1000	-444	-1104	-701	1085
1400	-1174	-447	-1239	-343	-1151	-317	-1081	-466	-1188	-757	1163
1500	-1291	-469	-1363	-347	-1266	-303	-1192	-490	-1302	-831	1272
1600	-1429	-519	-1506	-338	-1399	-268	-1316	-511	-1432	-915	1386
1700	-1551	-512	-1632	-312	-1514	-212	-1423	-519	-1546	-986	1477
1800	-1684	-502	-1769	-249	-1634	-116	-1533	-508	-1665	-1056	1544
1900	-1898	-429	-1997	-81	-1827	118	-1711	-433	-1836	-1145	1623
2000	-2019	-352	-2152	115	-1953	363	-1828	-322	-1895	-1155	1651

(Continued)

TABLE A-58 MODEL C, DISTRIBUTION OF LONGITUDINAL STRAIN (ϵ_x) IN COMPRESSION FLANGE LONGITUDINAL STIFFENERS AND IN WEB PANELS

$\epsilon \times 10^6$ in/in

$\frac{Lo}{PR}$	A_t	A_b	B_t	B_b	C_t	C_b	D_t	D_b	W_{cf}	W_{LS}	W_{tf}
2000Y	-2190	-317	-2364	202	-2130	585	-2046	-275	-1992	-1266	1687
2000Y	-2171	-320	-2342	206	-2107	584	-2025	-268	-1976	-1253	1662
0.0	-2176	-316	-2347	209	-2112	586	-2031	-268	-1981	-1262	1663

2000Y = plastic zone.

TABLE A-59 MODEL C, DISTRIBUTION OF LONGITUDINAL STRAIN (ε_x) IN LONGITUDINAL STIFFENERS OF THE COMPRESSION FLANGE (END PANEL)

$\varepsilon \times 10^6$ in/in

$\frac{Lo}{PR}$	A_t	A_b	B_t	B_b	C_b	D_b
Initial	-160	-74	-108	-33	-2	-8
300	-191	-82	-132	-36	-5	-15
500	-304	-114	-219	-61	-24	-50
700	-413	-141	-303	-83	-39	-78
800	-484	-156	-355	-95	-49	-95
900	-551	-174	-406	-111	-61	-114
1000	-620	-188	-457	-122	-71	-128
1100	-670	-201	-494	-135	-82	-142
1200	-734	-215	-541	-149	-95	-158
1300	-805	-231	-593	-163	-110	-173
1400	-864	-240	-636	-172	-121	-184
1500	-939	-253	-690	-186	-137	-197
1600	-1024	-262	-752	-198	-153	-206

(Continued)

TABLE A-59 MODEL C, DISTRIBUTION OF LONGITUDINAL STRAIN (ε_x) IN LONGITUDINAL STIFFENERS OF THE COMPRESSION FLANGE (END PANEL)

$\varepsilon \times 10^6$ in/in

$\frac{Lo}{PR}$	A_t	A_b	B_t	B_b	C_b	D_b
1700	-1097	-262	-807	-196	-159	-201
1800	-1182	-245	-873	-177	-151	-168
1900	-1374	-142	-1036	-59	-64	11
2000	-1677	93	-1351	246	184	463
2000Y	-2658	810	-4295	1726	1854	2559
2000Y	-2655	809	-4302	1731	1861	2552
0.0	-2670	812	-4328	1738	1869	2559

2000Y = plastic zone.

TABLE A-60 MODEL C, STRAIN IN WEB PANELS AT DIFFERENT LOADINGS

$\varepsilon \times 10^6$ in/in

PR / Lo	INITIAL	300	500	700	8[illegible]	900	1000	1100	1200	1300
1	17	23	59	94	114	137	157	175	199	225
2	-89	-119	-250	-375	-449	-527	-599	-662	-737	-820
3	-48	-50	-62	-71	-75	-81	-84	-89	-93	-98
4	67	74	113	146	164	185	204	219	236	255
5	-35	-42	-73	-101	-116	-137	-154	-170	-189	-210
6	-11	-26	-96	-168	-213	-256	-294	-317	-323	-304
8	131	164	325	504	615	744	872	987	1144	1344
9	-45	-54	-87	-114	-128	-148	-165	-178	-199	-227
11	-95	-122	-222	-316	-368	-433	-496	-549	-620	-708

(Continued)

TABLE A-60 MODEL C, STRAIN IN WEB PANELS AT DIFFERENT LOADINGS

$\varepsilon \times 10^6$ in/in

$\frac{PR}{Lo}$	INITIAL	300	500	700	800	900	1000	1100	1200	1300
12	100	126	251	372	440	527	607	678	771	885
13	-76	-101	-222	-341	-410	-477	-529	-579	-644	-716
14	34	43	101	180	235	294	340	394	458	522
15	-118	-149	-283	-406	-474	-552	-620	-673	-745	-830
16	92	116	250	379	449	536	573	646	730	826

TABLE A-61 MODEL C, STRAIN IN WEB PANELS AT DIFFERENT LOADINGS

$\varepsilon \times$ in/in

PR / LO	1400	1500	1600	1700	1800	1900	2000	2000Y	2000Y	0.0
1	245	272	303	332	361	414	454	522	519	520
2	-887	-974	-1072	-1154	-1234	-1348	-1412	-1568	-1557	-1559
3	-101	-105	-109	-112	-118	-138	-159	-242	-240	-2110
4	268	285	302	313	325	363	392	594	589	590
5	-228	-259	-331	-471	-846	-1666	-2156	-6709	-6714	-6736
6	-279	-234	-159	-24	197	878	1223	2592	2593	2602
8	1522	1783	2182	2711	3547	6024	9220	OUT	1629[R]	1628[R]
9	-252	-299	-383	-535	-937	-2265	-4336	-4011	-3997	-4004

2000 Y = plastic zone.

R = strain gage out.

(Continued)

TABLE A-61 MODEL C, STRAIN IN WEB PANELS AT DIFFERENT LOADINGS

ϵ_x in/in

$\frac{PR}{Lo}$	1400	1500	1600	1700	1800	1900	2000	2000Y	2000Y	0.0
11	-790	-955	-1205	-1557	-2382	-4256	-3776	-1541	-1319	-1286[R]
12	988	1155	1435	1916	3035	6950	OUT[R]	1341[R]	1209[R]	1202[R]
13	-769	-841	-911	-968	-1021	-1317	-1814	-3720	-3712	-3721
14	572	639	707	763	819	1111	1435	2954	2948	2958
15	-899	-1003	-1146	-1333	-1861	-3476	-5388	-1591[R]	-1583[R]	-1613[R]
16	909	1031	1193	1387	1717	3102	5548	1628[R]	1627[R]	1624[R]

2000Y = plastic zone.

R = strain gage out.

APPENDIX B

LARGE DEFLECTIONS ANALYSIS OF ULTIMATE BUCKLING STRENGTH OF STIFFENED PANEL WITH CONSIDERATION OF INITIAL IMPERFECTIONS

APPENDIX B

LARGE DEFLECTIONS ANALYSIS OF ULTIMATE BUCKLING STRENGTH OF STIFFENED PANEL WITH CONSIDERATION OF INITIAL IMPERFECTIONS

B.1 INTRODUCTION

A steel box-girder bridge is an assembly of stiffened panels. Due to the complexity of the mathematical formulcation of the buckling behaviour of the whole cross-section, it is current practice to analyse the buckling behaviour of those stiffened panel elements that compose the cross-section. Such investigation is discutable. This is why such experimental tests are required as those provided in the present work.

For the analysis of stiffened panels typical to those of steel box-girder bridges, the large deflections theory accounting for the effect of initial imperfections is recommended. This method is an extension of the large deflections theory of naturally-orthotropic plates. A historical note on its development is given in the main part of this thesis, in Section 3.5.1, as well as a review of the solutions given by some proposed approximate methods. In this section, the development of basically large fundamental deflection equations of stiffened panels is made, and an approximate solution is given.

Different techniques for the transformation of the stiffened plate element as a natural orthotropic plate, are well summarized by Troitsky [120]. The main difficulty is the accurate interpretation of the interaction between the plate and stiffeners. Some points still need more investigation, among those being the neutral plane about which unit rigidities are to be computed, the consideration of the eccentricities of the stiffeners, with regard to the neutral axis of the plate element, the fact that the stress state is two-dimensional in the plate, and in one direction for the stiffener.

In this section, fundamental equations are developed for two cases:

a) First, it is assumed that the stress acts in two directions for the plate element, and in one direction for the stiffener; therefore, the horizontal shear stress acts only upon the plate element.

b) In the second case, the stress is assumed to be the same in both the plate and stiffener. This latter case is conservative. However, it may be remembered that in both cases, the fundamental equation of equilibrium remains the same; only the compatibility equation is affected.

B.2 LARGE DEFLECTIONS EQUATIONS: ASSUMING THE STRESS TO BE DIFFERENT IN THE PLATE AND STIFFENER

The equilibrium method is used for the development of fundamental equations. Considering a typical element of the stiffened panel, Figure B.1, is subjected to the action of the lateral and in-plane loading, as shown. The stiffened panel is transformed as a continuous natural orthotropic plate by defining the unit membrane force per unit width, as follows:

$$n_x = \frac{N_x}{a_x} , \quad n_y = \frac{N_y}{a_y} , \quad n_{xy} = \frac{N_{xy}}{a_x} , \quad N_{yx} = \frac{N_{yx}}{a_y} \qquad (B.1)$$

For a stiffened plate subjected to lateral loading $p(x,y)$, Huber's Equation can be written as

$$B_x \frac{\partial^4 w}{\partial x^4} + 2H \frac{\partial^4 w}{\partial x^2 \partial y^2} + B_y \frac{\partial^4 w}{\partial y^4} = p(x,y) \qquad (B.2)$$

where

$$B_x = \frac{EI_x}{a_x} , \quad B_y = \frac{EI_y}{a_y} \qquad (B.3)$$

and

I_x, I_y = the moment of inertia about the middle plane of the plate's stiffener

a_x, a_y = stiffener's spacing

$H = H^*$ = effective torsional stiffness

$$= B + \frac{(B_{xy}+B_{yx})}{2} + \nu e_x e_y \bar{D} + (e_x+e_y)^2 \frac{(1-\nu)\bar{D}}{4}$$

Due to the curvature during the deformation of the plate, the components of n_x, n_y and n_{xy} in a z-direction give the relation

$$n_x \frac{\partial^2 w}{\partial x^2} + 2n_{xy} \frac{\partial^2 w}{\partial x \partial y} + ny\frac{\partial^2 w}{\partial y^2}, \qquad (B.4)$$

The differential equation of the stiffened plate under the action both of the lateral and the membrane forces comprises the combination of Equations (B.2) and (B.4), and is given by

$$B_x \frac{\partial^4 w}{\partial x^4} + 2H \frac{\partial^4 w}{\partial x^2 \partial y^2} + B_y \frac{\partial^4 w}{\partial y^4} = p(x,y) + n_x \frac{\partial^2 w}{\partial x^2}$$

$$+ 2n_{xy} \frac{\partial^2 w}{\partial x \partial y} + n_y \frac{\partial^2 w}{\partial y^2} \qquad (B.5)$$

The forces per unit width, Equation (B.1), can be expressed, using the Function F, of Airy, as

$$n_x = E\frac{\partial^2 F}{\partial y^2}\ ,\ n_y = E\frac{\partial^2 F}{\partial x^2}\ ,\ n_{xy} = -E\frac{\partial^2 F}{\partial x \partial y} \qquad (B.6)$$

An introduction of Equation (B.6) into Equation (B.5), gives

$$B_x \frac{\partial^4 w}{\partial x^4} + 2H\frac{\partial^4 w}{\partial x^2 \partial y^2} + B_y \frac{\partial^4 w}{\partial y^4} = p(x,y)$$

$$+ E\left(\frac{\partial^2 F}{\partial y^2}\frac{\partial^2 w}{\partial x^2} - 2\frac{\partial^2 F}{\partial x \partial y}\frac{\partial^2 w}{\partial x \partial y} + \frac{\partial^2 F}{\partial x^2}\frac{\partial^2 w}{\partial y^2}\right) \qquad (B.7)$$

This is the equilibrium equation of a stiffened plate subject to lateral and in-plane loading.

The membrane equation (compatibility of strains) is found to assume the following three hypotheses.

1) Horizontal shear N_{xy} and N_{yx} will be transferred only by the plate alone. Therefore, for the plate, the forces are

$$\tau_{xy} = \tau_{yx}$$

$$N_{xy} = \tau_{xy}\, a_x t$$

$$N_{yx} = \tau_{yx}\, a_y t$$

2) Unit elongation at the plate and stiffener connection is the same.

$$\varepsilon_{pl} = \varepsilon_{st}$$

3) The stresses act in two directions for the plate and in one direction for the stiffener.

$$\sigma_{pl} \neq \sigma_{st}$$

Therefore, the stresses acting in both the x and y-directions are given by

$$\text{y-direction} \begin{cases} \sigma_{pl} = \dfrac{E}{1-\nu^2}(\varepsilon_y + \nu\varepsilon_x) \\ \sigma_{st} = E\,\varepsilon_y \end{cases} \qquad \text{(B.8a)}$$

$$\text{x-direction} \begin{cases} \sigma_{pl} = \dfrac{E}{1-\nu^2}(\varepsilon_x + \nu\varepsilon_y) \\ \sigma_{st} = E\,\varepsilon_x \end{cases} \qquad \text{(B.8b)}$$

The membrane forces N_x and N_y are

$$N_y = \sigma_{pl} ta_y + \sigma_{st} A_y = E \left[\left(\frac{ta_y}{1-\nu^2} + A_y \right) \varepsilon_y + \frac{\nu ta_y}{1-\nu^2} \varepsilon_x \right] \quad (B.9)$$

$$N_x = \sigma_{pl} ta_x + \sigma_{st} A_y = E \left[\left(\frac{ta_x}{1-\nu^2} + A_x \right) \varepsilon_x + \frac{\nu ta_x}{1-\nu^2} \varepsilon_y \right] \quad (B.10)$$

Solving Equations (B.9) and (B.10), for ε_x and ε_y gives

$$\varepsilon_x = \frac{\nu N_y}{(1-\nu^2) E ta_y} \cdot \frac{1}{\{\quad\}} - \frac{N_x}{E ta_x} \left(\frac{1}{1-\nu^2} + \frac{A_y}{ta_y} \right) \cdot \frac{1}{\{\quad\}} \quad (B.11)$$

$$\varepsilon_y = \frac{N_y}{E ta_y} \left(\frac{1}{1-\nu^2} + \frac{A_x}{ta_x} \right) \frac{1}{\{\quad\}} + \frac{\nu}{(1-\nu^2)} \frac{N_x}{E ta_x} \frac{1}{\{\quad\}} \quad (B.12)$$

$$\gamma_{xy} = \frac{2(1+\nu)}{E} \frac{N_{xy}}{ta_x} \quad (B.13)$$

where

$$\{\quad\} = \left\{ \frac{\nu^2}{(1-\nu^2)^2} - \left(\frac{1}{1-\nu^2} + \frac{A_x}{ta_x} \right) \left(\frac{1}{(1-\nu^2} + \frac{A_y}{ta_y} \right) \right\}$$

Introducing into Equations (B.11), (B.12) and (B.13), the values from Equation (B.1), and using Airy's Function, Equation (B.6), the deformation ε_x, ε_y, and γ_{xy} can be expressed as

$$\varepsilon_x = \frac{\nu}{t(1-\nu^2)} \frac{\partial^2 F}{x^2} \cdot \frac{1}{\{\ \}} - \frac{\partial^2 F}{y^2} \frac{1}{t} \left(\frac{1}{1-\nu^2} + \frac{A_y}{ta_y}\right) \cdot$$

$$\cdot \frac{1}{\{\ \}}$$

$$\varepsilon_y = \frac{\partial^2 F}{x^2} \frac{1}{t} \left(\frac{1}{1-\nu^2} + \frac{A_x}{ta_x}\right) \frac{1}{\{\ \}} + \frac{\partial^2 F}{y^2} \frac{\nu}{t(1-\nu^2)} \cdot \qquad \text{(B.14)}$$

$$\cdot \frac{1}{\{\ \}}$$

$$\gamma_{xy} = -\frac{2(1+\nu)}{t} \frac{\partial^2 F}{\partial x \partial y}$$

Due to the membrane forces, there is an elongation in the middle plane of the plate. It may be demonstrated that the compatibility condition of the strains in the middle plane of the plate give the following Equation.

$$\frac{\partial^2 \varepsilon_x}{\partial y^2} + \frac{\partial^2 \varepsilon_y}{\partial x^2} = \frac{\partial^2 \gamma_{xy}}{\partial x \partial y} + \left(\frac{\partial^2 w}{\partial x \partial y}\right)^2 - \frac{\partial^2 w}{\partial x^2} \frac{\partial^2 w}{\partial y^2} \qquad \text{(B.15)}$$

But, in Equation (B.15), $\varepsilon_y, \varepsilon_y$ and γ_{xy} can be replaced by their values from Equation (B.14).

$$\frac{\partial^2 \varepsilon_x}{\partial y^2} = \frac{\nu}{t(1-\nu^2)} \frac{\partial^4 F}{\partial y^2 \partial x^2} \cdot \frac{1}{\{\quad\}} - \frac{\partial^4 F}{\partial y^4} \frac{1}{t} \left(\frac{1}{1-\nu^2} + \frac{A_y}{t a_y}\right)$$

$$\cdot \frac{1}{\{\quad\}} \qquad \text{(B.16)}$$

$$\frac{\partial^2 \varepsilon_y}{\partial x^2} = \frac{\partial^4 F}{\partial x^4} \frac{1}{t} \left(\frac{1}{1-\nu^2} + \frac{A_x}{t a_x}\right) \frac{1}{\{\quad\}} + \frac{\partial^4 F}{\partial x^2 \partial y^2} \frac{\nu}{t(1-\nu^2)}$$

$$\cdot \frac{1}{\{\quad\}}$$

$$\frac{\partial^2 \gamma_{xy}}{\partial x \partial y} = -\frac{2(1+\nu)}{t} \frac{\partial^4 F}{\partial x^2 \partial y^2}$$

Introducing Equation (B.16) into Equation (B.15), after rearranging the terms, the compatibility equation becomes

$$D_x \frac{\partial^4 F}{\partial x^4} + D_y \frac{\partial^4 F}{\partial y^4} + \left[-\frac{2\nu}{(1-\nu^2)} + 2T\right] \frac{\partial^4 F}{\partial x^2 \partial y^2} = R\left[\left(\frac{\partial^2 w}{\partial x \partial y}\right)^2 - \frac{\partial^2 w}{\partial x^2} \frac{\partial^2 w}{\partial y^2}\right] \qquad \text{(B.17)}$$

where

$$D_x = \left(\frac{1}{1-\nu^2} + \frac{A_x}{ta_x}\right)$$

$$D_y = \left(\frac{1}{1-\nu^2} + \frac{A_y}{ta_y}\right)$$

$$R = t\left[D_x D_y - \frac{\nu^2}{(1-\nu^2)^2}\right]$$

$$2T = 2(1+\nu)\left[D_x D_y - \frac{\nu^2}{(1-\nu^2)^2}\right]$$

If

$$2S = -\frac{2\nu}{(1-\nu^2)} + 2(1+\nu)\left[D_x D_y - \frac{\nu^2}{(1-\nu^2)^2}\right]$$

then, Equation (B.17) becomes

$$D_x \frac{\partial^4 F}{\partial x^4} + D_y \frac{\partial^4 F}{\partial y^4} + 2S \frac{\partial^4 F}{\partial x^2 y^2} = R\left[\left(\frac{\partial^2 w}{\partial x \partial y}\right)^2 - \frac{\partial^2 w}{\partial x^2}\frac{\partial^2 w}{x^2}\right] \quad (B.18)$$

For the plane state of the stresses and when the deflection w(x,y) is relatively small, the right-hand side of Equation (B.18) can be neglected, and this yields

$$D_x \frac{\partial^4 F}{\partial x^4} + 2S \frac{\partial^4 F}{\partial x^2 \partial y^2} + D_y \frac{\partial^4 F}{\partial y^4} = 0 \quad (B.19)$$

Equations (B.7) and (B.18) are fundamentally large deflection equations of stiffened plates, and are called in technical literature, the "equilibrium" and "compatibility" equations, respectively. If the lateral load is zero, Equations (B.7) and (B.19), can be used to investigate the buckling of stiffened plates.

The compatibility Equation (B.18) is derived by assuming the stress to be different in the plate and stiffener. But, it is current practice to assume that the stress is the same in both the plate and stiffener. This is the hypothesis used when stiffened plates are analysed on the basis of the equivalent thickness principle. Hereafter, the compatibility equation is derived, assuming the stress to be the same in both the plate and stiffener.

B.3 COMPATIBILITY EQUATION ASSUMING THE STRESS TO BE THE SAME IN BOTH THE PLATE AND STIFFENER

If the stress is assumed to be the same in both the plate and stiffener, Equations (B.9) and (B.10) for membrane forces N_x and N_y become

$$N_y = \sigma_y(ta_y+A_y) = \frac{E}{1-\nu^2}(\epsilon_y+\nu\epsilon_x)(ta_y+A_y) \qquad (B.20)$$

$$N_x = \sigma_x(ta_x+A_x) = \frac{E}{1-\nu^2}(\epsilon_x+\nu\epsilon_y)(ta_x+A_x) \qquad (B.21)$$

Solving Equations (B.20) and (B.21) for ε_x and ε_y give

$$\varepsilon_x = \frac{N_x}{Eta_x(1+\frac{A_x}{ta_x})} - \frac{\nu}{E}\frac{N_y}{ta_y(1+\frac{A_y}{ta_y})}$$

$$\varepsilon_y = \frac{N_y}{Eta_y(1+\frac{A_y}{ta_y})} - \frac{\nu}{E}\frac{N_x}{ta_x(1+\frac{A_x}{ta_x})} \qquad \text{(B.22)}$$

$$\gamma_{xy} = \frac{2(1+\nu)}{E}\frac{N_{xy}}{ta_x}$$

Introducing into Equation (B.22), the values from Equations (B.1) and (B.6), and rearranging them, the terms ε_x, ε_y and γ_{xy} are given by

$$\varepsilon_x = \frac{1}{tD_x}\frac{\partial^2 F}{\partial y^2} - \frac{\nu}{tD_y}\frac{\partial^2 F}{\partial x^2}$$

$$\varepsilon_y = \frac{1}{tD_y}\frac{\partial^2 F}{\partial x^2} - \frac{\nu}{tD_x}\frac{\partial^2 F}{\partial y^2} \qquad \text{(B.23)}$$

$$\gamma_{xy} = -\frac{2(1+\nu)}{t}\frac{\partial^2 F}{\partial x \partial y}$$

where

$$D_x = (1+\frac{A_x}{ta_x}), \quad D_y = (1+\frac{A_y}{ta_y})$$

After the second differentiation of $\varepsilon_x, \varepsilon_y$ and γ_{xy} in Equation (B.23) about y,x and xy, respectively, and introducing these new terms into the compatibility Equation (B.15), this latter becomes

$$D_x \frac{\partial^4 F}{\partial x^4} + 2H\frac{\partial^4 F}{\partial x^2 \partial y^2} + D_y \frac{\partial^4 F}{\partial y^4} = tD_x D_y\left[\left(\frac{\partial^2 w}{\partial x \partial y}\right)^2 - \frac{\partial^2 w}{\partial x^2}\frac{\partial^2 w}{\partial y^2}\right] \quad (B.24)$$

where

$$2H = 2(1+\nu)D_x D_y - \nu D_y - \nu D_x = 2(1+\nu)D_x D_y - \nu(D_x+D_y)$$

Compatibility Equation (B.24) and equilibrium Equation (B.7) are the fundamentally large deflection equations of the stiffened plates, assuming the stress to be the same in both the plate and stiffener.

B.4 SOLUTION OF FUNDAMENTALLY LARGE DEFLECTION EQUATIONS BY THE ENERGY METHOD

The exact solution of the system of the equilibrium Equation (B.7) and the compatibility Equation (B.18) or (B.24) is too complex, therefore, some approximate solutions are proposed, among those being the solution by energy method. This is relatively acceptable. In this section, a general description of the solution by the energy method is presented for the system formed by Equations (B.7) and (B.24). In other words, only the example that assumes the stress to be

the same in both plate and stiffener, is considered.

B.4.1 General Expression of Strain Energy for the Plane Problem

The expression of strain energy for the plane problem is given by

$$d\,U_t = 1/2 \iint (\sigma_x\varepsilon_x+\sigma_y\varepsilon_y+\tau_{xy}\gamma_{xy})\,dxdy \qquad (B.25)$$

where

U_t is the total virtual work due both to the bending and membrane stresses.

Using Hooke's law, strains ε_x, ε_y and γ_{xy} can be be expressed as:

$$\varepsilon_x = \frac{\sigma_x}{E_x} - \nu_y \frac{\sigma_y}{E_y}$$

$$\varepsilon_y = \frac{\sigma_y}{E_y} - \nu_x \frac{\sigma_x}{E_x} \qquad (B.26)$$

$$\gamma_{xy} = \frac{\tau_{xy}}{G_{xy}}$$

Introducing Equation (B.26) into Equation (B.25) gives

$$dU_t = 1/2 \iint \left[\frac{\sigma_x^2}{E_x} + \frac{\sigma_y^2}{E_y} - \left(\frac{\nu_x}{E_x}+\frac{\nu_y}{E_y}\right)\sigma_x\sigma_y + \frac{\tau_{xy}^2}{G_{xy}}\right] dxdy \qquad (B.27)$$

where

$$\sigma_x = \sigma_x^b + \sigma_x^m$$

where

b = bending.

$$\sigma_y = \sigma_y^b + \sigma_y^m$$

where

m = membrane.

$$\tau_{xy} = \tau_{xy}^b + \tau_{xy}^m$$

Equation (B.27) is now separately developed for bending, and for the membrane stresses.

B.4.1.1 Strain energy of bending

The strains $\varepsilon_x, \varepsilon_y$ and γ_{xy} can be expressed as a function of the curvature, as follows:

$$\varepsilon_x = \frac{z}{\rho_x}, \quad \varepsilon_y = \frac{z}{\rho_y}, \quad \gamma_{xy} = \frac{z}{\rho_{xy}} \qquad (B.28)$$

The curvature $1/\rho$ can also be expressed in terms of the deflection surface function w, where

$$\frac{1}{\rho_x} = -\frac{\partial^2 w}{\partial x^2}, \quad \frac{1}{\rho_y} = -\frac{\partial^2 w}{\partial y^2}, \quad \frac{1}{\rho_{xy}} = -\frac{\partial^2 w}{\partial x \partial y} \qquad \text{(B.29)}$$

Introducing Equation (B.29) into Equation (B.28), gives

$$\varepsilon_x = -\frac{Z\partial^2 w}{\partial x^2}, \quad \varepsilon_y = -Z\frac{\partial^2 w}{\partial y^2}, \quad \gamma_{xy} = -2Z\frac{\partial^2 w}{\partial x \partial y} \qquad \text{(B.30)}$$

If Equation (B.26) is solved for stresses σ_x, σ_y and τ_{xy}, and using the values of strains from Equations (B.30), it follows that the stresses are given by

$$\sigma_x^b = -\frac{E_x Z}{1-\nu_x \nu_y}\left(\frac{\partial^2 w}{\partial x^2} + \nu_y \frac{\partial^2 w}{\partial y^2}\right)$$

$$\sigma_y^b = -\frac{E_y Z}{1-\nu_x \nu_y}\left(\frac{\partial^2 w}{\partial y^2} + \nu_x \frac{\partial^2 w}{\partial y^2}\right) \qquad \text{(B.31)}$$

$$\tau_{xy}^b = -2G_{xy} Z \frac{\partial^2 w}{\partial x \partial y}$$

When Equation (B.31) is introduced into Equation (B.27), after some transformation, the strain energy of bending is given by Equation (B.32).

$$U_b = 1/2 \int\int \{B_x \left(\frac{\partial^2 w}{\partial x^2}\right)^2 + B_y \left(\frac{\partial^2 w}{\partial y^2}\right)^2 + 2H \frac{\partial^2 w}{\partial x^2} \frac{\partial^2 w}{\partial y^2}$$

$$+ 4B_{xy} \left[\left(\frac{\partial^2 w}{\partial x \partial y}\right)^2 - \frac{\partial^2 w}{\partial x^2} \frac{\partial^2 w}{\partial y^2}\right]\} \, dxdy \qquad (B.32)$$

where

$$2H = (B_x \nu_y + B_y \nu_x + 4B_{xy})$$

B_x, B_y and B_{xy} are respectively unit-flexural, and have torsional rigidities. For a stiffened plate, they can be approximated as

$$B_x = \frac{EI_x}{a_x}, \quad B_y = \frac{EI_y}{a_y} \qquad (B.33)$$

$$B_{xy} = \frac{1}{3a_x} G_{xy} \left(4h_s t_s^3 + 1/4 \, t^3\right)$$

where

I_x, I_y = movement of inertia of the stiffener and its adjacent plate about the neutral axis of the stiffened plate.

B.4.1.2 Strain energy of the membrane stresses

The strain energy U_m of the membrane stresses can be found by a similar process as that for bending stresses.

When the stress is assumed to be the same in both the plate and stiffener, the values of $\varepsilon_x, \varepsilon_y$ and γ_{xy} in Equation (B.22) can be directly expressed in terms of σ_x, σ_y and τ_{xy}. Introducing these latter into Equation (B.25) gives

$$U_m = \frac{1}{2E} \iint (\sigma_x^2 + \sigma_y^2 - 2\nu\sigma_x\sigma_y + 2(1+\nu)\tau_{xy}^2)\, dxdy \quad (B.34)$$

Using Equation (B.22), after simplification, Equation (B.34) can be rewritten as:

$$U_m = 1/2 \iint \left[\frac{N_x^2}{Et^2a_x^2D_x^2} \quad \frac{N_y^2}{Et^2a_y^2D_y^2} - \frac{2\nu}{Eta_x^2a_y} \frac{N_xN_y}{D_xD_y}\right.$$

$$\left. + \frac{1}{G_{xy}} \frac{N_{xy}^2}{t^2a_x^2}\right] dxdy \quad (B.35)$$

Introducing Airy's function (Equation (B.6)), in Equation (B.35) yields

$$U_m = \frac{E}{2t^2} \iint \frac{1}{D_x^2} \left(\frac{\partial^2 F}{\partial y^2}\right)^2 + \frac{1}{D_y^2} \left(\frac{\partial^2 F}{\partial x^2}\right)^2$$

$$\left. - \frac{2}{D_xD_y} \frac{\partial^2 F}{\partial x^2} \frac{\partial^2 F}{\partial x^2} + 2(1+\nu) \left(\frac{\partial^2 F}{\partial x \partial y}\right)^2 \right] dxdy \quad (B.36)$$

where

$$\Delta_x = \left(\frac{1}{1-\nu^2} + \frac{A_x}{ta_x}\right)$$

$$\Delta_y = \left(\frac{1}{1-\nu^2} + \frac{A_y}{ta_y}\right)$$

B.4.1.3 Ritz Method

Equations (B.32) and (B.36) give the strain energy of the bending and of the membrane stresses, respectively. To be complete, Equation (B.25) has to include that strain energy due to the lateral load in (x,y) or $\rho(x,y)$, as well as that of the in-plane forces N_x and N_y.

When there is no lateral load and the in-plane force acts only in one direction, assuming only N_x exists, the total strain energy is given by

$$U_t = U_b + U_m + \int_{a_x} N_x \, u \, dx \qquad (B.37)$$

where

u is the unit end displacement in the x-direction.

The necessary and sufficient condition of static equilibrium requires that the first variation of Equation (B.37) be zero. This yields

$$\delta U_t = \delta\left(U_b + U_m + \int_{a_x} N_x \, u \, dx\right) = 0 \qquad (B.38)$$

The critical buckling stress is that stress corresponding to the critical load N_x that satisfies Equation (B.38). The solution of Equation (B.38) requires the determination both of the deflection and the membrane stress functions w and F, respectively. This can be done by the Ritz approximate method [120]. This method can be summarized as follows:

a) The deflection function w can be assumed and is given by

$$w = a_1 f_1(x,y) + a_2 f_2(x,y) + \ldots + a_n f_n(x,y) \quad \text{(B.39a)}$$

in which the functions $f_1, \ldots, f_n$ are chosen to accurately represent the deflection surface, and at the same time, satisfy the required boundary conditions.

b) The function w is then introduced into the membrane, Equation (B.24), which is integrated according to those boundary conditions of the membrane stresses. It follows that the membrane stress functions, F, will be expressed as the function of unknown coefficients, $a_1, \ldots, a_n$.

c) The assumed deflection function w and the stress functions F computed in b), are then introduced into Equation (B.38). The unknown coefficient,

$a_1, \ldots, a_n$ as determined from the system of n nonlinear equations, given by the first variation of w, are as follows.

$$\frac{\partial w}{\partial a_1} = 0$$

$$\frac{\partial w}{\partial a_n} = 0 \qquad \text{(B.39b)}$$

Once the coefficients, $a_1, \ldots, a_n$, are determined the expressions for both w and F can be established, from which the displacements and stresses are computed.

B.4.2 Deflection Surface Function

As explained in Section B.4.1, the choice of the deflection surface function w is important. It must accurately represent the deflected surface and satisfy the boundary conditions.

In this section, only the case of a simply-supported plate is assumed, as is the current practice. Considering an element of the stiffened panel, Figure B.2, the deflection surface function w can then be expressed in the Navier form:

$$w = \sum_{m=1}^{\infty} \sum_{n=1}^{\infty} a_{mn} \sin \frac{m\pi x}{a} \sin \frac{n\pi y}{b} \qquad (B.40)$$

where

m and n are equal to 1,2,3,4, ...

The simply-supported boundary conditions at all four edges require that both the displacement w and the moment M, be zero at all four edges. This can be written as

a) at $x = 0$ and $x = a$

$$w = 0$$

$$M_x = \left(\frac{\partial^2 w}{\partial x^2} + \nu \frac{\partial^2 w}{\partial y^2}\right) = 0 \qquad (B.41)$$

b) at $y = 0$ and $y = b$

$$w = 0$$

$$M_y = \left(\frac{\partial^2 w}{\partial y^2} + \nu \frac{\partial^2 w}{\partial x^2}\right) = 0$$

It can easily be demonstrated that Equation (B.40) satisfies all boundary conditions in Equation (B.41).

B.4.3 Determination of the Membrane Stress Functions, F

As the deflection surface function w is chosen and satisfies assumed boundary conditions, the next stage is the

determination of the membrane stress functions, F. This will be done by introducing w into the compatibility Equation (B.24).

The function w must account for the effect of the initial deflection w_o. As a first simplification, both w and w_o are considered to be given by Equation (B.42). They will be generalized later, after the whole mathematical development is completed.

$$w_o = f_o \cos \frac{m\pi x}{a} \cos \frac{n\pi y}{b}$$

$$w = f \cos \frac{m\pi x}{a} \cos \frac{n\pi y}{b} \qquad \text{(B.42)}$$

When the effect of the initial deflection w_o is accounted for, the compatibility Equation (B.24) can then be rewritten as:

$$D_x \frac{\partial^4 F}{\partial x^4} + 2H \frac{\partial^4 F}{\partial x^2 \partial y^2} + D_y \frac{\partial^4 F}{\partial y^4} =$$

$$tD_x D_y \left[\left(\frac{\partial^2 w}{\partial x \partial y}\right)^2 - \frac{\partial^2 w}{\partial x^2} \frac{\partial^2 w}{\partial y^2} + 2 \frac{\partial^2 w_o}{\partial x \partial y} \frac{\partial^2 w}{\partial x \partial y} - \frac{\partial^2 w_o}{\partial x^2} \frac{\partial^2 w}{\partial y^2} \right.$$

$$\left. - \frac{\partial^2 w_o}{\partial y^2} \frac{\partial^2 w}{\partial x^2} \right] \qquad \text{(B.43)}$$

This can be written as

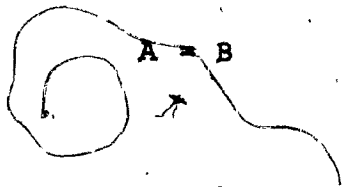

The right-hand sided member is considered first.

The following derivations are computed for both w and w_o.

$$\frac{\partial^2 w}{\partial x \partial y} = \frac{nm\pi^2}{ab} f \sin\frac{m\pi x}{a} \sin\frac{n\pi y}{b}$$

$$\frac{\partial^2 w_o}{\partial x \partial y} = \frac{nm\pi^2}{ab} f_o \sin\frac{m\pi x}{a} \sin\frac{n\pi y}{b} \qquad \text{(B.44)}$$

$$\frac{\partial^2 w}{\partial x^2} = -\frac{m^2\pi^2}{a^2} f \cos\frac{m\pi x}{a} \cos\frac{n\pi y}{b}$$

$$\frac{\partial^2 w_o}{\partial x^2} = -\frac{m^2\pi^2}{a^2} f_o \cos\frac{m\pi x}{a} \cos\frac{n\pi y}{b} \qquad \text{(B.45)}$$

$$\frac{\partial^2 w}{\partial y^2} = -\frac{n^2\pi^2}{b^2} f \cos\frac{n\pi y}{b} \cos\frac{m\pi x}{a}$$

$$\frac{\partial^2 w_o}{\partial y^2} = -\frac{n^2\pi^2}{b^2} f_o \cos\frac{n\pi y}{b} \cos\frac{m\pi x}{a} \qquad \text{(B.46)}$$

Introducing Equations (B.44), (B.45) and (B.46) into the right-hand sided member of Equation (B.43) becomes

$$B = \frac{m^2n^2\pi^4}{a^2b^2} f^2 \left(\sin^2 \frac{m\pi x}{a} \sin^2 \frac{n\pi y}{b} - \cos^2 \frac{m\pi x}{a} \cos^2 \frac{n\pi y}{b}\right) \tag{B.47}$$

$$+ 2 \frac{m^2n^2\pi^4}{a^2b^2} f_o f \left(\sin^2 \frac{m\pi x}{a} \sin^2 \frac{n\pi y}{b} - \cos^2 \frac{m\pi x}{a} \cos^2 \frac{n\pi y}{b}\right)$$

Making

$$k = \frac{m\pi x}{a} \ , \ \ell = \frac{n\pi y}{b}$$

rewriting Equation (B.47) now yields

$$B = f(f+2f_o)\frac{m^2n^2\pi^4}{a^2b^2} (\sin^2 k \sin^2 \ell - \cos^2 k \cos^2 \ell) \tag{B.48}$$

Making a few trigonometric transformations in Equation (B.48) then gives

$$B = - f(f+2f_o)\frac{m^2n^2 4}{2a^2b^2} (\cos 2k + \cos 2\ell) \tag{B.49}$$

Then, the compatibility Equation (B.43) becomes

$$D_x \frac{\partial^4 F}{\partial x^4} + 2H\frac{\partial^4 F}{\partial x^2 \partial y^2} + D_y \frac{\partial^4 F}{\partial y^4} = - tD_xD_yf(f+2f_o)\frac{m^2n^2\pi^4}{2a^2b^2}(\cos 2k + \cos 2\ell) \tag{B.50}$$

If both w and w_o are expressed in series, as in Equation (B.40), Equation (B.50) can therefore be rewritten as

$$D_x \frac{\partial^4 F}{\partial x^4} + 2H \frac{\partial^4 F}{\partial x^2 \partial y^2} + D_y \frac{\partial^4 F}{\partial y^4} =$$

$$- tD_x D_y \sum_{m=1}^{\infty} \sum_{n=1}^{\infty} f_{mn}(f_{mn}+2f_{omn}) \frac{m^2 n^2 \pi^4}{2a^2 b^2} (\cos 2\frac{m\pi x}{a}$$

$$+ \cos 2\frac{n\pi y}{b}) \qquad \text{(B.51)}$$

The compatibility Equation (B.51) is now solved as follows:

Making

$$- tD_x D_y \sum_{m=1}^{\infty} \sum_{n=1}^{\infty} (f_{mn}^2 + 2f_{omn} f_{mn}) \frac{m^2 n^2 \pi^4}{2a^2 b^2} = C$$

By identification, Equation (B.51) gives

$$D_x \frac{\partial^4 F}{\partial x^4} = C \cos 2 \frac{m\pi x}{a} \qquad \text{(B.52a)}$$

$$D_y \frac{\partial^4 F}{\partial y^4} = C \cos 2 \frac{n\pi y}{b} \qquad \text{(B.52b)}$$

The integration of Equations (B.52a) and (B.52b) give the components F_x and F_y, respectively

$$F_x = \frac{Ca^4}{16m^4 \pi^4 D_x} \cos \frac{2m\pi x}{a} \qquad \text{(B.53a)}$$

$$F_y = \frac{Cb^4}{16n^4\pi^4 D_y} \cos \frac{2n\pi y}{b} \qquad \text{(B.53b)}$$

Replacing C in Equations (B.53a) and (B.53b) by its value and introducing the coefficient $a/b = \alpha$, the components F_x and F_y can be rewritten as

$$F_x = - tD_y \sum_{m=1}^{\infty} \sum_{n=1}^{\infty} (f_{mn}^2 + 2f_{mn}f_{omn}) \frac{n^2\alpha^2}{32m^2} \cos \frac{2m\pi x}{a}$$

$$= A_1 \cos \frac{2m\pi x}{a} \qquad \text{(B.54a)}$$

$$F_y = - tD_x \sum_{m=1}^{\infty} \sum_{n=1}^{\infty} (f_{mn}^2 + 2f_{mn}f_{omn}) \frac{m^2}{32n^2\alpha^2} \cos \frac{2n\pi x}{b}$$

$$= A_2 \cos \frac{2n\pi y}{b} \qquad \text{(B.54b)}$$

Then the particular solution of the compatibility Equation (B.51) is

$$F_p = F_x + F_y = A_1 \cos \frac{2m\pi x}{a} + A_2 \cos \frac{2n\pi y}{b} \qquad \text{(B.55)}$$

The general solution of Equation (B.51), is given by

$$D_x \frac{\partial^4 F}{\partial x^4} + 2H \frac{\partial^4 F}{\partial x^2 \partial y^2} + D_y \frac{\partial^4 F}{\partial y^4} = 0 \qquad \text{(B.56)}$$

and this solution should be such that

$$F = F_p + F_G \tag{B.57}$$

To explain that there is compression in the x-direction, we have, as a first solution, F'_G, in which

$$F'_G = P_x \frac{y^2}{2} \tag{B.58}$$

Setting the following equation,

$$F = F_p + F'_G = A_1 \cos \frac{2m\,x}{a} + A_2 \cos \frac{2n\,y}{b} + P_x \frac{y^2}{2} \tag{B.59}$$

Equation (B.59) has to satisfy the following boundary conditions of the membrane stresses.

1) In the longitudinal direction (the x-direction), the buckling waves create similar states of stresses and deformations on each subpanel located between the transverse stiffeners. Consequently, the contraflexure edges $x = \pm a/2$ remain straight and no shearing forces act along them. This means that at $x = \pm a/2$

   a) $(u) = \text{cste}$

   b) $n_{xy} = 0$ (B.60)

2) Along the non-loaded edges $y = \pm b/2$, we now consider the following two cases:

   i) The unloaded edges are free to move in, but remain straight in their plane, due to distribution

of the normal stresses σ_y, of which the resultant is zero. This may be expressed by

$$\begin{aligned} &\text{a)} \quad (v)_y = \pm\, b/2 = \text{cste} \\ &\text{b)} \quad n_{xy} = 0 \end{aligned} \tag{B.61}$$

This case represents the membrane boundary conditions for an interior subpanel of a stiffened panel.

ii) Unloaded edges are free of stresses.

$$\begin{aligned} &\text{a)} \quad (n_y)_y = \pm\, b/2 = 0 \\ &\text{b)} \quad (n_{xy})_y = \pm\, b/2 = 0 \end{aligned} \tag{B.62}$$

Equation (B.62) may represent the boundary conditions at the flange/web edges of steel box-girder bridges.

Equation (B.51) gives the following forces per unit width.

$$\begin{aligned} n_y &= EtD_y \sum_{m=1}^{\infty} \sum_{n=1}^{\infty} (f_{mn}^2 + 2f_{mn}f_o)\frac{n^2\pi^2}{8b^2} \cos\frac{2m\pi x}{a} \\ n_x &= EtD_x \Sigma\Sigma (f_{mn}^2 + 2f_{mn}f_o)\frac{m^2\pi^2}{8a^2} \cos\frac{2n\pi y}{b} + EP_x \\ n_{xy} &= 0 \end{aligned} \tag{B.63}$$

The displacement u and v, can be expressed as

$$\epsilon_x = \frac{\partial u}{\partial x} + \frac{1}{2}\left(\frac{\partial w}{\partial x}\right)^2 + \frac{\partial w_o}{\partial x}\frac{\partial w}{\partial x}$$

$$\epsilon_y = \frac{\partial v}{\partial y} + \frac{1}{2}\left(\frac{\partial w}{y}\right)^2 + \frac{\partial w_o}{\partial y}\frac{\partial w}{\partial y} \qquad \text{(B.64)}$$

Solving Equations (B.64) for $\frac{\partial u}{\partial x}$ and $\frac{\partial v}{\partial y}$ and integrating the given strains u and v expressions for $x = \pm a/2$ and $y = \pm b/2$, respectively

$$u_x = D_x \frac{m^2\pi^2}{8Ea}(f^2+2ff_o)\cos\frac{2n\pi y}{a}$$

$$+ \frac{P_x a}{Et} - \frac{1}{4}\frac{m^2\pi^2}{a}(f^2+2ff_o)\cos^2\frac{n\pi y}{b} \qquad \text{(B.65)}$$

$$v_y = D_y \frac{n^2 2}{8Eb}(f^2 2ff_o)\cos\frac{2m x}{a}$$

$$- \frac{\nu P_x b}{Et} - \frac{1}{4}\frac{n^2\pi^2}{b}(f^2+2ff_o)\cos^2\frac{m\pi x}{a}$$

It may now be concluded from Equations (B.63) and (B.65), that Equation (B.59) satisfies the boundary conditions:

- In the longitudinal direction, Equation (B.60)

$$n_{xy} = 0 \qquad u_x = \text{cste} = \text{independent of } x$$

- In the transverse direction,

$$n_{yx} = 0 \qquad v_y = \text{cste} = \text{independent of } y$$

$$n_y \neq 0$$

Therefore, the membrane function given by Equation (B.59) applies in the transverse direction, only to the boundary conditions 1). In general, it must also satisfy boundary condition 2). To satisfy that, the force n_y has to disappear. To accomplish that, a new function F''_G is introduced into Equation (B.59), where

$$F = F_p + F'_G + F''_G \tag{B.66}$$

The function F''_G should not modify the already satisfied boundary conditions, only $(n_y)_{y = \pm b/2}$ must disappear. After a lengthy mathematical computation, Yamaki [127] and later Massonnet [64] concluded that F''_G had to be expressed as

$$F''_G = ch\beta y \cos \frac{2m\pi x}{a} \tag{B.67}$$

and had to satisfy Equation (B.56).

After numerous transformations, the general membrane function that was found to satisfy all the boundary conditions, 1) and 2). (Equations (B.60), (B.61) and (B.62)) is given by

$$F = A_1 \cos \frac{2m\pi x}{a} + A_2 \cos \frac{2n\pi y}{b} + P_x \frac{y^2}{2} + K_1 \cos \frac{2m\pi x}{a} \operatorname{ch}\beta_1 y + K_2 \cos \frac{2m\pi x}{a} \operatorname{ch}\beta_2 y \tag{B.68}$$

where

A_1 and A_2 are given in Equations (B.54).

$$\beta_1 = \frac{2\pi}{a} \sqrt{\frac{\Delta_x}{\bar{\Delta}}} \sqrt{1 + \sqrt{1-\theta^2}} = \frac{2\pi}{a} J_1$$

$$\beta_2 = \frac{2\pi}{a} \sqrt{\frac{\Delta_x}{\bar{\Delta}}} \sqrt{1 - \sqrt{1-\theta^2}} = \frac{2\pi}{a} J_2$$

$$K_1 = \frac{J_2 \operatorname{sh} \frac{\pi J_2}{\alpha}}{J_1 \operatorname{sh} \frac{\pi J_1}{\alpha} \operatorname{ch} \frac{\pi J_2}{\alpha} - J_2 \operatorname{sh} \frac{\pi J_2}{\alpha} \operatorname{ch} \frac{\pi J_1}{\alpha}} A_1$$

$$K_2 = \frac{J_1 \operatorname{sh} \frac{\pi J_1}{\alpha}}{J_1 \operatorname{sh} \frac{\pi J_1}{\alpha} \operatorname{ch} \frac{\pi J_2}{\alpha} - J_2 \operatorname{sh} \frac{\pi J_2}{\alpha} \operatorname{ch} \frac{\pi J_1}{\alpha}} A_1$$

$$\theta = \frac{\bar{\Delta}}{\sqrt{\Delta_x \Delta_y}} \qquad \bar{\Delta} = \frac{1 - \nu}{1 - \frac{\nu \Delta^2}{\Delta_x \Delta_y}}$$

$$\Delta = \frac{Et}{1 - \nu^2}$$

B.4.4 CONCLUSION

Once the deflection surface function w and the membrane stress functions F are accurately determined in Equations (B.40) and (B.68), respectively, the approximate Ritz method summarized in Equations (B.39a) and (B.39b) can be used to determine the critical buckling stress.

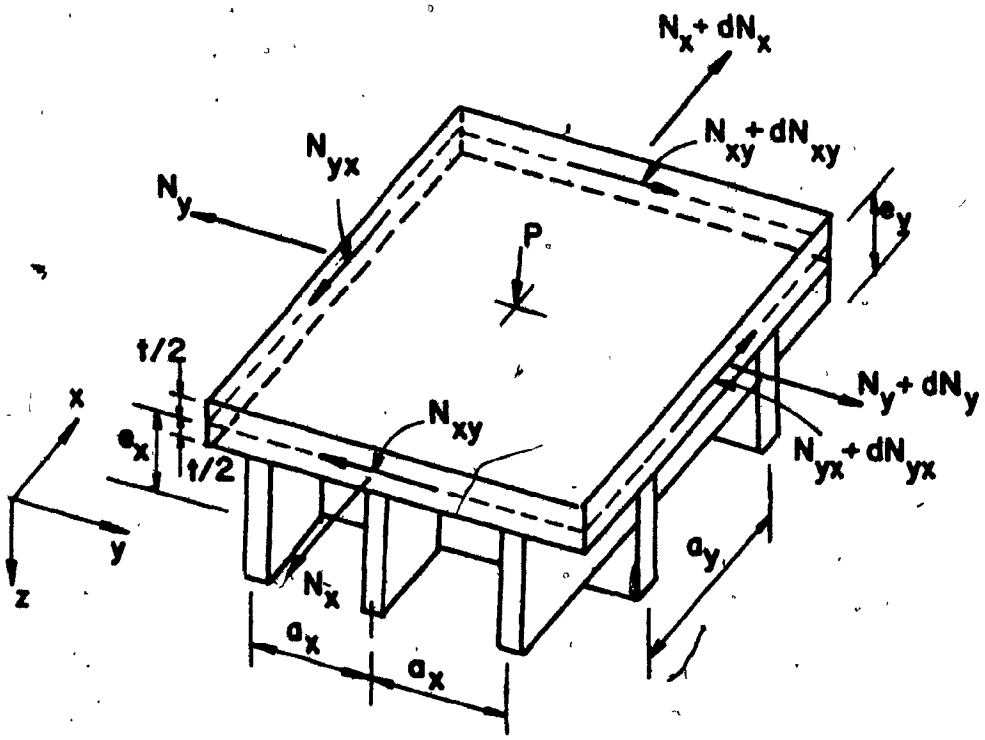

FIG. B-1 ELEMENT OF STIFFENED PLATE SUBJECTED TO IN-PLATE LATERAL FORCES

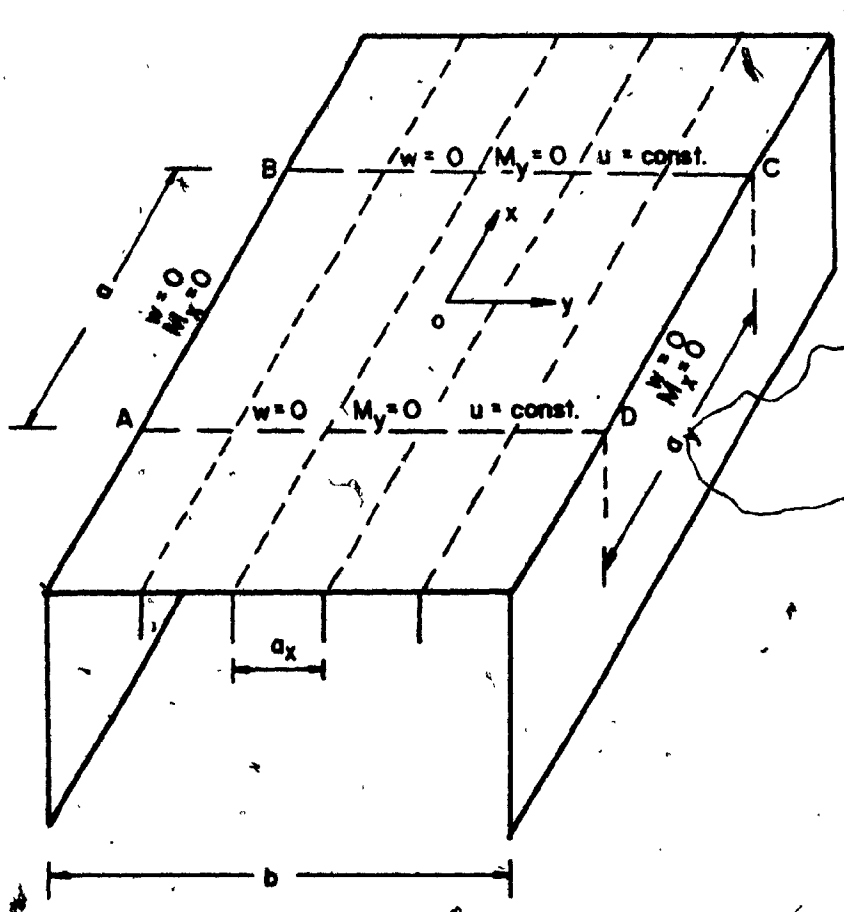

at $y = \pm b/2$ two cases: case ① a) $v \neq 0$ b) $n_{xy} = 0$ case ② a) $n_y = 0$ b) $n_{xy} = 0$

FIG. B-2 BOUNDARY CONDITIONS OF THE COMPRESSION FLANGE OF STEEL BASE-GIRDER BRIDGE